New Applications for Poly(ethylene-alt-maleic anhydride)

JOHNSON, DAVID,WARD

New Applications for Poly(ethylene-alt-maleic anhydride)

David Ward Johnson

A Thesis Presented for the Degree of

Doctor of Philosophy

Department of Chemistry

University of Durham

June 2010

Abstract

The project throughout is an iterative development of an understanding of poly(ethylene-alt-maleic anhydride) in terms of both its physical behaviour and chemistry.

Chapter one involves a thorough and rigorous characterisation of the polymer, and three principle things are established: the polymer is structurally uniform, reacts in a predictable and quantitative manner, closely analogous to that of small molecule anhydrides. It was with this knowledge that further applications could then be developed.

In chapter two the polymer is reacted with a series of different hydrophobic and hydrophilic amines in order to create a series of polymers which allowed the mechanism of ice re-crystallisation to be probed. The findings show that hydrophobic volume appears to play an important role in the mechanism of ice re-crystallisation. This finding allowed for tentative developments to be made on the existing theories surrounding antifreeze glycol protein mimicking polymers.

Chapter three involved the reaction of the polymer with varying amounts of hydrophobic and hydrophilic amines in order to induce their self assembly in water. The results demonstrated that when the concentration of hydrophobic amines is low that the polymer aggregates can disperse as a small molecule surfactant might. In addition, to this the hydrophobically modified polymers were able to self assemble intra-molecularly at concentration below the critical aggregation concentration

providing an opportunity to create complex encapsulation systems. In addition, it was shown that the introduction of small amounts of hydrophilic amines onto the polymer backbone resulted in aggregates forming wherein the remaining anhydride units form the core, consequently there was shown to be a limited period of time in which further reactions could be undertaken such as cross-linking or the immobilisation of nucleophilic compounds. This presents the opportunity for easily manufactured, multi –purpose carrier nano-aggregates for useful compounds, examples may include dispersing or solubilising a hydrophobic drug.

Chapter four deals with the production of hydrophobic surfaces by a trivial and easily replicable mechanism, namely by creating a phase separated polymer film and etching away of one of the polymer phases by dissolving it in a solvent selective for one polymer only. While this did not result in a super-hydrophobic surface the contact angle was observed to increase markedly over analogous flat thin films and presents ample opportunity for future optimisation.

Acknowledgments

I would like to start by thanking both Professor Neil R Cameron (Durham University) and Brian Tarbit (Vertellus Speciality Chemicals) for giving me the opportunity to spend three years working and learning. In addition, I'd especially like to thank Douglas Carswell for his uncomplaining help throughout the course of my study and for the selfless acts of generosity he has shown toward me.

I would like to thank my family and Alison Parry without whom I am certain that finishing my PhD would have been much harder. Finally, I'd like to thank all those people with whom I have worked, learned and laughed with over the past few years.

Funding

I would like to acknowledge both Vertellus Speciality Chemicals and the EPSRC for providing both the funding for this PhD and an opportunity for me to learn.

Contents

Abbreviations

[η]	intrinsic viscosity
Å	angstrom
A_2	second virial coefficient
AFGP	anti-freeze glyco-protein
AFP	anti-freeze protein
aq	aqueous
br	broad
CAC	critical aggregation concentration
CD	circular dichroism
$CDCl_3$	deuterated chloroform
cm^{-1}	reciprocal centimetres
cm^3	cubic centimetres
CMC	critical micelle concentration
Da	Dalton
dm^3	cubic decimetres
DMF	*N*,*N*-dimethylformamide
DMSO	dimethylsulphoxide
DP	degree of polymerisation
DSC	differential scanning calorimetry
E_a	activation energy
ETH	ethanol
FT	Fourier transform
g	grams
GPC	gel permeation chromatography
Hz	hertz
IR	infra-red
K_c	optical constant
kDa	kilo-Dalton
kg	kilograms
kJ	kilojoules

L	corona thickness
l_c	critical chain length of the hydrophobic group
m	multiplet
M	molarity
mg	milligrams
mL	millilitre
MLGS	mean largest grain size
mmol	millimoles
M_n	number average molecular weight
mol	moles
M_v	viscosity average molecular weight
M_w	weight average molecular weight
$M_{w/} M_n$	polydispersity
M_z	size average molecular weight
N_{agg}	aggregation number
NMR	nuclear magnetic resonance
NRET	non-radiative energy transfer
oop	out-of-plane
ov	overlapping
PDI	polydispersity index
ppm	parts per million
QLL	quasi-liquid layer
R_c	core radius
RI	inhibition of recrystallisation
RI	refractive index
s	singlet
SEC	size exclusion chromatography
SPR	surface plasmon resonance
T_c	crystallisation temperature
T_f	freezing temperature
TFB	trifluorobutanol
TFE	trifluoroethanol
T_g	glass transition temperature

TGA	thermogravimetric analysis
TH	thermal hysteresis
T_m	melting temperature
V	volume of the hydrophobic chain
XPS	X-ray powder solids
α	Mark-Houwink parameter
α_0	optimal surface area of the hydrophilic chains
ΔR	excess Raleigh constant
μL	microlitres
τ_c	correlation time

[On the narrator's admission to the Grand Academy of Lagado, the art wherein the Professors employ themselves.]

"The first man I saw was of a meagre aspect, with sooty hands and face, his hair and beard long, ragged, and singed in several places. His clothes, shirt, and skin, were all of the same colour. He has been eight years upon a project for extracting sunbeams out of cucumbers, which were to be put in phials hermetically sealed, and let out to warm the air in raw inclement summers. He told me, he did not doubt, that, in eight years more, he should be able to supply the governor's gardens with sunshine, at a reasonable rate: but he complained that his stock was low, and entreated me "to give him something as an encouragement to ingenuity, especially since this had been a very dear season for cucumbers." I made him a small present, for my lord had furnished me with money on purpose, because he knew their practice of begging from all who go to see them."

- *Gullivars' Travels by Jonathan Swift*

Author's Forward

Vertellus Speciality Chemicals are the manufacturers of poly(ethylene-alt-maleic anhydride), sold under the trade name of ZeMac. Such polymers have been in existence since the mid-1940s and have found myriad applications as emulsion stabilisers, detergent compositions and viscosity modifiers.

Vertellus' aim is to fully characterise, benchmark and develop new applications for these polymers, and it was to this brief that the following thesis was worked. As a result, the body of work covers a large range of systems and applications: Chapter one deals with the polymer's physical and chemical characterisation; Chapter two with its use in aqueous solution to inhibit the growth of ice crystals; Chapter three its application to colloidal systems, and Chapter four its use in surface applications.

The unifying theme throughout the thesis is the polymer itself rather than the development of an individual goal or system. Because of the broad range of systems to which the polymer has been applied, each chapter has been written to be semi-self contained, with its own literature review and experimental section. However, it should be noted that the fundamentals of polymer science discussed within Chapter one and, where necessary references are made between chapters, although this has been kept to a minimum in order to make the reading of this work easier.

Chapter One: **Physical and Chemical Characteristics of Poly(ethylene-alt-maleic anhydride)**

1.1 Introduction

1.1.1 Polymer chemistry

In 1953 Flory grouped all polymerisations into one of two categories: step growth and chain growth.[1,2] Chain growth polymerisations involve the sequential addition of a monomer unit onto the end of the polymer chain. That is to say, the polymer grows one residue at a time outwards from a reactive centre which is maintained at the end of the polymer chain. This mechanism, in its simplest form, is characterised by: the initiation of the chain, the growth of the chain by propagation and the subsequent termination of the chain. However, in addition to this there are two further considerations namely transfer of the active centre and the use of multifunctional initiators.

Transfer of the active centre involves the abstraction of an atom by a chain carrier from an inactive molecule. The inactive molecule's identity can be any of the following types: monomer, initiator, inactive sites on the polymer chain, solvent, or a molecule added to deliberately promote transfer (chain transfer agent).

The process of transfer will result in either the creation of a new active centre from which further propagation may occur, or the creation of a group too stable for further polymerisation. The latter possibility is particularly notable in radical polymerisations

where transfer to vinylic monomers can lead to resonance stabilised radicals in a process known as degradative transfer.

Multifunctional initiation involves the use of initiators capable of generating a molecule with more than one active centre. Propagation is then able to occur in more than one direction. In the simplest case, a bi-functional initiator this will lead to a polymer chain growing in two directions still producing a linear polymer chain. When there are more than two active centres the final structure will be branched. Step growth polymerisation involves the reaction of multi-functional (usually di-functional) molecules with other multi-functional molecules of complementary reactivity, for example the reaction of a diamine with an acyl chloride. The reaction rate is dependent on the concentration of functional groups in the reaction mixture, therefore the reaction initially proceeds rapidly with the formation of short oligomeric chains; however, beyond this point the concentration of functional groups is significantly reduced resulting in long reaction times and the use of forcing conditions to drive the combination of the oligomers into long chain polymers.

There are significant difficulties in ensuring the success of step growth polymerisations, including the need for precise stoichiometric control of the reactants as the polymerisation relies on the reaction of increasingly scarce functional groups. Even a slight excess of one monomer over the other will prematurely terminate the reaction, as will the presence of even small amounts of mono-functional material. An exception to this is when an A-B type monomers are used, that is to say where the complementary functional groups are on the same molecule. Here the stoichiometric amount of each functional group is determined by the identity of the monomer.

1.1.2 Free radical polymerisation

Free radical polymerisation is a form of chain growth polymerisation and is characterised by five stages: initiator decomposition, initiation, propagation, termination and transfer.

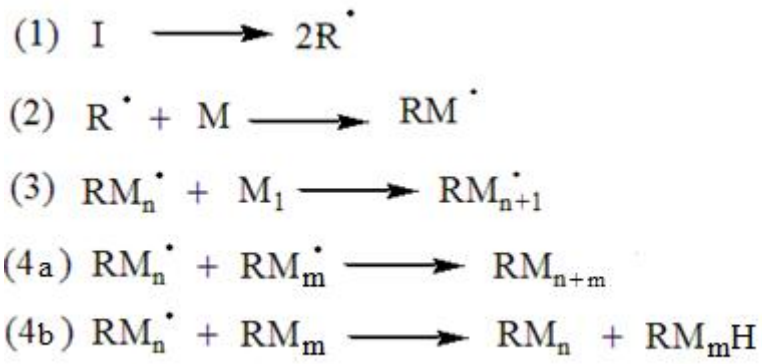

Figure 1-1: Reaction steps in free radical polymerisation: (1) decomposition of initiator; (2) initiation; (3) propagation (growth) of polymer chains; (4a) termination by combination; and, (4b) termination by disproportionation

Figure 1-1 shows the various steps involved in radical polymerisation. The precise mechanism and rate of each step are dependent on a number of factors including temperature, solvent and the chemistry of each component. The process initiates and then continues until either the monomer is entirely consumed or all the growing free radical chains are terminated without the prospect for the further initiation and propagation of new polymer chains. The important point is that the entire process tends towards a steady state where rate of termination becomes equal to the rate of initiation.

1.1.3 Copolymerisation

When a polymerisation is conducted in the presence of more than one monomer, the monomers may react in one of two ways. They may react as independent monomers and polymerise to form two types of chains each composed of one type of monomer (homopolymer). Alternatively, they may polymerise together as co-monomers and form a chain which is a composite of the two, namely a copolymer.

It is this relative distribution of co-monomers that defines the architecture of the copolymer. There are five common copolymer architectures namely: statistical, alternating, block, gradient and graft copolymers.

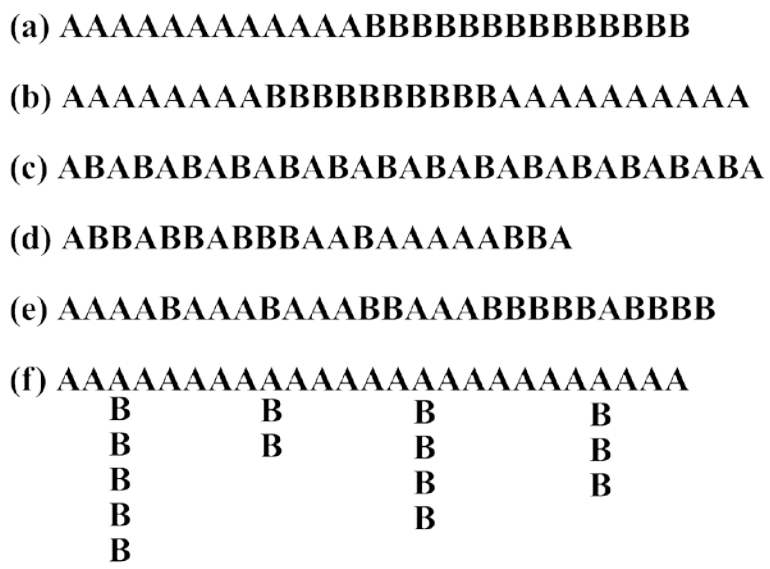

Figure 1-2: Structural representation of a variety of block copolymer architectures wherein A and B represent co-monomers (a) di-block copolymer, (b) tri-block copolymer, (c) alternating block, (d) statistical block copolymer, (e) gradient and (f) graft copolymer.

Block copolymers form when the co-monomers form distinct homopolymeric blocks within the overall copolymer structure (figure 1-2 (a, b)). Alternating block copolymers are formed when the co-monomers react in such a way that the comonomer residues periodically alternate between each co-monomer (figure 1-2 (c)). Statistical copolymers are formed when the monomers have an intermediate preference for reaction with themselves and their co-monomer. A special, but notable, case of a statistical copolymer is that of a random copolymer in which neither co-monomer has a bias for copolymerisation or homo-polymerisation. Gradient copolymers (figure 1-2(e)) exhibit a gradual change in composition along the polymer backbone. The simplest example would be a polymer chain in which the initiator end is predominantly composed of the first co-monomer, then proceeds in to a region where the polymer backbone is predominantly a mixture of both co-monomers and then into a third region where the second co-monomer predominates. The final structure represented (figure 1-2(f)) is a graft copolymer. In this case the initiation and growth of the second block generally occurs after the polymerisation of the backbone.

The final copolymer architecture is determined by two principle factors: the first is the relative concentration of the co-monomers (feed ratio), and the second is the reactivity ratio of the two co-monomers.

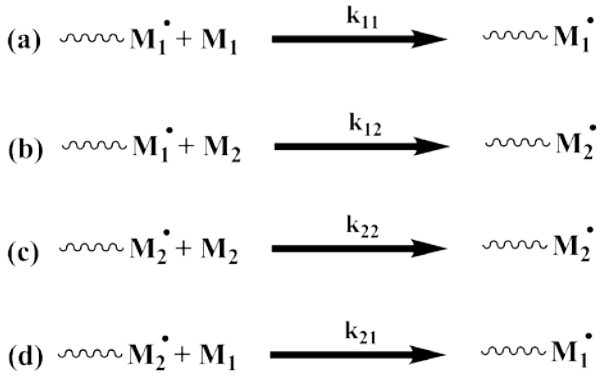

Figure 1-3: Possible propagation steps for the co-copolymerisation of monomers M_1 and M_2. (a, c) represent homo-polymerisation steps whereas (b,d) represent copolymerisation steps.

If two monomers are polymerised radically there are four possible propagation reactions (figure 1-3) each with an associated rate constant (k) which provides a direct measure of how favourable each reaction is. Therefore, the propensity of the monomers to react with either themselves or a co-monomer can be measured by the ratio of the rate constant of each reaction.

$$r_1 = \frac{k_{11}}{k_{12}} \qquad eqn\ (1.1)$$

$$r_2 = \frac{k_{22}}{k_{21}} \qquad eqn\ (1.2)$$

Equations (1.1) and (1.2) are defined as the relative reactivity ratios where r_1 and r_2 are measures of the reactivity of monomers M_1 and M_2 respectively. Therefore, the relative reactivity ratios can be used to predict the final copolymer architecture.

$$r_1 \approx r_2 \approx 1 \quad (1.3)\ Random\ \ copolymer$$

$$r_1 = r_2 = 0 \quad (1.4)\ Alternating\ copolymer$$

$$0 < r_1 r_2 < 1 \quad (1.5)\ \ Statistical\ copolymers$$

$$r_1 = r_2 > 1\ (1.6)\ Blocky\ copolymer$$

$$r_1 = r_2 \gg 1\ (1.7)\ Homopolymerisation$$

The factors which affect the relative reaction rates include: resonance, steric and polar effects both in the monomers and the nascent radicals.[3] It has been observed that alternating copolymers tend to be composed of monomers with opposite polarity, for example stilbene (strongly nucelophilic alkene) and maleic anhydride (strongly electrophilic alkene), neither of these monomers is easily homopolymerised but will copolymerise with each other to form a perfectly alternating copolymer. [3]

This model is limited in that it assumed the reactivity of the active centre is unaffected by the monomer unit which precedes it on the polymer chain. In other words the active centre on the propagating chain is assumed to be the same as an active centre on a single monomer molecule. Hence the model is often referred to as the ultimate model as it takes into account the identity of only the ultimate monomer residue.

It has been observed that many co-polymers, including maleic anhydride co-polymers,[4] have architectures which deviate from that predicted by the ultimate model. Fordyce and co-workers[5,6] first observed this effect in the polymerisation of styrene with fumaronitrile. Propagating chains are rich in fumaronitrile, and whose chain end co-polymer architecture is such that the penultimate residue is fumaronitrile, and the ultimate (active centre) is a styrene residue will show decreased reactivity towards fumaronitrile monomer. This is due to steric and polar repulsions between fumaronitrile monomer and fumaronitile residues within the chain.

The first mathematical treatment of this phenomenon was produced by Merz[7] and co-workers, and has subsequently been further developed by Fukuda and co-workers[8]. This has led to the development of two versions of the penultimate model namely the implicit and explicit forms.

The explicit model defined eight propagation reactions (fig 1-4).

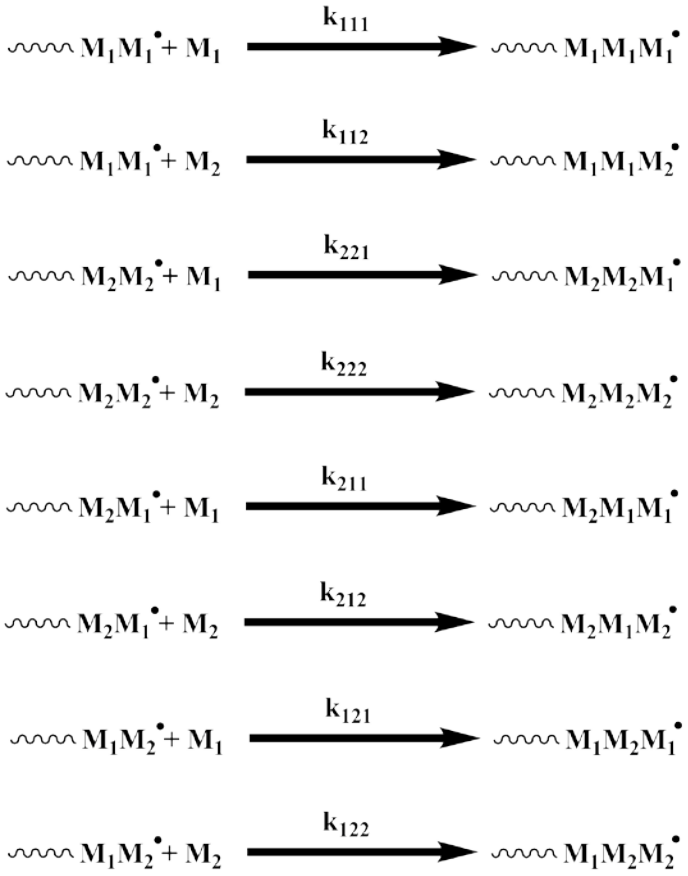

Figure 1-4: Propagation steps considered in the penultimate model

Each monomer is characterised by two reactivity ratios, one in which the propagating species and penultimate terminal monomer are the same and the other where they differ. The latter ratios are denoted by prime notations. In addition two radical reactivity ratios can be defined which are denoted by the letters.

$$r_1 = \frac{k_{111}}{k_{112}} \qquad eqn\ (1.8)$$

$$r_2 = \frac{k_{222}}{k_{221}} \qquad eqn\ (1.9)$$

$$r'_1 = \frac{k_{211}}{k_{212}} \qquad eqn\ (1.10)$$

$$r'_2 = \frac{k_{122}}{k_{121}} \qquad eqn\,(1.11)$$

$$s_1 = \frac{k_{211}}{k_{111}} \qquad eqn\,(1.12)$$

$$s_2 = \frac{k_{122}}{k_{222}} \qquad eqn\,(1.13)$$

The monomer and radical reactivity ratios are used to calculate the adjusted parameters $\bar{r}_1, \bar{r}_2, \bar{k}_{11}, \bar{k}_{22}$

$$\bar{r}_1 = r'_1 \frac{(f_1 r_1 + f_2)}{(f_1 r'_1 + f_2)} \quad eqn\,(1.14)$$

$$\bar{r}_2 = r'_2 \frac{(f_2 r_2 + f_1)}{(f_2 r'_2 + f_1)} \quad eqn\,(1.15)$$

$$\bar{k}_{11} = k_{111} \frac{(f_1 r_1 + f_2)}{\left(f_1 r_1 + {f_2}/{s_1}\right)} \quad eqn\,(1.16)$$

$$\bar{k}_{22} = k_{222} \frac{(f_2 r_2 + f_1)}{\left(f_2 r_2 + {f_1}/{s_2}\right)} \quad eqn\,(1.17)$$

These corrected values are used in place of r_1, r_2, k_{11}, k_{22}, in the ultimate model.

The implicit penultimate model was proposed for copolymers where the terminal model successfully describes the copolymer composition and the monomer sequence, but not the propagation rate or rate constant.

1.2 Physical properties of polymers

1.2.1 Molecular weight

The nature of most polymerisation reactions means that the final polymeric material is composed of macromolecules which, while chemically identical, are of different molecular weights. This presents a challenge as to how best to quantify the molecular weight of the material and it necessitates molecular weight to be expressed in terms of statistical averages and distributions.

There are four well established means of describing molecular weight: number average (M_n), weight average (M_w), viscosity average (M_v) and the z average (M_z). Typically, $M_n<M_v<M_w<M_z$ with M_n and M_w being the most widely quoted.

$$M_n = \frac{\sum N_i M_i}{\sum N_i} \qquad \textit{eqn} (1.18)$$

$$M_w = \frac{\sum N_i M_i^2}{\sum N_i^2 M_i} \qquad \textit{eqn} (1.19)$$

$$M_z = \frac{\sum N_i M_i^3}{\sum N_i M_i^2} \qquad \textit{eqn} (1.20)$$

$$M_v = \left(\frac{\sum N_i M_i^{1+a}}{\sum N_i M_i}\right)^{\frac{1}{a}} \qquad \textit{eqn} (1.21)$$

Where M_i is the molecular weight of chain i, N_i is the number of polymer chains of mass M_i and *a* is the Mark Houwink parameter (a measure of the polymer's conformation in solution.)

The number average molecular weight (M_n) is the unweighted mean molecular weight. In physical terms this average is important for colligative effects where the number of molecules, rather than their size or identity, is the important factor. The weight average molecular weight (M_w) is the average molecular weight of the sample weighted in favour of the higher molecular weight chains. This measure accounts for the fact that higher molecular weight chains contribute more to the total molecular weight of the sample than the lower molecular weight chains. In physical terms weight average molecular weight is important to any physical property which is dependent on the square of the molecular weight. An example would include light scattering; indeed, this is the useful way of measuring M_w.

The viscosity (M_v) and z average molecular weight (M_z) are less commonly quoted. The viscosity average molecular weight depends upon the solvent-polymer interactions, reflected in the Mark Houwink parameter (equation 1.21), and is actually a measure of the polymer's hydrodynamic volume in a particular solvent. The z average molecular weight results from centrifugation of a polymer at low speed which, over time, results in a molecular weight gradient in the centrifuged solution.

Measuring the spread of data, that is to say how wide the distribution is about the mean, is usually measured by taking the ratio of M_w against M_n to give a value known

as the polydispersity index (PDI). The further from unity the ratio the larger the spread of molecular weight in the sample.

While a variety of techniques is available to determine the various molecular weight average, the most common is gel permeation chromatography (GPC), the principle of which involves the permeation of a dissolved polymer sample through a cross-linked gel containing various pore sizes. Separation of molecular weights is achieved by the greater access of low molecular weight chains into the pores of the gel as compared to the higher molecular weight chains. Therefore lower molecular weight polymers have a longer path length through the gel as compared with higher molecular weight chains and, as a result, the large chains will elute first.

Data obtained from GPC can be analysed in three principle ways: conventional calibration, universal calibration, and light scattering. Conventional calibration involves using narrow molecular weight polymer standards to calibrate the column. That is to say the elution times of the standards are recorded for the column and then used as reference values. However, this requires the false conflation of molecular weight with hydrodynamic volume which is not necessarily the case.

The second technique, universal calibration, is intended to overcome the problems of conflating the hydrodynamic volume and molecular weight. This is achieved by producing a calibration curve of elution time against $[\eta]M$ where: $[\eta]$ is the intrinsic viscosity of the polymer eluent, and M is the molecular weight. For the majority of polymers the elution time directly relates to $[\eta]M$ and therefore the chemical identity of the standards is unimportant. The assumption is that the product $[\eta]M$ scales with

hydrodynamic volume, and that the migration of the polymer in and out of the gel's pores is influenced only by hydrodynamic volume.

The third technique is light scattering in which the scatter intensity of the sample is related back to the molecular weight of the polymer.

$$\frac{K_c}{\Delta R} = \frac{1}{M_w} + 2A_2c \qquad eqn.(1.22)$$

Equation 1.22 outlines how scattering relates to molecular weight, where K_c is the optical constant, ΔR is the excess Rayleigh ratio (the additional scattering resulting from a polymer chain's presence), M_w(weight average molecular weight), A_2 (second virial coefficient) and c (concentration g dm^{-3}). Light scattering is often referred to as an absolute measure of molecular weight, however, this is only true when measurements are taken at an angle $\theta = 0^o$ to the incident light, which is a technical impossibility. Therefore, measurements are either taken at low angles where $\theta \approx 0^o$ or else the measurement is taken at non-zero angles and a model applied to account for the additional (excess) scattering events occurring from different parts of an individual chain. This requires assumptions to be made of the polymer's solution conformation, which must be considered when interpreting results.

1.2.2 Thermal properties

Polymers can be broadly characterised into those which are amorphous and those which are crystalline. Crystalline polymers, which are in fact usually only semi-crystalline, display a characteristic, melt temperature (T_m). The process of melting is a

thermodynamic transition although the T_m is often broad due to imperfections in the polymer's crystalline structure.

Amorphous polymer solids are visualised as being frozen polymer liquids. In fact, neutron scattering studies and Flory Huggins theory suggest that purely amorphous polymers adopt their unperturbed dimensions.[3,9] As a result of this lack of crystallinity there is no melt transition in the normal thermodynamic sense. Instead, as an amorphous polymer is cooled, the melt becomes increasingly viscous then rubbery and finally, at the characteristic glass transition temperature (T_g), the polymer becomes a glassy solid and kinetically frozen. Therefore, T_g is a kinetic, rather than thermodynamic phenomenon, and the transition seen by differential scanning calorimetry (DSC) is a result of the greater conformational freedom of polymer chains at temperatures above the T_g, thus raising the specific heat capacity of the material. As a result, the transitions are relatively weak as compared to thermodynamic melt transitions.

There are several factors which effect the T_g including molecular symmetry, structural rigidity and secondary attractive forces. High inter-chain attractive forces decrease the mobility of polymer chains leading to a high glass transition temperature. Increased rigidity in the backbone also increases the glass transition temperatures as the chain mobility in necessarily lower than in less rigid polymers. Finally, highly symmetric polymers will tend to pack more efficiently thereby increasing the glass transition as mobility is reduced.

As a consequence of this the addition of side groups onto a polymer backbone can have unpredictable results. The presence of bulky or numerous side groups will increase chain rigidity thereby increasing the glass transition. However, if the side groups are capable of inducing inter-chain attractive forces the glass transition temperature can again be expected to increase. However, if the side groups are less numerous the resulting drop in symmetry may well decrease the glass transition temperature.

An example of this unpredictability is demonstrated by a comparison of polypropene, poly(vinyl chloride), poly(vinyl fluoride) with polyisobutylene, poly(vinylidene chloride, and poly(vinylidene fluoride) respectively shows that the 1,1-disubstituted ethylene have lower glass transitions than mono-substituted ethylenes. This is somewhat surprising as the 1,1 disubstituted ethylenes are of greater polarity and symmetry, but nevertheless in this instance the presence of two side groups appears to result in the greater separation of polymer chains.[3]

Finally, molecular weight also influences the glass transition, with it increasing with molecular weight. However, this trend rapidly plateaus and in most instances this effect is not relevant.

1.3 Alternating co-polymers of maleic anhydride literature review

1.3.1 Introduction

Maleic anhydride is well known in the literature as being a monomer incapable of homopolymerisation.[4,10] Although it is actually possible to synthesise oligomers of maleic anhydride[11,12] and polymers proper can be produced by plasma, the vast

majority of MA polymerisation involves its co-polymeristion with a less electropositive monomer. Suitable co-monomers include among others: styrene, divinylbenzene, heptene, octadecene, methyl vinyl ether, ethylene, propylene, octadecene, trananthenole[13-15] In contrast conjugated dienes have been shown to yield alternating or near alternating copolymers.[3,16] By contrast non-conjugated dienes have been shown by Butler[17], to form the 1:1 Diels-Alder product as opposed to copolymerising.

Another MA polymerisation of note is that of graft polymerisation, wherein MA is reacted with the backbone of a polymer chain either by generating the radical on the MA or on the polymer backbone. [18-20] The grafting reaction is brought about by abstraction of polymer backbone protons with an alkoxy radical. The nascent carbon centred radical is then able to react with the vinyl group of maleic anhydride via a conventional radical addition reaction. However, competing pathways exist including β-scission of the polymer chain leading to its fragmentation into two chains, one with a chain end saturated α-olefin and the other with a chain end macro radical.[21] This grafting process is dependent on a number of factors, not least the identity of the starting polymer.

The following review deals with the polymerisation, mechanism and reactivity of maleic anhydride co-polymers.

1.3.2 Mechanism of polymerisation

The co-polymerisation of maleic anhydride (MA) has attracted interest due to the fact that such co-polymers include virtually no MA-MA diads within the polymer chain.[22]

There is also a general acceptance that the polymers have a tendency to be alternating. The mechanistic reasons behind these phenomena are a subject of debate within the literature,[4] with two models proposed.

The first is that alternation depends on the co-monomer to MA being sufficiently electron rich to cause the formation of a charge transfer complex between it and the electron poor MA monomer. It has been suggested that monomers which appear to form charge transfer complexes co-polymerise by what is known as the complex addition mechanism.[23-25] It has been demonstrated that such complexes form[26] and the model proposes that as the polymer propagates the monomer added brings with it a co-monomer as part of a charge transfer complex. That is not to say the addition of both monomers in the charge transfer complex occurs in one step, rather the second co-monomer in the charge transfer complex is readily available for the next propagation step.

However, the charge transfer complex model has somewhat fallen out of favour with the parallel development of the participation model.[4] The reason for this is partly that the participation model uses the widely known, and understood, penultimate model of polymerisation which states that co-polymer architecture is determined by the relative reaction rates of every possible propagation step. This, in turn, is determined by both the identity of the co-monomer residue at the active site and that of the preceding co-monomer residue. In addition, there is no convincing evidence of a correlation between the charge transfer complex concentration, with MA co-polymerisations typically following fast kinetics despite the charge transfer complex concentration being low.[27] Finally, the life time of charge transfer complexes is typically two or

three magnitudes faster than the rate constant of propagation.[28] All of which suggests that charge transfer complexes cannot, alone, account for the either the kinetics or the final co-polymer architecture.

Fitting the penultimate model to MA polymerisation does, however, require the model to be restricted in order for good correlation with the empirical data to be achieved. In the case of styrene – MA co-polymerisation the concentration of any triad which requires the presence of MA-MA diads must be set to zero.[4,29] This is a reasonable assumption given the difficulties in achieving MA homo-polymerisation and the absence of examples of this being achieved in the presence of a co-monomer. However, this means that the penultimate model, while being predictive of MA co-polymerisation behaviour, does not provide a rationalisation of it.

Kinetic studies on the co-polymerisation of MA with acrylamide, ethyl acrylate[30], various pentene derivatives,[31] and isobutene[32] demonstrates that the copolymerisation rate is dependent both on the co-monomers electron density at the olefinic group, and steric hindrance during MA's addition to the radical chain end. The importance of sterics in the co-polymerisation of MA is evident in the structural work of Komber *et al*[33,34]who demonstrated, in the case of poly(ethylene-alt-maleic anhydride) and poly(iso-butene-alt-maleic anhydride), that the less sterically hindered threo triad forms preferentially over the more sterically hindered erythro diad. The importance of sterics is presumably due to the conformational restriction the anhydride ring places on MA.

Rationalising this requires consideration to be given the molecular orbitals of the propagating MA radical. The unpaired electron of the propagating MA possesses a low energy SOMO, due to its adjacency to the partially occupied p-orbitals. This has the effect of creating an electrophilic radical and so the HOMO of the incoming monomer is decisive. In the case of MA system it is always the olefin co-monomer that reacts. By contrast the olefin monomer has a high energy SOMO which facilitates its reaction with the low energy LUMO of MA.

1.3.3 Ultra-violet initiation

MA co-polymers have been obtained by a variety of initiation techniques including: thermal[13,35-38], UV[39, 27,32,40]and radiation.[41] Of particular interest is UV polymerisation, Arnold *et al*[27,31,32,40] have demonstrated that charge transfer complexes form between the MA and co-monomer, or the MA and solvent. These charge transfer complexes can be excited by exposure to UV radiation which then may go on to initiate polymerisation.

This is supported by Ratzsch and Schicht's work on the UV initiation of styrene MA systems in which they determined the presence of a styrene cation.[42] In addition, they report a significant acceleration in the rate of initiation occurs when solvents capable of forming charge transfer complexes with MA are chosen.[10] In particular MA -THF charge transfer complexes have been shown to be elevated to an excited singlet state on UV irradiation. This excited state may then either relax back to the ground state or undergo a non-radiative transfer to a triplet state. Both the singlet and triplet state may dissociate into a radical and ion[43] which, stabilised by the solvent, may then either go onto initiate polymerisation or recombine (figure 1-5)

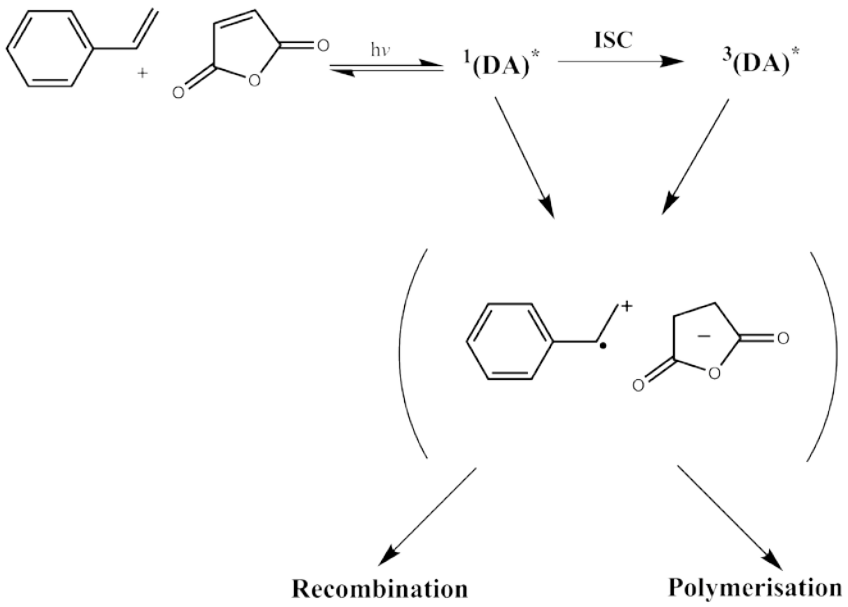

Figure 1-5: Proposed mechanism for the initiation of styrene MA copolymerisation via the excitation and degradation of a charge transfer complex under UV radiation where DA is a donor acceptor pair.

As a MA copolymerisation by UV is heavily dependent on both the co-monomer and solvent choice the results of such a radical initiation can be unpredictable. However, it does offer a viable alternative to the addition of conventional initiators such as benzoyl peroxide or AIBN.

1.3.4 Controlled polymerisation

Controlled radical polymerisation techniques have been successfully applied to styrene MA copolymer systems with examples of nitroxide mediated polymerisation (NMP), and reversible addition fragmentation chain transfer (RAFT) being present in the literature.[29,35,36,38,44-48] Atom transfer radical polymerisation has been attempted but appears to be incompatible with the chemistry of the anhydride[49].

The use of controlled radical polymerisation has allowed for the production of block co-polymers. An interesting example of the chemistry this makes available is presented by Wooley *et al*[50] who reported the polymerisation of poly(styrene-alt-maleic anhydride)-b-(styrene), and its self assembly, in a one pot reaction. This was achieved by co-polymerising MA in the presence of excess styrene using a RAFT agent. The polymerisation proceeds in the following manner, first the alternating styrene MA block is formed until MA is consumed, once consumed the polymerisation continues as a homo-polymerisation of a styrene block. Water can then be added to hydrolyse the anhydride moiety which, on further addition of water, allows the self assembly of the polymer chains into micelles. The same co-polymerisation behaviour has been observed for NMP systems[18,51]

This phenomena of copolymerisation followed by homo-polymerisation in a one pot reaction is in stark contrast to conventional radical polymerisations the result of which would be a mixture of copolymer and styrene homo-polymer. Studies on the kinetics of these reactions have demonstrated that lower temperatures are beneficial to the production of block copolymers as opposed to a mixture of copolymer and block copolymer.[52] A similar phenomena has also been observed by early research in to the free radical co-polymerisation of MA where high temperatures where shown to increase the instance of the other co-monomer's homo-polymerisation as either diads or oligomers.[10,30] However, to date no rationalisation of this observation has been made.

Kinetic studies on controlled radical polymerisation also show that certain RAFT polymerisations are initiated much more quickly in the presence of MA. For example

cumyl dithiobenzoate takes 240min to fully initiate in the presence of styrene alone, whereas initiation takes only 5min in the presence of a catalytic amount of MA and styrene under similar conditions. The cumyl radical was shown to add exclusively to MA, and this was rationalised as being due to the electron rich nature of the cumyl radical. By contrast cyanopropyl dithiobenzoate initiates at a similar rate regardless of the presence of MA in the styrene polymerisation, in this instance the cyanopropyl initiator was found to add exclusively to the styrene.[29,53,54]

1.3.5 Structure of maleic anhydride copolymers

As has already been discussed the structure of copolymers of MA, synthesised by radical polymerisation, are typically alternating or close to alternating copolymers with MA MA diads being non-existent within the polymer chain. The fine structure of these polymers has been the subject of several groups' research and an understanding of the polymer micro-structure has incrementally improved with the development of spectroscopic techniques.[33,34,55-58]

Gaylord's research on the structure of MA piperylene copolymers using ^{13}C NMR demonstrated that no difference in the final copolymer composition occurred when using either cis or trans piperylene. However the stereochemistry about the MA carbons remained unexamined. The production of low molecular weight model compounds of 2,3-diethyl succinic anhydride and the corresponding erythro and threo forms of the anhydride have subsequently been used in the interpretation of maleic anhydride copolymers.[55,59] The results indicate that at 60^{o}C ethylene MA copolymers exist in an erythro to threo configuration in a ratio of 12 to 88% respectively. The threo form, being the less sterically hindered, forming preferentially even with

relatively unhindered monomers like ethylene. This configuration has also been shown to persist after hydrolysis of the anhydride.[55]

Komber and co-workers have since confirmed these observations in the polymers proper, as opposed to model compounds, by the direct NMR measurement of a variety of MA copolymers.[60,61] Their work demonstrates that, when the co-monomer is relatively unhindered, a minority of MA residues will be in the more sterically hindered erthyro isomer. However, the addition of bulkier co-monomers results in all the MA residues existing in the threo form. For example poly(ethylene-alt-maleic anhydride) is approximately 12 to 17% erythro, and poly(propylene-alt-maleic anhydride) is 20 to 33% erythro, whereas poly(isobutene-alt-maleic anhydride) contains no erthyro isomers.[60-63]

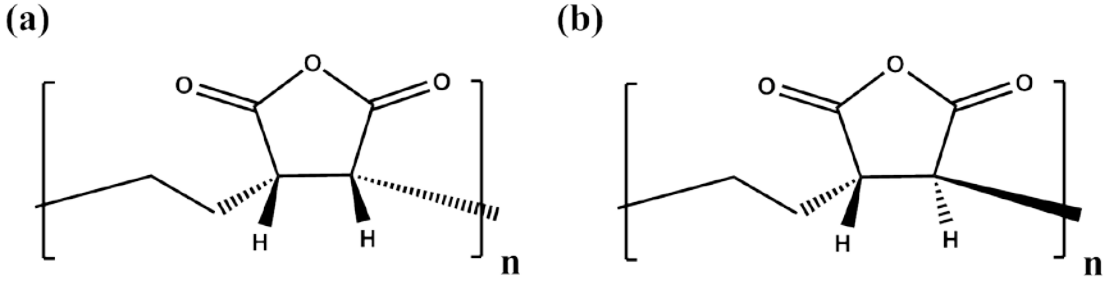

Figure 1-6: Threo and erythro form of the poly(ethylene-alt-maleic anhydride)

The importance of the MA isomerism becomes clear from the work of Ratzsch, who observed that the erythro anhydride is more reactive towards nucleophiles than the threo form due to the increased steric stain on the erythro ring. [64] Once ring opened the erythro form becomes less reactive towards nucleophiles and ring closure. In addition the erthyro diacid displays different pKa values to the threo form.[60,61,65]

Komber, using the known chemistry of small molecule succinic acid derivatives as a lead, was able to demonstrate that it is possible to isomerise the threo and erythro forms of the polymer by heating salts of the diacid (hydrolysed) form of the polymer.[57] The resulting increase in erthyro composition is of interest as subsequent closure of the diacid to anhydride results in a polymer with increased reactivity towards nucleophiles and different solution properties (principally pKa) as a polyelectrolyte. In addition some control over the isomers formed can be achieved by polymerising half esters of maleic anhydride.[61]

1.3.6 Reactivity

The anhydride functional group of the polymer had been shown to react readily with any moderate to strong nucleophile. The most common examples of reaction include: amidation,[66-69] esterification,[70-72] thioesterification,[73] hydrolysis,[33] dehydration and imidization (figure 1-7).[74]

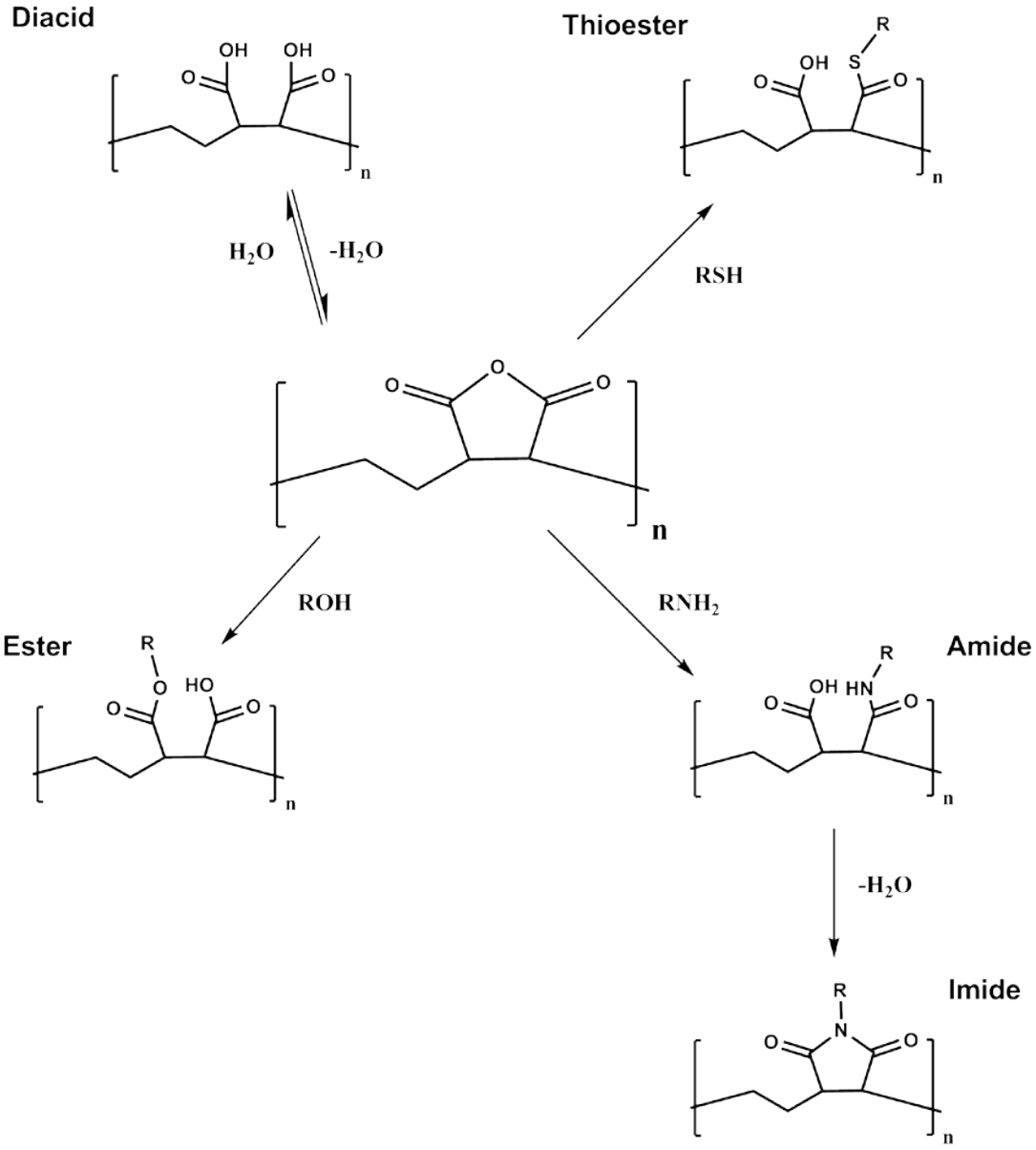

Figure 1-7: Common reactions of poly(ethylene-alt-maleic anhydride)

1.3.7 Amidation

Work by Ratzsch and Phien on the amidation of MA copolymers with aromatic amines demonstrates that at equimolar concentration of amine to anhydride the kinetics follow a second order rate equation. They also observed that, at least in the case of poly(ethylene-alt-maleic anhydride), the kinetics do not deviate from that of small molecule cyclic anhydrides. However, rate acceleration beyond 60% conversion

of anhydride to half amide was observed, and this was attributed to autocatalysis brought about by the nascent carboxylic acid groups. The results demonstrate a clear dependence of the rate of amidation with both the steric bulk and the basicity of the amine.[75]

Similarly there was a clear correlation between the rate constant and the steric hindrance resulting from the co-monomer of MA. The rate constant followed the order of norbornene < styrene < cyclopentane < propene < ethane. In other words the reaction rates increase with decreased steric bulk about the MA functional group.[10] This trend has also be confirmed for the hydrolysis of the MA co-monomer.[75]

The addition of either base or acid is generally understood to catalyse the reaction of amines with carbonyls. However, attempts to quantify the increase in the amidation rate of MA copolymers in the presence of glacial acetic acid have failed. Although, the kinetic plots may be sufficiently similar to small molecule model compounds to allow some qualitative predictions to be made regarding reaction rates.[10] In the case of base catalysis there are even some instances of retardation, for example Hue and Ratzsch[76] report a significant decrease in the amide yield on the addition of organic bases. However, in the case of trialkylamine catalysts there exists at least one example of rate acceleration between MA copolymers and amines.[77]

Ratzsch and co-workers,[10] has also examined the influence of solvents on amidation, with reaction rates typically decreasing with increasing solvent dielectric constants. However, these considerations were further complicated by the conformation the polymer is placed in by the solvent. Indeed, the addition of a small amount of DMF to

a reaction of poly(styrene-alt-maleic anhydride) with aniline in THF results in a drastic decrease in the reaction rate. This is attributed to a change in the solution conformation of the structure bringing about a decrease in reaction rate.

The yield of amide in the reaction of poly(propylene-alt-maleic anhydride) with a variety of amines in DMF has also been extensively studies by Ratzsch and co-workers. [76] It was observed that conversion was near 100% for all primary aliphatic amines but decreasing markedly for secondary amines with diethylamine attaining only 60% conversion.[76] Examination of the degree of conversion with increasing co-monomer sterics demonstrated an inverse relationship.

Away from model systems Donati *et al*[67] have demonstrated that poly(styrene-alt-maleic anhydride) is able to react with amino-galactose, glucose and lactose derivatives to yield 56, 54 and 94% of the half amide respectively in THF. The kinetics of each of these reactions were followed by colourmetric assay of the free amine, the results suggested that the reaction came to a halt after 3 hours. However, Uzawa et al[78] have demonstrated that an acetylated galactopyranosyl amine derivative reacts with poly(ethylene-alt-maleic anhydride) to approximately 96% conversion within 5 minutes in DMSO. The latter observation may be attributable to the decreased steric hindrance about the MA co-monomer in poly(ethylene-alt-maleic anhydride). However, more difficult to explain is the higher limiting conversion of the amino- lactose derivative compared with amino-galactose and glucose derivatives. Lactose, being a disaccharide, would intuitively be expected to have a lower limit of conversion due to its steric bulk, however, this is not the case, and serves to

demonstrate the complex relationship between competing factors involved in the amidation of MA copolymers.

1.3.8 Esterification

The esterification of MA co-polymers is well documented in the literature.[70,71,79,80] Early results by Ratzsch and co-workers[81] demonstrated that the rate of esterification, after an initial drop from methanol to ethanol increases and then plateaus with the alcohol's C number. The general observations made by Ratzsch and co-workers on esterification rates are closely analogous to those of amidation, with factors such as the steric bulk about the hydroxyl and MA playing a role in determining rate constants.[27,32,64,81,82]

However, there are a number of limiting factors to the successful esterification of MA copolymers. Firstly, alcohols often precipitate the polymer at relatively low concentrations, the formed esters are often not soluble in the same solvents as the MA polymer, therefore it is often the case that the esterification occurs on a surface, in a gel or simply as a heterogeneous reaction.[79]

Recognising these difficulties Badyal et al.[**83**] conducted an examination of the gas phase reaction of poly(ethylene-alt-maleic anhydride) surfaces with the following alcohols: 2,2,2 trifluoroethanol, 4,4,4-trifluorobutanol, and ethanol (figure 1-8).

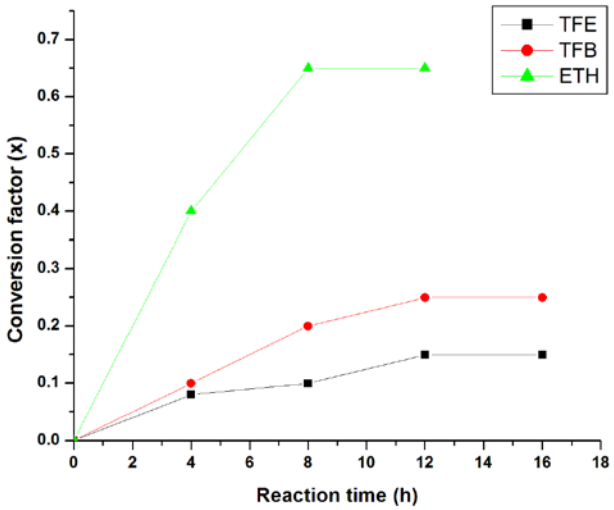

Figure 1-8: Conversion of surface maleic anhydride groups of a thin film of poly(ethylene-alt-maleic anhydride) to mono-esters of trifluoroethanol (TFE), trifluorobutanol (TFB) and ethanol (ETH) at room temperature. Determined by XPS analysis. Reprinted from Badyal et al. [83]

While Badyal et al.'s work demonstrates the potential for the reaction of maleic anhydride copolymers with alcohols it must be remembered that these reactions are surface modifications and carried out at room temperature. Therefore, it is probable the reaction could be pushed to higher conversion in homogenous conditions, at elevated temperature or in the presence of catalysts.

1.3.9 Hydrolysis

The hydrolysis of MA copolymers is arguably the most important reaction in terms of their application given their widespread use as polyelectrolytes and in surfactant systems.[84,85] The un-catalysed hydrolysis of cyclic anhydrides do not always appear to follow simple reaction kinetics for example Koskikallio has demonstrated an overall

reaction order of 3 for succinic anhydride hydrolysis in water, this presumably being the result of autocatalysis from the nascent maleic acid residues[86]

The catalysis of the hydrolysis of poly(propylene-alt-maleic anhydride) has been studied by Elberson who determined that triethylamine does indeed catalyse the hydrolysis of the MA component with a seven fold increase in the reaction rate occurring on the addition of 0.1 mol of triethylamine to a hydrolysis reaction (10mol water, 1 mol of anhydride). Interestingly, no evidence of acid catalysis of hydrolysis was found, possibly due to the existent electron deficiency of the anhydride ring.

1.3.10 Imidization

Imidation is another reaction which has received some attention in both the patent literature and academic literature, particularly in reference to films.[74] The work of Lee *et al*.[87] on imide-functionalised solid supports approached the problem of ring closing the mono-amidic maleic anhydride groups by increasing the electrophilicity of the carboxylic acid adjacent to the amine (figure 1-9).

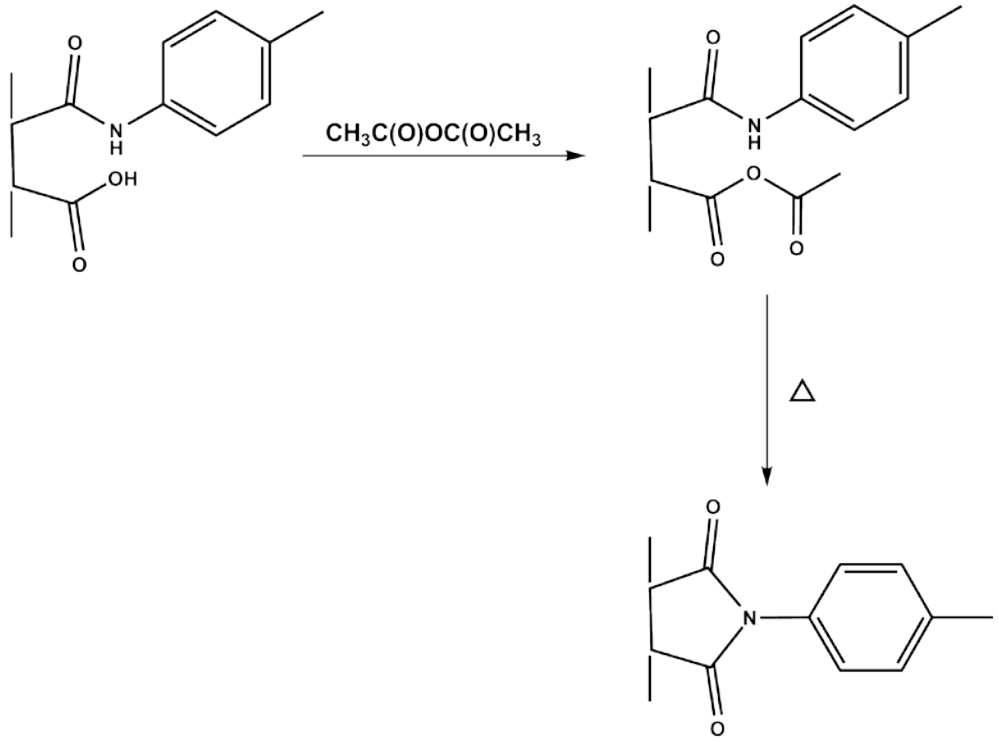

Figure 1-9: Reaction scheme for conversion of styrene – MA to amide to imide as outlined by Lee *et al.*[88]

Optimal conditions led to a conversion to imide of 95% but more typically conversions were less than 60%. Driving this system to completion required the use of strongly dehydrating conditions, including the use of acetic anhydride, sodium acetate and triethylamine which were subsequently found to be hard to remove. The result was that reliable conversion of amide to imide proved difficult to achieve.

1.3.11 Solution properties

Most current applications for these polymers utilise the polymer in this form.[89-98] The aqueous solution behaviour of these polyelectrolytes is complex and behaviour is often thought to be analogous to biological polymers.[89] An understanding of the hydrolysed forms behaviour is fundamental to understanding many current applications of the polymer.

It is understood that succinic acid has two distinct pKa values at 4.19 and 5.27. Therefore, it is not surprising to state that polymers containing the diacids should display at least two pKa values[99,100]. Bianchi[99] compared the titration curves of MA with different co-monomers: ethylene, propylene, isobutylene, 2-methylpentene and styrene. All polymers were titrated from the carboxylate to the acid; it is noticeable that the first protonation is distinct with a less distinct second protonation in all cases, with the exception of the ethylene copolymer in which there is significant overlap between the two curves. It is also worth noting that as the length of the alkyl side chain increases the pK_1 (most acidic proton) decreases whereas the pK_2 (least acidic proton) increases.

This was rationalised by assuming the presence of a neighbouring dipole moment, i.e. the second acid in the maleic acid pair, favours the de-protonation of the first acid group, as the nascent carboxylate may be stabilised by the second acid delocalising its proton between the two. On second ionisation the interaction becomes a repulsive ion-ion interaction.

While the explanation based on changes to the local dielectric constant is compelling, no argument is presented as to why increasing alkyl chain length results in this. It seems possible that steric hindrance results in a lack of rotation about the bonds thus forcing a favourable conformation, i.e. eclipsing acid groups, for the first deprotonation while simultaneously maintaining an unfavourable conformation for the second deprotonation. The differences between pK_1 and pK_2 in all cases are shown to be at least a unit larger than the difference associated with succinic acid.[101]

In order to explain the indistinct titration curves of poly(ethylene-alt-maleic acid) Schultz *et al*[100] attempted a model fitting exercise from which they concluded that there is interaction between neighbouring dicarboxylic acid units i.e. across the olefin moiety. Based on the polyelectrolyte models applied it was found that there is a strong tendency, at intermediate ionization $1 \leq \alpha \leq 2$ (pH intermediate between the two pKa values), for the doubly ionized and singly ionized diacid to alternate along the backbone. This is thought to be the result of an extraordinarily large hydration sphere about the doubly charged diacid. However, should the co-monomer present a large steric bulk between the adjacent diacid moieties the hydration sphere is disrupted and so the dependency of one pair of acid's pKas on the ionization state of its neighbouring diacid pair is reduced.

As has previously been mentioned hydrolysed maleic anhydride copolymers find utility as surfactants in the chemical industry. However, work by Garnier *et al*[102] demonstrated by surface tension measurements that poly(styrene-alt-maleic acid) does not behave as an ordinary surfactant. Although poly(styrene-alt-maleic acid) has been demonstrated to exist at the air water interface when added to aqueous solution it has also been observed that aggregates form in solution before the surface is saturated. Compression of the polymer chains at the surface using a Langmuir trough, demonstrated that the polymer chains enter the solution rather than pack further and saturate the surface. The formation of aggregates in solution is confirmed by the work of Kuo *et al*[97] who demonstrated that hydrophobic fluorophores were being encapsulated within the aggregates.

Garnier[102] went onto observe that the equilibrium between the solution and the air water interface varies depending on pH. At pH 12.5 and pH 3 the surface tension reaches equilibrium rapidly. However, at pH 6.5 the surface tension measurements indicate that several hours are required to reach equilibrium. This implies that the solution behaviour is much more complex at intermediate ionization with respect to fully ionized and fully protonated equivalents. However, it was also noted that at pH 6.5 the aggregate concentration was at a maximum. This is unusual as normal self assembly of amphiphiles into aggregates requires that the air water interface be saturated before they form (chapter 3). However, it appears here that the thermodynamic barrier between the air water interface, solution and aggregate is comparatively low. Garnier proposes a mechanism in which the polymer can easily form either an aggregate with another polymer chain or position itself at the interface, the only unstable position is that of a free chain in solution which results in either its relatively rapid return to the surface or aggregate. However, an alternative possibility that the polymer chains enter conformations, or chain collapsing, in such a way as to exclude the styrene moieties from the water, as is discussed by McCormick.[103] As a result the systems behaviour is much more subtle than that of a normal amphiphile. This is discussed in more detail in chapter 3.

Conclusion

Despite being the subject of extensive study both the polymerisation and solution behaviour of MA copolymers remains ill defined. This is problematic as both impact on the reactivity of the polymer. Recent work on the controlled polymerisation of MA co-polymers, combined with a desire for functionalisable polymers, has triggered something of a resurgence of interest in this class of polymers. There remains useful

work to be done especially surrounding the mechanism of polymerisation and solvation studies of the anhydride, di-acid, and derivatives thereof.

1.4 Characterisation

1.4.1 Aims

Vertellus speciality chemicals produce two copolymers of ethylene and maleic anhydride E60 and E400. Both are sold as poly(ethylene-alt-maleic anhydride) with E60 and E400 being low and high molecular weight products respectively. Due to the potential application of this polymer to complex systems: colloid, surface and gels, it was necessary to gain a thorough understanding of the physical and chemical properties of the polymers. Commercially, it is also useful to benchmark the polymer against competitor materials.

In order to address this, a thorough physical and chemical characterisation was carried out in order to provide useful data points for the application of the polymers.

1.5 Results and Discussion

1.5.1 Molecular structure

Q-e model calculation on the maleic anhydride (Q = 0.23, e = 2.25) and ethylene (Q = 0.015, e = -0.20) gave an r_1r_2 value of 0.0025, in other words the electronics of this polymerisation would highly favour an alternating structure. In addition to this, the work of Kombre *et al*[44] has already demonstrated the alternating structure of these polymers. However, there are myriad variables which might result in a deviation from the alternating structure including: complete consumption of the maleic anhydride monomer ahead of termination and inhomogeneous reaction conditions.

Consequently, it is important to establish the polymer, as produced by Vertellus, conforms to Kombre's proposed structure.[44]

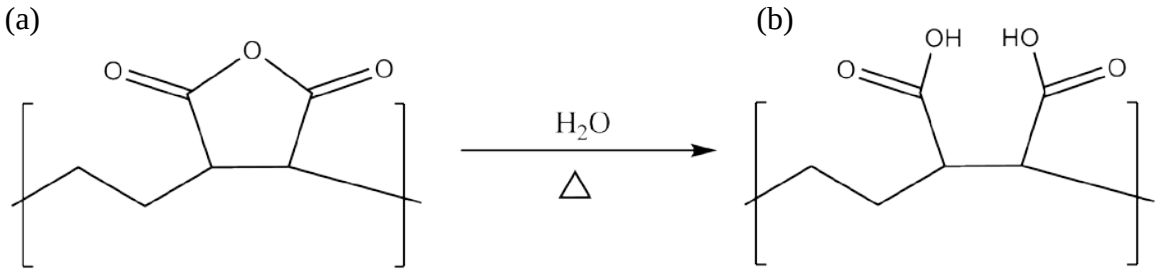

Figure 1-10: Proposed structures of E60 and E400, in their ring-closed and ring-opened forms: (a) poly(ethylene-alt-maleic anhydride) and (b) poly(ethylene-alt-maleic acid) (hE60)

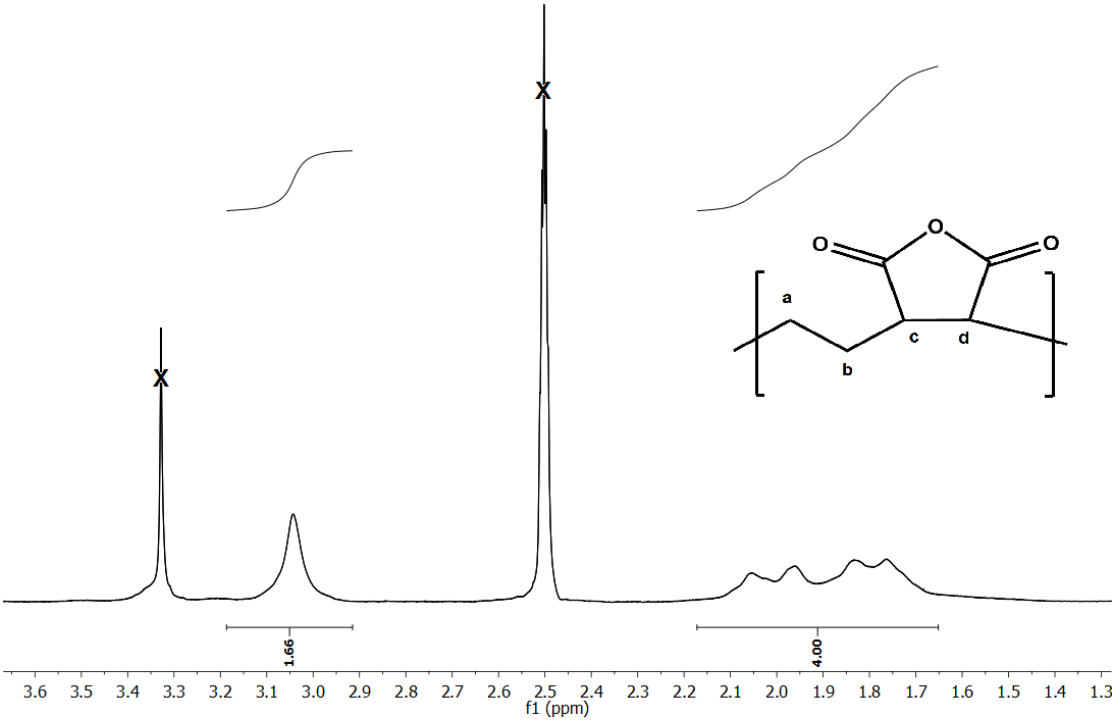

Figure 1-11: (400MHz, d_6-DMSO) ^{1}H NMR spectrum of E60

An examination of the ^{1}H NMR of both E60 and E400 (figure 1-11, table 1-2) demonstrates that maleic anhydride and ethylene monomer residues are present in a ratio close to 1:1 with a slight excess of ethylene units in both cases. The COSY spectrum of both polymers demonstrated coupling between the ethylene and maleic anhydride peaks, suggesting that the polymer is an alternating structure (figure 1-12).

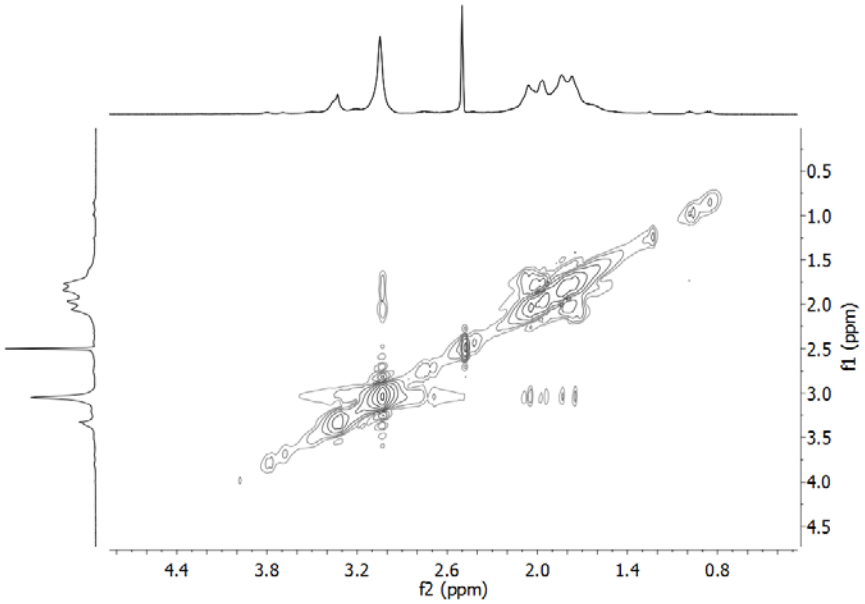

Figure 1-12: (d_6-DMSO, 400MHz) 1H COSY spectra of E60

The peaks between 1.4 and 2.0ppm correspond to the ethylene protons which are all coupled to the maleic anhydride protons at circa 3.0ppm. The peak at 3.3ppm corresponds to erythro maleic anhydride isomers.

Table 1-1 show the integrals of pol(ethylene-alt-maleic anhydride) as both the E60 and E400 derivatives. The theoretical ratio of ^{1}H for an entirely alternating co-polymer would be 1:2 maleic anhydride to ethylene. That is to say maleic anhydride's 2 ^{1}H to ethylene's 4 ^{1}H. By comparing the integrals of both ^{1}H NMR peaks it is possible to determine the relative amount of each co-monomer.

Table 1-1: The integrals of maleic anhydride relative to ethylene peaks in the ^{1}H NMR spectra of E60 and E400.

Polymer	Integral ethylene	Integral maleic anhydride	% Anhydride	Error
E400	4.0	1.9	43%	+/- 5%
E60	4.0	1.7	48%	+/- 3%

The composition was confirmed by determining the mass of potassium hydroxide required to neutralise the acid form of the polymer (figure 1-13). This number is expressed as mgs of KOH per g of polymer and termed the acid number (table 1-2). The values were obtained by the neutralisation of the acidic form of the polymer with potassium hydroxide solution. Once the pH was seen to plateau the end point of titration was taken to have been reached.

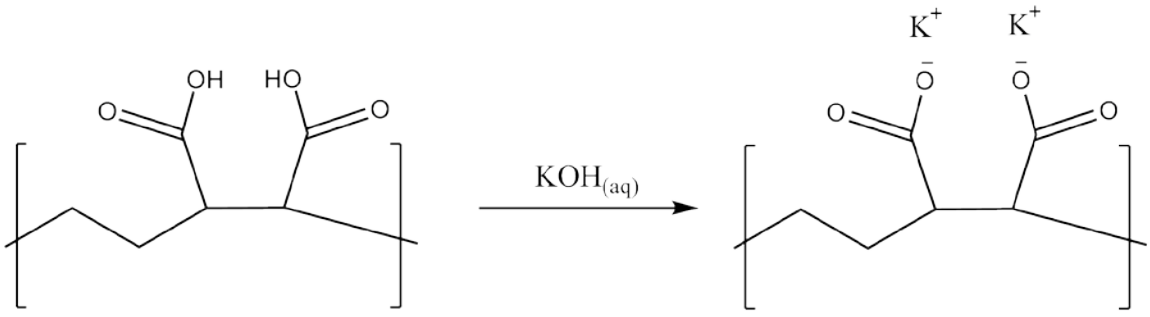

Figure 1-13: Schematic for the determination of poly(ethylene-alt-maleic acid)'s acid number measured in mg of KOH per g of polymer

This technique also allowed for the pKa of the acidic groups to be determined (fig 1-13). To determine the pKas of the protons titration of purified, hydrolyzed batches of E60 and E400 against NaOH(aq) was conducted.

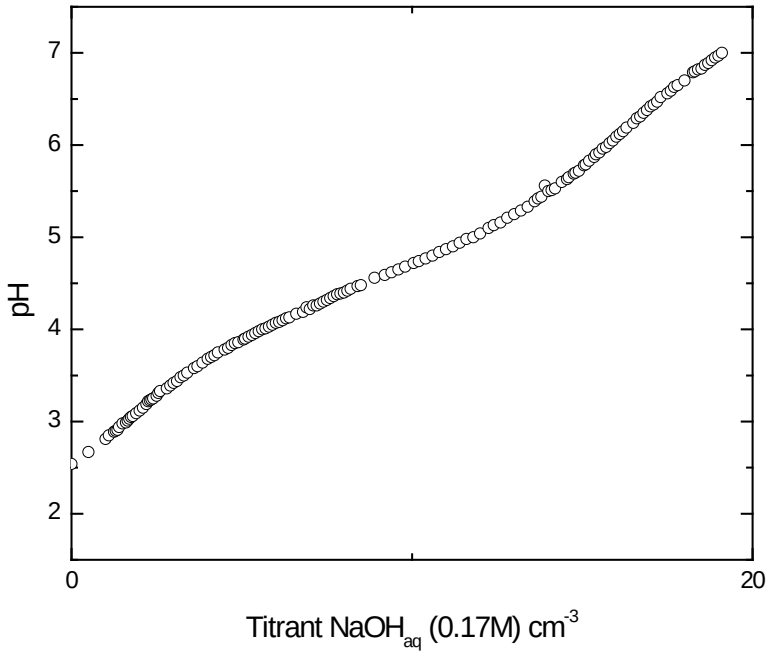

Figure 1-14: Titration curve of hE60. Note the indistinct pKa transitions of both diacid protons as described in the literature.

As can be observed there are no definite pKa transitions, rather the pH changes in two broad curves (figure 1-14). The presence of two curves is attributable to the two acid groups on each repeat unit. After the deprotonation of the first acid group the increased charge inhibits the removal of the second carboxylic proton, this effect is observed in some small molecule di-acids such as succinic acid which has carboxylic protons with pKa values of 4.16 and 5.61.

The broadness of these two pKa curves is an attribute of many acidic polymers when in aqueous solution, the close proximity of the acidic moieties result in the pKa of a `particular acid being affected by the identity of adjacent carboxylic groups. An acid group adjacent to predominantly carboxylate anions will have a higher pKa than one adjacent to carboxylic groups. In addition, there is some evidence that fast proton transfer is able to occur along a partially neutralised polyacid chain thereby further averaging the pKa value.[60,61,101,100]

As can be seen the resolution is poor but average pKa values can be extracted by first derivative plots which indicate pKa values of 3.41 and 6.26. Kombre's detailed NMR analysis of poly(ethylene-co-maleic acid) demonstrated that it has four pKa values (two pairs at; 4.1, 4.2, 6.1 and 6.8) resulting from the erythro and threo configurations.[60,61]

It can be concluded, given that the titrations result in comparable curves to those obtained in the literature that Kombre's values are taken to be applicable to the diacid form of the polymer. The apparent pKa values based on a model fitting treatment of titration data can be taken to be 3.65 and 6.40 and practically these are perhaps more useful.[100]

Table 1-2: The measured acid number of hydrolysed E60 and E400 quoted in KOH mg per g of polymer

Polymer	Average (mg)	Error (mg)	Theoretical (mg)	Diacid content (mole %)
E400	**748**	**+/- 17**	**778**	**48**
E60	**763**	**+/- 11**	**778**	**49**

This confirms the evidence from ^{1}H NMRs spectroscopy that the ethylene to maleic anhydride ratio is approximately 1:1. Evidence that the monomer residues are alternating is also found in the ^{13}C spectrum (figure 1-15). For clarity, the spectrum has been cut between ~ 30 and 145 ppm.

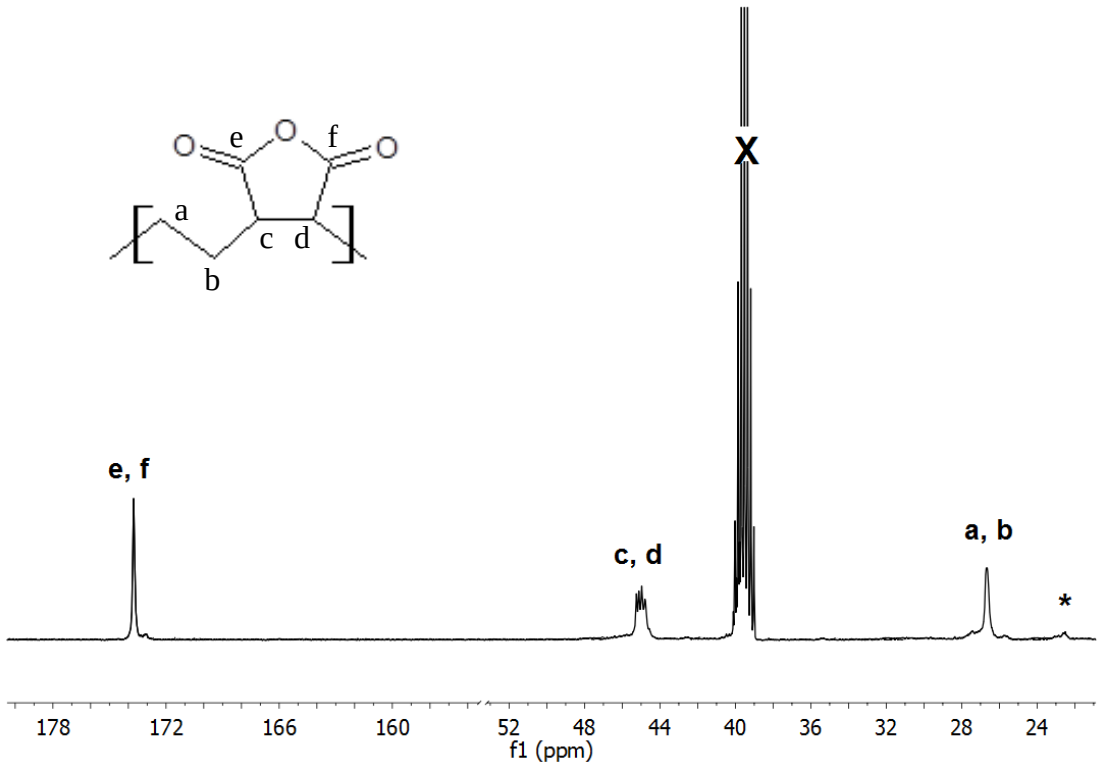

Figure 1-15: (d_6-DMSO, 100mHz) ^{13}C NMR of E60.

Figure 1-15 shows the ^{13}C NMR spectrum of E60 demonstrating the presence of three carbon environments, namely the ethylene backbone, maleic anhydride backbone and carbonyl carbons at 27.5, 43.1 and 174ppm respectively. The small peak at circa 23ppm, indicated by an asterisk, suggests the presence of a small amount of ethylene-ethylene environments which is supported by the slight excess of ethylene in the proton NMR and acid number. In addition the shoulder on the carbonyl C peak has been attributed by others to the erythro isomer of maleic anhydride.[61]

In summary, the evidence overwhelmingly suggests a polymer structure that is almost entirely alternating with an approximate relative ethylene to maleic anhydride composition of 1:1, which is consistent with that reported by Kombre *et al.* [44]

1.5.2 Molecular weight

Determining the molecular mass of both E60 and E400 proved more difficult than expected. Early attempts to analyse the polymer using DMF GPC were unsuccessful with either no detectable polymer eluting from the column or very broad, weak signals in all detectors (RI, viscometer, and RALS). It was subsequently found that the poly(ethylene-alt-maleic acid) forms of both E60 and E400 would not pass through the DMF GPC columns, leading to speculation that trace water in the DMF, combined with the low polymer concentrations and elevated temperature, resulted in the hydrolysis of the maleic anhydride form of the polymer as it passed through the column. While there are examples of the addition of 5% acetic acid to aqueous GPC eluents for the elution of poly acids the use of acidic aqueous solvents did not result in the polymers elution from the column.

In order to address this, three experiments were conducted: the first was to pass the polymer through the column using freshly prepared, and therefore drier, eluent, the second to analyse the molecular mass of the hydrolysed polymer by aqueous GPC and the third to modify the polymer to a form less susceptible to hydrolysis but still soluble in DMF. The structures of these polymers are shown in figure 1-16.

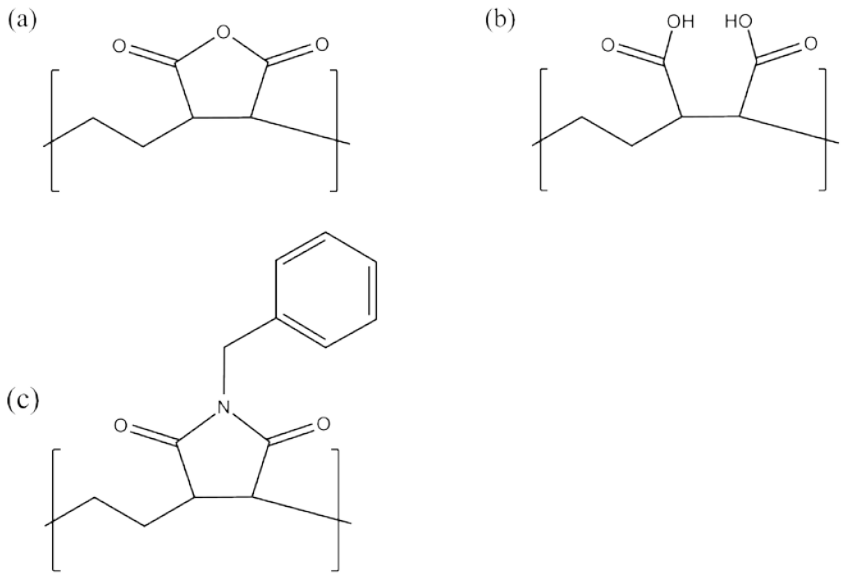

Figure 1-16: Polymers for GPC measurements: (a) anhydride, (b) di-acid, and (c) benzylimide forms of E60 and E400

The anhydride and benzylimide forms of E60 and E400 (figure 1-16 (a) and (c) respectively) were characterised with DMF GPC whereas the acid form of E60 and E400 (figure 1-16 (b)) were characterised by aqueous GPC at pH 9. The DMF GPC was calibrated against a poly(styrene) standard and the data obtained from the light

scattering detector. The aqueous GPC was calibrated against poly(ethylene oxide) standards and the data obtained from the light scattering detector.

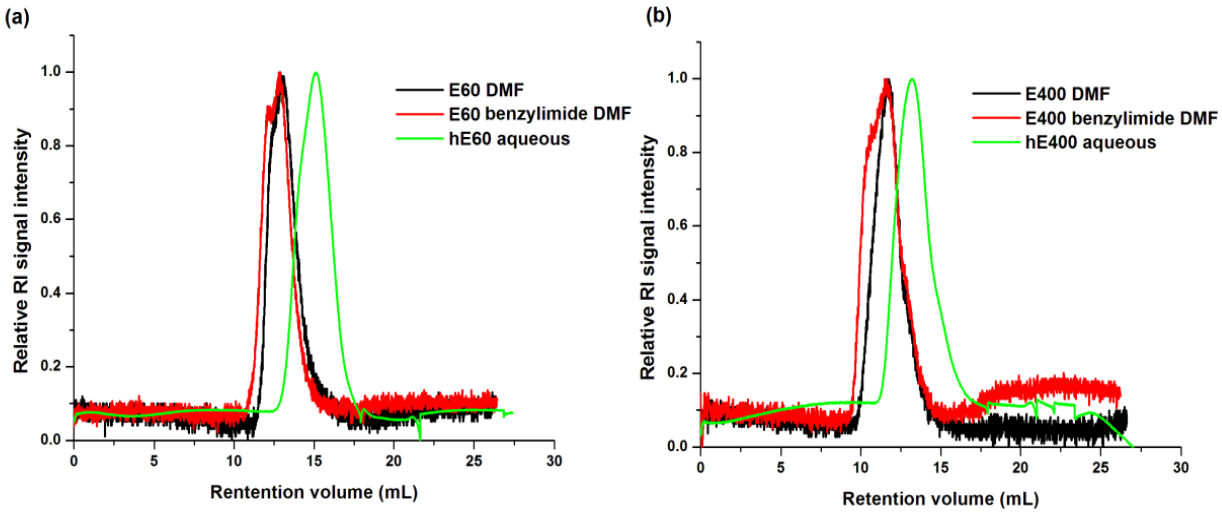

Figure 1-17: GPC traces of (a) E60 derivatives and (b) E400 derivatives.

Table 1-3: GPC results of poly(ethylene-alt-maleic anhydride) and its derivatives.

Polymer	M_n (Da)	M_w (Da)	PDI	dn/dc	Calculated M_n (Da)†
E60	**40,500**	**71,000**	**1.8**	**0.09**	**N/A**
E400	**214,000**	**610,000**	**2.8**	**0.09**	**N/A**
Hydrolysed E60	**14,500**	**33,000**	**2.3**	**0.22**	**12,700**
Hydrolysed E400	**85,000**	**346,000**	**4**	**0.22**	**74, 500**
Imide E60	**89,000**	**149,000**	**1.7**	**0.1**	**47,000**
Imide E400	**364,000**	**951,000**	**2.8**	**0.1**	**197,000**

† Molecular weight of E60 and E400 calculated from E60 and E400 derivative M_n values.

The GPC results for both the hydrolysed and imide forms of the polymer were then used to calculate a theoretical E60 and E400 molecular weights. As can be observed

the aqueous results (hydrolysed E60 and hydrolysed E400), once corrected, are significantly below those obtained for both E60 and E400. However the E60 and E400 molecular weights as calculated from the imide derivatives are of approximately the same values as those obtained from the virgin polymer. As a result, the M_n of E60 and E400 can be estimated to at 40,000 and 214,000Da respectively and the hydrolysed polymer result rejected as being meaningless. This is somewhat suprising as elsewhere in the literature there are several examples of both basic and acidic

1.6 Chemical modification

The potential for the chemical modification of the polymer post polymerisation sets it apart from the majority of polymers. However, control over the final product is necessary as unwanted side reactions on the polymer backbone cannot be removed by purification. This combined with the paucity of data in the literature meant it was necessary to characterise the chemical reactivity of these polymers. Reactions examined include: amidation, esterification, hydrolysis, dehydration and imidation.

1.6.1 Amidation

Primary and secondary amines are strong nucelophiles and consequently are good candidates for reaction with the polymeric anhydrides, as the reaction should out-compete potential side reactions such as esterification and hydrolysis. The efficiency of this reaction is demonstrated by reaction of E60 with benzylamine. The ^{1}H NMR of the product is shown in figure 1-18.

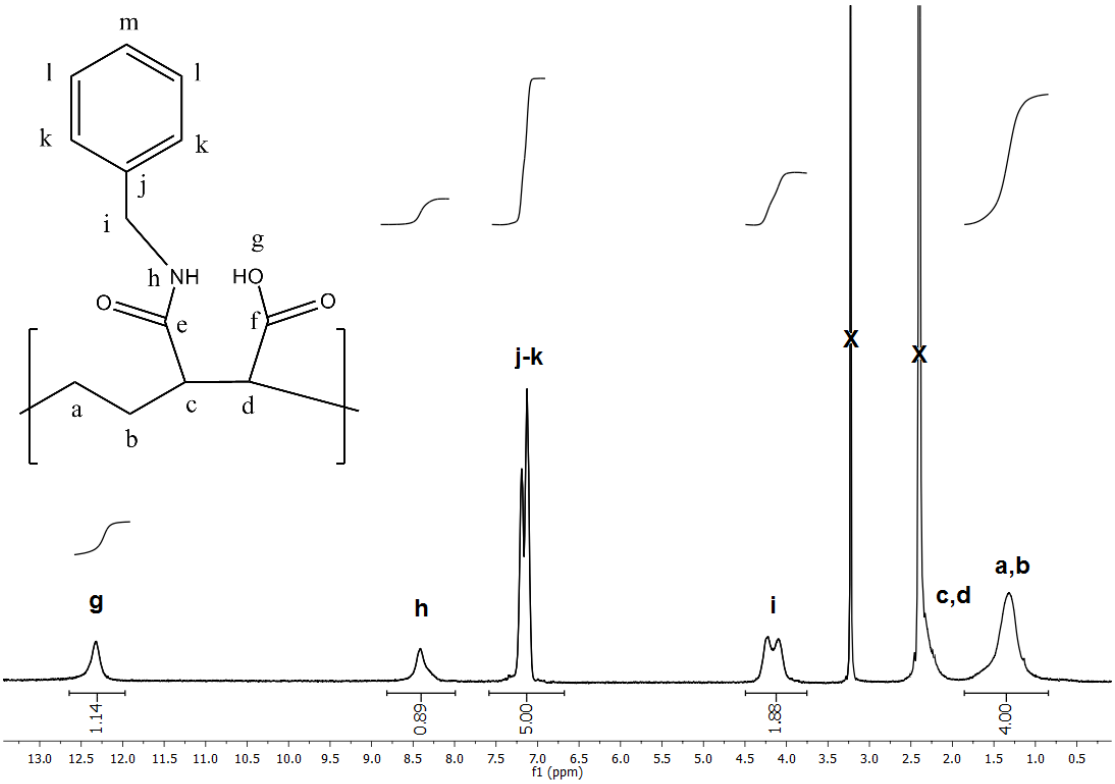

Figure 1-18: (400MHz, d_6-DMSO) ^{1}H NMR of benzylamine modified E60

Reaction of the backbone anhydride with benzylamine in DMF was observed to go to 100% conversion within 10 seconds of the amines addition. As a result, attempts to follow the reaction kinetics failed. However, the reaction proved trivial with a variety of amines going to near 100% conversion (table 1-4) as determined by ^{1}H NMR

Table 1-4: Conversion of anhydride to mono-amide for E60[*]

Amine	Conversion (%)[†]
Benzylamine	**100[†]**
N-methylbenzylamine	**100[†]**
Hexylamine	**96[‡]**
Napthylmethylamine	**98[†]**

* Reaction at room temperature in DMF over 10 minutes.

†Calculated by comparision of ethylene to aromatic region of ^{1}H NMR

‡Calculated by comparison of CH_2 alkane to amide alpha protons by ^{1}H NMR

The principle problem found when reacting the polymer with amines is the tendency for the product polymer to gel. While this is unimportant in forming the amide it does hinders both the purification of the product, especially as high boiling point solvents tend to be necessary, and attempts to achieve partial conversion of anhydride to amide.

Despite these difficulties the reaction does offer a great degree of control when optimised as the reaction was found to be quantitative (figure 1-19).

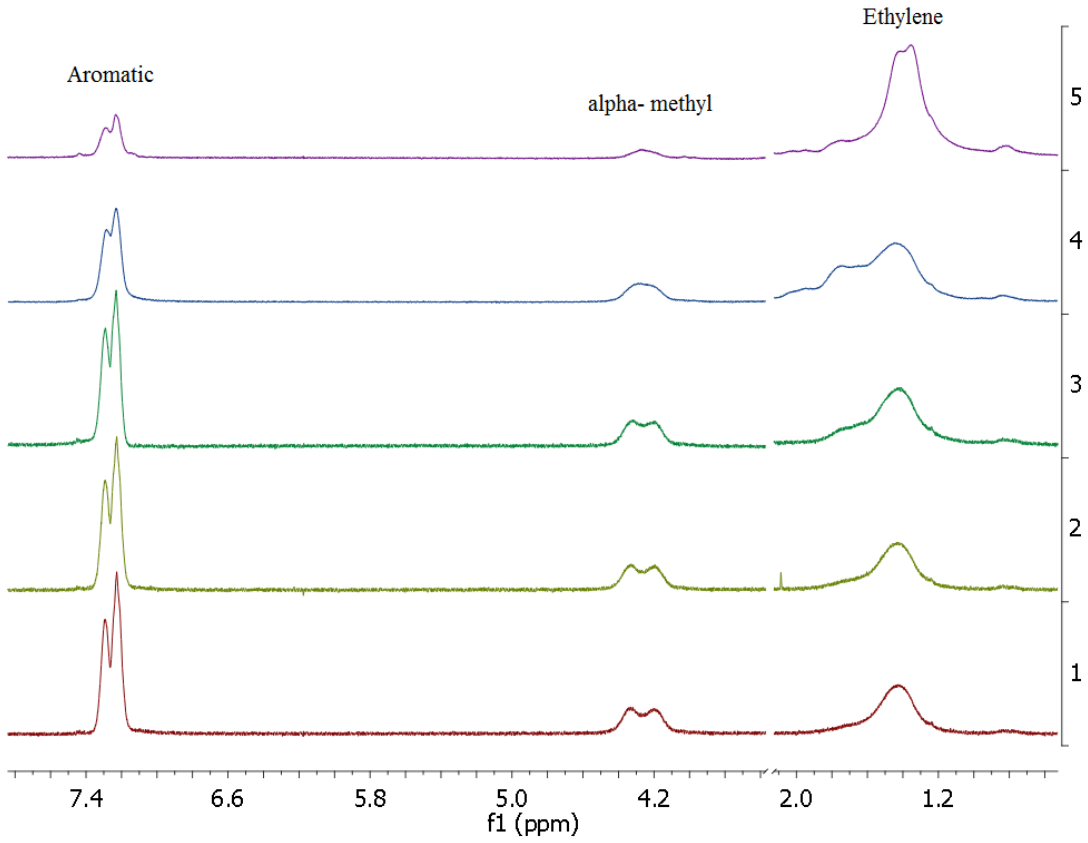

Figure 1-19: Stacked ^{1}H NMR spectra of reaction product of (1) 1 (mol amine/mol anhydride), (2) 0.8 (mol amine/mol anhydride), (3) 0.5 (mol amine/mol anhydride), (4) 0.2 (mol amine/mol anhydride), and (5) 0.1 (mol amine/mol anhydride).

.

1.6.2 Hydrolysis

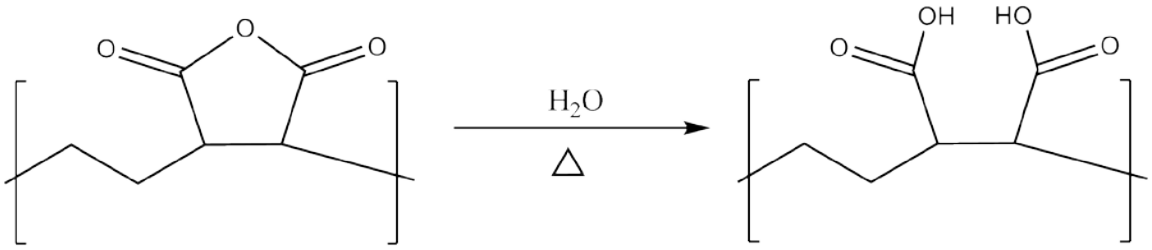

Figure 1-20: Hydrolysis of poly(ethylene-alt-maleic anhydride) to poly(ethylene-alt-maleic acid).

Hydrolysis of the polymer (figure 1-20), while a potentially useful reaction, may allow for significant potential side reactions, as well as presenting a challenge in storing the material before its use. As a result, a characterisation of the hydrolysis reaction was conducted in: solution, bulk water and water vapour.

The anhydride polymer was observed to form an orange coloured solution in DMF with an absorbance maximum at 475nm, whereas the hydrolysed polymer in the same solvent is colourless. The origin of this colouration is likely to be due to charge transfer complexes between the solvent and anhydride. A plot of anhydride concentration vs absorbance closely fitted a polynomial function. This deviation from the Beer Lambert Law is expected at high concentration (figure 1-21(a)).

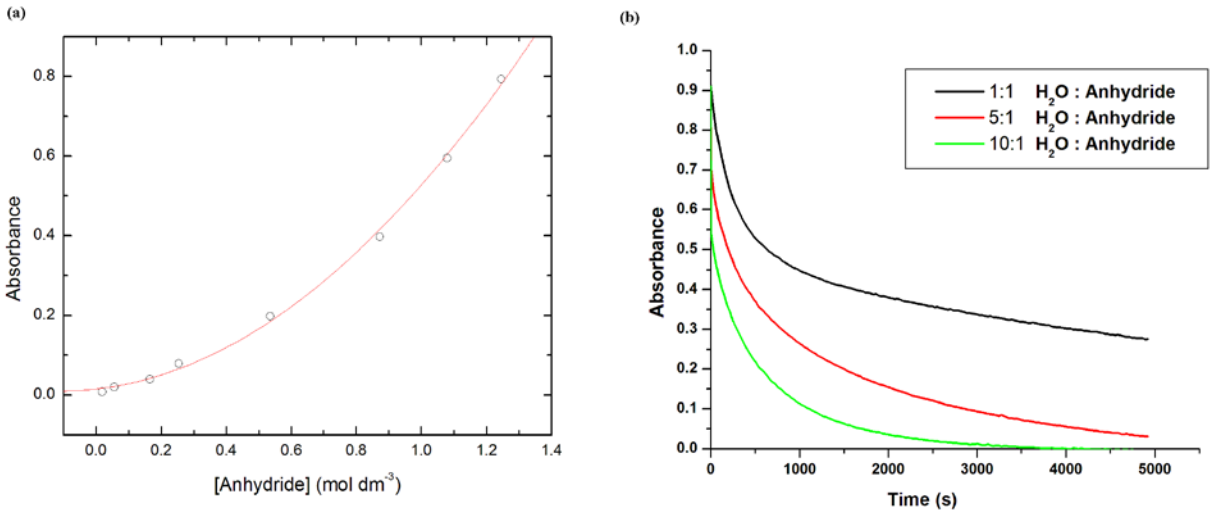

Figure 1-21: (a) Calibration curve of anhydride concentration vs absorbance at 475nm, (b) change in absorbance at 475nm with time at 60°C in the presence of varying amounts of water.

In order to follow the kinetics of hydrolysis a known mass of E60 was dissolved in to freshly obtained anhydrous DMF. The polymer solution was then transferred in to a sealed cuvette and then held for 10 minutes at the required temperature within the UV-vis instrument with efficient stirring. To this solution an appropriate volume of water was then added, the cuvette resealed, and the ensuing reaction followed at 475nm. Measurements were taken at 30 second intervals.

Hydrolysis by this method was demonstrated to be complete by ^{13}C NMR (figure 1-22).

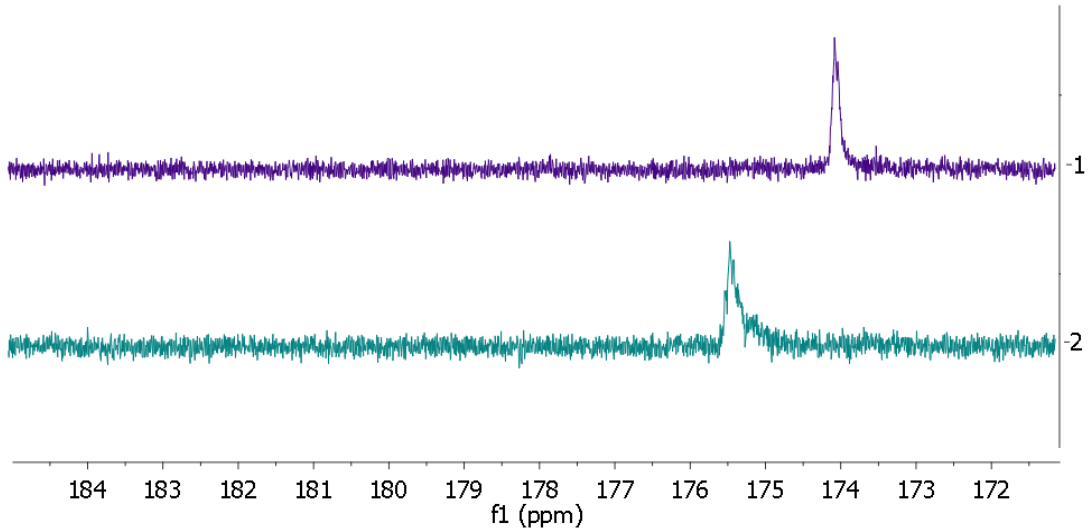

Figure 1-22: (100MHz, d_6-DMSO) ^{13}C NMR spectra of (1) poly(ethylene-alt-maleic acid) and (2) poly(ethylene-alt-maleic anhydride).

The data obtained (figure 1-22) was used to calculate anhydride concentration vs time which in turn was used to determine the kinetics of the reaction. This was achieved using the integrated rate equations, to determine the overall order of the rate equation at a water to anhydride mole ratio of 1:1 and comparing this with the order of the reaction when the water is in large excess. The latter experiment assumes that the concentration of water is constant throughout and therefore the rate of reaction is determined only by the anhydride concentration.

$$rate = k\,[Anhydride]^n\,[Water]^m \quad (eqn\ 1.22)$$

$$rate = k\,[Anhydride]^n \quad (eqn\ 1.23)$$

As a result it is possible to determine both the overall order of the reaction and the approximate order in the anhydride only, from this it is them possible to estimate the order in the water.

However, the rate constant expresses the dependence of rate on the energy of the system and a reaction specific constant known as the Arrheius constant. These relationships are expressed by the Arrheius equation.

$$k = A\, e^{\frac{-Ea}{RT}} \quad (eqn\ 1.24)$$

Therefore, by fixing the concentration of both water and anhydride, but varying the temperature it is possible to determine both the activation energy and Arrheius constant.

The order of the reactions were determined using the graphical method (figure 1-23)

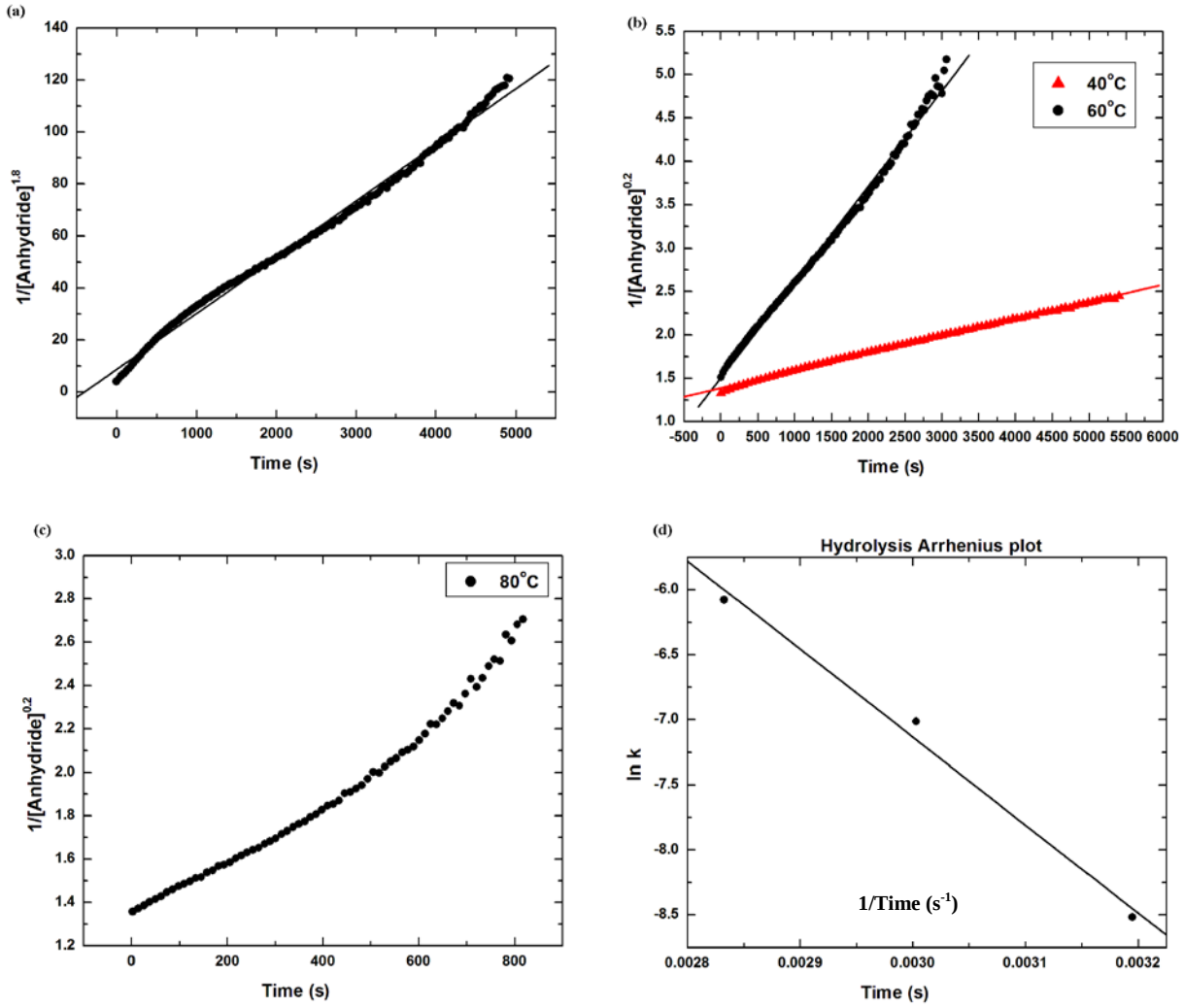

Figure 1-23: Kinetic plots of: (a) 1:1 anhydride:water hydrolysis at 60°C, (b) 1:10 anhydride:water at 40°C and 60°C, (c) 1:10 anhydride:water 80°C, (d) Arrhenius plot of k' determined from 1:10 anhydride:water at varying temperature.

When the concentration of anhydride and water are in a molar ratio of 1:1 the overall order of the reaction was shown to be 2.8. When water is added in a ten fold excess and steady state conditons assumed the overall order in the anhydride is 1.2. Therefore, the rate equation can be written as eqn 1-22.

$$rate = k\,[Anhydride]^{1.2}[H_2O]^{1.6} \qquad (eqn. 1-22)$$

Experiments at varying temperature demonstrated the E_a to be 56 kJmol^{-1}, which is the same value obtained by other researchers for small molecule anhydrides.[104] The Arrhenius constant was determined as being 1.8x10^6 s^{-1}.

In addition to this, experiments were conducted to follow the conversion of anhydride to diacid in both heterogenous bulk water and with water vapour (figure 1-24). Both of these are important when considering the storage and formulation conditions of the polymer.

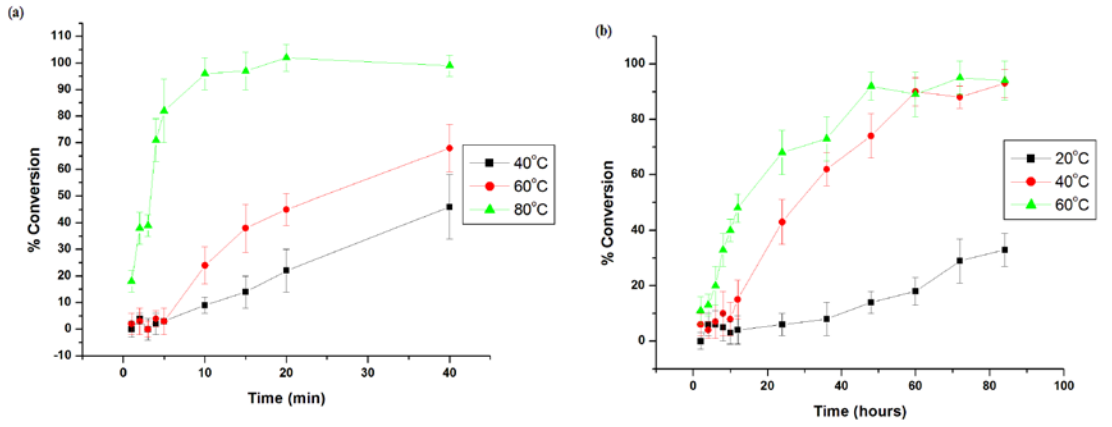

Figure 1-24: Reaction of E60 with (a) bulk water and (b) water vapour at various temperatures.

Heterogeneous hydrolysis, both in bulk water and with water vapour, initially proceeds slowly followed by a rapid increase in rate. This is likely to be the result of an increasing solubility/hydrophilicity with increasing conversion of the anhydride to

diacid, resulting in increased contact between water molecules and the remaining anhydrides. Further kinetic treatment in both cases was unnecessary. In the case of hydrolysis in bulk water the polymer is initially insoluble, then forms a gel and then enters solution hence the observed lag in the reaction rate. This in turn is dependent on the grain size and how efficiently the initial slurry is stirred. As a result, the data can only be taken as an empirical guide and can be expected to vary significantly on such factors as polymer grain size, stirrer speed and reactor design.

1.6.3 Esterification

Esterification of the anhydrides can be forced under heterogeneous conditions using strongly dehydrating conditions (figure 1-25).

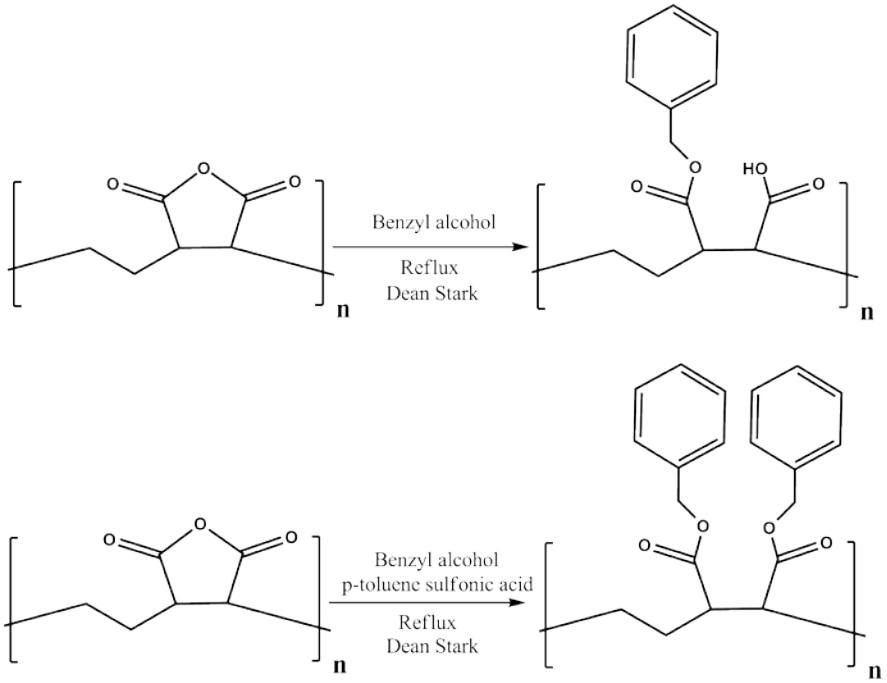

Figure 1-25: Esterification conditions for (a) mono esterification, and (b) di-esterification.

The formation of each of these products (figure 1-26) can be determined from the carbonyl region of their respective ^{13}C NMR spectra, note again the shoulder at lower chemical shift indicating the presence of erythro forms of the polymer. Unfortunately better resolution of the peaks could not be obtained due to the high viscosity of the polymer d_6-DMSO solutions.

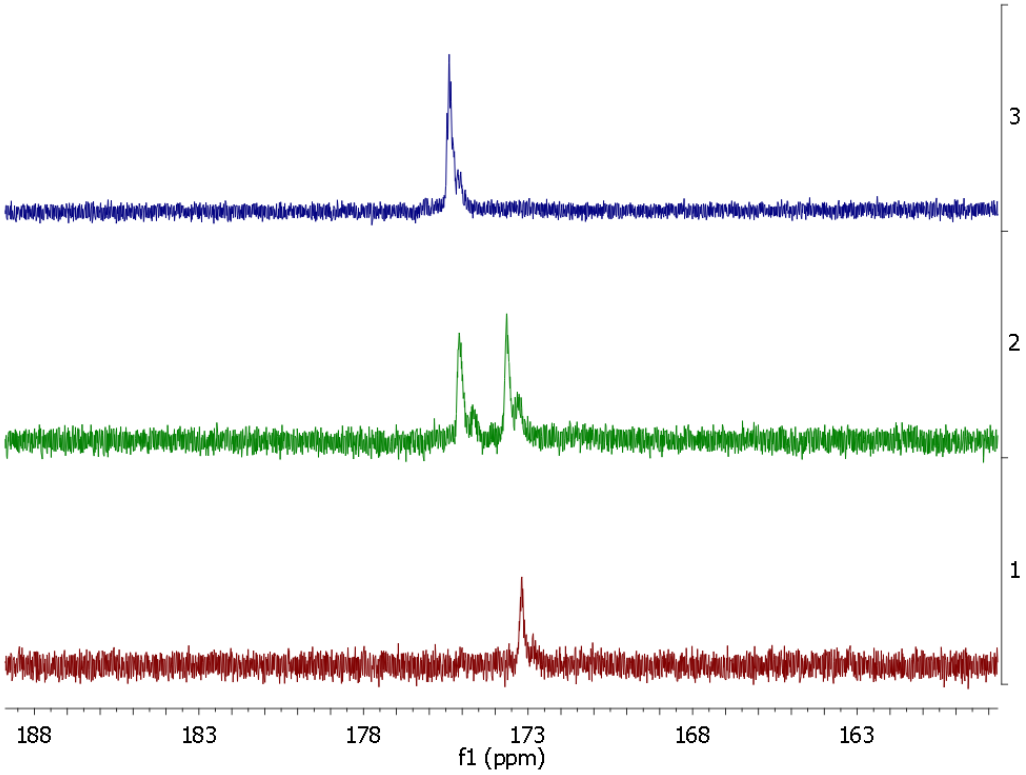

Figure 1-26: (100MHz, d_6-DMSO) ^{13}C NMR spectra of (3)hydrolysed E60, (2) mono-benzyl ester E60 derivative (fig 23 (a)), and (3) di-benzyl ester E60 derivative (fig 23 (b)).

Although conversion to the mono and di-esters is trivial, the forcing conditions used mean the reaction must be conducted in heterogeneous conditions. Clearly, it would

be advantageous to be able to work in conditions that allowed for only partial conversion of backbone anhydrides to esters. However, because of the limited solubility of the polymer, this requires the use of high boiling point hygroscopic solvents, which presents two challenges: firstly in excluding water from the system and secondly in removing the nascent water from the reaction. Additionally, because of the high concentration of anhydrides relative to polymer chains per gram of material, the amount of alcohol which must be added means that there are limitations as to what concentration of polymer may be used without the polymers precipitating. Although there are reports of reactive extrusion as a viable method in the literature this is not always practicable given the high glass transition temperature of poly(ethylene-alt-maleic anhydride).[79]

However, with careful optimisation of the conditions it was found that working in rigorously dry conditions and in the presence of molecular sieves meant it was possible to affect complete conversion of the anhydrides to the monoester (figure 1-25). As a result it was possible to follow the reaction kinetics by ^{1}H NMR (figure 1.27).

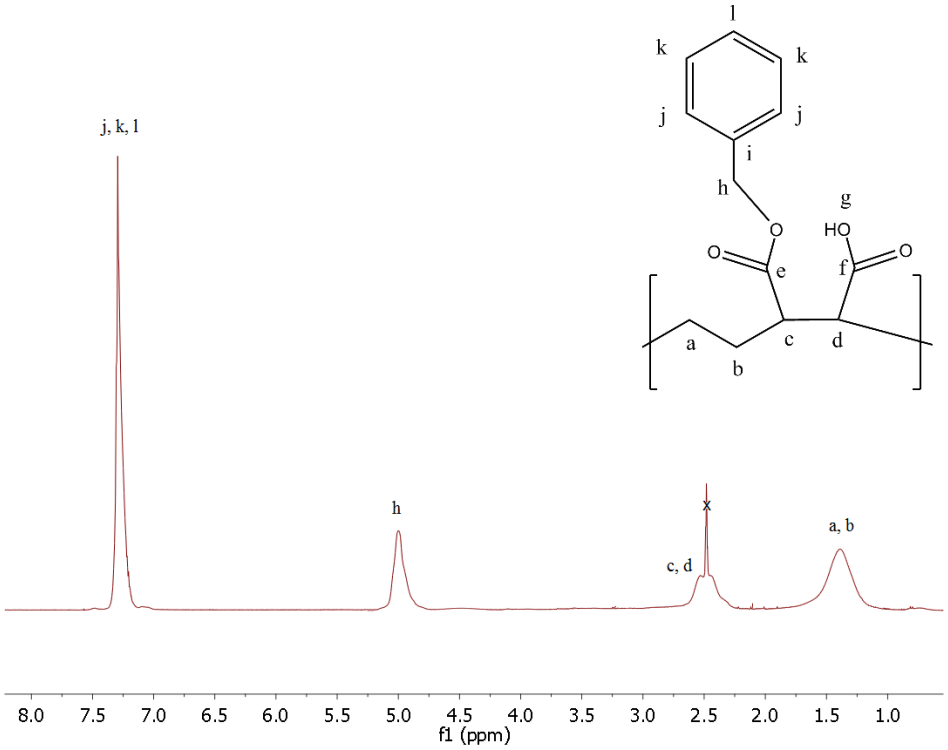

Figure 1-27: (400MHz, d_6-DMSO) ^{1}H NMR of mono benzyl ester E60.

Kinetics were followed by reaction of anhydrous benzyl alcohol with E60 in anhydrous DMF under a flow of N_2 gas over 4Å molecular sieves. The solutions were then heated to an appropriate temperature and stirred. Samples were then taken at appropriate times and the polymer recovered by precipitation into diethyl ether. The polymer was then analysed by ^{1}H NMR without further purification, comparison of polymeric ethylene proton integral with the α-methyl proton integral of the formed ester allowed the degree of esterification to be calculated, assuming no esterification of the nascent carboxylic acids, for which there is no evidence without the use of forcing conditions.

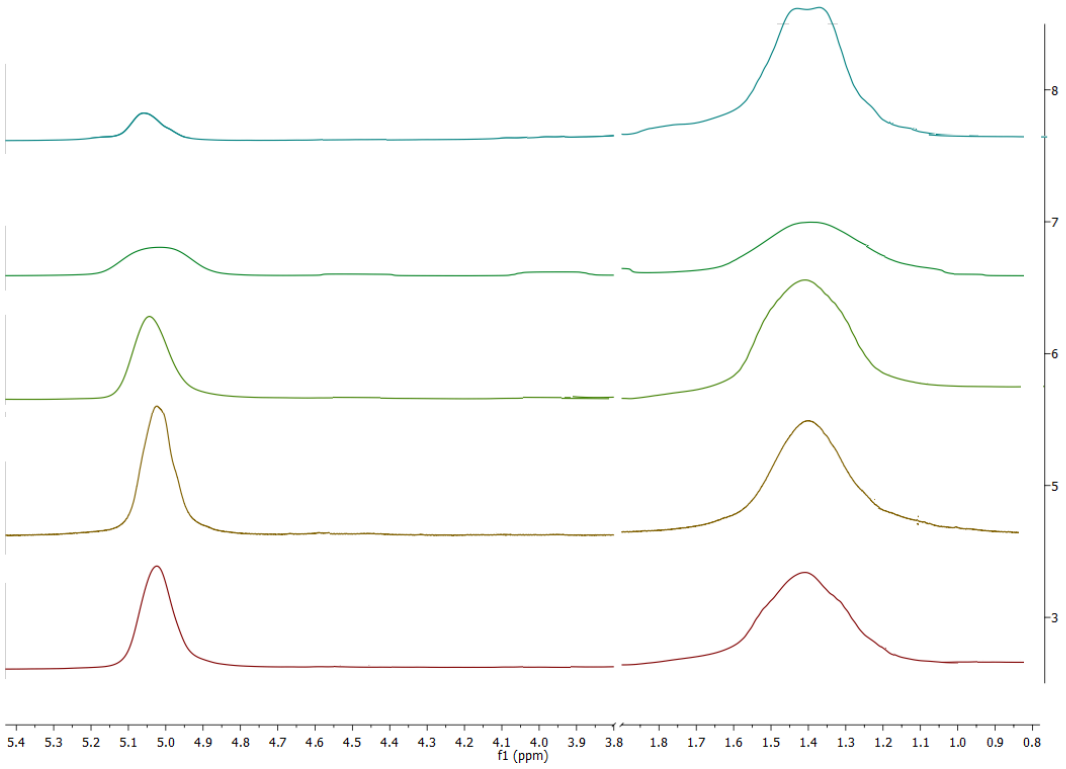

Figure 1-28: ^{1}H NMR spectra of the product of esterification of E60 anhydrides with benzyl alcohol (2mol: 5mol) in DMF at 50^{o}C after times: (6) 30 minutes, (5) 60 minutes, (4) 90 minutes, (3) 180 min, (2) 300 minutes, and (1) 12 hrs. The peaks monitored are the ethylene protons and protons α to the nascent ester.

As expected conversion was seen to be dependent both on concentration of benzyl alcohol and on the reaction temperature (figure 1-29, figure 1-30).

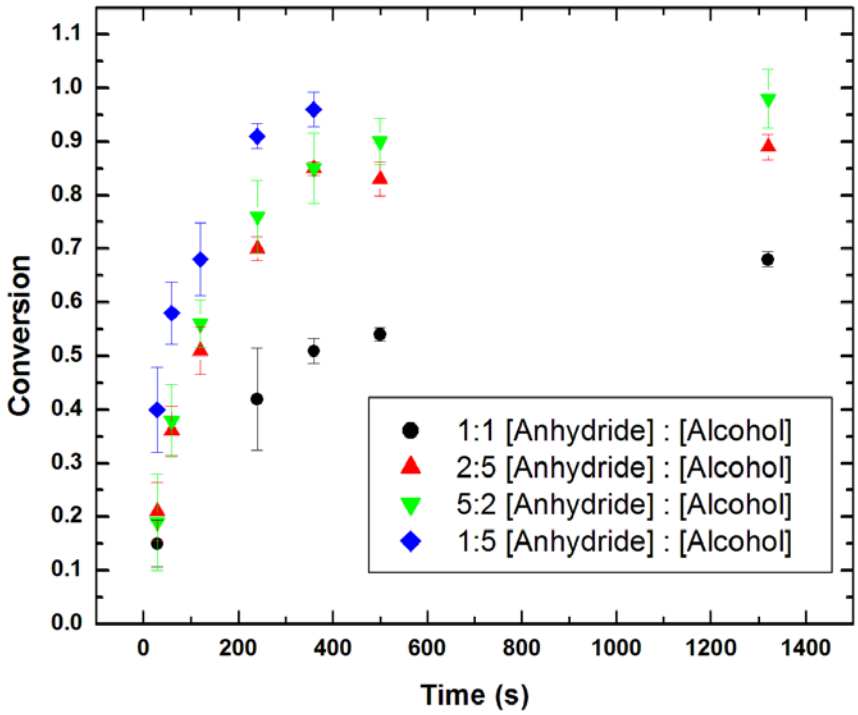

Figure 1-29: Conversion of E60 to the benzyl alcohol mono-ester vs time at 50°C

This data was then plotted according to the integrated rate equations to obtain the reaction rate equations and activation energies. The methodology for interpreting the kinetic data was the same as was used for the hydrolysis kinetics (section 1.6.2)

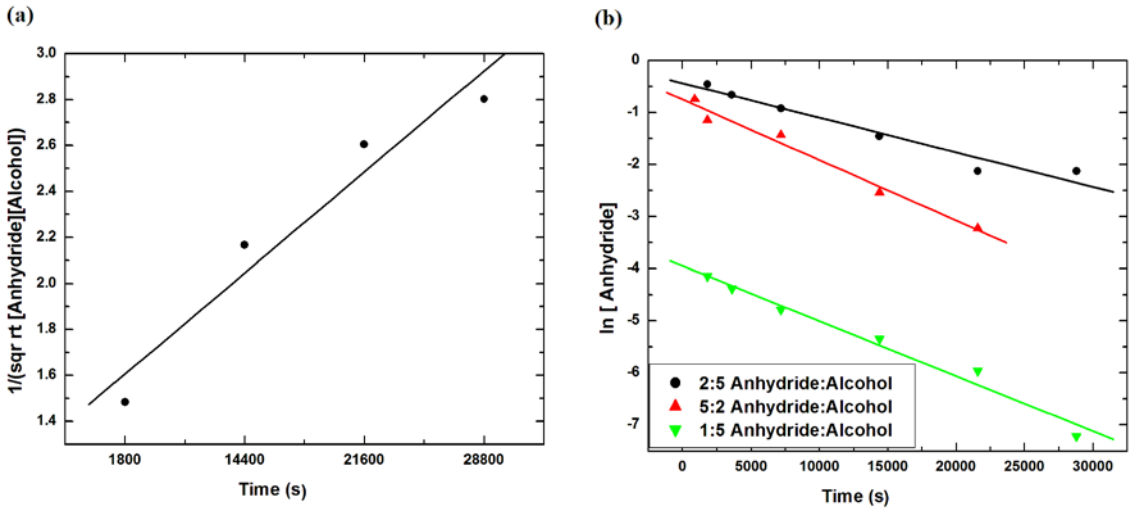

Figure 1-30: (a) Linear rate plot of ester kinetics at 50°C with relative concentration of alcohol:anhydride being 1:1 (b) linear rate plots at 50°C when benzyl alcohol is in excess to anhydride.

When the anhydride and benzyl alcohol concentration are equal the overall rate of reaction is 2. In the presence of excess alcohol, and steady state kinetics are assumed, the order in the anhydride is pseudo first order. In other words the overall order is 2 with the order in the alcohol and anhydride individually being 1.

$$rate = k\,[Anhydride][Alcohol] \quad (eqn\ 1.32)$$

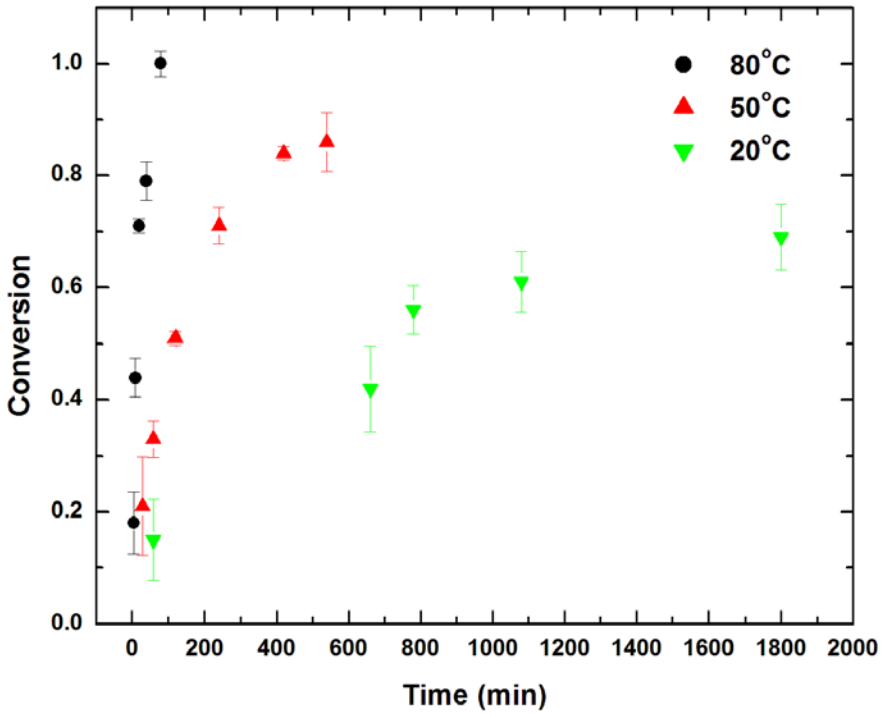

Figure 1-31: Formation of the mono-benzyl ester derivative of E60 at varying temperature with relative concentration of anhydride to alcohol of 1:5.

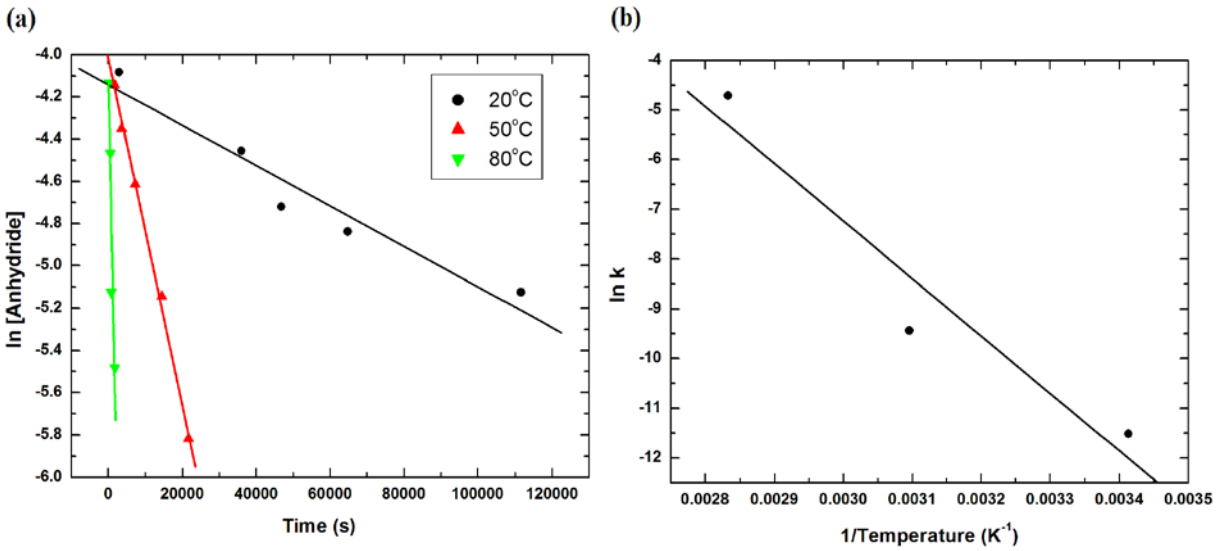

Figure 1-32: (a) Rate plot assuming pseudo first order kinetics with a 5 mole excess of alcohol to anhydride , (b) Arrhenius plot of pseudo first order rate constants.

An Arrhenius plot of this reaction yielded an E_a of 63 kJmol^{-1} (figure 1-32(b)). A comparison with the literature values for E_a demonstrates that the reaction's activation energy is approximately the same value as small molecule cyclic anhydrides. As a consequence the reactivity of the polymer can be closely modelled on the behaviour of small molecule anhydrides.

1.6.4 Dehydration

The dehydration of poly(ethylene-alt-maleic acid) to poly(ethylene-alt-maleic anhydride) is of interest as it represents the reverse reaction of a potential side reaction, namely, hydrolysis. It was found that heating a sample of poly(ethylene-alt-maleic acid) to 120^{o}C for 18 hours, under vacuum, resulted in the formation of a cyclic anhydride via a ring closing dehydration reaction mechanism.

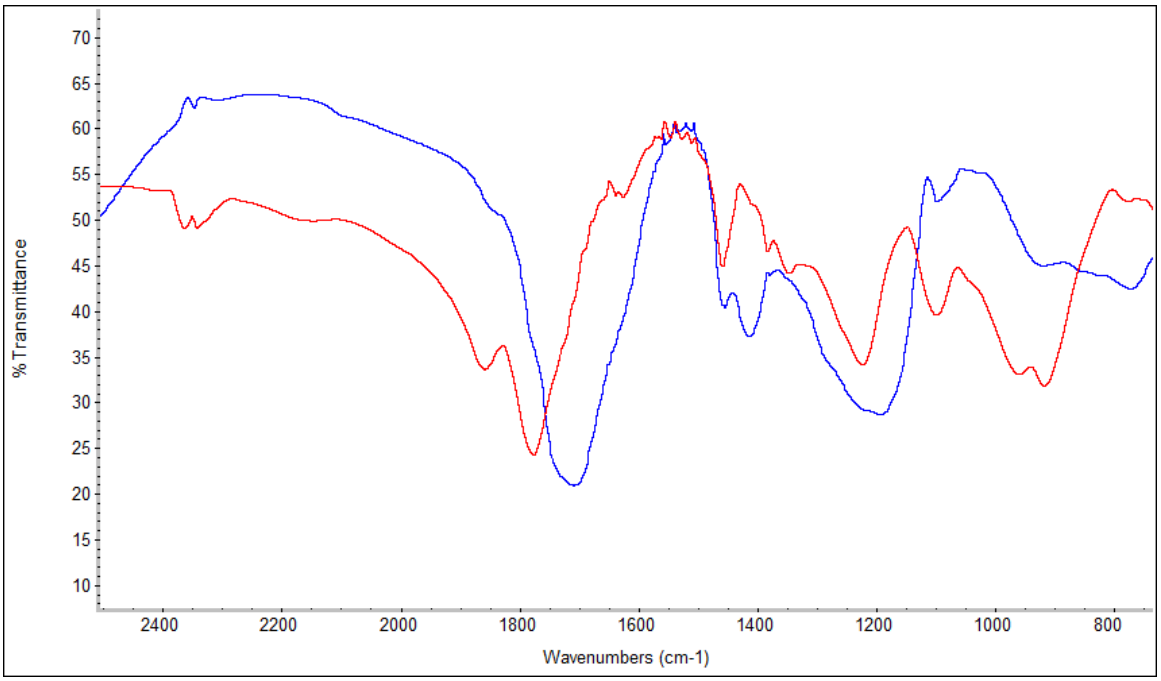

Figure 1-33: FTIR (KBr) spectra: (Blue) hE60, (Red) hE60 after 18 hours at 120°C.

Table 1-5: Principle IR stretches (see fig. 1-33)

hE60	ν (cm^{-1})	18 hrs at 120°C	ν (cm^{-1})
C=O acid	1740	C=O anhydride	1860
C-C	1460	C=O anhydride	1790
C-C	1400	C-C	1470
C-O carbonyl	1210	C-C	1410
		C-O`	1290-1110

FT-IR spectroscopy on hydrolysed E60 before and after heating (120°C 18h) confirmed the dehydration of diacid groups and the formation of cyclic anhydrides (figure 1-33). The kinetics of dehydration were followed by isothermal thermogravimetric analysis (TGA), with the mass loss over time being attributable to the expulsion of water (figure 1-34).

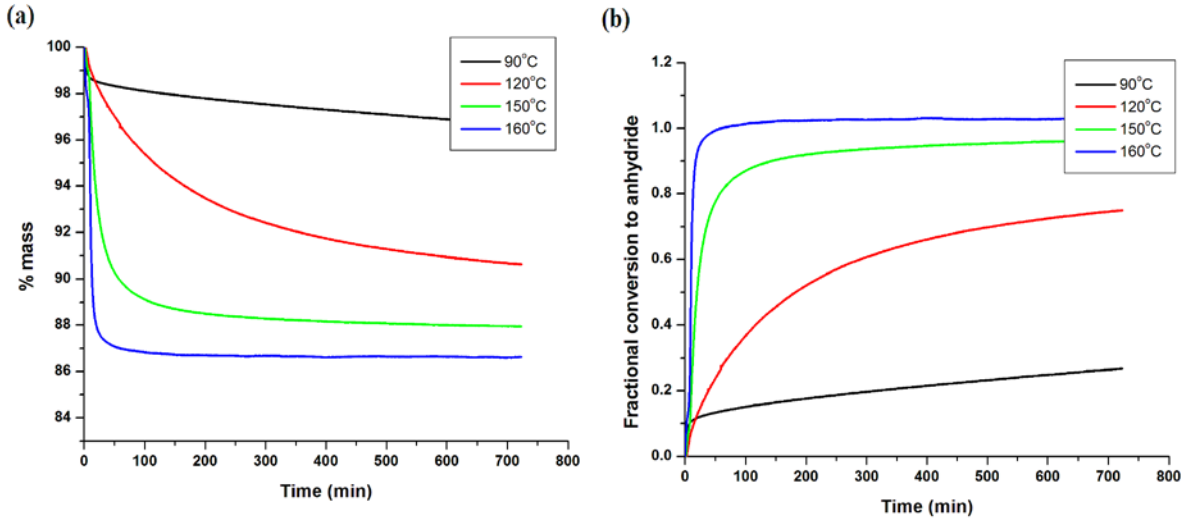

Figure 1-34: (a) Dehydration of hE60 under a flow of nitrogen as % mass loss, (b) fractional conversion of hE60 to E60 as calculated from TGA.

The time taken to reach any particular fractional conversion (t_α) is directly proportional to the rate of the reaction, and this can be used to calculate E_a .

$$\alpha(t) = \frac{(m_i - m_t)}{(m_i - m_f)} \qquad (eqn\ 1-33)$$

Where α(t) is the conversion of the reaction at time t, m_i is the initial mass, m_t is the mass at time t, and m_f is the final mass at 100% conversion to anhydride.

$$-\ln t_\alpha = \ln A - \frac{E_a}{RT} \qquad (eqn\ 1\text{-}34)$$

This is a model-free method of determining the rate of reaction, that is to say no assumptions are made about the time taken for the water to diffuse out of the solid.[105]

However, there is also another factor to take into account: as the reaction proceeds, water is released by the dehydration mechanism, at these elevated temperatures it is possible that the nascent water will ring-open previously formed anhydrides. The mechanism is in fact an equilibrium which is driven, by the removal of water by vacuum or nitrogen flow, towards the anhydride product (figure 1-35).

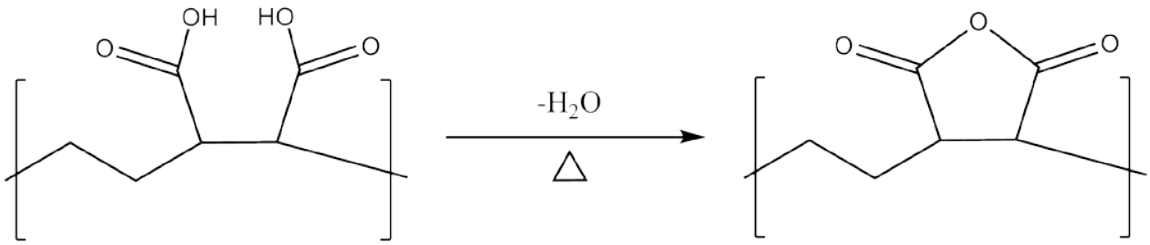

Figure 1-35: Dehydration mechanism in the solid state.

At low conversion the equilibrium will lie predominantly in the forward direction due to the scarcity of anhydrides for the nascent water to react with. Consequently, at low α the forward reaction will dominate and the back reaction can be assumed to be negligble, whereas at high α the back reaction becomes increasingly important.

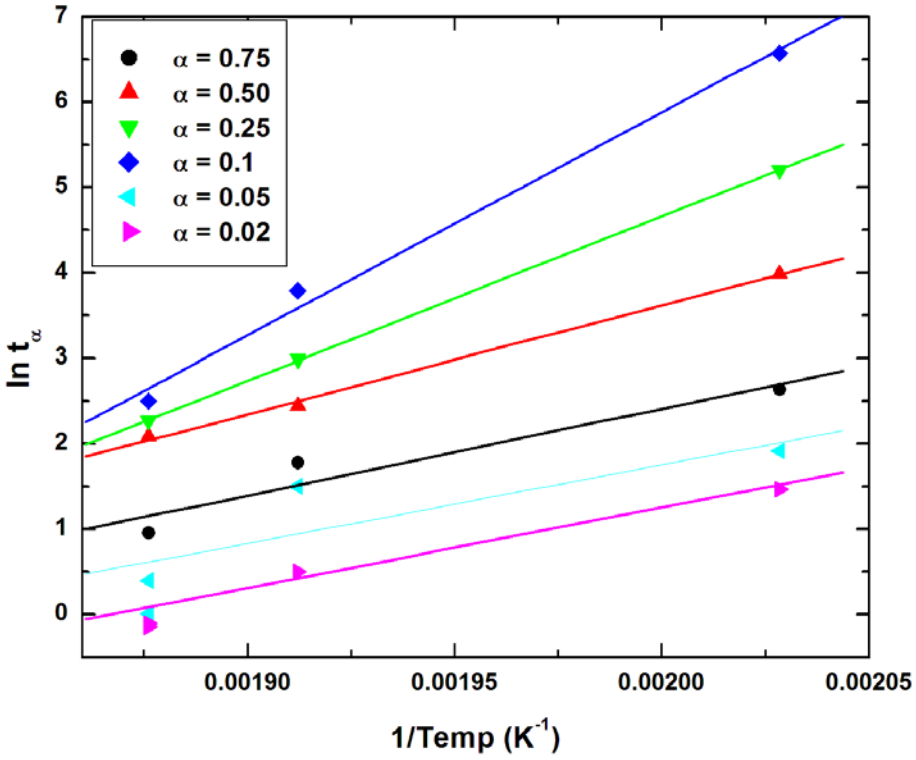

Figure 1-36: Kinetic plot of ln t_α vs 1/T where t_α is the time taken to reach conversion α

As can be seen at low α values the gradient, and therefore E_a, is approximately constant. However, at high conversion the back reaction, hydrolysis, decreases the apparent rate of the forward reaction thereby increasing the apparent E_a of dehydration (figure 1-36).

Therefore, in calculating the E_a of dehydration it is important to regress the plot back to α(t)= 0, in effect providing the instantaneous E_a, which can be approximated as being the absolute E_a of the dehydration reaction (figure 1-37).

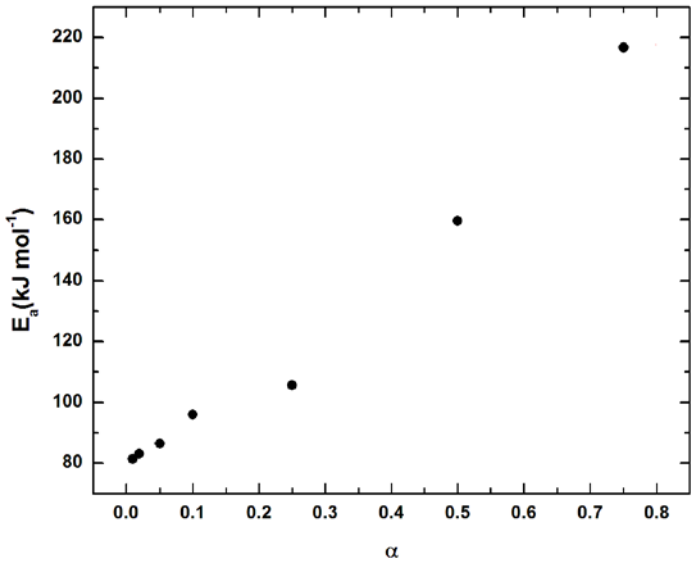

Figure 1-37: Plot of the apparent activation energy with varying conversion (α)

The measured E_a is 81 kJmol^{-1}, which compares favourably with the literature value for the ring closing of small molecule di-acids in solution, 92 kJmol^{-1}. The reduced value for the polymeric material may reflect the fact that fewer conformations are available to the diacid groups thereby lowering the entropy penalty on ring closing.

1.6.5 Imidization

The formation of imides is important for two reasons. Firstly, it represents a functional group which is less susceptible to hydrolysis than the starting amide, and secondly, the formation of an imide is a convenient way to remove the carboxylic acid residues which may be problematic for particular applications (figure 1-38).

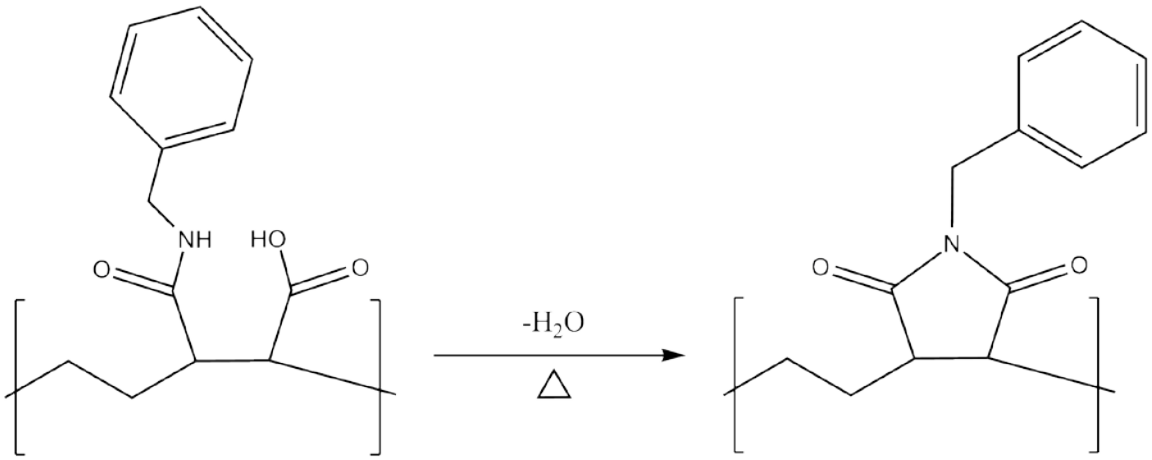

Figure 1-38: Synthesis of the benzylimide from the benzylamide E60 derivative.

The formation of the imide was achieved by heating a solid sample of the benzylamide derivative of E60 under vacuum for 12 hours at 150^{o}C. Conversion was found to go to approximately 100%, as determined by ^{13}C NMR (figure 1-39).

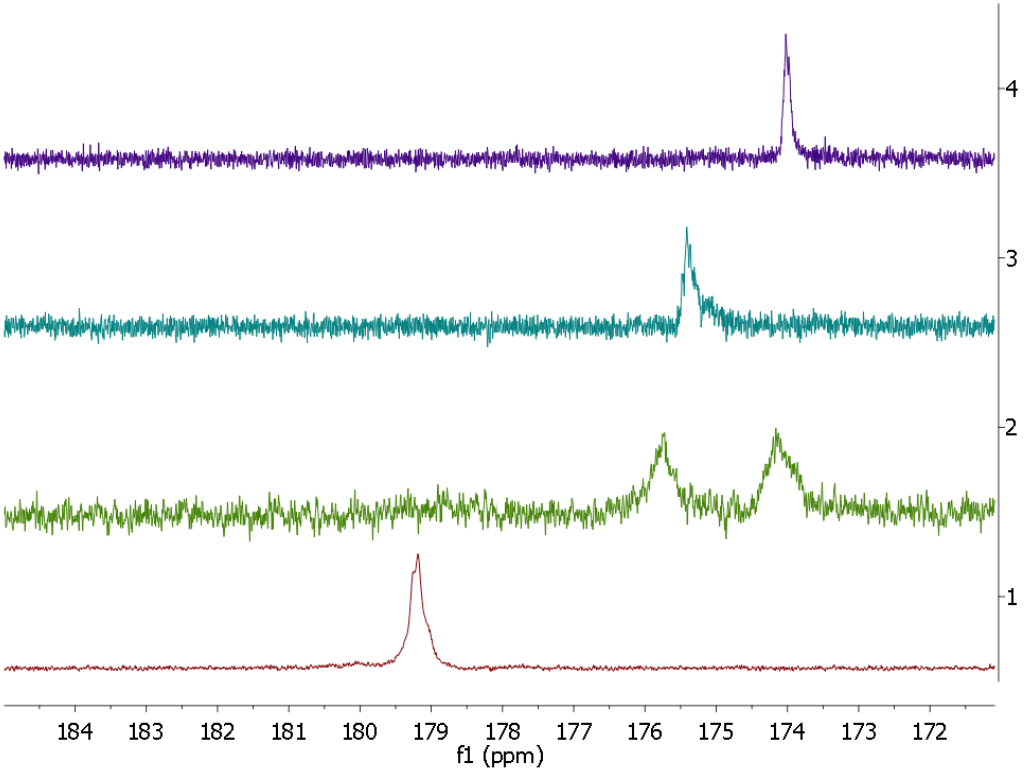

Figure 1-39: ^{13}C NMR spectra of (4) anhydride E60, (3) hE60, (2) benzylamide E60 and, (1) benzylimide E60

Analysis of the ^{13}C NMR spectra of the final product demonstrated the disappearance of carboxylic and amidic carbon signals and the appearance of a single carbonyl carbon signal at 179.3ppm, which is attributable to the imide functional group. In addition, the ^{1}H NMR spectra demonstrated the disappearance of acid, but the persistence of aromatic, protons.

The kinetics of this solid state reaction were followed by isothermal TGA with the mass loss being attributed to the expulsion of water from the sample (figure 1-40).

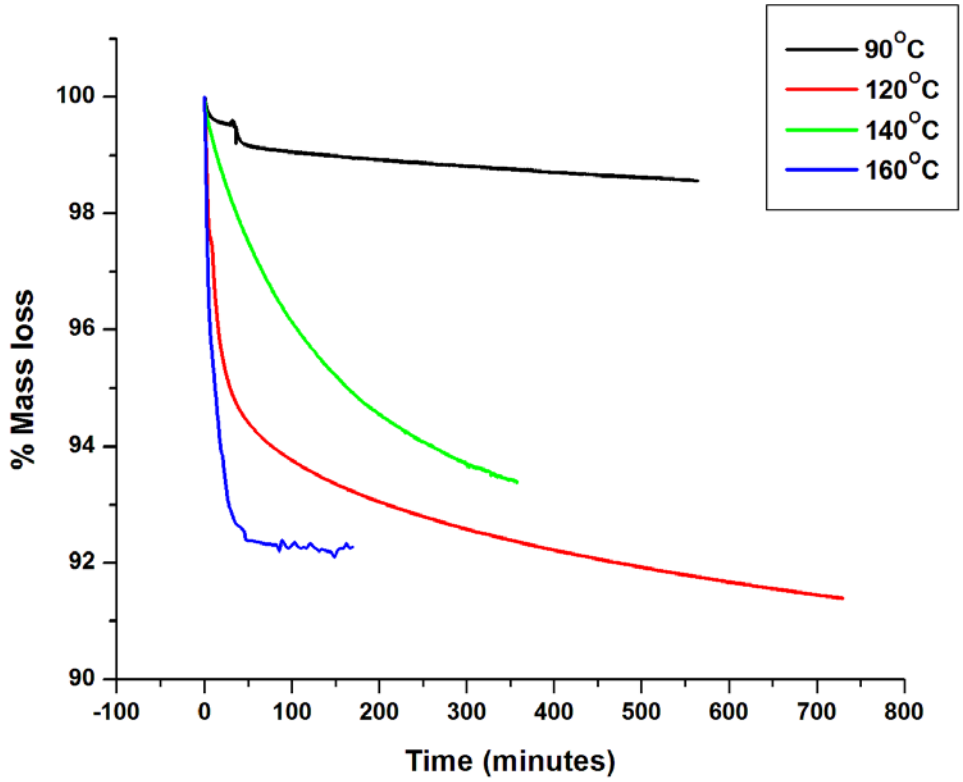

Figure 1-40: (a) Dehydration of benzylamide E60 to benzylimide E60

The model free solid state reaction kinetics model was applied and the resulting plot t_{α} vs 1/temperature yielded linear fits with gradient E_a (figure 1-41).

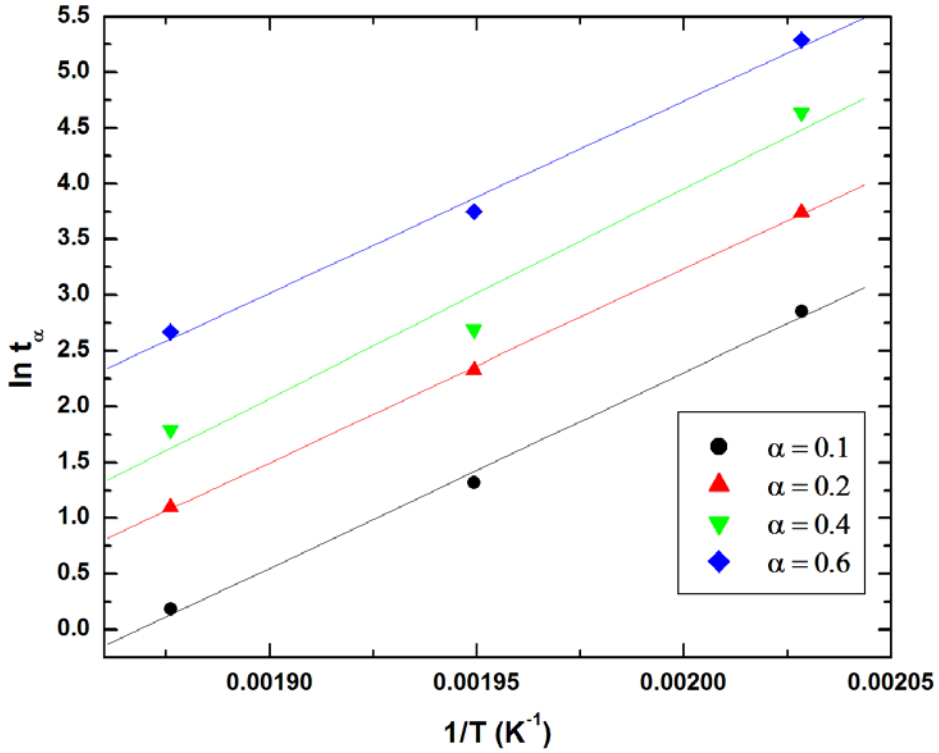

Figure 1-41: Model free Arrhenius plot of benzylimidization of E60

It is notable that, unlike the dehydration kinetics, the gradient of the plot does not vary significantly with α. This suggests the back reaction, namely hydrolysis of the imide, does not occur to any significant extent even at high conversion. Based on this the reaction was found to have an E_a of 147.3 (+/- 5.85) kJmol^{-1}. Literature values for the E_a of imidation range from 105 kJmol^{-1} to 260 kJmol^{-1}.[106]

1.6.6 Thermal analysis

Given that it is desirable to heat the polymer as a powder in order to easily effect dehydration and imidization it was necessary to thermally characterise the material to find both its glass transition and decomposition temperature (table 1-6).

Table 1-6: Glass transition (T_g) and decomposition temperature (at onset, N_2)

Polymer	T_g (°C)	Decomposition Temp*(°C)
E60	165	276
E400	168	280

*In nitrogen gas

As can be seen under inert atmosphere the decomposition temperature is beyond those necessary for dehydration and esterification. The glass transition temperature is rather closer, although it must be remembered any derivative of E60/E400 will be likely to have a different T_g to the virgin polymer. It is also notable that the T_g for both polymers is approximately the same, indicating that the molecular mass of E60 is beyond that of the region where molecular mass and T_g are interdependent.

1.7 Conclusion

The polymers were successfully characterised yielding information of its structure, physical properties and reactivity. Importantly, the anhydride moieties were found to react at rates, temperatures and yields comparable to small molecule anhydrides. Therefore, the limiting factor in most reactions is the polymer's solubility, the

difficulties in removing impurities and unwanted side reactions occurring along the chain which, necessarily, cannot be removed post reaction.

1.8 Experimental

1.8.1 Materials and instruments

E60 and E400 were received from Vertellus speciality chemicals and purified as outlined in section 1.9.2. All other chemicals were purchased from standard chemical suppliers and used without further purification unless otherwise stated.

Dry solvents were purchased from Fischer Scientific and dried by passage through two alumina columns using an *Innovative Technology Inc.* solvent purification system and stored under N_2.

Nuclear magnetic resonance (NMR) spectra were recorded using a Varian Inova 500 spectrometer at 499.87 (^{1}H) and 125.67 MHz (^{13}C, 1H decoupled at 500 MHz), a Bruker Avance 400 spectrometer at 400.13 MHz (1H) or 100.26 MHz (^{13}C, ^{1}H decoupled at 400 MHz) or a Varian Inova-700 spectrometer at 700MHz (1H) and 176MHz (13C), at ambient temperature in $CDCl_3$, DMSO, D_2O, MeOD. NMR spectra were analysed using MestReNova v6.04 software and referenced internally to the residual protons in the NMR solvent. IR spectra were recorded on a Nicolet Nexus FT-IR spectrometer using samples prepared as pressed KBr discs. DMF gel permeation chromatography was performed using a triple detection method (with angular correction) and measurements were performed on a Viscotek TDA 301 triple detection SEC fitted with two (300 x 7.5 mm) GMPWxl methacrylate-based mixed bed columns with an exclusion limit of 5,107 g mol^{-}1, having refractive index, viscometer and RALLS detectors. The eluent was DMF with added LiBr salt at a flow rate of 1.0 ml/minute. For aqueous GPC, the eluent was 0.05 M NaNO3 solution (80/20 v/v water/methanol) containing 2.5 mL/liter 1.0 M NaOH, at a flow rate of 1.0 mL/minute and at a constant temperature of 30 °C and calibrated with narrow

polydispersity index (PDI) PEO standards. UV-Vis measurements were carried out on either a Perkin Elmer Lambda 900 UV/Vis/NIR Spectrophotometer or a Varian 'Cary 100 Bio' UV-Vis spectrophotometer. The results were analysed using the integrated software in each case. Dynamic scanning calorimetry (DSC) measurements were performed on a Perkin Elmer Pyris 1, from room temperature to 200^{o}C at a rate of 30^{o}C min^{-1} with three heat cool cycles. The T_g was determined from the third heat cycle. Thermogravimetric analysis (TGA) was performed using a Perkin Elmer Pyris 1 instrument. The sample was heated over a range from room temperature to 400^{o}C at a rate of 10^{o}C min^{-1}. The mass loss was followed and the decomposition temperature taken as the intercept between a tangent between two lines.

1.8.2 Polymer purification

Prior to their use both E60 and E400 were heated overnight to 120^{o}C and then dissolved in acetone (10% w/v) followed by precipitation into a 10 volume excess of diethyl ether. The polymer was then recovered by filtration and the process repeated a second time. The sample was then dried under vacuum and then heated under vacuum to 120^{o}C overnight and then stored in a desiccator.

The polymer was heated to 120^{o}C for 2h immediately before its use.

1.8.2.1 Characterisation of E60/E400

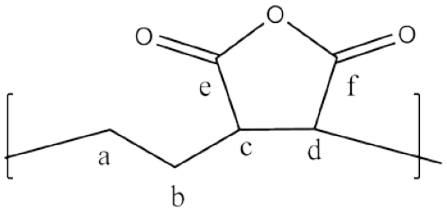

^{1}H NMR: δ_H (400MHz, d_6-DMSO) 3.2-2.9 (br, 2H, c, d); 2.15-1.5 (br, 4H, a, b)

^{13}C NMR: δ_C (100MHz, d_6-DMSO) 154.8, 26.1, 7.8

FTIR: ν_{max} (KBr)/cm^{-1}: 2939 C-H sp^3; 1859 anhydride C=O; 1777 anhydride C=O; 1224; 1099; 917;720

1.8.3 Hydrolysis (synthesis of hE60 and hE400).

E60 (2.00g, 0.05mmol) was added to distilled water (10mL) and stirred at 60^{o}C for 6h. The water was then removed by freeze drying. The hydrolysis of E400 (2.00g, 0.029mmol) was conducted by the same procedure as E60.

1.8.3.1 Characterisation of hE60 and hE400

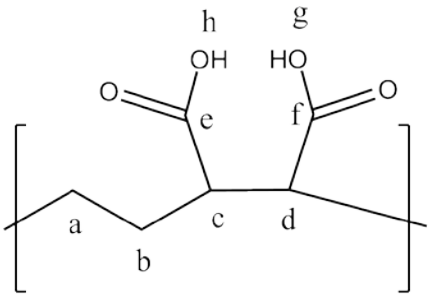

^{1}H NMR: δ_H (400MHz, D_2O) 2.9-2.68 (br, 2H, c, d); 1.8-1.4 (br, 4H, a, b)

^{13}C NMR: δ_C (100MHz, d_6-DMSO) 175.0, 46.37, 25.99

FTIR ν_{max} (KBr)/cm^{-1}: 3171 (broad) OH; 2939 C-H; 1708 (strong) C=O; 1454; 1193 acid C-O; 770

1.8.4 Acid number

hE60 (0.50g, 0.011mmol) was dissolved into $NaOH_{(aq)}$ (1M , 10mL). The polymer was then precipitated into THF (10mL) and removed by filtration. The THF was then removed from the filterate under vacuum. The resulting NaOH solution was then titrated against $HCl_{(aq)}$ (0.1M) to determine the final NaOH concentration. This was then used to calculate the number of moles of carboxylic acid on the starting polymer.

This procedure was repeated for hE400 (0.50g, 0.0071mmol).

1.8.5 Benzylamide E60 derivatives

E60 (0.5g, 0.012mmol, 0.004mol anhydride) was dissolved into anhydrous DMF (5mL). To this a 1.1 mole excess of benzylamine (0.46g, 0.0044mol) to anhydride was added dropwise. The solution was then allowed to stir for 10min before its precipitation into $HCl_{(aq)}$ (50mL, 0.5M). The polymer was isolated by filtration, and washed with distilled water. The polymer was freeze-dried to remove excess water.

This process was then repeated using amine/anhydride mole ratios of 0.8, 0.5, 0.2, and 0.1.

1.8.5.1 Characterisation of benzylamide E60 derivative

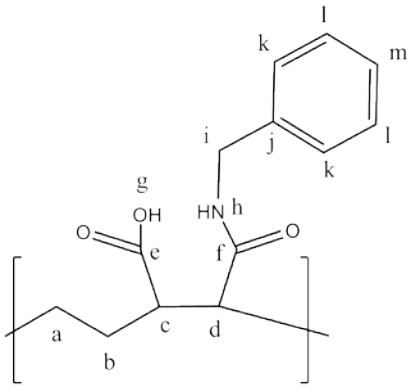

^{1}H NMR: δ_H (400MHz, δ_6-DMSO) 12.7-12.2 (br, 1H, g), 8.7-8.3 (br, 1H, h), 7.5-6.9 (br, 5H, j, k, l, m), 2.5-2.2 (br, ov, 2H, c, d), 1.8-1.1 (br, 2H, a, b)

^{13}C NMR: δ_C (100MHz, d_6-DMSO) 175.2, 173.1, 129.3, 127.7, 127.1, 46, 43, 26

FTIR ν_{max} (KBr)/cm^{-1}: 3100cm^{-1} (strong) amide N-H; 2930cm^{-1} (strong) C-H sp^3; 2500cm^{-1} (br, strong) acid OH; 1709cm^{-1} (strong) acid C=O; 1641cm^{-1} (strong) amide C=O; 1560cm^{-1} (strong) amide II band N-H; 1498 aromatic C=C; 1406 aromatic C=C; 1195 acid C-O.

1.8.6 Other E60 derivatives

E60 (0.5g, 0.012mmol, 0.004mol anhydride) was dissolved into anhydrous DMF (5mL). To this a 1.1 mole excess of amine (0.0044mol) to anhydride was added dropwise. The solution was then allowed to stir for 10min before its precipitation into $HCl_{(aq)}$ (50mL, 0.5M), isolation by filtration and washing with copious amounts of distilled water. Residual water was removed from the polymer by freeze drying.

This procedure was followed for N-methylbenzylamine (0.533g), hexylamine (0.445g), and napthylmethylamine (0.692g).

1.8.6.1 Characterisation of *N*-methylbenzylamide

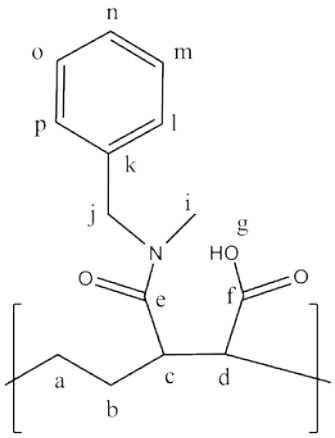

^{1}H NMR: δ_H (400MHz, δ_6-DMSO) : 12.5-12.1 (br, 1H, g); 7.4-7.0 (br m, 5H, p, o, n, m, l); 4.5-4.2 (br δ, 2H, j); 3.45-3.2 (br, 3H, i); 2.9-2.6 (br m, ov, 2H, c, d);´(1.8-1.1 (br, 2H, a, b).

1.8.6.2 Characterisation of hexylamide E60 derivative

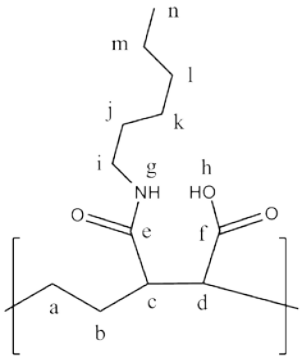

^{1}H NMR: δ_H (400MHz, d_6-DMSO) : 12.7-12.2 (br, 1H, h); 8.16 (br, 1H, g); 3.15-2.95 (br, 2H, i); 2.6-2.4 (br, ov, 2H, c, d); 1.7-1.2 (br m ov, 12H, a, b, j, k, l, m); 0.96 (br t, 3H, n)

1.8.6.3 Characterisation of napthymethylamide E60 derivative

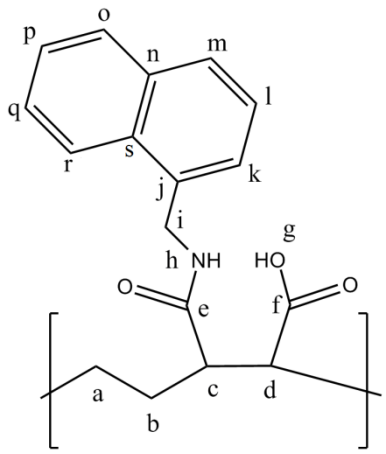

^{1}H NMR: δ_H (400MHz, δ_6-DMSO): 8.7-8.45 (br, 1H, η); 8.0-7.3 (br ov, 7H, k, l, m, o, p, q, r); 5.0-4.6 (br d, 2H, i); 2.8-2.4 (br ov, 2H, c, d); 1.7-1.2 (br, 4H, a, b)

1.8.7 Benzylimide synthesis

A sample of the benzylamine E60 derivative (see section 1.9.5) was ground into a fine powder and heated to 140oC under vacuum for 18h and then recovered without further purification.

1.8.7.1 Characterisation

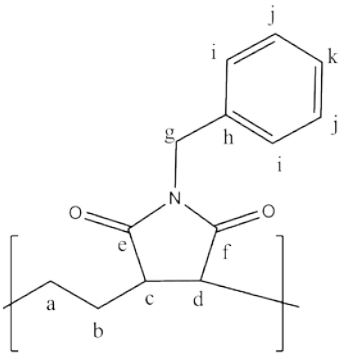

^{1}H NMR: δ_H (400MHz, δ_6-DNSO) : 7.4-7.34 (br m, 5H, i, j, k); 4.34 (br, 2H, g); 2.33-2.25 (br ov, 2H, c, δ); 1.8-1.2 (br, 4H, a, b)

^{13}C NMR: δ_C (100MHz, d_6-DMSO) 175.2, 140.0, 129.53, 129.3, 128.94, 127.7, 127.34, 126.1, 48.01, 39.51, 27.01

FTIR (KBr) : 3407 C-H sp^2; 2934 C-H sp^3; 1851 imide C=O; 1724 imide C=O; 1548 aromatic C=C; 1496 aromatic C=C; 1452 aromatic C=C; 1384; 1236

1.8.8 Benzyl alcohol esterification

1.8.8.1 Monoesterification

E60 (0.5g. 0.012mmol, 0.004mol anhydride) was stirred as a dispersion in toluene (100mL), and to this anhydrous benzyl alcohol (4.28g, 0.04mol) was added. The mixture was then refluxed in a Dean Stark apparatus for 18h at 140^{o}C. The toluene was then removed *in vacuo* and the excess benzyl alcohol removed by precipitation into dichloromethane (50mL). The polymer was then recovered by filtration.

1.8.8.2 Diesterification

The diesterification was performed using the same procedure as for monoesterification (1.9.8.1) but with the addition of p-toluene sulfonic acid (0.50g, 0.003mol) to the reflux mixture.

1.8.8.3 Characterisation of monoester

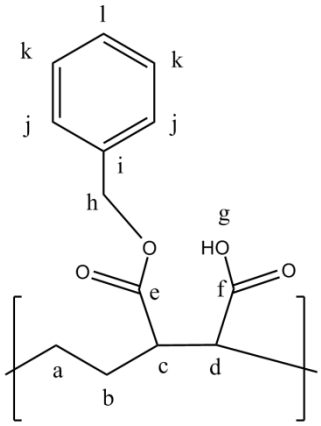

^{1}H NMR: δ_H (400MHz, d_6-DMSO) : 7.5-7.0 (br, 5H, i, j, k, l); 5.3-4.7 (br, 2H, h); 2.6-2.4 (br ov, 2H, c, d); 1.8-1.2 (br, 4H, a, b)

^{13}C NMR δ_C (100MHz, d_6-DMSO): 175.09, 173.65, 136.31, 128.79, 128.38, 126.90, 66.12, 48.23, 46.0, 26.29

FTIR ν_{max} (KBr)/cm^{-1}: 3600-2500 (strong, broad) acid OH; 3033(weak) C-H sp^2; 2956^{-1} (strong) C-H sp^2; 1731 (strong) ester C=O; 1709 (medium) acid C=O; 1497 (medium) aromatic C=C; 751, 699 (strong) aromatic C-H o.o.p.

1.8.8.4 Characterisation of di-ester

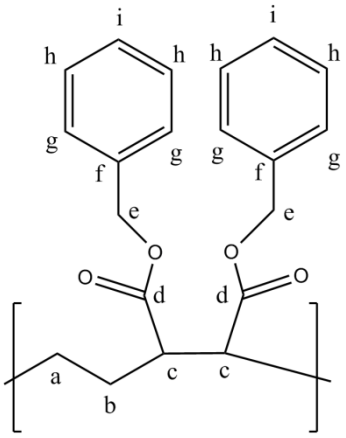

^{1}H NMR: δ_H (400MHz, δ_6-DMSO) : 7.4-7.0 (br, 10H, g, h, i); 5.25-4.75 (br, 4H, e); 2.75-2.25 (br, ov, 2H, c); 1.75-1.25 (br, 4H, a, b)

^{13}C NMR δ_C (100MHz, d_6-DMSO): 173.19, 136.0, 128.7, 127.03, 126.8, 66.3, 46.0, 26.8

FTIR ν_{max} (KBr)/cm^{-1}: 3036 (weak) C-H sp^2; 2965^{-1} (strong) C-H sp^3; 1711 (strong) acid C=O; 1497 (medium) aromatic C=C; 757, 697 (strong) aromatic C-H o.o.p.

1.8.9 Esterification kinetics

A series of E60 (1.00g, 0.024mol, 0.008mol anhydride) solutions were prepared with anhydrous DMF (10mL). To these solutions was added powdered molecular sieve (0.10g, 4Å) and the mixture maintained under a flow of dry nitrogen. Anhydrous benzyl alcohol was then added in differing amounts to the different solutions to give a final benzyl alcohol to anhydride mole ratio of 1:1, 2:5, and 5:2.

These solutions were then stirred and maintained at either room temperature, 50°C or 80°C. The mixtures were periodically sampled and the polymer recovered by precipitation into toluene and filtration through a celite plug. The polymers were then dissolved through the celite with acetone, precipitated into toluene and filtered through the celite plug a second time. The polymer was then washed off the celite plug with acetone and the solvent removed *in vacuo* to yield the final polymer. ^1H NMR (d_6-DMSO, 400MHz) was then conducted without further purification; the conversion to ester was determined by comparison of the ethylene peaks (1.7-1.2ppm) to methyl group α- to both the phenyl and carbonyl group.

1.8.10 Hydrolysis kinetics

1.8.10.1 E60 DMF solution calibration curve

A series of anhydrous DMF E60 solutions were prepared to a polymer concentration of between 3.17×10^{-5} and 4.13×10^{-4} mol dm^{-3} (anhydride concentration between 0.01 to 1.3 mol dm^{-3}). The absorbencies of these solutions were recorded at 475nm, the resulting curve of absorbance vs. anhydride concentration was then fitted to a polynomial.

1.8.10.2 Hydrolysis solution kinetics

A series of E60 water-DMF solutions were prepared to an anhydride concentration of 1.21 mol dm^{-3}. The amount of water within the solution ranged from 1, 5 and 10 mole excess to anhydride. The hydrolysis of these solutions was followed by UV-vis spectroscopy (475nm) at 40, 60, and 80^{o}C.

1.8.10.3 Heterogeneous hydrolysis

1.8.10.3.1 Vapour

E60 was ground into a fine powder and heated to 120^{o}C overnight. The powder was then weighed into a series of sample vials to a mass of ~100mg. These were then placed into a sealed oven with a beaker holding 200mL of distilled water. The oven was then heated to 40^{o}C and the vials removed periodically. The vials were then dried in a desiccator, weighed, heated under vacuum (120^{o}C, 18h) and weighed again. The degree of hydrolysis was then calculated gravimetrically. This procedure was repeated in triplicate.

The same procedure was then repeated at 60^{o}C and 80^{o}C.

1.8.10.3.2 In bulk water

Several dispersions were prepared by the addition of E60 (1.00g, 0.025mmol) to water (10mL) which had been preheated in a reflux apparatus to 40, 50 or 60^{o}C. The dispersion was allowed to stir for a period of time before it was rapidly frozen in liquid nitrogen. The water was then removed by freeze drying and the samples weighed, heated (120^{o}C, 18h) under vacuum and then weighed again. The degree of hydrolysis was then calculated gravimetrically. All experiments were conducted in triplicate.

1.8.11 Dehydration kinetics of hE60

hE60 was ground into a fine powder and a sample weighed into a TGA instrument. Dry nitrogen was then allowed to flow over the sample for 2h before it was rapidly heated to 90^{o}C. The sample was then held at this isotherm for 12h and the mass loss recorded. The loss of mass was attributed to the loss of water resulting from the dehydration of the hE60 di-acids.

This procedure was repeated at 120^{o}C, 140^{o}C and 150^{o}C.

The reaction product, E60, was confirmed by heating hE60 (0.10g, 0.0022mmol) to 120^{o}C under a flow of nitrogen for 18h. The product was then characterised by NMR and FT-IR.

1.8.12 Imidation kinetics

A sample of benzylamide E60 derivative (see section 1.9.5) was ground into a fine powder and weighed into a TGA pan. The sample was then held under a flow of dry

nitrogen for 2h before it was rapidly heated to 90^{o}C. The sample was then held at this isotherm for 12h and the mass loss recorded.

The reaction product, a benzylimide E60 derivative, was confirmed by heating a sample of benzylamide E60 derivative (0.10g, 0.0022mmol) to 120^{o}C under a flow of nitrogen for 18h. The product was then characterised by NMR and FT-IR.

1.8.13 Thermal analysis

1.8.13.1 Differential scanning calorimetry

Samples of E60 and E400 were ground into a fine powder heated (120^{o}C, 18h) and weighed into a DSC pan. The sample was then heated within the instrument from room temperature to 200^{o}C at a rate of 300^{o}Cmin^{-1} with three heat cool cycles. The T_g was determined from the third heat cycle.

1.8.13.2 Thermo-gravimetric analysis

Samples of E60 and E400 were ground into a fine powder heated (120^{o}C, 18h) and weighed into a TGA pan. The sample was then heated within the instrument from room temperature to 400^{o}C at a rate of 10^{o}C min^{-1}. The mass loss was followed and the decomposition temperature taken as the intercept between a tangent between two lines.

1.8.14 pKa

A sample of hE60 (0.50g, 0.011mmol, 0.0069mol of acid) was dissolved into water (50mL) to a carboxylic acid concentration of 0.069M. A sample of this solution

(10mL) was then titrated against $NaOH_{(aq)}$ (0.05M) and the pH followed. This process was repeated with hE60 (0.50g, 0.007mmol).

1.9 References

(1) Staudinger, H. *Berichte der Deutschen Chemischen Gesellschaft* **1920**, *53*, 1073.

(2) Morris, P. J. T. *Polymer Pioneers*; University of Pennsylvania Press: Pennsylvania, 1989.

(3) Cowie, J. M. G. *Polymers: Chemistry & Physics of Modern Materials*; 2 ed.; Blackie Academic & Professional: London, 1997.

(4) Klumperman, B. *Polymer Chemistry* **2010**, *1*, 558–562.

(5) R. G. Fordyce, G. E. H. *Journal of Polymer Science* **1948**, *3*, 891.

(6) R. G. Fordyce, G. E. H. *J. Am. Chem. Soc.* **1951**, *73*, 1186.

(7) E. Merz, T. A., G. Goldfinger *Journal of Polymer Science* **1946**, *1*, 75.

(8) T. Fukuda, A. G., Y Kwak, C. Yoshikawa, and Y. D. Ma *Macromolecules Symposium* **2002**, *182*, 53.

(9) Young, R. J.; Lovell, P. A. *Introduction to Polymers*; 2 ed.; Chapman & Hall: London, 1997.

(10) Ratzsch, M. *Prog. Poly. Sci.* **1988**, *13*, 227.

(11) Al-Roomi, Y. M.; Hussain, K. F. *Journal of Applied Polymer Science* **2006**, *102*, 3404–3412.

(12) John L. Lang, W. A. P., H. D. Clarey *J. Polym. Sci. Part A: General Papers* **1963**, *1*, 1123.

(13) Akperov, O. H.; Mamedova, R. E.; Akperov, E. O. *Materials Research Innovations* **2008**, *12*, 210-212.

(14) Braun, D.; Hu, F. *Journal of Macromolecular Science, Part A: Pure and Applied Chemistry* **2005**, *42*, 1127–1146.

(15) Zeng, W.; Shirota, Y. *Macromolecules* **1989**, *22*, 4204-4208.

(16) Cowie, J. M. G. *Alternating Copolymers*; Plenum Press: New York, 1985.

(17) Butler, G. B. *Pure Applied Chemistry* **1970**, *23*, 255.

(18) Wang, Z. M.; Hang, H.; Chung, T. C. *Macromolecules* **2005**, *38*, 8996.

(19) Priola, A.; Bongiovanni, R.; Gozzelino, G. *European Polymer Journal* **1994**, *30*, 1047.

(20) Heinen, W.; Rosenmoller, C. H.; Wenzel, C. B.; Groot, H. J. d.; Lutenberg, J.; Duin, M. v. *Macromolecules* **1996**, *118*, 705.

(21) Ruggeri, G.; Aglietto, M.; Petragnori, A.; Ciardelli, F. *European Polymer Journal* **1983**, *19*, 863.

(22) D. J. T. Hill, J. H. O. D., P.W. O'Sullivan *Macromolecules* **1985**, *18*, 9-17.

(23) P. C. Deb, G. M. *Polymer* **1985**, *26*, 629.

(24) Gaylord, N. G. *Journal of Polymer Science Part C* **1970**, *31*, 247.

(25) S. Iwatsuki, T. I. *Macromolek Chemie* **1967**, *104*, 263.

(26) E. Tsuchida, T. T. *Mackromol. Chem* **1971**, *141*, 265-298.

(27) M. Arnold, M. R. *Acta. polym.* **1981**, *32*, 300.

(28) C. Brevard, J. M. L. *J. Am. Chem. Soc.* **1970**, *92*, 4987.

(29) Klumperman, B. *Macromolecular Chemistry and Physics* **2006**, *207*, 861–863.

(30) Ratzsch, M. *J. Macromolec.Sci-Chem* **1987**, *A24*, 507.

(31) M. Ratzsch, M. A., V Steinert *Acta. polym.* **1985**, *36*, 8.

(32) M. Arnold, M. R. *Makromolek. Chem.* **1986**, *187*, 1593.

(33) Kombre, H. *Macromolecular Chemical Physics* **1995**, *196*, 669.

(34) Kombre, H. *Macromolecular Chemical Physics* **1996**, *197*, 343.

(35) Barr, D.; Davies, M. C.; Dawkins, J. V.; Hourston, D. J. *Polymer* **2005**, *46*, 1739-1753.

(36) Brouwer, H. D.; Schellekens, M. A. J.; Klumperman, B.; Monteiro, M. J.; German, A. L. *Journal of Polymer Science: Part A: Polymer Chemistry* **2000**, *38*, 3596–3603.

(37) Can, H. K.; Dogan, A. L.; Rzaev, Z. M. O.; Uner, A. H.; Guner, A. *Journal of Applied Polymer Science* **2005**, *96*, 2352–2359.

(38) Hu, Z.; Zhang, Z. *Macromolecules* **2006**, *39*, 1384-1390.

(39) L. Tong, J. P., Z. Zhang *Mackromol. Chem* **1988**, *190*, 1319-1324.

(40) M. Arnold; Raetzsch, M. *Plaste und Kautschuk* **1982**, *29*, 381-387.

(41) Wu, D.; Zou, Y.; Pan, C. *Chinese Journal of Polymer Science* **2002** *20*, 525-530.

(42) M. Ratzsch, G. S. *Acta. polym.* **1982**, *33*, 441.

(43) H. Kaperski, J. H., H K Roth and M Ratzsch *Physical Chemistry* **1978**, *259*, 167.

(44) Bonilla-Cruz, J.; Guerrero-Sánchez, C.; Schubert, U. S.; Saldívar-Guerra, E. *European Polymer Journal* **2010**, *46*, 298–312.

(45) Brouwer, H. D.; Schellekens, M. A. J.; Klumperman, B.; Monteiro, M. J.; German, A. L. *Journal of Polymer Science: Part A: Polymer Chemistry* **2000**, *38*, 3596–3603.

(46) Chernikova, E.; Terpugovab, P.; Buia, C.; Charleuxa, B. *Polymer* **2003**, *44*, 4101–4107.

(47) Han, J.; Silcock, P.; McQuillan, A. J.; Bremer, P. *European Polymer Journal* **2010**, *46*, 1824–1832.

(48) Vasile, C.; Bumbu, G.; I.Mylonas; Bokias, G.; Staikos, G. *Polymer International* **2004**, *53*, 1176–1179.

(49) G.Q. Chen, Z. Q. W., J.R. Wu, Z.C. Li, F.M. Li *Macromolecules* **2000**, *2000*, 1505.

(50) Wooley, S. H. a. K. L. *Chem. Comm.* **2005**, 3259-3261.

(51) D. Benoit, C. J. H., E. E Huang, Z. Lin, T. P. Russell *Macromolecules* **2000**, *33*, 1505-1507.

(52) Lessard, B.; Mari, M. *Macromolecules* **2010**, *43*, 879–885.

(53) E. T. A. van den Dungen, J. R., N. O. Pretorius, J. M. McKenzie, J. B. McLeary, R. D. Sanderson, B. Klumpermann *Austrian J. of Chem.* **2006**, *59*, 742-748.

(54) J. B. McLeary, F. M. C., J. M. McKenzie, M. P. Tonge, R. D. Sanderson, B. Klumpermann *Macromolecules* **2005**, *38*, 3151-3161.

(55) Koneig, K. E. *Macromolecules* **1983**, *16* 99.

(56) Appelhans, D. R.; Wang, Z.; Zschoche, S.; Zhuang, R.; Haussler, L.; Friedel, P.; Simon, F.; Jehnichen, D.; Grundke, K.; Eichhorn, K.; Komber, H.; Voit, B. *Macromolecules* **2005**, *38*, 1655-1664.

(57) Komber, H.; Steinert, V. *Macromolecular Rapid Communications* **2005**, *26*, 168–171.

(58) Werner, K.; Komber, H.; Reinhardt, S.; Steinert, V. *European Polymer Journal* **1998**, *34*, 327-333.

(59) M. Ratzsch, S. Z., V. Steinert, K. Schlothaur *Mackromolekular Chemie* **1986**, *187*, 1669.

(60) Komber, H. *Macromolecular Chemical Physics* **1995**, *196*, 669.

(61) Komber, H. *Macromolecular Chemical Physics* **1996**, *197*, 343.

(62) Koenig, K. E. *Macromolecules* **1983**, *16*, 99.

(63) B. Bacskai, L. P. L., D. L. Rabenstein *Journal of Polymer Science Part A* **1972**, *10*, 1297.

(64) M Ratzsch, S. Z., V. Steinert, *Journal of Macromolecular Science: Chemistry* **1987**, *A24*, 949.

(65) K. Werner, V. S., S. Reinhardt *Macromolecules Rapid Communications* **1995**, *16*, 673.

(66) Hu, G. H.; Lindt, J. T. *Polymer Bulletin* **1992**, *29*, 357-363.

(67) Donati, I.; Gamini, A.; Vetec, A.; Compa, C.; Paoletti, S. *Biomarcomolecules* **2002**, *3*, 8025.

(68) Bergbreiter, D. E.; Liu, Y. S. *Tetrahedron Letters* **1997**, *38*, 3703.

(69) Marcucci, F.; Gregory, R. US 6172202, 2001.

(70) Serbin, A. V.; Kareva, G. Y.; Stotskaya, L. L.; Krentsel, B. A. *Vysokomolekulyarnye Soedineniya, Seriya A* **1989**, *31*, 1975-1982.

(71) Stoilova, O.; Ignatova, M.; Manolova, N.; Godjevargova, T.; Mita, D. G.; Rashkov, I. *European Polymer Journal* **2010**, *46* 1966–1974.

(72) Russel, G. S. WO 9109883, 1991.

(73) Stamm, W. US 3725508, 1971.

(74) Morduchowitz, A. US 3810276, 1974.

(75) O'Rogne *Perkin Transactions II* **1972**, *4*, 472.

(76) M. Ratzsch, N. T. H. *Acta. polym.* **1979**, *30*, 93.

(77) M. Dror, M. L. *Perkin Transactions II* **1974**, *1425*.

(78) Uzawa, H.; Ito, H.; Izumi, M.; Tokahisa, H.; Tasuchi, K.; Minaura, N. *Tetrahedron* **2005**, *61*, 5895.

(79) Chiellini, E.; Leonardi, G.; Giannasi, D.; Solaro, R. *Journal of Bioactive and Compatible Polymers* **1992**, *7*, 161-174.

(80) Singhal, R.; A. Mishra; Nagpal, A. K.; Mathur, G. N. *Journal of Polymer Materials: An International Journal*, *27*.

(81) M. Ratzsch, B. W. *Acta polym.* **1986**, *37*, 708.

(82) M Ratzsch, V. S., K Schlothaur *Mackromolekular Chemie* **1986**, *187*.

(83) Evenson, S. A.; Fail, C. A.; Badyal, J. P. C. *Journal of Physical Chemistry Part B* **2000**, *104*, 10608.

(84) Caykara, T. *Journal of Applied Polymer Science* **2004**, *92*, 763-769.

(85) Ignatova, M.; Stoilova, O.; Manolova, N.; Markova, N.; Rashkov, I. *Macromolecular Bioscience* **2010**, *10*, 944–954.

(86) Koskikallio, L. *Acta Chim. Scandinavia* **1956**, *10*, 822.

(87) Lee, S. S.; Ahn, T. O. *Journal of Applied Polymer Science* **1999**, *71*, 1187.

(88) Lee, Y. C. US 4108913, 1977.

(89) Tuchibana, T.; Inokuch, K.; Inokkuchi, T. *Nature* **1955**, *176*, 1119.

(90) Piret, W. H.; Masson, N. A. US 6896963, 2005.

(91) Kumar, L. D.; Schobel, A. M. US 4980391, 1990.

(92) Prosise, W. E. US 5286764, 1994.

(93) Black, S. A.; Feinston, W. H. US 3821363, 1974.

(94) Rowe, C. T.; Foster, S. L. US 5427690, 1995.

(95) Lee, F.; Fearnley, C.; Fordham, G. H. US 4083794, 1978.

(96) Miyoshi, T.; Kishida, S. US 968531, 1999.

(97) Jan, B.; Jia-Huey, H.; Ho, C. W.; Liu, Y. C.; Pan, C. C.; Chow, Z. S.; Chang, Y. S.; Wa, C. T.; Kuo, W. H. US 6960468, 2005.

(98) Chakrabarti, P. M. US 4178204, 1979.

(99) Bianchi, E.; Ciferri, A.; Parodi, R.; Tealdi, A. *Journal of Polymer Chemistry* **1970**, *74*, 1050.

(100) A. W. Schultz, U. P. S. *Journal of Physical Chemistry* **1972**, *76*.

(101) J. J. Christennen, R. M. I., L. D. Hansen *Journal of the American Chemical Society* **1967**, *89*.

(102) Garnier, G.; Duskova-Smrckura, M.; Vyhnalkova, R.; Ven, T. G. M. v. d. *Langmuir* **2000**, 3757.

(103) McCormick, C. L.; Chang, Y. *Macromolecules* **1994,**, *27*, 2151-2158.

(104) Bunton, C. A.; Fendler, J. H. *Journal of Organic Chemistry* **1965**, *30*, 1365.

(105) Lee, Y. C.; Sheth, A.; Mikker, J. M. *ParmSciTech* **2006**, *7*, 65.

(106) Lee, Y. C.; Sheth, A.; Miller, J. M. *PharmSciTech* **2006**, *7*, 65.

Chapter Two: Ice Crystal Growth Inhibition

2.1 Literature review

2.1.1 Introduction

It is necessarily the case that organisms which are exposed to temperatures at or below the freezing point of water require a mechanism of protection. This is because the formation of ice within the organism has two effects: dehydration resulting from the unavailability of the liquid water required for normal metabolic processes,[1] and physical injury incurred by ice re-crystallisation,[2] a spontaneous process in which small ice crystals coalesce into large, damaging masses of ice.[3]

'Warm blooded' organisms solve this problem by regulation of their metabolic rate in order to maintain thermal homeostasis regardless of the ambient temperature.[4] However, many organisms, including plants,[3] insects[5] and polar fish,[6] have evolved a series of proteins and glyco-proteins which are capable of mitigating the damage caused by ice. There has been a sustained interest in these macromolecules because of their potential application in the fields of cryomedicine and food preservation.

There are two general types of biological antifreeze molecules: antifreeze glyco-protein (AFGP) and antifreeze proteins (AFP). The effect of these molecules on ice crystal formation include: non colligative freezing point depression; dynamic ice shaping; and inhibition of recrystallisation (RI).

This effect is distinct from colligative freezing point depression which results merely from the presence of solutes reducing the chemical potential of the solvent. The

colligative freezing point depression occurs as the dissolved material is unable to form part of the growing solid particle. As a result, the equilibrium between liquid and solid which is normally established in pure solvents at their freezing point is disrupted and is not attained until lower temperatures. A non-colligative freezing point depression is an effect which does not simply affect the equilibrium attained at the freezing point, rather it causes a thermal hysteresis (TH) in which the freezing point (T_F) decreases but the melting point (T_m) remains constant. The molecule causing a non-colligative freezing point depression is acting to stabilise the liquid phase relative to the solid phase.[7]

Recrystallisation describes the spontaneous, thermodynamically driven, process in which ice crystals coalesce to form larger ones or larger crystal grow at the expense of smaller ones. The latter process is, in fact, an example of Ostwald ripening, the physical origin of which is the relatively high free energy of molecules at interfaces compared with those in the bulk. In other words, smaller ice crystals are of higher energy than larger ones due to their higher surface area to volume ratios. As a result, molecules at the interfaces migrate from smaller ice crystals to larger ones. The rate of coalescence is proportional to the total surface area of the sample, consequently as recrystallisation continues the total surface area decreases and the process slows to a halt. AF(G)Ps are able to inhibit this process, the mechanism by which this occurs is discussed later. For clarity it is worth noting that recrystallisation can refer to other processes which involve the correction of defects within or at the surface of crystals, however, for the remainder of this work recrystallisation should be understood as being synonymous with crystal coalescence.[8]

The final effect of ‘antifreeze activity’ is dynamic ice shaping which describes the process by which AF(G)Ps alter the shape of growing ice crystals away from the normal structure. The final shape of the crystal is thought to indicate as to which crystal faces the AF(G)P is bound.[9]

Although qualitative links between these phenomena have been suggested,[10] they do not appear to be interdependent, indeed there are examples of RI active molecules which display little or no TH activity.[3,11]

In summary, these biological macromolecules not only have interesting properties but real commercial value. However, the current costs of AFP and AFGPs make them unsuitable for bulk applications and therefore inexpensive antifreeze polymers would represent an improvement in the field.

2.1.2 Structure of Antifreeze (glyco) proteins

AF(G)Ps were first identified in studies of the blood serum of polar fish.[12,13] Over time, four classes of structurally diverse AFPs were identified and classified as type I, type II, type III and type IV (table 2-1).[14] In addition, a single class of glycosylated proteins were identified as being involved in inhibiting the formation and growth of ice.[6]

Table 2-1: Characteristic structural properties of antifreeze proteins. Reprinted from Harding *et al.*[6]

Characteristic	AFGP	Type I AFP	Type II AFP	Type III AFP	Type IV AFP
Mass (Da)	2600-33000	3300-4500	11000-24000	6500	12000
Structure	Ala-Ala-Thr repeat; disaccharide	Alanine rich α-helix	Disulfide bonded	β sandwich	Alanine rich helical bundle

The structural diversity of AFPs suggests that secondary structure alone is not enough to explain their activity. However, studies on oligo- and poly-peptide model compounds have demonstrated that primary structure is not enough to explain activity either.[1,15] Despite the unlikely prospect that a simple relation would be found, much research has focussed on structure-function relationships.[1,16-20] In aggregate, these results point to the importance of some form of well defined structure or conformation but not any particular secondary structural motif.

In contrast to the structural complexity of AFPs, the structure of AFGPs is predictable and relatively well understood (figure 2-1).

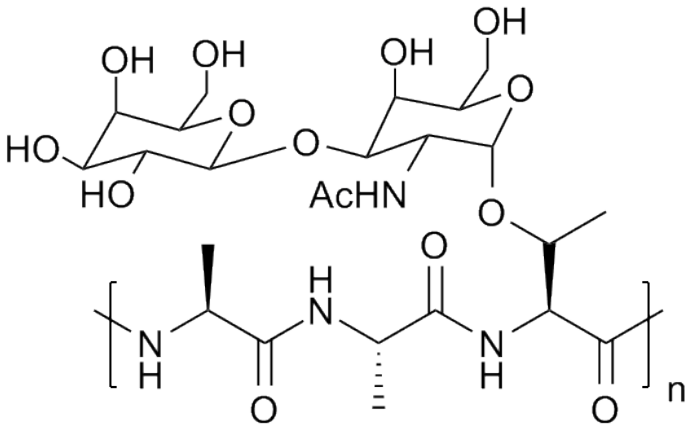

Figure 2-1: Schematic representation of AFGP. Bond angles and conformation are to direct the eye only.

Despite the relative structural simplicity of AFGP, it exists in at least eight different molecular weights varying between 2.6 and 34kDa.[6] These are characterised as $AFGP_x$ where x = 1 to 4 are of high molecular weight and x= 5 to 8 are low molecular weight. In addition to this, recent work has identified $AFGP_6$ as being composed of two fractions at 6026Da and 9784Da in 14 different isoforms.[21] The predominant observation regarding AFGPs is that activity is linked with molecular weight and, possibly, with the solution conformation of the glycoside.

2.1.3 Mechanism of action of antifreeze glycoproteins

The first hypothesised mechanism by which AFPs act was put forward by DeVries who suggested that they bind to the surface of the ice crystal through strong hydrogen bonds, the presence of the AFP on the surface then prevents the normal growth of the ice crystal.[13] An adsorption mechanism can be inferred from the ability of AFPs to alter the shape of growing ice crystals. Pure water, when flash frozen, will form disc shaped ice crystals (figure 2-2 (b)), however, the introduction of an AFP results in the

shaping of ice crystals into hexagonal prisms (figure 2-2 (c)) with the degree of shaping becoming more pronounced with increasing concentration (figure 2-2 (c-e)).

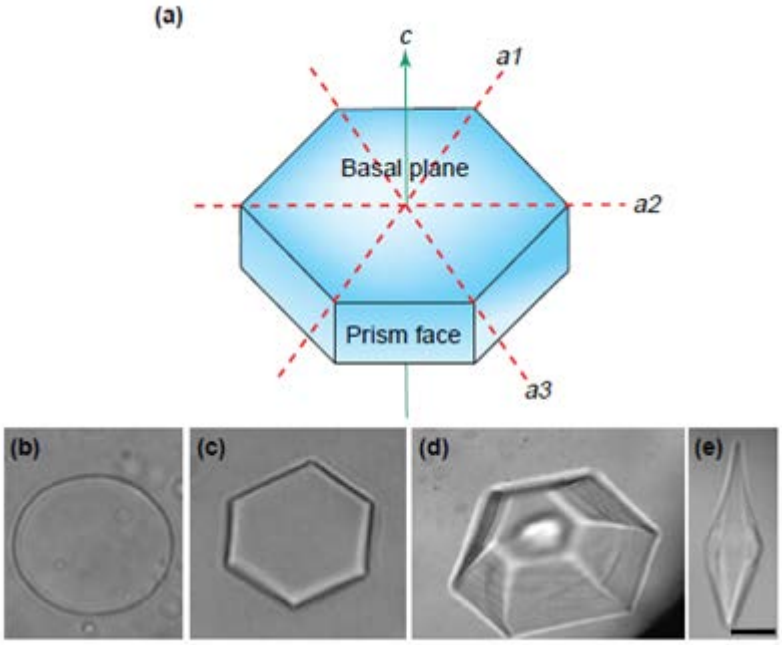

Figure 2-2: (a) the structure of hexagonal ice. (b) in water, or a solution of 'antifreeze' inactive substances, ice forms a disc shaped crystal. (c) In dilute solution, AFPs bind to the prism faces creating hexagonally shaped crystals. (d) Adsorption of AFPs on the prism face inhibits the binding of further water molecules making it energetically favourable for the basal plane to grow. (e) At high concentration AFPs force the ice crystals into bipyramidal structures with hexagonal cross-section. Scale 200µm Reprinted from Griffiths *et al.*[14]

In the absence of AFP, the basal plane of hexagonal ice is the slowest growing. However, the formation of bi-pyramidal structures in the presence AFPs (figure 2-2(e)) demonstrates that the basal plane is growing at a faster rate than the prism faces.[18] From this it has been inferred that, typically, AFPs have a greater affinity for the prism face over the basal plane. Chao *et al.*'s[22] examination of the activity of

representative AFPs from type I and II demonstrates that in all cases the AFPs were more active against the prism face than the basal face resulting in preferential growth along the c axis.

Neutron scattering experiments on the adsorption of AFPs on ice surfaces have demonstrated that, at concentrations associated with activity, the adsorption of AFP was at sub-monolayer levels.[23] Evidence such as this has led Knight[24] to propose a mechanism wherein the AFP binds and then 'pins' the ice. Briefly, the AFP binds tightly to the surface, preventing the growth of ice at the point of binding. As a result further crystal growth in the locality of the adsorbed AFP requires the opening of new growth planes, thereby lowering the localised T_f due to the Kelvin effect which describes the phenomena by which curved liquid surfaces are of higher vapour pressure than flatter liquid surfaces. In the context of ice in water an increase in the ice surfaces curvature will result in the equilibrium at the surface shifting in favour of the liquid phase thereby inhibiting further growth.[3]

In order for this effect to occur, it is necessary that the molecule be tightly bound to the surface of the ice to prevent it merely being pushed ahead of the advancing crystal face [18] The mechanism by which this binding occurs is a matter of debate. DeVries originally proposed a model of AFP activity involving the tight binding of the molecule to the ice crystal's surface through hydrogen bonding.[9] This model has supported by studies on peptide AFP mimics which suggest that hydrogen bonding, as opposed to hydrophobicity, is important in the binding mechanism.[16,19]

However, this has since been somewhat undermined by mutation studies which demonstrate that the removal of hydrophilic amino acids from the proposed binding face of AFPs does not, necessarily, result in the loss of activity.[25,26] Consequently, an alternative hypothesis was proposed by Yang *et al.* who suggested that the binding face is a flat, hydrophobic surface.[18,27] The physical origin for its binding is rationalised as the increase in entropy as the AFP sheds its hydration sphere.

Further complicating the situation is the apparent specificity of AFP for the prism faces of the ice. It has been suggested that the secondary structure plays a role in ensuring good complementarity, and by extension tight binding.. However, each attempt to rationalise specific activities or attributes to a particular secondary structure, as occurred with the discovery of hyperactive AFPs, has been countered with examples of other structures which exhibit the same attributes.[28,29]

Therefore, the evidence suggests that secondary structure alone cannot be used to explain the activity nor can activity be attributed to an abundance of hydrogen bonding or hydrophobic groups.

Siemer *et al.'s* solid state NMR study of a ^{13}C and ^{15}N enriched type III fish AFP demonstrated that seven hydrophilic amino acid residues on the proposed binding face underwent significant shifts when in the presence of frozen water (figure 2-3).[30]

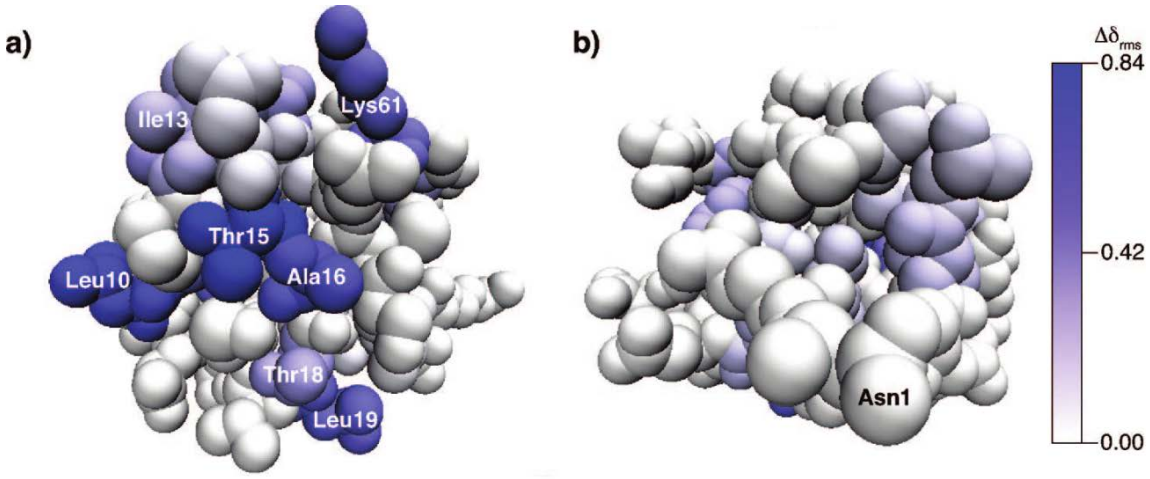

Figure 2-3: Relief representation of the solution-state NMR structure of type III AFP isoform HPLC-12. (a) view normal to the proposed ice binding surface each amino acid is coloured according to the rms ^{13}C change in chemical shift between water and ice with white indicating no change and dark blue indicating a maximum change. (b) as (a) but protein rotated 180^{o} to shoe non-ice binding site. Reprinted from Siemer *et al.*[30]

This indicates a strong hydrogen bonding interaction between a small number of hydrophilic amino acids and the surface of ice. However, despite the apparent importance of these hydrogen bonding groups, it is also the case that 52% of the ice binding surface in Siemer *et al.'s* study is composed of non-hydrogen bonding residues, and as previously discussed, mutation studies have demonstrated that hydrophobic residues play an important role in activity. Indeed, mutation and structural studies of type III AFPs have shown while the hydrophilic residues Gln 9, Asn 14, Thr 15, and Gln 44 are conserved across species,[31-33] the truncation of flanking hydrophobic residues significantly reduces the antifreeze activity.[34]

The combined evidence indicates that both hydrophilic and hydrophobic groups play a role in the binding activity of AFPs but that this synergistic activity is not simply expressed through the secondary structure adopted. Evidence for this is provided in the modelling work of Smolin and Daggett.[35] The results (figure 2-4) indicate that water in the first hydration sphere of the ice binding face adopts a tetrahedral arrangement close to that of ice. This implies the binding environment is tailored to ensure the enthalpy of the AFP-ice binding to ice is close to that of water-ice binding, thereby ensuring tight, irreversible protein binding.

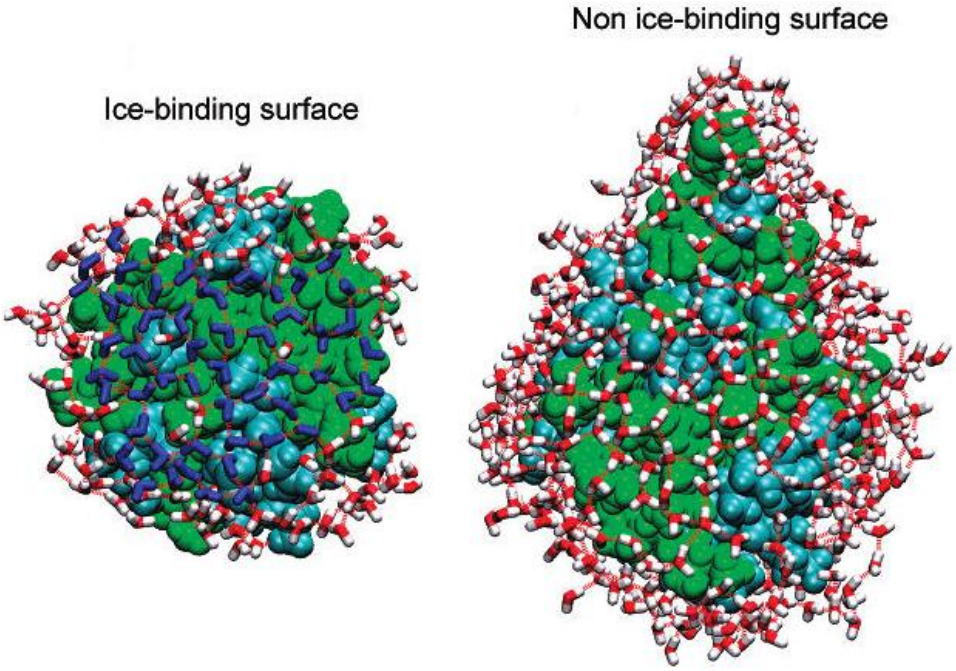

Figure 2-4: Molecular dynamics image of Type III fish AFP in water. Green surfaces represent hydrophobic residues, pale blue hydrophilic residues. Blue solvent molecules represent tetrahedral "ice like" water. Reprinted Yang *et al.*[27]

The evidence indicates that while overall secondary structure is not an indication of activity, the ability of the ice binding face to 'fit' the ice surface is dependent on how the secondary structure local to the ice binding face shapes the hydration layer. This

model is augmented by the experiments of Zelent *et al.*[36] who studied the changes in amide I and II IR bands of AFP mimic polypeptides while in an aqueous solution undergoing freeze thaw cycles. The results demonstrated that both poly-L-arginine and AFPs give no change in their amide I bands between the liquid and frozen state, which is interpreted as being indicative that the structure of the hydrating water is close to that of ice.

Consequently, the mechanism of AFP activity appears to fit the original DeVries model even if the mechanism of the binding does not. In other words, surface binding and pinning is still the accepted hypothesis in explaining antifreeze activity but the nature of that binding appears to be much more subtle than previously believed.

2.1.4 Antifreeze glycoproteins and their synthetic mimics

The current evidence for AFPs points to a bind and pin mechanism based on the pre-ordering of the hydrated water; the mechanisms of action of AFGP and synthetic 'antifreeze' polymers however is less clear. Indeed, a range of structures, in addition to AFGP, which give rise to activity include: poly(vinyl alcohol)s,[37] polyglycidols,[38] polytartars,[39] and certain polypeptides.[19] In most of these cases there is little evidence of a rigid, ordered structure as in the case for AFPs. However, their solution conformation does appear to play a role, [11,4] as does molar mass.[21]

The importance of hydrogen bonding was investigated by Hederos *et al.*[41] in their modelling of AFGP using self assembled monolayers (SAMs). This involved the introduction of two different thiol amides, one bearing a terminal methyl group the other the AFGP disaccharide, in varying relative concentrations. The result was to

produce a series of surfaces with varying relative amounts of disaccharide and methyl groups (see figure 2-5).

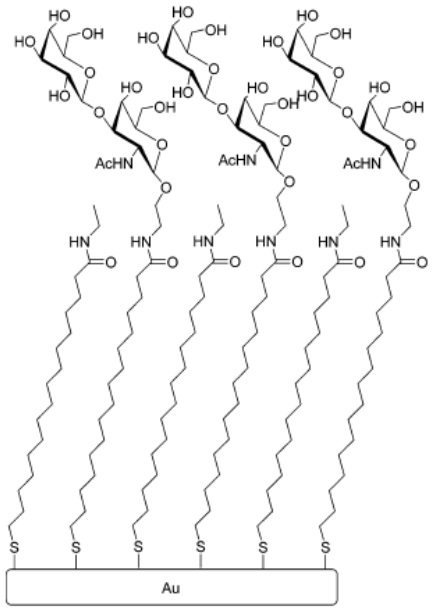

Figure 2-5 Schematic representation of the surfaces tested by Hederos *et al.*[41]. Reprinted from Hederos *et al.* [44]

The surfaces were then analysed by cooling the substrates in a chamber at a controlled humidity, the temperature at which ice crystals were observed to form (T_c) was then used as a measure of antifreeze activity. The results demonstrated that surface energy is inversely proportional to the T_c. It was also observed that T_c increases when the disaccharide is substituted with a hydroxyl group, the activity decreases even when the surface energies are engineered to be equivalent. This indicates two things: firstly, that hydrogen bonding is important to activity and secondly, that the nature of the hydrogen bonding group, or perhaps the density of hydrogen bonding groups, is important to activity. The importance of the presence of hydrogen bonding groups, all else being equal, is also demonstrated by studies on poly(vinyl alcohol-co-vinyl acetate)s with varying amounts of acetates.[42]

Gibson *et al's*[40] analysis of a series of different hydrogen bonding polymers (figure 2-6) demonstrated that RI activity had the following trend carboxylic acid < amine < hydroxyl.

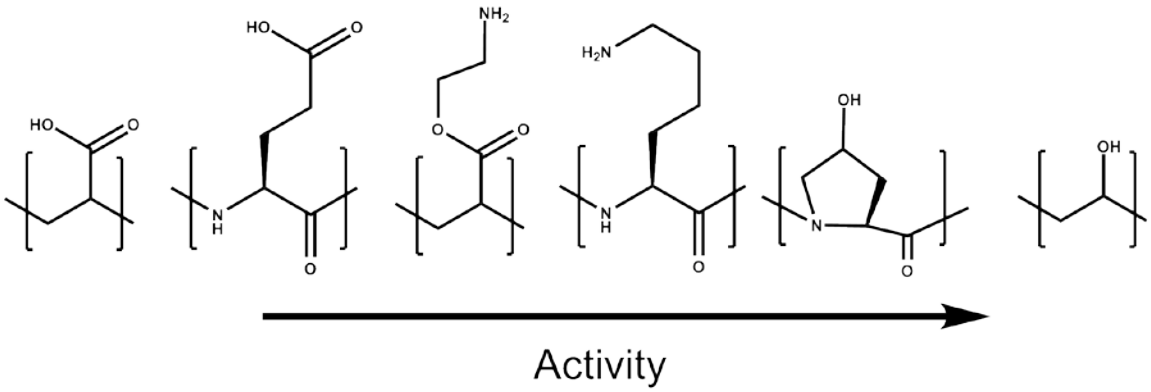

Figure 2-6: Macromolecules tested for RI activity by Gibson *et al.*[40]

However, it is not possible to explain the trend in activity simply in terms of hydroxyl concentration. Gibson *et al*[43] compared the activity of a series of glycopolymers with poly(vinyl alcohol) and demonstrated that, despite the higher proportion of hydroxyl per unit mass, the saccharide polymers are less active than poly(vinyl alcohol).

The importance of complementarity to the ice surface is a concept which has been pursued vigorously in the study of AFPs. Indeed, the ice shaping property of many 'anti freeze' macromolecules necessarily means that some faces of the ice crystal must be more strongly affected than others which implies the macromolecules preference for that surface. For example: poly(vinyl alcohol) demonstrates strong RI activity[37], marginal thermal hysteresis[42] and a strong capacity for ice shaping.[3] While there is

some evidence that PVA presents a strong complementarity to the surface it is not the result of an elegant structural motif, rather of an abundance of hydroxyl groups and a flexible backbone which allows the polymer to adopt a conformation that maximises its contact with the ice surface (figure 2-7 (i) and (j)).

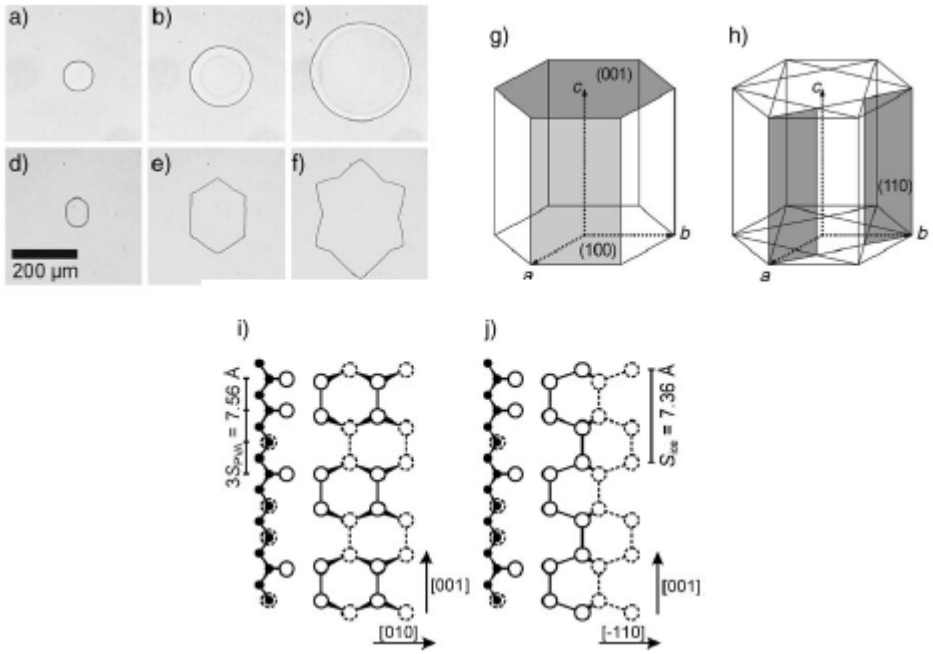

Figure 2-7: (a-c) Growth of ice in pure water, (d-f) growth of ice with increasing aqueous poly(vinyl alcohol) concentration, (g-h) prism planes of hexagonal ice, (i-j) proposed binding mechanism of poly(vinyl alcohol) to ice crystal planes. Reprinted and adapted from Koop *et al*.[3]

Further indications that conformation plays a role in activity despite the lack of formal secondary structure is highlighted by Ben *et al*[46] who synthesised a series of C and O linked glycosides with varying linker lengths between the H-bonding unit and the backbone (figure 2-8).

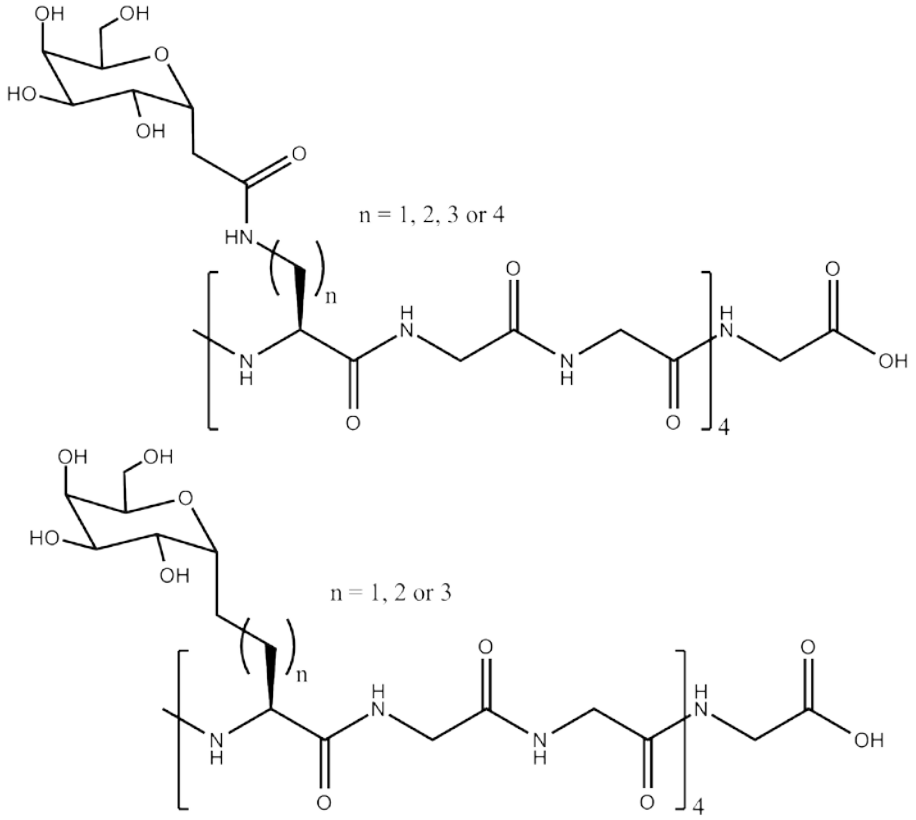

Figure 2-8: Structure of AFGP mimics synthesised by Ben *et al*.[43]

In both cases, activity was observed when n = 3 (figure 2-8) with little or no activity when n≠3. This behaviour cannot be attributed to long range structures as circular dichroism (CD) demonstrates, in all cases, that the structure is random coil. In addition, NMR studies also discount the possibility of hydrogen bonding between the peptide backbone and carbohydrate. However, molecular dynamic simulations do suggest that when n=3 the sugar moiety sits in a conformation which placed it physically close to the peptide backbone.[43] This observation correlates well with evidence that native AFGP-8 adopts a similar conformation wherein the glycoside is orientated toward the backbone hypothetically via intramolecular hydrogen bonds between the hydroxyls and backbone amides.[44,45] The hypothesis put forward by Ben

et al. was that the conformation is favourable to ice binding which in turn explains their RI activity.

However, later work by Ben *et al*.[46] went onto examine the activity of a variety of glycoside bearing peptides where the variable is the identity of the saccharide unit. It was found that RI activity is inversely proportional to the molar compressibility of the sugar moiety (figure 2-9).

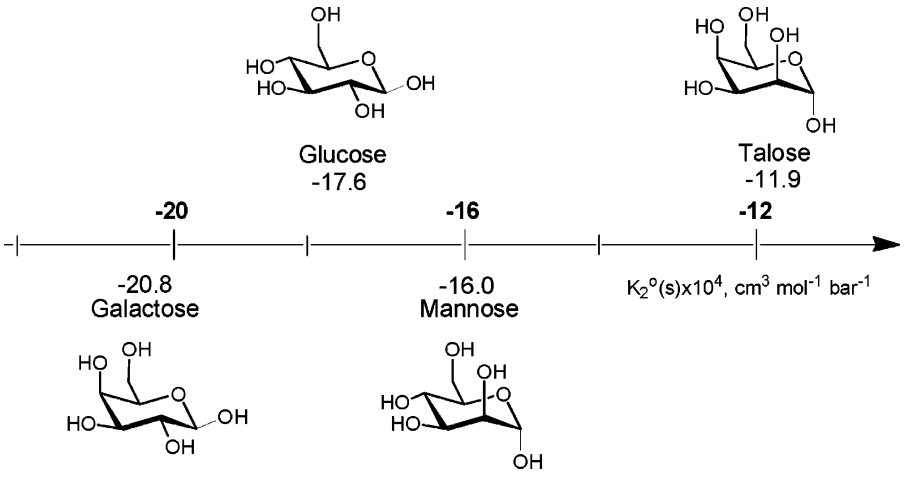

Figure 2-9: Partial molar compressibility of monosaccharides.

Reprinted from Ben *et al*.[46]

From this they were able to demonstrate that the hydration index (the ratio of hydration number to molar volume) correlates extremely closely to their RI activity. In rationalising this, Ben *et al* departed from the bind and pin model proposed by Knight to explain AFP activity.[24] Instead they propose a model which involves the polymers presence in the quasi liquid layer (QLL) which exists between ice crystal interfaces. The hypothesis is that the more hydrated sugars distort the structure of the QLL water, thereby preventing it from reorganising ahead of coalescence. In contrast,

the less well hydrated sugars do not impact so greatly on the QLL layer and therefore are not as potent in RI.

This concept is somewhat contradicted by Gibson *et al.*[40] who synthesised two glycoside methacrylates and tested their RI activity (figure 2-10).

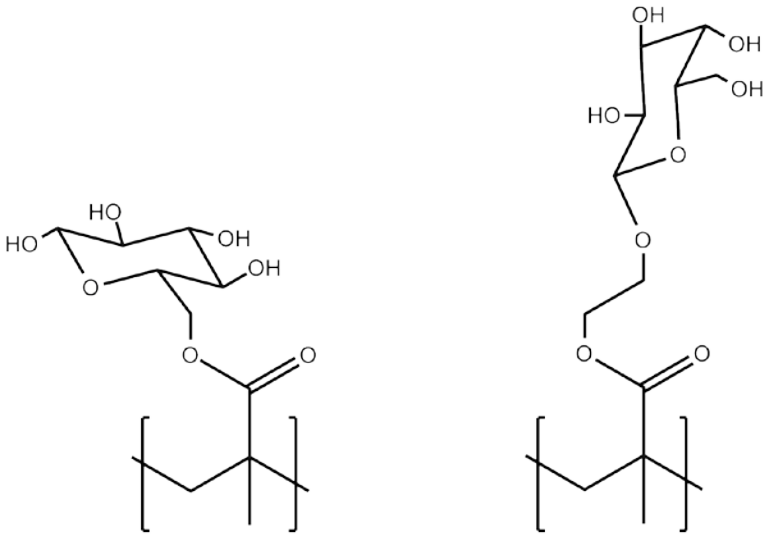

Figure 2-10: Structure of glycopolymers synthesised by Cameron *et al*.[40]

Despite the superior RI activity of galactose with respect to glucose demonstrated by Ben *et al.*, the glucose methacrylate was shown to be more active than the galactose methacrylate. This was attributed to the longer linker lengths between the methacrylate backbone and the galactose compared with the glucose methacrylate. This fits in with the RI potency of poly(vinyl alcohol); the linker length in PVA is zero placing it close to the backbone.[3] The rationale for this apparent trend was

suggested by Gibson *et al.* to be the result of shorter linker lengths allowing for tighter binding of the polymer to the ice crystal's surface.

Another important attribute in 'antifreeze' activity is molecular mass. It has been observed that a greater TH occurs for AFGPs with higher molecular masses.[16] Indeed, the low molecular weights AFGPs demonstrate only two thirds the activity of higher molecular weight AFGPs. Similarly, there are reports that higher molecular mass PVAs have more pronounced TH[3] and RI[40] activities. Rationalising this remains a problem with no obvious explanation as to why this correlation should exist.

To date an explanation of activity in AFGP and its mimics remains unclear. What has been established is that RI activity appears to be dependent on molecular mass, chemical structure and solution conformation. Unlike AFPs, there is not even a consensus of the mechanism of action, at least in regard to RI activity, with evidence being presented which supports both the bind and pin model and QLL disruption model of RI activity.

2.2 Aim

The ability for E60 to undergo reaction with amines in a quantitative and controlled manner opens up the possibility to make several, structurally different polymers, in a trivial way. The polymer's regular structure means the composition of the final polymer post reaction is predictable as 100% conversion to the amide preserves the alternating copolymer structure. If reacted with a mixture of amines sequentially the end product is that of a random copolymer (chapter 1).

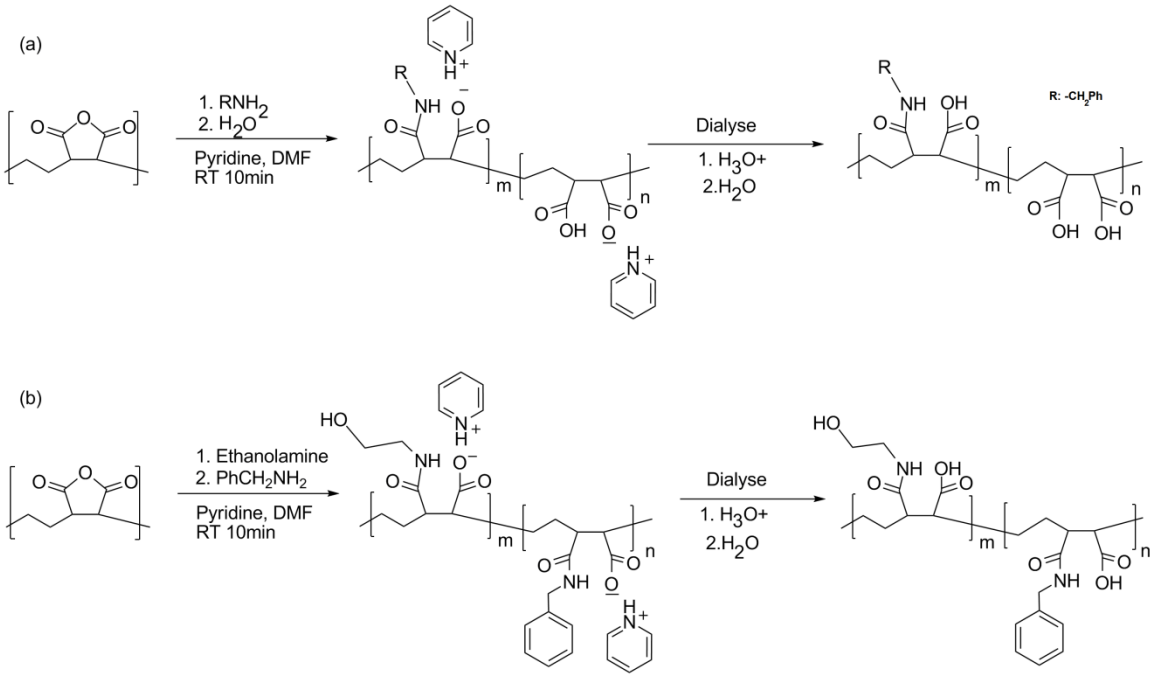

Figure 2-11: Reaction scheme for the production of RI active polymers: (a) production of benzylamide ethanolamide copolymer. (b) reaction production of alcohol bearing polymers m = 63 to 315, n = 0 to 315 Note reactions are assumed to occur randomly along the polymer chain

With this in mind, it is possible to see how this polymer could be useful in probing the factors which determine the RI activity of macromolecules. It allows structural changes to be made easily while fixing other variables such as backbone structure and degree of polymerisation. In addition, the polymer is commercially available and inexpensive compared with AFGP. Consequently this presents the opportunity to develop a synthetic route to inexpensive RI polymers (figure 2-11).

As the literature review has demonstrated there are several variables which are believed to impact on RI activity including: hydrogen bonding; molecular mass; the composition of the polymer backbone; the presence of hydrophobic groups, and the distance between the backbone and the hydrogen bonding component. Therefore, a series of E60 derivatives were synthesised in order to probe the relation between composition, hydrophobicity and structure (figure 2-12, table 2-2), and these are referred to through-out the chapter.

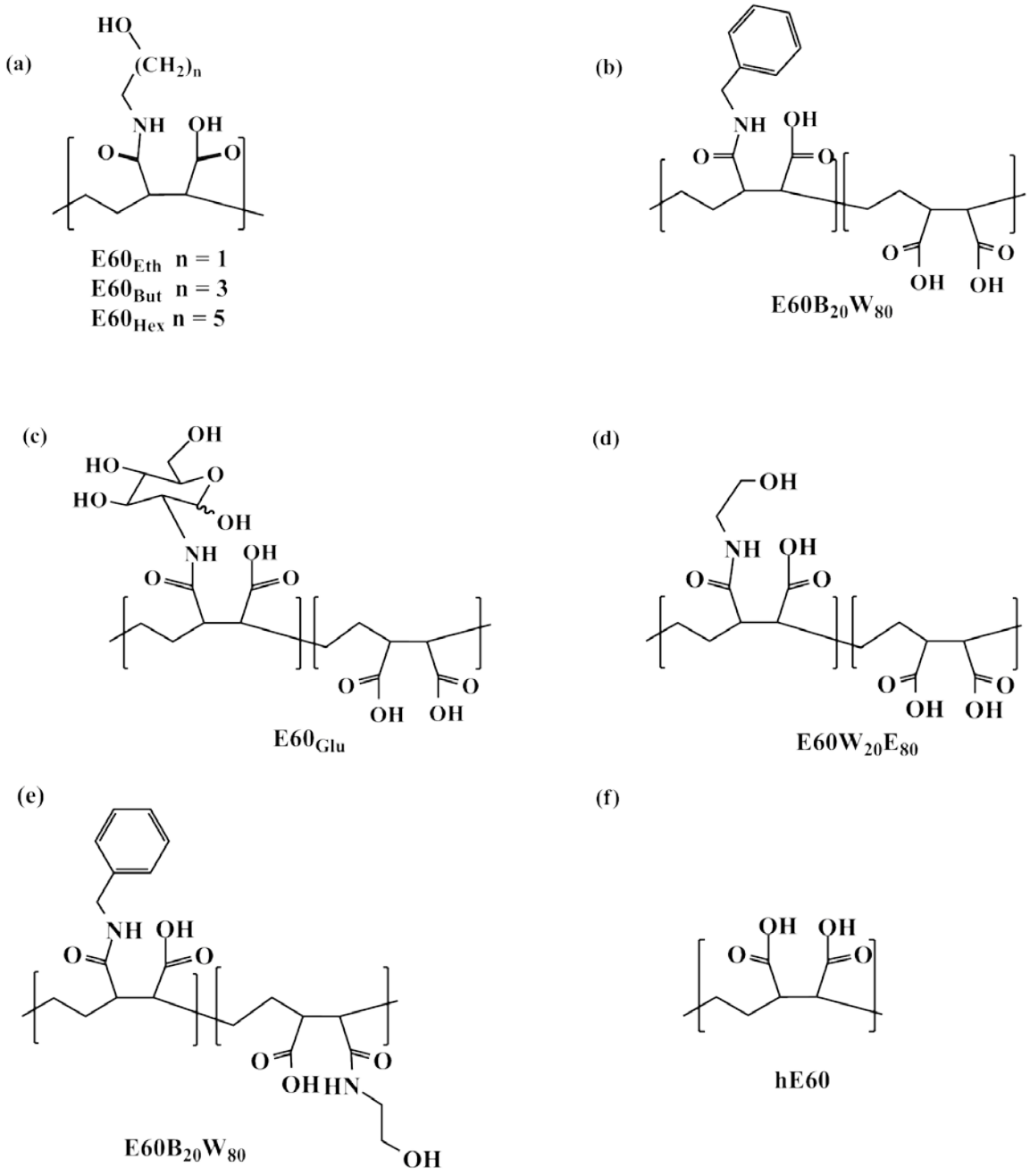

Figure 2-12: Structure of polymers synthesised for antifreeze testing

Table 2-2: Table of chemical and physical properties of polymers tested.

Polymer	Structure	Composition*	Mn (kDa)†	Alcohols per chain
$E60_{Eth}$	Fig.15 (a)	n = 1, m = 315	73.9	315
$E60_{But}$	Fig.15 (a)	n = 3, m = 315	85	315
$E60_{Hex}$	Fig.15 (a)	n = 5, m = 315	96.1	315
$E60_{Gluc}$	Fig.15 (c)	n = 250, m = 69	106.6	1000
$E60_{Acid}$	Fig.15 (f)	n = 315	56.9	0
E60E8020W	Fig.15 (e)	n = 76, m = 240	69.8	300
E60B2080W	Fig.15 (b)	n = 63, m = 252	65.4	0
E60B20E80	Fig.15 (d)	n = 57, m = 258	77.2	324
PVA_{2623}			115.5	2623
PVA_{205}			9	205

***Calculated from ^{1}H NMR**

†: Calculated from GPC values of E60 (chapter 1)

2.3 Results and discussion

The activity of polymers was tested by the splat test methodology, in which 10µl of liquid is dropped a distance onto metal plate cooled with dry ice. The nascent ice disc is then removed with a chilled blade and annealed on a -6^{o}C microscope stage for 30 minutes. The disc was then imaged under a cross polarised microscope and an image captured of no less than 8 locations on each wafer (figure 2-13). The thirty largest crystals in each image were then measured across their longest axis using the microscope's proprietary software and the largest of these taken as the largest grain size for that image. These measurements were then combined to calculate the largest mean grain size.

This procedure was carried out at least three times for each solution. Activity is measured in terms of largest mean grain size (LGMS) and compared to a PBS control LGMS of 248µm +/- 4µm.

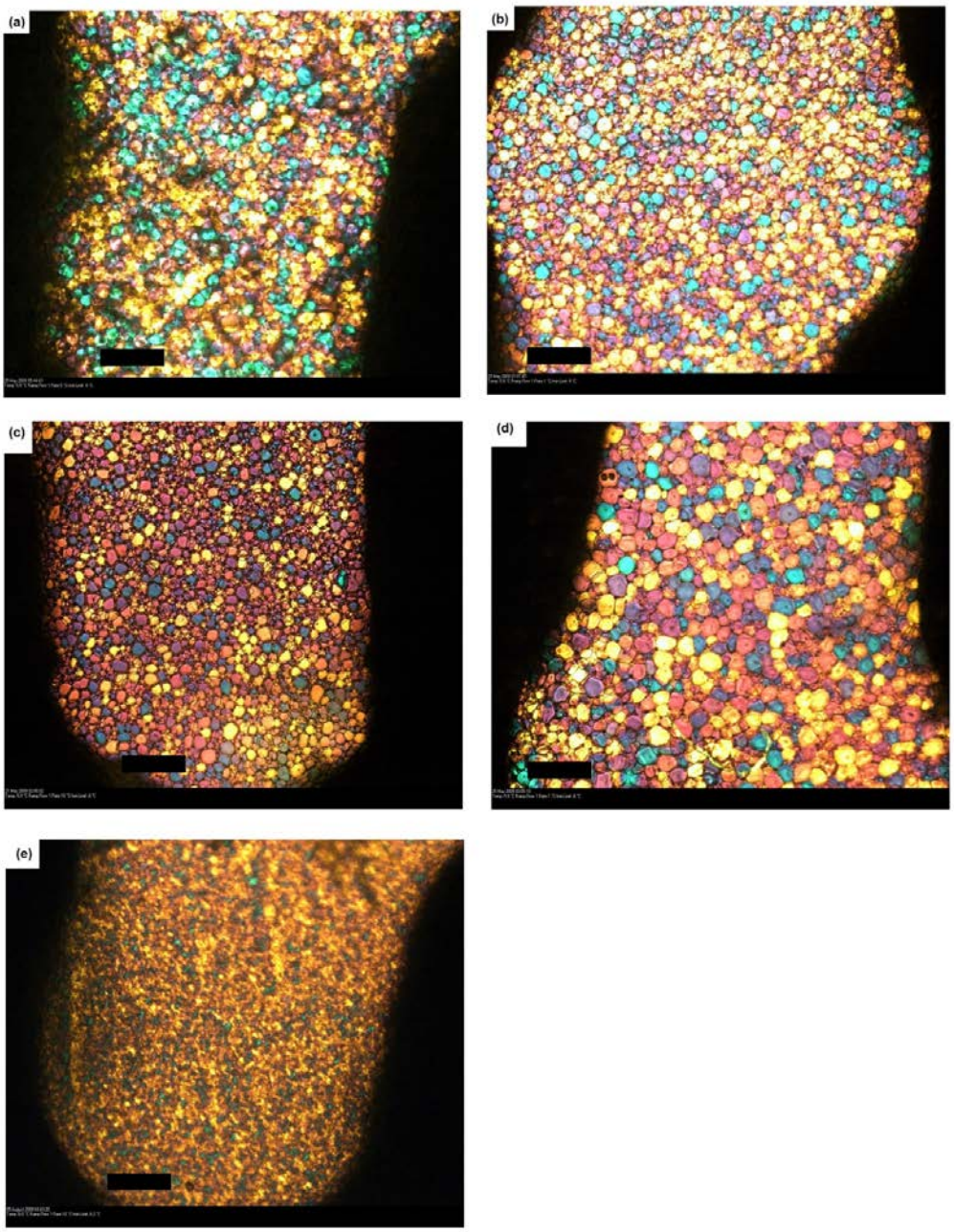

Figure 2-13 Microscope image of ice crystals after 30min at -6^{o}C (a) E60$_{Eth}$ (b)E60$_{But}$, (c)E60$_{Hex}$, (d)hE60, and (e)PVA$_{205}$. Testes solutions are at 0.4mmol L^{-1}. Scale bar is 200µm.

Phosphate saline buffer (pH 7) when subjected to the splat test, results in a LMGS of circa 254µm. The ethanolamine, butanolamine and hexanolamine derivatives of E60

($E60_{Eth}$, $E60_{But}$ and $E60_{Hex}$ respectively) all display a marked RI activity, that is a capacity to suppress ice crystal growth, as compared to phosphate buffered saline (PBS) (see figure 2-13 and 2-14). The RI activity is in the order $E60_{Hext}$ < $E60_{But}$ < $E60_{Eth}$, although the change in activity between the $E60_{Eth}$ and $E60_{But}$ polymers is marginal.

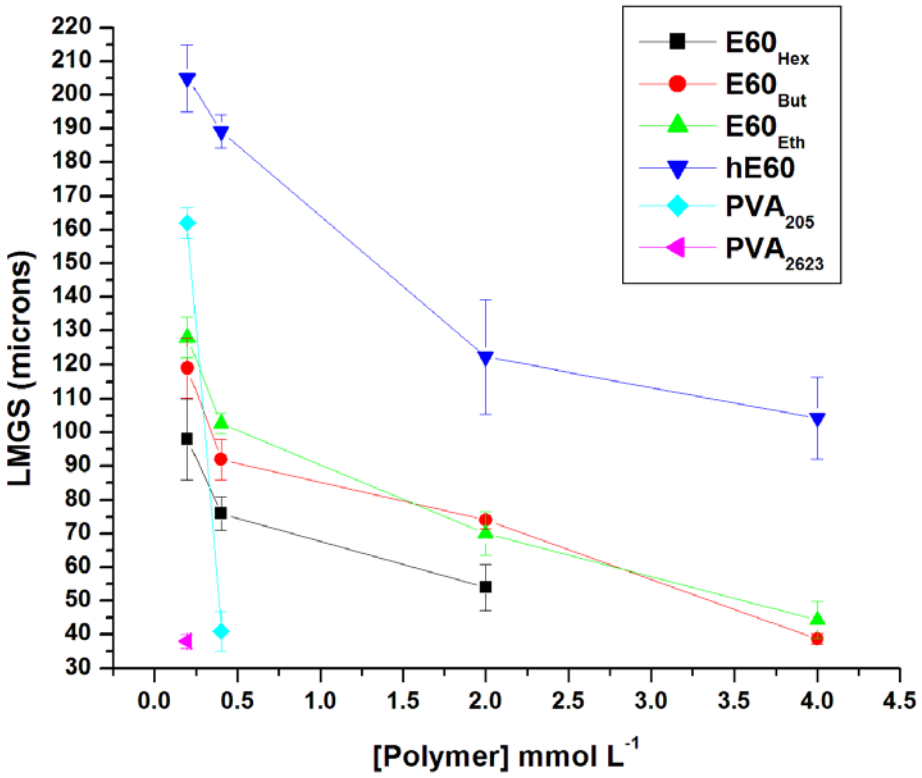

Figure 2-14: Largest mean grain size (LGMS) vs. [Polymer] for a variety of tested polymers. Note that at 4mmol L^{-1} $E60_{Hex}$ forms a gel and therefore could not be tested.

An observation made previously by Gibson *et al*[40] is that the linker length between the polymer backbone and hydroxyl group is inversely proportional to activity. This would also explain the higher activity observed in both this study and others[37] for

poly(vinyl alcohol), where the carbon atom length between the back bone and hydroxyl is zero. In order for this theory to fit the data obtained it is necessary to assume that, as Ben *et al* observed, longer linker lengths with hydroxyls which are spatially closer to the polymer backbone, due to solution conformation, results in higher RI activity than shorter lengths where the hydroxyl in more remote. Currently, no data exists to suggest that this is the case and resolution of this would require computational modelling.

Re-plotting figure 2-14 in terms of hydroxyl concentration provides an insight into the RI activity per hydroxyl (figure 2-15).

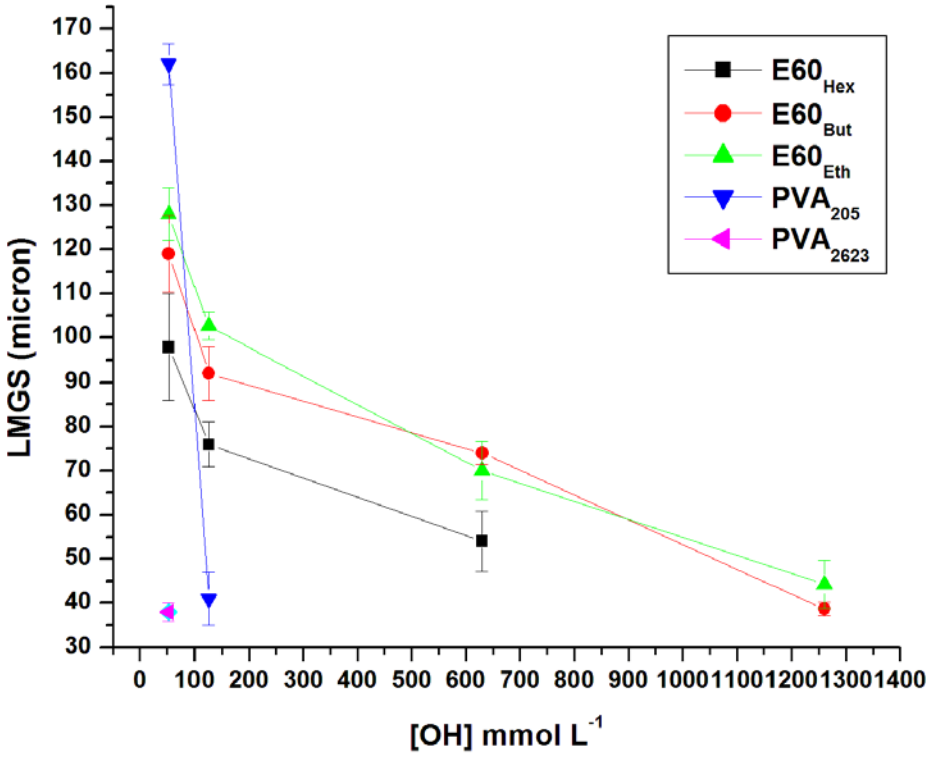

Figure 2-15: Largest mean grain size (LGMS) vs. hydroxyl concentration for a variety of hydroxyl bearing polymers.

What is apparent is that PVA is more active per hydroxyl than the E60 polymers. In addition, the molecular mass of PVA_{205} (9kDa) is significantly lower than that of the E60 polymers (57-106kDa). This demonstrates that PVA's RI potency is in some way structural and not merely a product of hydroxyl concentration or molecular mass of the polymer.

Rationalising this data depends which model is accepted. The model developed by Knight[24] rationalises activity as resulting from the bind and pin mechanism (figure 2-3). Here, activity is dependent on how firmly the polymer can bind to the ice crystal's surface. In terms of linker length this makes sense entropically; the binding of more conformationally restricted polymer would incur a much lower entropy penalty than a polymer which has a great degree of freedom. Indeed, this model would also explain the results of Ben *et al*.[43] whose AFGP mimics show no direct relation between linker length and activity but do indicate that the most conformationally restricted polymer is most active.

However, perhaps the most surprising result is the activity of hE60 (figure 2-15) which, although the least active of the polymers tested, still has a marked impact on LGMS. This is in stark contrast with the work of Gibson *et al*.[40] who, based on measurements of poly(acrylic acid) and poly(glutamic acid), concluded that carboxylic acid groups have no RI beyond a small colligative effect. This is likely to be to be the result of the unusual acid dissociation constants of poly acids and more particularly polymers bearing succinic acid moieties (chapter 1). In other words despite being buffered to pH 7 the polymer still bears carboxylic hydroxyl groups.

In response to the short comings of the bind and pin model in explaining the inverse relation between hydration number and RI activity, Ben *et al* proposed a model in which, briefly, the mode of action is the polymers ability to disrupt the re-organisation of the QLL between adjacent ice crystals, thereby preventing coalescence. However, this model does not explain the ice shaping behaviour of, for example, poly(vinyl alcohol) which demonstrates the macromolecule is preferentially active against the prism faces of the ice.

Clearly there are conflicting data and theories, and in order to address the activity of E60 derivatives it is necessary to consider further how these polymers may interact with water.

It has already been established that hydrated polymers have three types of water associated with them: closely bound water, intermediate water and free water.[51] Free water consists of water molecules which have a structure similar to that of the bulk with polymer-water interactions being negligible. Bound water is generally associated with polymer chains capable of forming strong hydrogen bonds or which interact strongly with ionic groups. Finally, intermediate water lies between the bound and free water. The relative amount of these water types is dependent on a variety of factors including the chemical nature of the hydrogen bonding groups. It is notable that the freezing temperature (T_F) for bound, intermediate and free water is: 173K, 248K and 273K respectively.[51-53] This can only be interpreted as the polymer conferring a conformation on the bound water which in turn perturbs the structure of intermediate water thereby lowering the freezing point of the water.

Hydrophobic volumes impact markedly on water's structure by forcing it to organise into a clathrate structure. This process is actually well understood with reference to surfactants. The self assembly of micelles is driven by entropy. The enthalpy of micelle formation is thought to be slightly positive (1-2 kJ mol^{-1})[7] which means that self assembly is favourable in terms of entropy due to the collapse of the clathrate cage that water is required to form in order to solubilise a hydrophobic volume.

The conventional model of liquid water is that of a tetrahedral array of hydrogen bonded molecule. However, despite this rigid, highly organised structure, it has been shown, in numerous spectroscopic studies, that water has picosecond relaxation times and that the diffusion of water at room temperature is very close to that of a simple liquid.[47-50] This is at odds with the concept of a system in which each molecule is formally hydrogen bonded in a tetrahedral arrangement which would severely inhibit diffusion even at room temperature.[47] However, this problem appears to have been resolved with the discovery of the bifurcated hydrogen bond. (figure 2-16)[51]

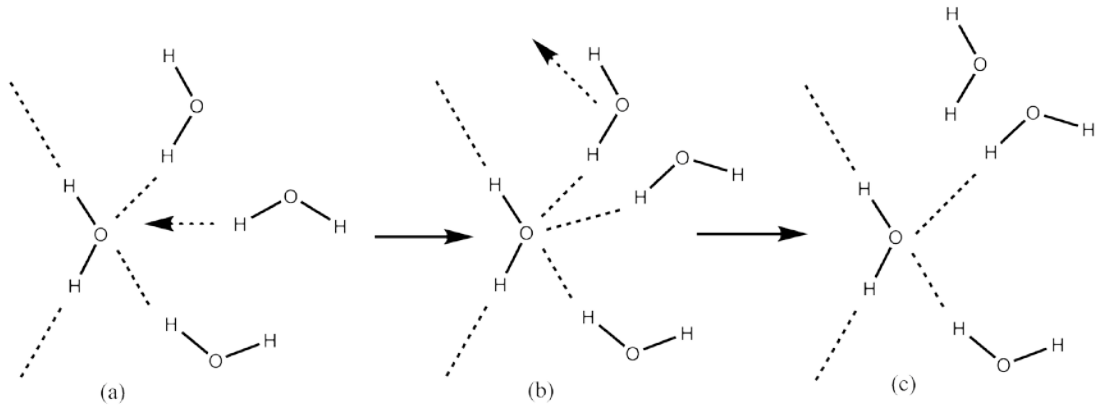

Figure 2-16: Mechanism of water's reorientation via bifurcation. (a) tetrahedral water, (b) bifurcated water, (c) tetrahedral water. Dashed lines represent hydrogen bonds, dashed arrows show motion of molecules

This bonding mechanism allows for the formation of a water unit cell in which a fifth water molecule approaches and disturbs the tetrahedral hydrogen bonding network. This disruption, of what would otherwise be a rigid structure, allows for greater re-orientational motion. The fifth water molecule is sometimes described as a catalyst to reorientation.[52]

The fast reorientation of water is therefore dependent on the presence of this 'catalytic water'. This can be related to the correlation time (τ_c) of the water which can be loosely defined as the time taken for a molecule to either rotate one radian or move a distance within the order of its own size. There are indications that both hydrophobic and hydrogen bonding groups can restrict the motion of water and, in some cases, work synergistically as evidenced by the work of Yang *et al.* on AFP type III.[27]

NMR experiments on natural abundance water-solute systems allow the correlation time of hydrating water to be studied. Experiments with small molecule alcohols in water have demonstrated that the hydrating water can readily reorientate in the presence of hydroxyl groups; in other words, τ_c^h is short. However, an increase in the hydrophobicity of the hydroxyl bearing molecule leads to an increase in the correlation time. For example, Ishihara *et al*.[53] demonstrated that the of the hydrating water correlation time for a series of n-alcohols increases with the alkyl chain length.

However, this effect is not simply a function of the molecules surface area, Ishihara *et al.* went on to demonstrate that the hydrating water correlation time increases when the hydrophobic volume close to the hydroxyl groups increases, the ratio τ_c^h to the correlation time of water (τ_c^0) for: n-butanol, i-butanol, s-butanol and t-butanol is

1.86, 1.91, 1.99, and 2.22 respectively. In other words an increase in the hydrophobic volume close to the hydroxyl decreases the motion of its hydrating water molecules [53] It is important to note the water accessible surface area of the different isomers of butanol is approximately the same, in other words the increase in correlation time is not simply a function of an increased hydrophobic volume, rather it is the distribution of that volume around the hydroxyl group which is important.

In addition to this, studies on the structure of water near large, sterically hindered, surfaces suggests that the geometry excludes the fifth, bifurcating, water molecule from approaching the hydrating water thereby inhibiting its reorientation.[52,54] In other words, hydrating water is more dense due to the exclusion of bifurcated bonds. This is somewhat confirmed by Uedaria *et* al's work on the correlation times of peptides[55] in which they demonstrate that τ_c^h is proportional to molecular mass of oligoleucines but not oligoglycines. The implication being that steric bulk and hydrophobic volume influence the waters correlation time.

Strong hydrogen bonding also decreases τ_c^h, a trend identified by Uedaria *et al.*[53,55] in their NMR study of a series of monosaccharides and cyclohexanols which demonstrated that τ_c^h is linearly proportional to the number of equatorial hydroxyl groups are present

In summary, the thermal motion of hydrating water can be restricted by: strong hydrogen bonding; hydrophobic volumes, and the shape of the molecule.

This allows for a rationalisation as to how the distance of hydroxyl groups from the backbone may affects RI activity. An increase in the hydrophobicity of the environment close to the hydroxyl groups results in a decrease the hydrating water mobility. This effect can either then be interpreted as presenting a more ice like water structure surrounding the hydroxyl, thereby promoting binding to ice crystal surfaces, or alternatively causing a disruption to the quasi liquid layer between ice crystals thereby inhibiting Ostwald ripening and crystal coalescence.

While it is possible to infer that RI activity may be dependent on the mobility of the hydrating water it is not clear how this results in RI activity. To recall there are two proposed mechanisms for the RI activity of synthetic AFGP mimics namely: Knight's 'bind and pin model' which relies on the tight binding of the molecule onto the surface; and Ben *et al.'s*[56] model, which involves the disruption of the QLL water molecules thereby inhibiting their reorganisation ahead of the coalescence of two adjacent ice crystals.

Both mechanisms are dependent on the polymer perturbing the waters structure, but differ as to whether it is the surface ice or QLL molecules with which this interaction is important. There is no obvious way of concluding this at the moment, however, what can be concluded is that the distance of a hydroxyl group from the backbone of a polymer is related to its RI ability and this by implication suggests hydrophobic volume, surrounding the hydroxyl groups influences the polymers RI activity.

2.3.1 Hydrophobic groups and inhibition of recrystallisation activity

In order to probe the importance of hydrophobic components for RI activity, the polymers shown in figure 2-12 (a-d) were synthesised. The rationale was to probe whether a decrease in the hydroxyl content would significantly impact on activity and as to whether the introduction of hydrophobic amides would affect RI activity. The link between molar mass and activity is not clearly established; rather it appears it is the number of hydroxyl groups which is seemingly important. As a result the polymers were tested on a mg mL^{-1} which ensures that the number of 'active' sites is constant between the samples even if the number of chains is not. Further testing at other concentrations is desirable but lack of material and time prohibited this. Clearly this would be a starting point for any future work.

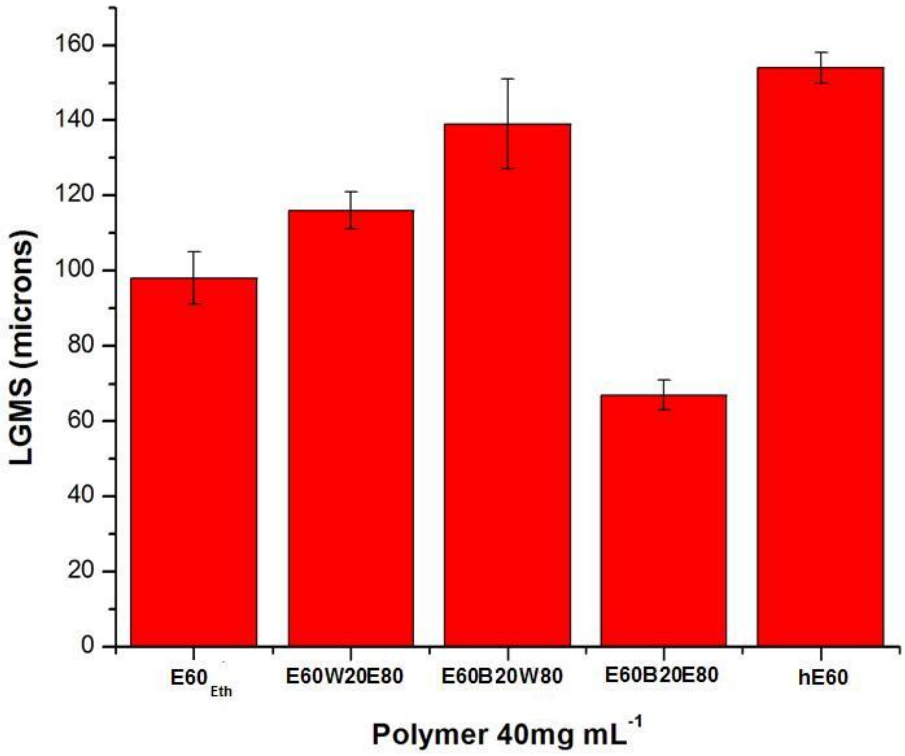

Figure 2-17: LMGS measurements of a 40mg mL^{-1} PBS solution of E60 derivatives

It is clear that hydroxyl groups contribute to RI activity, as evidenced by the decrease in activity with decreasing hydroxyl content in polymers: $E60_{Eth}$<$E60W_{20}E_{80}$<hE60. However, a more surprising result is that activity increases with the introduction of hydrophobic amides evidenced by hE60<$E60B_{20}W_{80}$ and $E60_{Eth}$<$E60B_{20}E_{80}$. The role of hydrophobic groups is not normally considered for RI polymers, however, it is not a new observation with regards to AFPs where the link between hydrophobic residues and activity has already been established.[27]

The data indicates that activity is dependent on the number of hydroxyls per polymer chain as evidenced by the drop in activity from $E60_{Eth}$ to $E60W_{20}E_{80}$. In other words ,

acid groups are less RI active than hydroxyls, an observation already made by Gibson *et al*.[43] Secondly, the presence of benzylamide groups increases the activity.

The activity of benzylamide groups may be the result of the entropy increase when these groups are removed from solution. This would create a thermodynamic drive for the polymer to deposit onto the ice crystal's surface. Given the distance between the benzyl and hydroxyl groups it seems unlikely that, in this case, the hydrophobic volume of the benzyl groups impacts on the τ_c^h of the hydroxyl groups as has been observed elsewhere.

However, there is a second possibility. While NMR and light scattering gave no indication that any intermolecular aggregation is occurring there is the possibility of intramolecular aggregation evidence for which is presented in chapter 3. In other words, the polymer adopts a conformation which removes the hydrophobic groups from the water. However, it is not clear how this would contribute to RI as it would result in an overall increase in entropy. In addition, the measurements taken in chapter 3 were taken at the polymer's native pH of 4.2, that is to say significantly below the pH 7 buffer conditions of these experiments. Indeed, as observed in chapter one, at this pH the polymers acid groups should be almost entirely deprotonated thereby decreasing the probability of intramolecular aggregation.

2.4 Glucosamide polymer

Glucose has previously been shown to be active in RI[46] and it was rationalised that testing a glucosamine based E60 derivative would prove an instructive comparison with the n-amino alcohol derivatives of E60 tested and the work of others. The

advantage of glucosamine is that the amide formed is very close to the backbone of the polymer which translates as a short linker length. This has been previously identified as being advantageous to activity.[40]

Unlike reactions with n-alkylamino alcohols (ethanolamine etc.) the reaction with glucosamine did not go to completion with a final amide yield of only 78%. The remaining 22% of anhydrides ring opened to form the diacid. The reason for this is unclear but may either be a result of: steric hindrance; the heterogeneous nature of the reaction, or the partial hydrolysis of the amides during purification.[57]

$E60_{Gluc}$ was observed to have an activity greater than $E60_{Eth}$ in terms of polymer concentration (figure 2-18).

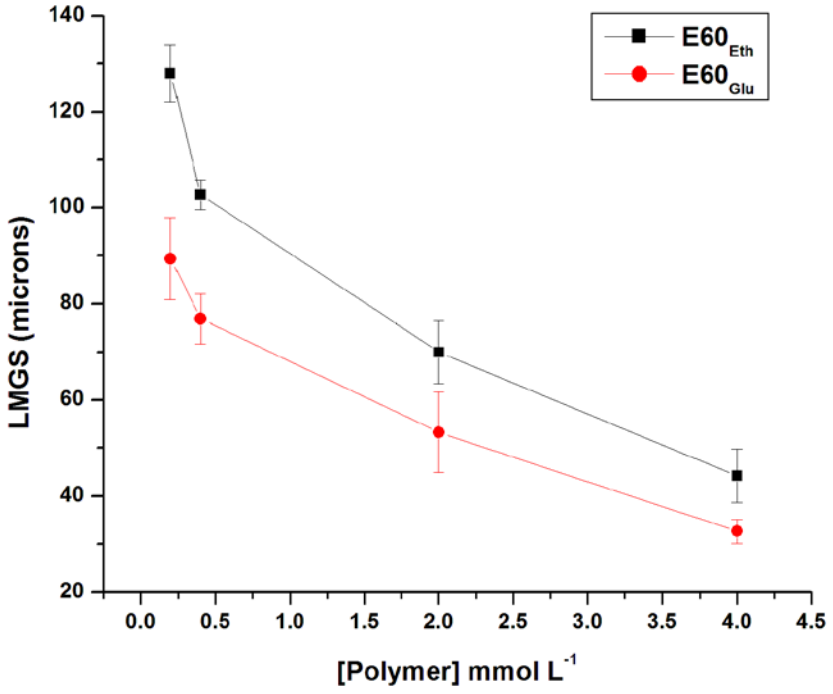

Figure 2-18: Largest mean grain size vs. polymer concentration. Comparison of ethanolamine and glucosamine E60 derivatives.

However, it must be remembered that the moles of hydroxyls per chain is much greater for the glucosamine than the ethanolamine derivative. Consequently, re-plotting of the data in terms of LMGS against hydroxyl concentration provides an insight into activity, or efficiency, per hydroxyl.

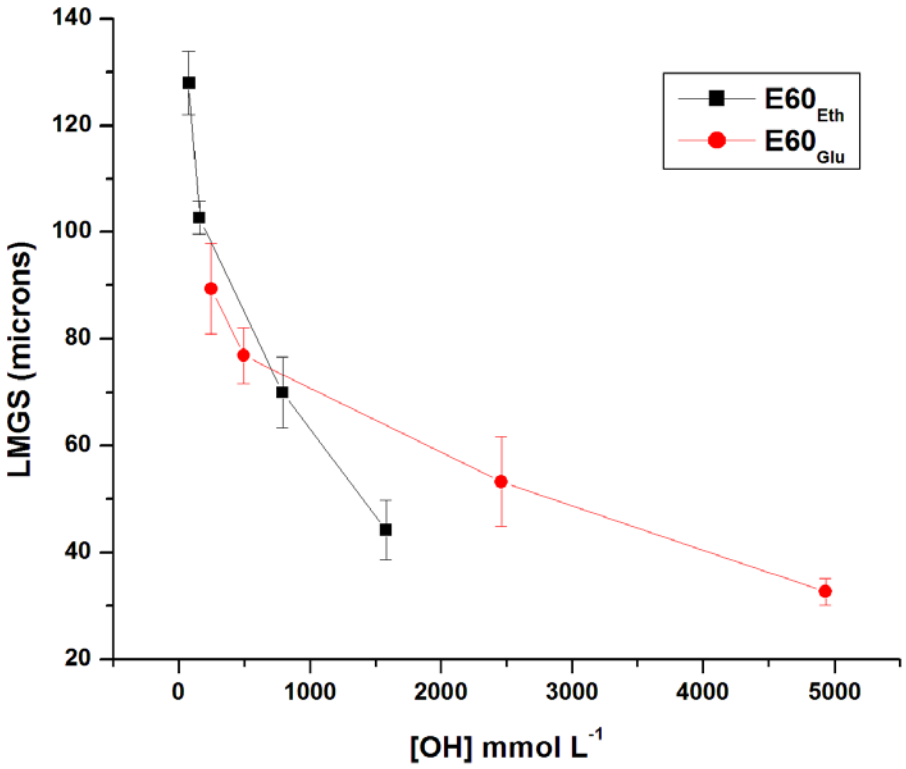

Figure 2-19: Largest Mean Grain Size vs. hydroxyl concentration. Comparison of ethanolamine and glucosamine E60 derivatives.

As figure 2-19 shows, the activity per hydroxyl is significantly lower for the glucosamine bearing polymer. The reason for this in unclear but does indicate that it is not hydroxyl concentration alone which determines activity. The hydration number of ethanol and glucose is 15 and 8.4 respectively.[46] This perhaps indicates that the $E60_{Eth}$

is more hydrated than $E60_{Gluc}$. However, a complete understanding of the polymer's hydration structure would require some measurement of the dynamics of the hydrating water.

2.5 Conclusion

It has been demonstrated that in this instance linker length is proportional to RI activity, possibly resulting from the increasing distance of those hydroxyls from the polymer backbone. It is hypothesised that the hydrating water molecules are more mobile around the polymer, or more specifically the hydroxyl groups, as the linker length decreases.

The benefit of introducing hydrophobic groups is a new observation in terms of synthetic AFGP mimics. This points to the importance of disrupting the structure of the water either as an end in itself, to disrupt the quasi-liquid layer, or to promote binding to the surface. However, the influence of intramolecular aggregation, although seemingly unlikely, cannot be ruled out.

2.5.1 Future work

A more thorough understanding of the solvation structure of these polymers would provide a greater insight into their mechanism of action. A computational study, ideally a molecular dynamics simulation of the entire polymer and *ab initio* study of representative fragments would also provide useful insights. In addition, measurements of the τ_c^h of a series of small molecule structural analogues would provide some indication as to whether the mobility of hydrating water influences activity.

Future work in this area would benefit from a study of changes to the polymer backbone either by variation of the α-olefin in a series of poly(α-olefin-alt-maleic anhydride) copolymer or by the study of a variety of poly(α-olefin-co-vinyl alcohol) polymers. A detailed study of RI active – hydrophobic block copolymers would also be beneficial as current studies tend to focus on the introduction of hydrophilic blocks to a RI active block.[38] It would be useful to probe the activity of those polymers which are close in composition to those which self assemble i.e. where the water is highly ordered in a clathrate cage.

2.6 Experimental

2.6.1 Materials and instrumentation

E60 was received from Vertellus speciality chemicals and purified as outlined in Chapter 1, section 1.9.2. All other chemicals were purchased from standard chemical suppliers and used without further purification unless otherwise stated.

NMR spectra were recorded using a Varian Inova 500 spectrometer at 499.87 (^{1}H) and 125.67 MHz (^{13}C, 1H decoupled at 500 MHz), a Bruker Avance 400 spectrometer at 400.13 MHz (1H) or 100.26 MHz (^{13}C, ^{1}H decoupled at 400 MHz) or a Varian Inova-700 spectrometer at 700MHz (1H) and 176MHz (13C), at ambient temperature in $CDCl_3$, DMSO, D_2O, MeOD. NMR spectra were analysed using MestReNova v6.04 software and referenced internally to the residual protons in the NMR solvent. IR spectra were recorded on a Nicolet Nexus FT-IR spectrometer either as thin films on KBr discs cast from a suitable solvent or pressed as KBr discs. Ice wafers were annealed on a Linkam THMS600 thermostatted microscope stage using liquid nitrogen as the coolant. CD spectra were recorded on a JASCO J-810 spectropolarimeter using a scan rate of 10 nm per min and a bandwidth of 1 nm. Five accumulations were collected for each sample. The concentration of the aqueous polymer solutions was 1 g L^{-1}.

2.6.2 Synthesis of n-alcohol amide derivatives

E60 (0.5g, 0.01mmol, 4mmol of anhydride) was dissolved in 10mL of anhydrous DMF with efficient stirring. To this, anhydrous trimethylamine (0.8g, 8mmol, Aldrich) was added. To this mixture, amino alcohol (4.4mmol) in 2mL DMF was

added dropwise. The reaction was allowed to stir for 20 minutes at room temperature. The reactions were observed to form gels over time, the reaction was then quenched with $HCl_{(aq)}$ (5mL, 0.01M) to dissolve the gel before transferring into a dialysis tube (Aldrich, M_n cut off 12kDa). The solution was dialysed against 0.01M $HCl_{(ag)}$ (1000mL) for 6h with efficient stirring. The solution was then dialysed against deionized water over 36h with frequent water changes. The polymer was then recovered by freeze drying.

Table 2-3: Summary of reaction conditions and products

Polymer	Amine	Mass of amine (mg)	Recovered polymer (mg)	Yield (%)	Conversion to amide (%)
$E60_{Etha}$	Ethanolamine	240	683	92	100
$E60_{But}$	Butanolamine	360	835	98	100
$E60_{Hex}$	Hexanolamine	465	626	65	100

2.6.2.1 Characterisation of ethanolamine poly(ethylene-alt-maleic anhydride) derivative

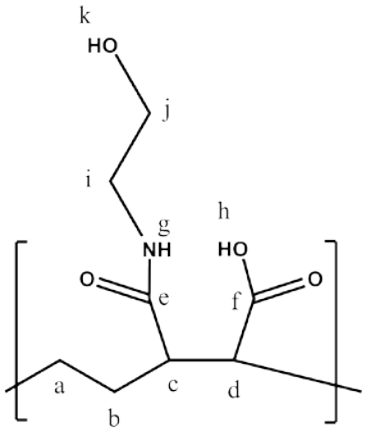

Figure 2-20: Labelled structure of $E60_{Eth}$

^{1}H NMR (400MHz, D_2O): δ 3.52 (br s, 2H, j), 3.21 (br s, 2H, i), 2.32 (br s, 2H, c -d), 1.33 (br s, 4H, a-b).

FTIR (KBr): 3260 cm-1 (broad, strong) OH, 3100 cm-1 (strong) amide N-H; 2930 cm-1 (strong) C-H; 2860 cm-1 (strong) –CH; 2500 cm-1 (broad strong) acid –OH;1700 cm-1 (strong) acid C=O; 1620 cm-1 (strong) amide C=O; 1550 cm-1 (sharp) amide N-H; 1390 cm-1 alcohol –OH; 1350 cm-1, 1190 cm-1; 1060 cm-1; 737 cm^{-1}

2.6.2.2 Characterisation of butanolamine poly(ethylene-alt-maleic anhydride) derivative

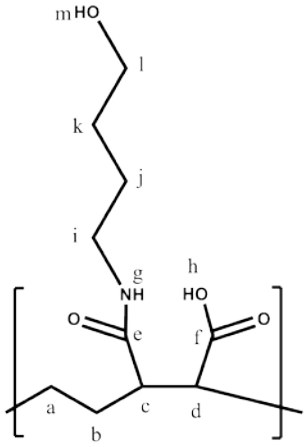

^{1}H NMR: δ_H (400 MHz, D_2O) 3.50 (br, 2H, a, b), 3.07 (br, 2H, i), 2.30 (br, 2H, c-d), 1.43-1.30 (br ov, 8H, a, b, c, d)

FTIR (KBr) : 3260 cm^{-1} (broad, strong) OH, 3100 cm^{-1} (strong) amide N-H; 2930 cm^{-1} (strong) C-H; 2860 cm^{-1} (strong) –CH; 2500 cm^{-1} (broad strong) acid –OH; 1710 cm^{-1} (strong) acid C=O; 1640 cm^{-1} (strong) amide C=O; 1560 cm^{-1} (strong) amide II band N-H; 1480 cm^{-1} C-H; 1380 cm^{-1} alcohol –OH; 1240 cm^{-1}; 1000 cm^{-1}

2.6.2.3 Characterisation of hexanolamine poly(ethylene-alt-maleic anhydride) derivative

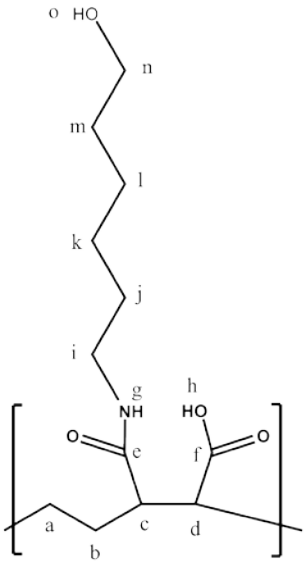

^{1}H: δ_H (400 MHz, D_2O) 3.51 (br t, 2H, ν), 3.06 (br s, 2H, i), 2.36 (br, 2H, c, d), 1.45-1.23 (br ov, 12H, a, b, j, k, l, m).

FTIR (KBr) : 3260 cm^{-1} (broad, strong) OH, 3100 cm^{-1} (strong) amide N-H; 2930 cm^{-1} (strong) C-H; 2860 cm^{-1} (strong) –CH; 2500 cm^{-1} (broad strong) acid –OH; 1710 cm^{-1} (strong) acid C=O; 1635 cm^{-1} (strong) amide C=O; 1555 cm^{-1} (strong) amide II band N-H; 1480 cm^{-1} C-H; 1380 cm^{-1}; 1240 cm^{-1}; 1000 cm^{-1}

2.6.3 Synthesis of glucosamine poly(ethylene-alt-maleic anhydride) derivative

E60 (0.5g, 0.01mmol, 4mmol of anhydride) was dissolved in 10mL anhydrous DMF with efficient stirring. To this anhydrous pyridine (2g, 0.02 mmol) was added. Glucosamine hydrochloride (1.7g, 0.008mmol) was then added to this mixture. The heterogenous reaction was allowed to proceed for 24 hours before quenching with $HCl_{(aq)}$ (5mL, 0.01M) and transferred into a dialysis tube (Aldrich, M_n cut off~

12kDa). The solution was then dialysed against 0.01M $HCl_{(ag)}$ (1000mL) for 6h with efficient stirring followed by dialysis against deionized water over 36h with frequent water changes. The polymer was then recovered by freeze drying (1.03g, 94% yield).

2.6.3.1 Characterisation of glucosamine poly(ethylene-alt-maleic anhydride) derivative

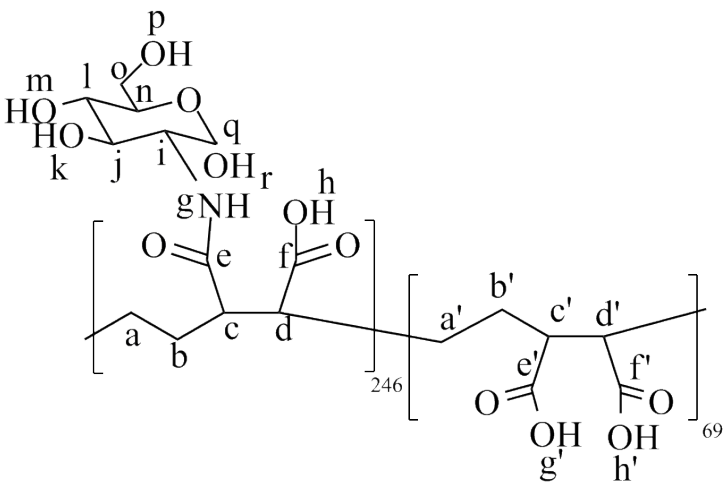

^{1}H NMR: δ_H (400 MHz, D_2O) 5.08 (br s, i), 3.73-3.33 (br, j, l, n, o, q), 2.47 (br s, c, d, c', d'), 1.43 (br s, a, b, a', b')

FTIR (KBr): 3300 cm^{-1} (broad , strong) alcohol –OH; 2920 cm^{-1} C-H; 2870 cm^{-1} C-H; 2620 cm^{-1} (broad, strong) acid –OH; 1710 cm^{-1} (strong) acid C=O; 1690 cm^{-1} (strong) amide C=O; 1620 cm^{-1} amide N-H; 1380 cm^{-1}; 1180 cm^{-1} (strong) carbohydrate C-O; 1000 cm^{-1}.

2.6.4 Synthesis of poly(ethylene-alt-maleic acid)

E60 (0.5g, 0.01mmol, 4mmol of anhydride) was added to 30mL of deionized water and heated with efficient stirring at 60^{o}C for 8 hours. The polymer was then recovered by freeze drying, (0.57g, 100% yield).

2.6.4.1 Characterisation of $E60_{Acid}$

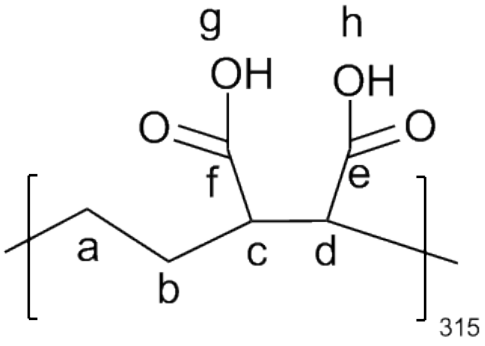

NMRQ d_H (400 MHz, D_2O) 1.4 (br s, 4H, a, b), 2.4 (br s, 2H, c, d).

FTIR (KBr): 3060 cm^{-1} (broad, strong) acid –OH; 2940 cm^{-1} (strong) C-H; 2550 cm^{-1} (broad) acid –OH; 1700 cm^{-1} (strong) acid C=O; 1430 cm^{-1} C-H; 1390 cm^{-1} (define) –OH; 1170 cm^{-1}; 890 cm^{-1}

2.6.5 Synthesis of 80% ethanolanolamide 20% benzylamide poly(ethylene-alt-maleic anhydride) derivative

E60 (0.5g, 0.01mmol, 4mmol of anhydride) was added to 10mL anhydrous DMF with anhydrous triethylamine (0.8g, 8mmol, Aldrich). To this benzylamine (0.085g, 0.79mmol, Aldrich) was added in 2mL DMF dropwise. The reaction was allowed to stir for 20 minutes at room temperature. To this mixture ethanolamine (0.252g, 4mmol, Aldrich) in 2mL DMF was added to the reaction mix and left to stir

20minutes at room temperature. The reaction was then quenched with $HCl_{(aq)}$ (5mL, 0.01M) and transferred into a dialysis tube (Aldrich, M_n cut off 12kDa). The solution was dialysed against 0.01M $HCl_{(ag)}$ (1000mL) for 6hrs then dialysed against water over 36 hours with frequent changing of the water. The polymer was then recovered by freeze drying (0.73g, 94%)

2.6.5.1 Characterisation E60 80% ethanolamide 20% benzylamine

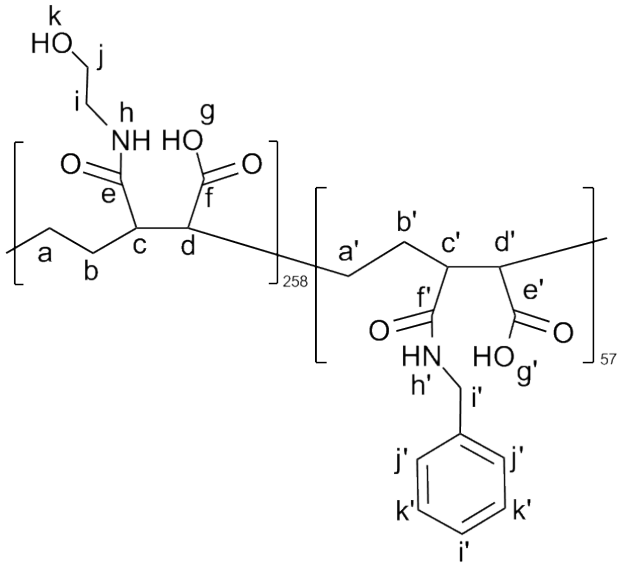

NMR: δ_H (400 MHz, D_2O) 6.96 (br m, j', k', l'), 3.98 (s, i'), 3.26 (br s, 1.4H, j), 2.96 (br s, i), 2.2 (br s, 2H, c, d), 1.17 (br, a, b).

FTIR (KBr): 3300 cm^{-1} (broad, strong) alcohol –OH; 3090 cm^{-1} (strong) amide N-H; 2930 cm^{-1} (strong) aromatic C-H; 2880 cm^{-1} (strong) C-H; 2550 cm^{-1} (broad) carboxylic –OH; 1700 cm^{-1} (strong) acid C=O; 1690 cm^{-1}(strong) amide C=O; 1550 cm^{-1} amide N-H; 1440 cm^{-1} C-H; 1390 cm^{-1} alcohol –OH; 1200 cm^{-1} (broad); 1050 cm^{-1}; 750 cm^{-1}.

2.6.5.2 Synthesis of 20% diacid 80% ethanolamine poly(ethylene-alt-maleic anhydride) derivative

E60 (0.5g, 0.01mmol, 4mmol of anhydride) was added to 10mL anhydrous DMF with anhydrous triethylamine (0.8g, 8mmol, Aldrich). To this benzylamine (0.085g, 0.79mmol, Aldrich) was added in 2mL DMF dropwise. The reaction was allowed to stir for 20 minutes at room temperature. The reaction was then quenched with $HCl_{(aq)}$ (5mL, 0.01M) and transferred into a dialysis tube (Aldrich, M_n cut off~ 12kDa). The solution was dialysed against 0.01M $HCl_{(ag)}$ (1000mL) for 6hrs then dialysed against water over 36h with frequent water changes. The polymer was then recovered by freeze drying (0.45g, 87%).

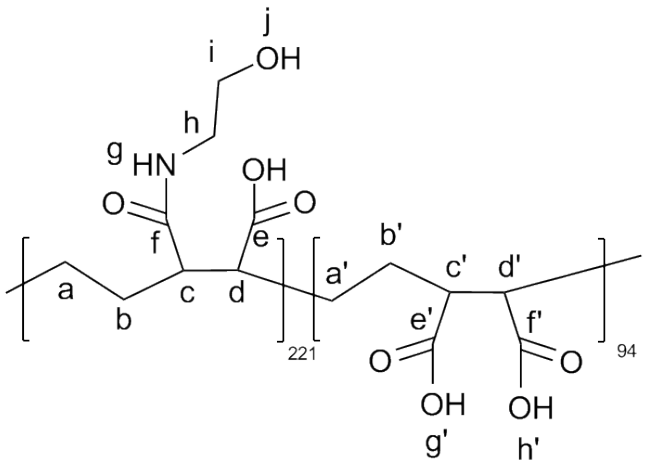

NMR d_H (400 MHz, D_2O) 3.26 (br s, j), 2.96 (br s, i), 2.24 (br s, c, d), 1.22 (br s, a, b)

FTIR (KBr): 3300 cm^{-1} (broad, strong) alcohol O-H; 3080 cm^{-1} (strong) amide N-H; 2920 cm^{-1} C-H; 2870 cm^{-1} C-H; 2550 cm^{-1} (broad) acid O-H; 1710 cm^{-1} (strong) acid C=O; 1650 cm^{-1} (strong) amide C=O; 1530 cm^{-1} amide N-H; 1440cm^{-1} C-H; 1300 cm^{-1} alcohol O-H; 1180 cm^{-1} (broad strong) alcohol O-H; 1080 cm^{-1}.

2.6.6 Synthesis of 20% benzylamide poly(ethylene-alt-maleic anhydride) derivative

E60 (0.5g, 0.01mmol, 4mmol of anhydride) was added to 10mL anhydrous DMF with anhydrous triethylamine (0.8g, 8mmol, Aldrich). To this benzylamine (0.087g, 0.79mmol, Aldrich) in 2mL DMF was added in dropwise. The reaction was allowed to stir for 20 minutes at room temperature. To this mixture deionized water (5mL, mmol) was added and the solution heated to 60^{o}C for 2h. The reaction was then quenched with $HCl_{(aq)}$ (5mL, 0.01M) and transferred into a dialysis tube (Aldrich, M_n cut off 12kDa) and dialysed against 0.01M $HCl_{(ag)}$ (1000mL) for 6h with efficient stirring. The solution was then dialysed against deionized water over 36h with frequent water changes. The polymer was then recovered by freeze drying. (0.62g, 97%).

2.6.7 Characterisation of 20% benzylamine poly(ethylene-alt-maleic anhydride) derivative

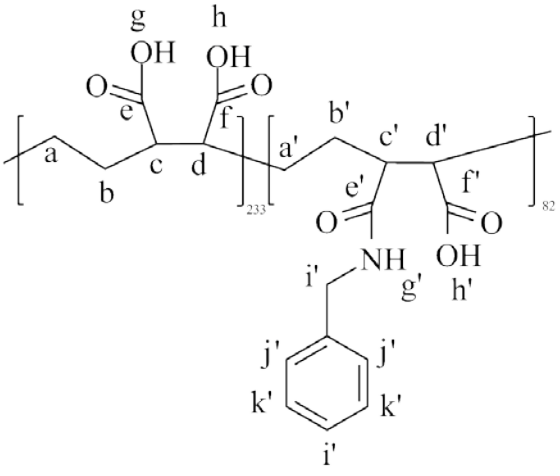

NMR: δ ^{1}H (400 MHz, D_2O): 6.96 (br s, j', k', l), 4.04 (br s, i'), 2.32 (br ov, c, d, c', d'), 1.22 (br s, a, b, a', b').

FT-IR (KBr plate, thin film cast from MeOH) 3100cm^{-1} (broad , strong) acid -OH, amide N-H; 2950cm^{-1} (strong) alkane C-H; 2600cm^{-1} (broad) acid –OH; 1700cm^{-1} (strong) acid C=O; 1650 cm^{-1} (strong, shoulder) amide C=O; 1440cm^{-1} amide N-H; 1400cm^{-1} aromatic C-H; 1180cm-1; 900cm^{-1}; 760cm^{-1}.

2.6.8 Circular dichroism

Samples of $E60_{Acid}$, $E60_{Glu}$ and $E60_{Etha}$ were dissolved in phosphate buffered saline (10mL, pH=7, Aldrich) at a concentration of 1mg mL^{-1}. The solutions were sonicated for 15 minutes and allowed to equilibrate for 3 hours. CD experiments were performed on a JASCO J-810 spectropolarimeter at 20^{o}C under a flow of nitrogen between the range of 320 to 190nm, with the final plot being the average of five readings.

2.6.9 Recrystallization Inhibition Assay

A 10 μL sample of polymer dissolved in PBS buffer (pH 7.4) was dropped 1.5 m down a hollow acrylic tube onto a piece of polished aluminium sat upon dry ice. Upon hitting the aluminium, a wafer with diameter of approximately 10 mm was formed instantaneously. The wafer was transferred using a chilled blade to a glass slide onto the Linkam cool stage and held at -6 °C under N_2 for 30 min. Photographs through crossed polarizers, at a resolution of 2 megapixels, were taken of the initial wafer (to ensure that a polycrystalline sample had been obtained) and after 30 min. ImageJ was used to analyze the obtained images. A number of the largest ice crystals (30+) in each wafer were measured and the single largest length in any axis recorded. This was repeated for at least three wafers and the average (mean) value was calculated to find

the largest grain dimension along any axis. The average of this value from three individual wafers was calculated to give the mean largest grain size (MLGS).

2.7 References

[1] Wierzbicki. A.; Knight. C. A.; Rutland. T. J.; Muccio. D. D.; Pybus. B. S.; Sikes. C. S., *Biomacromolecules*, **2000**, *1*, 268-274.

[2] Knight. C. A.; Wen. D.; Laursen. R. A., *Cryobiology*, **1995**, *32*, 23-34.

[3] Budke. C.; Koop. T., *ChemPhysChem*, **2006**, *7*, 2601-2606.

[4] Stryer, L; Berg, J. M.; Tymoczko, J. L., *Biochemistry*, W H Freeman & Co. Ltd., edn. 5, 2002

[5] Scotter. A.; Marshall. C. B.; Graham. L. A.; Gilber. J. A.; Garnham. C. P.; Davies. P. L., *Cryobiology*, **2006**, *53*, 229-239.

[6] Harding. M. M.; Anderberg. P. I.; Haymet. A. D. J., *Eur. J. Biochem.*, **2003**, *270*, 1381-1392.

[7] Atkins, P., *Elements of Physical Chemistry*, Oxford University Press, edn.3, 2001, vol. 1.

[8] Flores. A. A.; Goff. H. D. , *J. Diary Sci.*, **1999,** *82*, 14908-11415.

[9] Raymond. J. A.; Wilson. P.; DeVries. A. L., *Proc. Natl. Acad. Sci USA*, **1989**, *86*, 881-885.

[10] Eniade. A.; Purushotham. M.; Ben. R. N.; Wang. J. B.; Horwath. K., *Cell Biochemistry and Biophysics*, **2003**, *38*, 115-124.

[11] Liu. S.; Ben. R. N., *Organic Letters*, **2005**, *7*, 2385-2388.

[12] Scholander. P. F.; Dam. L. V.; Kanwisher. J.; Hammel. T.; Gordon. M. S., *J. Cell. Compar. Physiol.*, **1957**, *29*, 5-24.

[13] De Vries. A. L., *Science*, **1969**, *163*, 1073-1075.

[14] Griffith. M.; Yaish. M. W. F., *Trends in plant science*, **2004**, *9*, 399-406.

[15] Knight. C. A.; Cheng. C. C.; DeVries. A. L., *Biophysical Journal*, **1991**, *59*, 409-418.

[16] Tachibana. Y.; Fletcher. G. L.; Fujitani. S. T.; Monde. K.; Nishimura. S., *Angew. Chem. Int. Ed.*, **2004**, *43*, 856-860.

[17] Xu. H.; Pernumal. S.; Zhao. X.; Du. N.; Liu. X.; Jia. Z.; Lu. J. R., *Biophysical Journal*, **2008**, *94*, 4405-4413.

[18] Wierzbicki. A; Knight. C. A.; Salter. E. A.; Henderson. C. N.; Madura. J. D., *Crystal Growth and Design*, **2008**, *8*, 3420-3429.

[19] Kim. J. S.; Domodaron. S. ; Yethiraj. A., *J. Phys. Chem. A.*, **2009**, *113*, 4403-4407.

[20] Ewart. K. V.; Lin. Q.; Hew. C. L., *Cell. Mol. Life Sci.* , **1999**, *55*, 271-283.

[21] Wu. Y.; Banoub. J.; Goddard. S. V.; Kao. M. H.; Fletcher. G. L., *Comp. Biochem. Physiol. B*, **2001**, *128*, 265-273.

[22] Chao. H.; DeLuca. C. I.; Davies. P. L., *FEBS lett.*, **1995**, *357*, 183-186.

[23] Nutt. D. R.; Smith. J. C., *J. Am. Chem. Soc.*, **2008**, *130*, 13066-13073.

[24] Knight. C. A., *Nature*, **2000**, *406*, 249-251.

[25] Haymet. A. D. J.; Ward. L. G.; Harding. M. M., *J. Am. Chem. Soc*, **1999**, *38*, 941.

[26] Baardsnes. J.; Jelokhani-Niaraki. M.; Kondejewski. L. H.; Hodges. R. S.; Davies. P. L., *Protein Sci.*, **2001**, *10*, 2566.

[27] Yang. D. S. C.; Hon. W.; Bubanko. S.; Xue. Y.; Seetharaman. J.; Hew. C. L.; Sicheri. F., *Biophysical Journal*, **1998**, *74*, 2142-2151.

[28] Liou. Y. C.; Tocilj. A.; Davies. P. L.; Jia. Z., *Nature* , **2000**, *206*, 322-324.

[29] Marshall. C.; Chakrabartty. A.; Davies. P. L., *J. Biol. Chem.*, **2005**, *280*, 17920-17929.

[30] Siemer. A. B.; McDermott. A. E., *J. Am. Chem. Soc*, **2008**, *130*, 17394-17399.

[31] Graether. S. P.; DeLuca. C. I.; Baardsnes. J.; Hill. G. A.; David. P. ; Jia. Z. C., *J. Biol. Chem.*, **1999**, *274*, 11842.

[32] Jia. Z. C.; DeLuca. C. I.; Chao. H. M.; Davies. P. L., *Nature*, **1996**, *284*, 285.

[33] Chao. H.; Sonnichsen. F. D.; DeLuca. C. I.; Sykes. B. D.; Davies. P. L., *Protein Sci.*, **1994**, *3*, 1760.

[34] DeLuca. C. I.; Davies. P. L.; Ye. Q. L.; Jia. Z. C., *J. Mol. Biol.*, **1998**, *275*, 515.

[35] Smolin. N.; Daggett. V., *J. Phy. Chem. B*, **2008**, *112*, 6193-6202.

[36] Zelent. B.; Bryan. M. A.; Sharp. K. A.; Vanderkooi. J. M., *Biophysical Chemistry*, **2009**, *141*, 222-230.

[37] Inada. T.; Lu. S., *Crystal Growth & Design*, **2003**, *3*, 747-752.

[38] Baruch. E.; Mastai. T., *Macromol. Rapid Commun.*, **2007**, *28*, 2256-2261.

[39] Yagci. Y. E.; Antonietti. M.; Borner. H. G., *Macromolecular Rapid Communications*, **2006**, *27*, 1660-1664.

[40] Gibson. M. I.; Barker. C. A.; Spain. S. G.; Albertin. L.; Cameron. N. R., *Biomacrolecules*, **2009**, *10*, 328-333.

[41] Hederos. M.; Konradsson. P.; Borgh. A.; Liedberg. B., *J. Phys. Chem. B*, **2005**, ***109***, 15849-15859.

[42] Inada. T ; Lu. S., *Chem. Phys. Lett*., **2004**, *394*, 361-365.

[43] Tam. R. Y.; Rowley. C. N.; Petroy. I.; Zhang. T.; Afagh. N. A.; Woo. T. K.; Ben. R. N., *J. Am. Chem. Soc*, **2009**, *131*, 15745-15753.

[44] Fields. G. B.; Fields. C. G., *J. Am. Chem. Soc*., **1991**, *113*, 4202-4207.

[45] Mimura. Y.; Yamamoto. Y.; Inoue. Y.; Chujo. R., *Int. J. Biol. Macromol*., **1992**, *14*, 242-248.

[46] Tam. R. Y.; Ferreria. S. S.; Czechura. P.; Chaytor. J. L.; Ben. R. N., *J. Am. Chem. Soc*, **2008**, *130*, 17494-17501.

[47] Laage. D.; Hynes. J. T., *Science*, **2006**, *311*, 832.

[48] Winkler. K.; Lindner. J.; Bursing. H.; Vohringer. P., *J. Chem. Phys.*, **2000**, *113*, 4674.

[49] Woutersen. S.; Emmerichsm. U.; Bakker. H. J., *Science*, **1997**, *278*, 658.

[50] Lawrence. C. P.; Skinner. J. L., *J. Chem. Phys*, **2003**, *118*, 264.

[51] Walraten. G. E.; Shokmabadii. M. S.; Yang. W. H.; Chu. Y. C.; Monosmith. B., *J. Phys. Chem*, **1989**, *93*, 2909.

[52] Sciortino. F.; Geiger. A.; Stanley. H. E., *Nature*, **1991**, *354*, 218.

[53] Ishihara. Y.; Okouchi. S.; Uedaira. H., *Faraday Trans*., **1997**, *93*, 3337.

[54] Blokzijl. W.; Engberts. B. F. N., *Angew. Chem. Int. Ed.*, **1993**, *32*, 1545.

[55] Ishimura. M.; Uedaira. H., *Bull. Chem. Soc. Jpn*., **1990**, *63*, 1-5.

[56] Czechura. P. ; Tam. R. M. ; Dimitrijevic. E. ; Murphy. A. V. ; Ben. R. N. *J. Am. Chem. Soc.*, **2008**, *130*, 2928-2929.

[57] Donati, I.; Gamini, A.; Vetec, A.; Compa, C; Paoletti, S. *Biomacromol*., **2002**, *3*, 8025.

Chapter Three: **Hydrophilic and Hydrophobic Modification of Poly(ethylene-alt-maleic anhydride) for Colloidal Applications**

3.1 Manipulating Matter at the Nanoscale

On December 29th 1959, Richard Fenyman delivered what was to become a seminal lecture entitled "There's plenty of room at the bottom"[1] In it he outlined how the ability to manipulate matter, first at a micro then nano-scopic level would allow for advances in computer processing power and data storage. In addition, Fenyman outlined the "weird" possibility of "swallowing the doctor", whereby a microscopic robotic doctor would conduct medical procedures internally.

Fenyman proposed this be achieved by building tools, with which to build smaller tools, with which to build smaller tools and so on until a tool exists which is small enough to manipulate matter at the appropriate scale. This defines what was to become the top down methodology wherein macroscopic materials are machined down to the appropriate scale. And remarkably successful this approach has been, with advances being made in areas as seemingly diverse as microprocessors and sunscreens.

While Fenyman commented on nature's success operating at this length scale, he did not explore in any detail nature's route to the nanoscale, namely the self assembly of molecules into supra-molecular structures. This approach has come to be known as the bottom up methodology and biological structures as diverse as DNA, cell membranes and enzymes are examples of species that have resulted from it.

In more recent years polymer chemistry has been of huge importance in synthetically replicating nature's approach. Polymeric materials have now been successfully employed in the self assembly of myriad supra-molecular architectures some of which are discussed in the following section.

3.2 Self assembly in organic and biological chemistry

In the context of organic chemistry self assembly involves the organisation of molecular species into higher order, supra molecular structures. It is worth briefly considering what is, and is not, self assembly.

The bulk precipitation of a substance from a solvent is, in a sense, self assembly in that molecules combine to form supra-molecular aggregates. However, this would not normally be regarded as self assembly which instead carries with it a distinct notion of an ordered and defined structure. In this sense crystallisation could be regarded as self assembly whereas bulk precipitation of an amorphous powder is not.

The term self assembly is a description of a process not of a system. As a result, self assembly can occur in organic solvents, water or even from a gas. However, for the remainder of this chapter the process of self assembly will be discussed in terms of self assembly in aqueous systems.

The process of self assembly is a spontaneous and thermodynamic one, and consequently a great deal can be understood through the physical processes which govern the free energy of self assembly for a given system.

The influence of enthalpy is most dramatic when multiple intra- or intermolecular forces act in concert to form complex structures. An elegant example is the polypeptide secondary structure known as the α-helix (figure 3-1).[2] Such structures are formed by hydrogen bonding between the carbonyl oxygens and amidic protons of peptide bonds at sites, remote to each other, along the peptide backbone. The overall effect is to induce a helical structure which results in hydrogen bonds between peptides four residues apart.

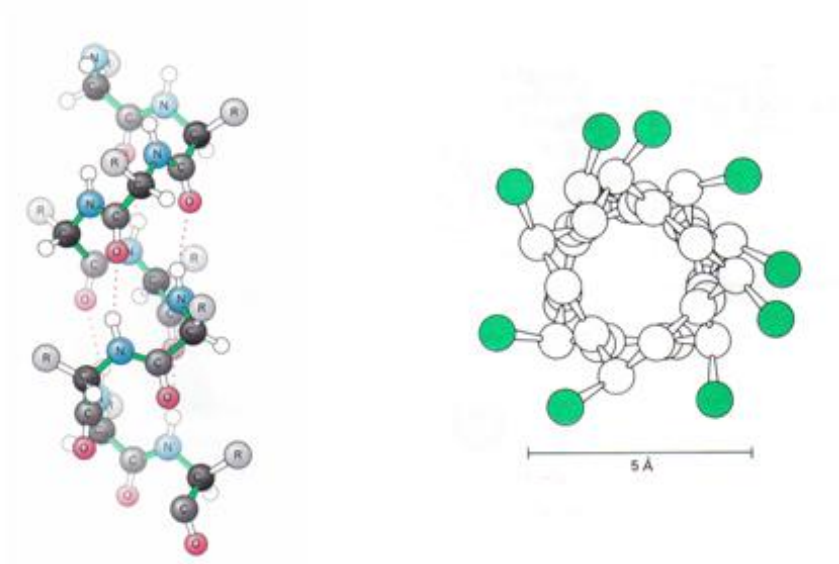

Figure 3-1: Left: representation of an α-helix. Hydrogen bonds are depicted by red-dotted lines. Right: α-helix as viewed from above. (Reprinted from Stryer).[2]

The second factor influencing the free energy of self assembly, and of more relevance to this chapter, is entropic and is known as the hydrophobic effect. Hydrophobicity, describes a molecule's propensity to "avoid" water. The physical basis for this aversion comes from water's capacity to form strong hydrogen bonds and the inability of the hydrophobic species to reciprocate.

In the bulk, water molecules are able to reorientate quickly due to the extended water-water hydrogen bonding network. From the perspective of an individual water molecule there are multiple orientations available which are enthalpically favourable. As a result, the water molecule is able to quickly move between these orientations thereby maintaining the molecule in a high entropy state and minimising the system's free energy.

However, if the water molecule is adjacent to a hydrophobe then, typically, it is not able to form hydrogen bonds in that direction, and in addition, bifurcated water is excluded from the surface (see chapter 2). As a result, the orientational freedom of the water molecule is restricted and a cage like solvating structure forms (figure. 3-2).[3]

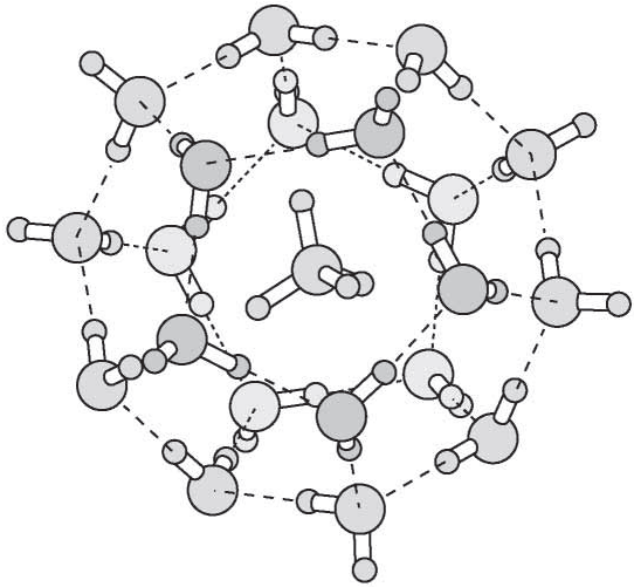

Figure 3-2: Idealised model of a water clathrate cage solvating a methane molecule. (Reprinted from Konrad *et al.*[3])

It should be noted that these clathrate cages are not entirely frozen and do retain some dynamism, in the case of methane Rezus and Baker[4] determined that around 20% of the solvating water molecules are frozen, with the remainder maintaining some of their conformational freedom.

As a result of this, the solvating water molecules are of low entropy and, therefore, there is a drive towards the coalescence of the hydrophobic structures into larger aggregates; which minimises the total hydrophobic surface area resulting in fewer water molecules being conformationally restricted.[5] As a result of this, most aggregates formed via this mechanism are spherical.

While intramolecular forces and the hydrophobic effect are distinct phenomena, it is important to note that in many systems both operate in concert to produce complex structures such as the tertiary and quaternary structures of proteins.

3.3 Amphiphiles and self assembly

Amphiphilic molecules, are composed of distinct hydrophilic and hydrophobic domains (figure 3-3), and are often able to self-assemble by excluding their hydrophobic moieties from water, whilst simultaneously maintaining the hydrophilic moieties contact with it, thereby maximising the system's entropy and therefore free energy.

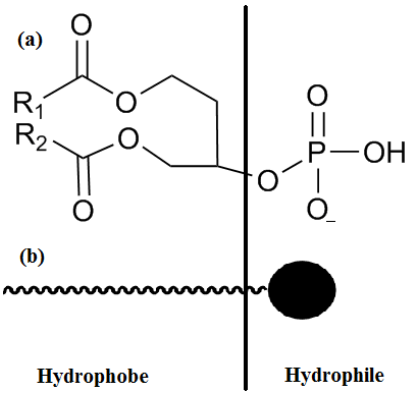

Figure 3-3: (a) Example of an amphiphilic molecule where R_1 and R_2 are alkyl chains; (b) schematic of an amphiphilic molecule. The vertical bar represents the separation of the molecule's hydrophobic and hydrophilic domains.

The process of an amphiphile's aggregation is governed by several factors including: its molecular identity, concentration and temperature (figure 3-4).[6] The concentration at which amphiphiles spontaneously aggregate occurs at a characteristic concentration, namely the critical aggregation concentration (CAC).

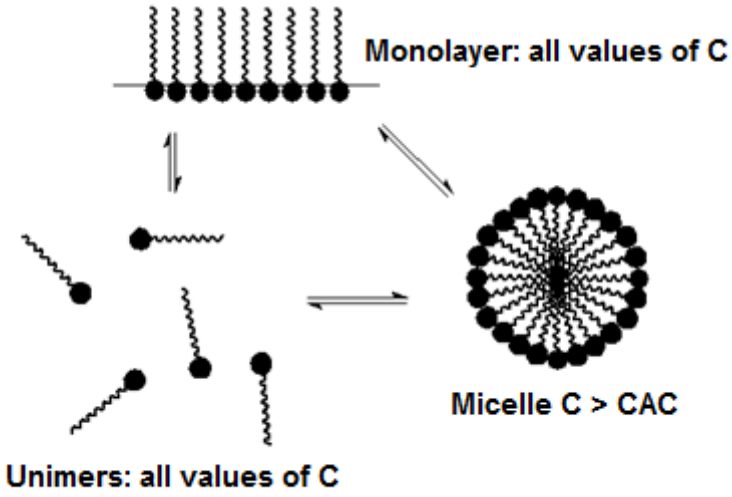

Figure 3-4: Schematic of amphiphilic self assembly where C is the amphiphile concentration; and, CAC the critical aggregation concentration.

Classical amphiphiles, surfactants, when introduced into water at a concentration below the CAC exist in equilibrium between a monolayer at the air-water interface and vessel-water interface, which allows the hydrophobic moieties to be excluded from the water, and the bulk solution as unimers. However, as the concentration of amphiphiles is increased the interface becomes saturated and so the concentration of unimers begins to increase with increasing concentration, eventually the concentration of unimers exceeds the CAC and aggregates form (figure 3-4). The thermodynamic drive for the self assembly of unimers in to aggregates is the increase in entropy resulting from the release of water molecules which form the solvent cages around the hydrophobic moieties.

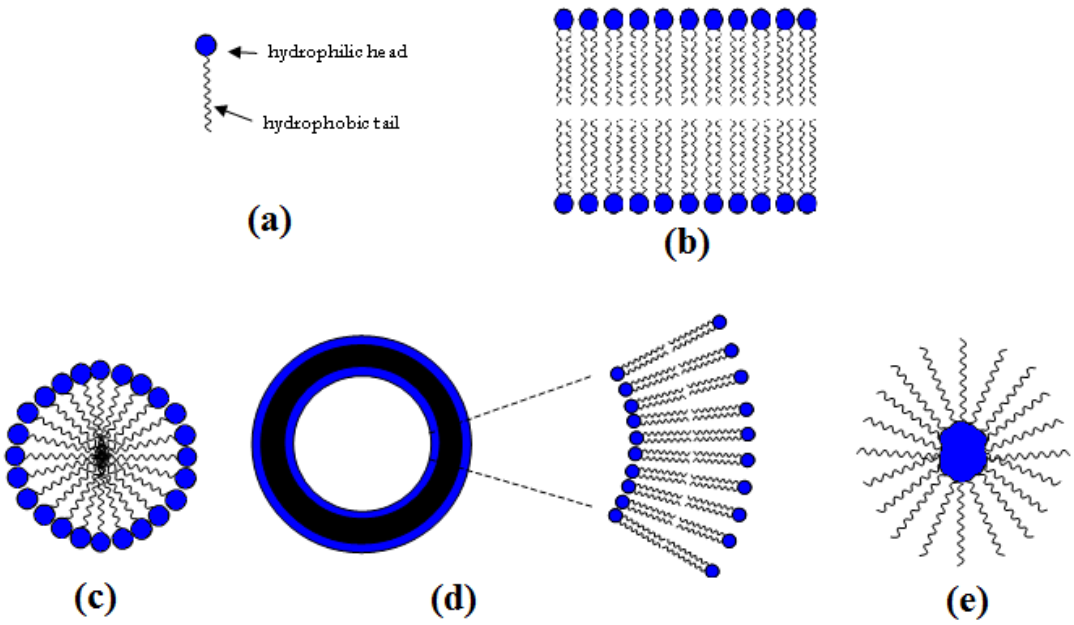

Figure 3-5: Representation of amphiphilic aggregates: (a) amphiphile, (b) bilayer, (c) micelle, (d) liposome (e) reverse micelle

Bilayers (figure 3-5 (b)) are double layers which describe a sheet wherein the hydrophobic groups are orientated towards the bilayer's centre (the core). Micelles (figure 3-5 (c)) are spherical structures wherein the hydrophilic moiety forms the interface with the water and the hydrophobic moiety the core. Finally, liposomes (figure 3-5 (d)), are bilayers of amphiphiles encloses an internal, solvent filled, cavity. In forming liposomes the hydrophobes at the edge of the bilayer are excluded from the solvent. Finally, reverse micelles (figure 3-5 (e)) are an example of self assembly in non-aqueous solvents; here the hydrophilic component forms the core and hydrophobic component the corona.

3.3.1 Aqueous polymeric self assembly

The advent of controlled polymerisation techniques has made the synthesis of amphiphilic block copolymers comparatively trivial.[7-9] Structurally, amphiphilic polymers are composed of at least two domains, one of which is hydrophilic the other hydrophobic, for example poly(styrene)-b-(acrylic acid). By convention the solubilised block is termed the corona whereas the block forming the aggregate's centre is termed the core (figure 3-6 (a)). However, it should also be noted that, if such a polymer is placed into a solvent which is selective for the hydrophobic block only a reverse micelle can form wherein the hydrophobic block forms the corona (figure 3-6 (b)).

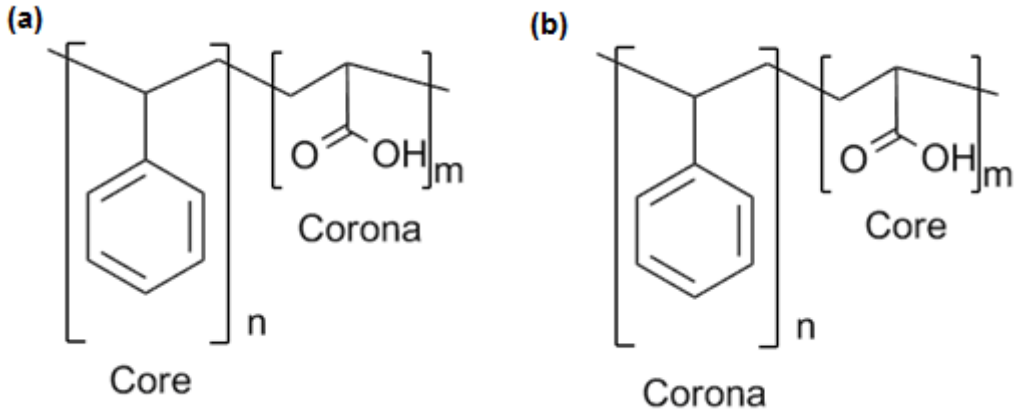

Figure 3-6: Structure of the amphiphilic block co(a) in water and (b) a solvent selective for the poly(styrene) block alone.

While the thermodynamics of amphiphilic block copolymer aggregation is entirely analogous to that of small molecule amphiphiles, there are a number of considerations which result in the self assembly of polymers being somewhat more complex than that of small molecules.

The large, entangled, nature of the polymer chain segments forming the core, the aggregates formed may be to be kinetically frozen providing the glass transition of the core forming block is lower than the solvents temperature. This often means that the products of self assembly with polymers are not entirely the thermodynamic product. In other words, the mobility of small molecule amphiphiles in and out of the aggregate allows the system to reach thermodynamic equilibrium, whereas polymeric amphiphiles can become kinetically frozen in thermodynamically sub-optimal structures. In practical terms this means that polymeric aggregates will persist even when diluted below the polymer's CAC and that they are affected, often indefinitely,

by the conditions at the time of aggregation such as: temperature, solvent, and the rate of precipitation.

The core and corona forming blocks heavily influences the structure's final morphology. Essentially, the number of chains which are able to aggregate (N_{agg}) is in proportion to the size of the aggregate. This, in part, is determined by the packing parameter (P) which provides a geometric rationalisation for the process of self assembly (equation 3-1). [10,11]

$$P = \frac{V}{l_c a_0} \qquad \text{(eqn. 3-1)}$$

Where a_0 is the optimal surface area, V the volume of the hydrophobic block, and l_c the end to end hydrophobic block length (figure 3-7). In other words, P is a ratio of two areas, one a steric area (V/l_C) and the other the actual area at the interface a_0.

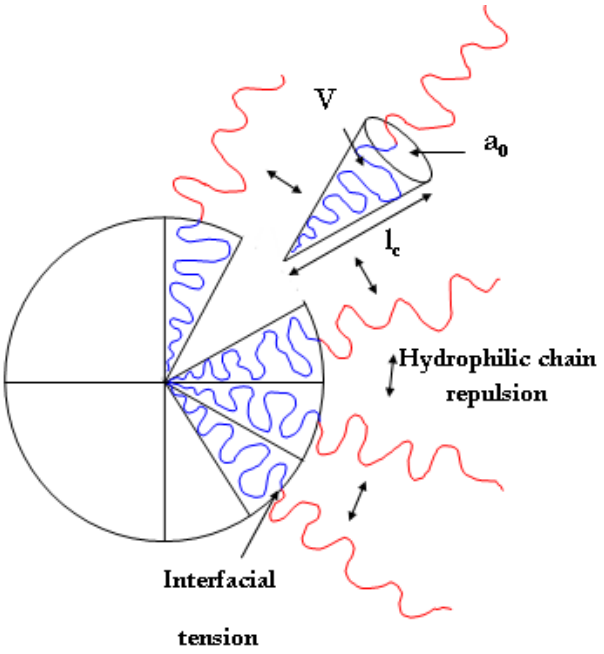

Figure 3-7: Schematic of surfactant packing according to the packing parameter principle

These geometric considerations provide a partial explanation for some of the possible aggregate structures which can form including: micelles, cylindrical micelles and liposomes (figure 3-8).[10]

For example, a spherical micelle which is packed so that there is no free space within the micelle, cannot be of radius longer than the fully extended length of the hydrophobic block. Introducing this constraint means that, for a spherical structure, $0 \leq P \leq 1/3$. Similarly, there are such constraints on the packing of other aggregate structures as determined by the geometry of the aggregate (figure 3-8).

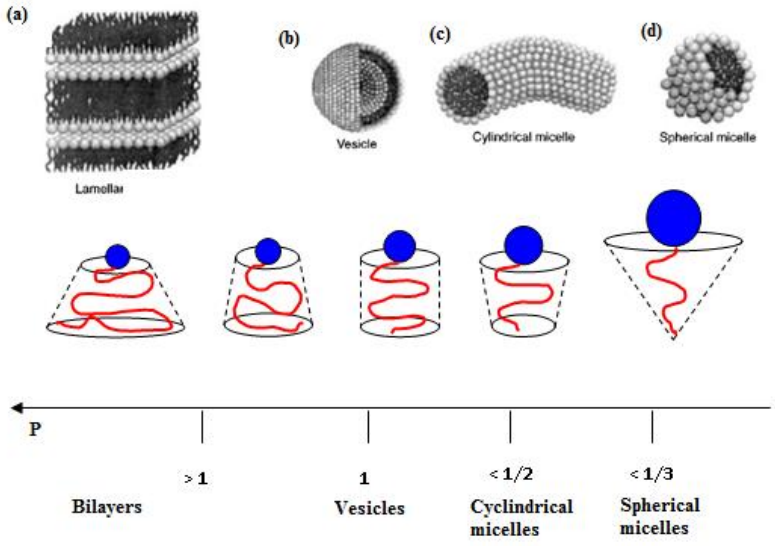

Figure 3-8: Amphiphile self-assembly leads to a range of different aggregates and their relation to the packing parameter (P), (a) lamellae (b) vesicles (c) cylindrical micelles (d) spherical micelles (figures (a-d) reprinted from Evans and Wennerstrom)[12]

The interfacial area is directly proportional to the area of the hydrophilic block. This means for a given hydrophilic block the interfacial area scales with the block length and, therefore, when both l_c and V (the hydrophobic block) are constant, the nature and size of the aggregate can be changed by altering the hydrophilic length; the shorter the length, the smaller a_0 and therefore the closer to unity is P. This is best described in terms of an example; Eisenberg and co-workers have conducted extensive work on poly(styrene)-b-(acrylic acid) and have found the following trends (figure 3-9).[13]

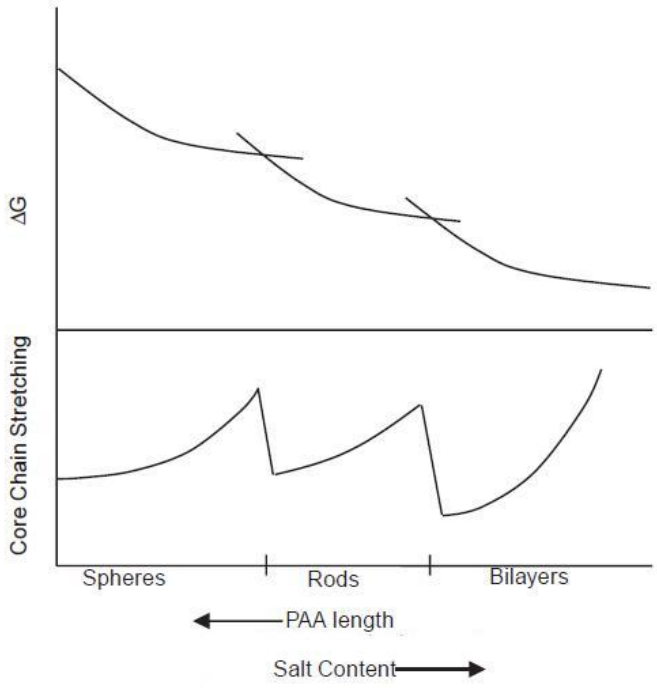

Figure 3-9: The effect of various variables on free energy, core chain end to end length and ultimate aggregate structure of poly(styrene)-b-(acrylic acid) (Reprinted from Eisenberg *et al*) [13]

This example also serves to highlight effects which, while they can be expressed geometrically, are not simply the result of the hydrophile's volume. The acrylic acid block, when de-protonated, bears a charge, the consequence of this is that adjacent hydrophilic blocks within the aggregate repel each other thereby preventing their close packing. This means hydrophilic blocks have a greater effective volume than their chain dimensions alone would suggest. This explains why, in the case of poly(styrene)-b-(acrylic acid), the salt content affects the aggregate structure, (figure 3-9) and, by extension, P. As the salt content increases so the charges on adjacent acrylic acid blocks are screened from each other, reducing the repulsion between adjacent acrylic acid blocks, thereby reducing the acrylic acid block's effective volume.

However, this purely geometric argument does not account for the thermodynamics of aggregation. While geometry enters into the free energy calculations as a boundary condition, the two main contributing factors are: the interfacial energy of the hydrophobic-hydrophilic interface, and the loss of entropy resulting from the aggregation of flexible polymer chains.[14]

Therefore, when the interfacial energy is large, and the loss of entropy on aggregation small, the minimisation of the interfacial energy dominates the thermodynamics of aggregation. In the case of conformationally restricted polymers, the entropy loss on their aggregation is low and such polymers will aggregate in such a way as to minimise the interfacial area per unit volume (equation 3-2).[14]

$$a_v = \frac{d\emptyset}{l} \qquad \text{(equation 3-2)}$$

Where a_v is the interfacial area per unit volume, d is the dimensionality of the structure formed, Ø is the volume fraction of the hydrophobe and l the hydrophobe's chain length normal to the interface.

The dimensionality of the various aggregates are as follows: bilayers d = 1 (vesicles d≈1), cylindrical micelles d=2, and micelles d=3. Therefore, the formation and stability of bilayer structures for low entropy polymers is often quite pronounced. [14,15]

In summary, the structure of self assembled polymer aggregates is determined by numerous factors including: the conditions of aggregation, the polymer's molecular

identity, the hydrophile to hydrophobe ratio, and the conformational freedom of the polymer backbone. While this makes predicting the final structure somewhat harder than small molecule amphiphiles it does present the opportunity to synthesise a wider variety of structures including kinetically frozen non-equilibrium structures such as: bicontinuous bilayers, toroids, and trapped vesicles.

3.3.2 Associating polyelectrolytes and polysoaps

It has been observed that polyelectrolytes, based on a hydrophilic backbone, which are modified with a small amount of a hydrophobic group (typically <2% but up to 10%) produce remarkably viscous aqueous solutions. This increase in solution viscosity is attributed to the formation of transitory hydrophobe-hydrophobe interactions between polymer chains in solution (figure 3-10).[16]

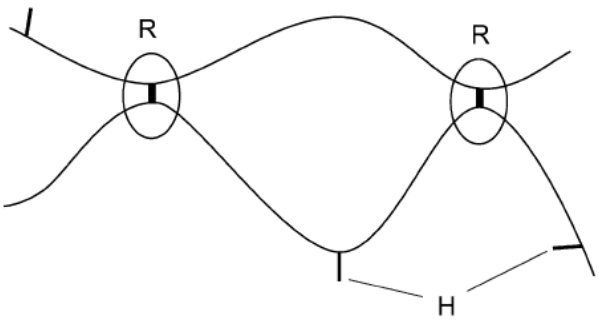

Figure 3-10: A simple model of an associative polymer. H: hydrophobic side chain R: reversible hydrophobic-hydrophobic bond (reprinted from Roger *et al*)

16

Typically, the higher the number of hydrophobic groups per chain the more marked the increase in viscosity, and the lower the concentration at which the increase occurs.

The molecular mechanism for these transitory chain-chain interactions is supported by both small angle x-ray and fluorescence studies.[17]

In 1956, Strauss *et al*[18,19] partially reacted poly(4-vinyl pyridine) with n-dodecylbromide in order to study its aqueous solution behaviour. The aqueous viscosity was observed to increase up to a critical n-dodecyl bromide incorporation of 13.6%, after which it dramatically fell. This was attributed to a significant change in conformation which allows the n-dodecyl moieties to be excluded from the water.

Strauss *et al*[20,21] went on to conduct a more extensive study on the solution behaviour of a series of poly(n-alkyl vinyl ether-co-maleic acid)s with varying n-alkyl chain lengths. By measuring changes in the intrinsic viscosity with n-alkyl chain length and pH, Strauss was able to conclude that, when the n-alkyl chain length is longer than three carbon atoms, the polymer chain changes conformation so as to bring about the intramolecular aggregation of the hydrophobic n-alkyl moieties.

This type of polymer belongs to a sub class of amphiphilic polymers known as polysoaps. Structurally they consist of low molecular weight amphiphilic moieties joined through a polymer backbone. In other words, they appear as if an amphiphilic monomer has been polymerised, although typically, the amphiphiles are introduced to the polymer backbone post polymerisation.[17]

As discussed, the distinguishing feature of polysoaps, and in contrast to block amphiphilic copolymers, is their ability to undergo intramolecular hydrophobic aggregation. Because the process is intramolecular, there is no critical aggregation

concentration in the conventional sense, although it may be possible to define one in terms of degree of polymerisation, consequently they are able to be used as concentration independent encapsulants.[22,23]

Since Strauss' early work potentiometric, calorimetric, fluorescence and neutron scattering studies have confirmed the formation of a compact coil stabilised by the alkyl side chains.[22,24-30]

However, the precise structure of these intramolecular aggregates is still subject to debate from which three models have emerged: the local micelle, molecular micelle and the regional micelle (figure 3-11).

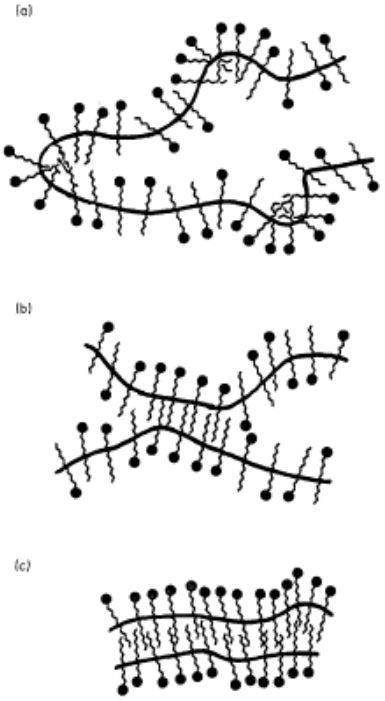

Figure 3-11: Schematic representation of: (a) the local micelle wherein adjacent amphiphiles aggregate, (b) the regional micelle wherein two remote parts of a chain superpose their amphiphilic moieties, and (c) the molecular micelle wherein the entire polymer chain forms a single micellar aggregate [31]

In their seminal work Strauss *et al*[32] proposed the formation of local micelles along the polymer backbone, by assuming the aggregation of a limited number of neighbouring surfactant moieties (figure. 3-11 (a)). As a result, the model is independent of the degree of polymerisation but requires a highly flexible polymer backbone. In order to account for the fact polymer backbones do not have absolute freedom Strauss assumed that the hydrophilic moieties would have to be in slight excess compared with small molecule surfactants.[32]

The molecular micelle model, (figure 3-11 (c)), assumes the intramolecular aggregation of all of the surfactant moieties of a given polymer. In other words the micelle's aggregation number is the same as the degree of polymerisation. Theoretical treatments of this model indicate that sterics is unimportant, fast exchange is unnecessary and that the balance of hydrophilic to hydrophobic moieties can be closer to that of a conventional surfactant.[33,34]

A compromise between the local and molecular models is the regional micelle, which assumes the aggregation of neighbouring surfactant moieties superposed by the aggregation of remote segments of the polymer chain. In other words, two remote parts of the same polymer chain enter a conformation which allows the mutual aggregation of their surfactant moieties (figure 3-11(b)). Therefore, as with the local micelle, fast exchange of amphiphilic groups is possible but in a manner which circumvents the extreme geometric and steric restrictions of the local micelle.[35,36]

It should be noted that because all of these are intra-chain are processes there is no critical concentration at which they occur. In other words such aggregates occur at all concentrations. However, should the polymer chains begin to inter-molecularly aggregate, at some critical (inter-chain) aggregation concentration, this would clearly reduce the concentration of intra-molecular aggregates.

In more recent year consensus has been building around the regional micelle model. Theoretical treatments by Borisov and Hugouvieux[37,38] indicate that the polymer chains appear to fold then collapse as if segments of the polymer backbone were "sticky" towards each other.

In addition, there is strong evidence of intermolecular aggregation processes occurring at higher concentrations, which would be expected to compete with intramolecular aggregation under the regional micelle model. Of particular interest is the work of Hu *et al*. [30] who incorporated two fluorophores, namely amine bearing derivatives of pyrene and naphthalene, onto the backbone of a poly(sodium maleate-alt-ethyl vinyl ether). By measuring the extent of non-radiative energy transfer (NRET) between two different fluorophores the distance between them can be estimated.

The results demonstrated three things: firstly, intramolecular micelles are observed to form at low to intermediate pH and at high ionic strength; secondly, the micelle's NRET signal was observed to diminish as the pH increased indicating the dispersion of intramolecular aggregates; and thirdly, inter chain NRET was observed to occur at high salt concentrations.

In order to rationalise this increase in interchain NRET with ionic strength, Hu *et al* proposed that an increase in salt concentration allows the fluorophores to migrate to the intramolecular micelle's surface, however, it seems equally plausible that the increased ionic strength allows the charged intramolecular aggregates to approach one and other.

Despite this, the formation of inter-chain aggregates receives less attention than that of intra-chain aggregates. This is possibly because, in most instances, even when inter chain aggregation appears to be extensive the micelles do not grow into higher order structures.

Notable exceptions are found in the work of Nayak *et al* who demonstrated, with a variety of dodecyl based polymers, including: poly[sodium 11-acrylamidoundecaonate][39] and poly[sodium N-(11-acrylamidoundecanoyl)-L-valinate],[40] that intermolecular aggregates can be formed (figure 3-12).

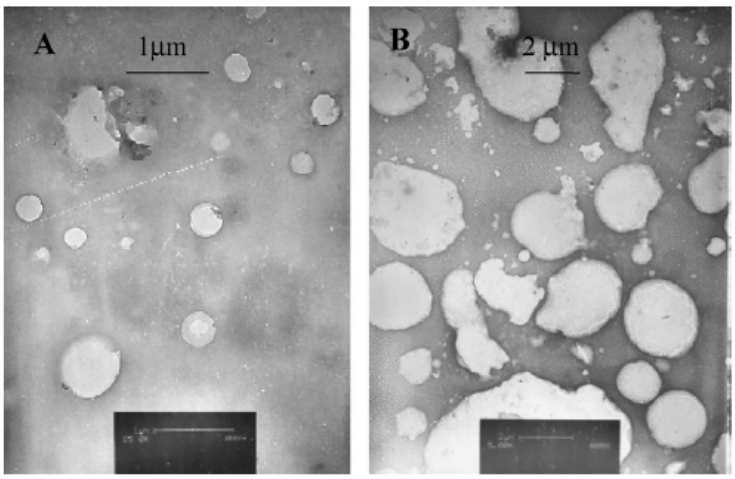

Figure 3-12 Negatively stained TEM image of poly[sodium N-(11-acrylamidoundecanoyl)-L-valinate] (Reprinted from Roy et al) [40]

In explaining these structures, Roy *et al*[40] proposed the following structures (figure 3-13) wherein the polysoap aggregates either intramoleculary (figure 3-13(b)) or as bilayer structures (figure 3-13 (c)) which can take the form of either bicontinuous or vesicular morphologies.

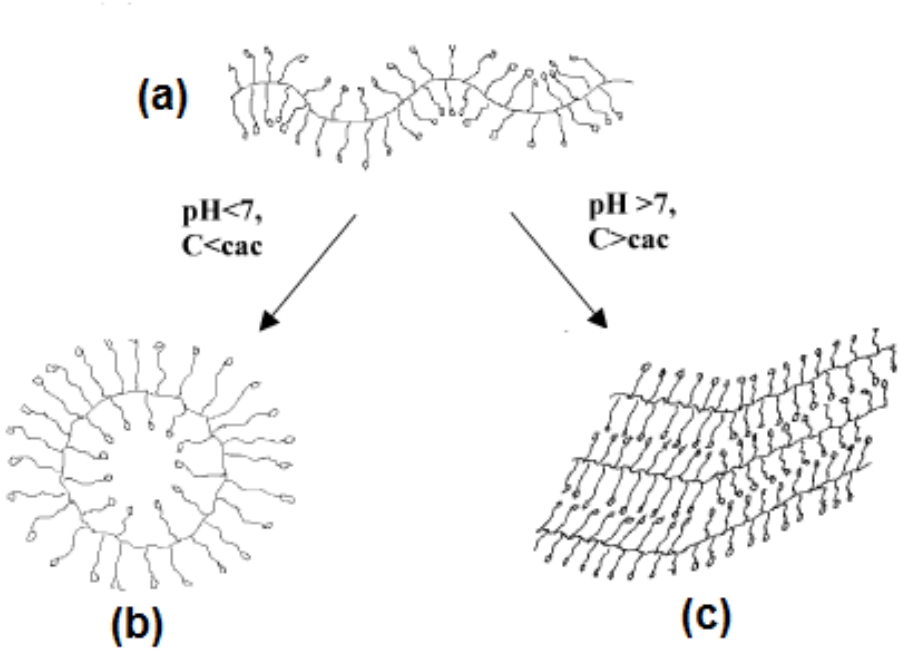

Figure 3-13: Proposed mechanism of poly[sodium N-(11-acrylamidoundecanoyl)-L-valinate aggregation: (a) free polymer chain, (b) intramolecular aggregation, (c) intermolecular aggregation.[39]

The fluorescence of pyrene is dependent on its environment; in a polar matrix such as water the intensity of its first fluorescence band is significantly reduced as compared to a non-polar matrices. Given pyrene's hydrophobicity there is a strong tendency for it to concentrate in the hydrophobic core of aggregates which then results in a fluorescence intensity much greater than that which would be expected of an aqueous pyrene solution. Therefore, pyrene provides a useful probe for hydrophobic environments within an aqueous colloidal system.

Roy *et al*[39] employed pyrene fluorescence in their study on polysoap aggregates and were able to demonstrate a CAC of 0.2 g L^{-1}, but importantly found that at no point did pyrene's I_1 band become independent of the polymer's concentration (figure 3-14).

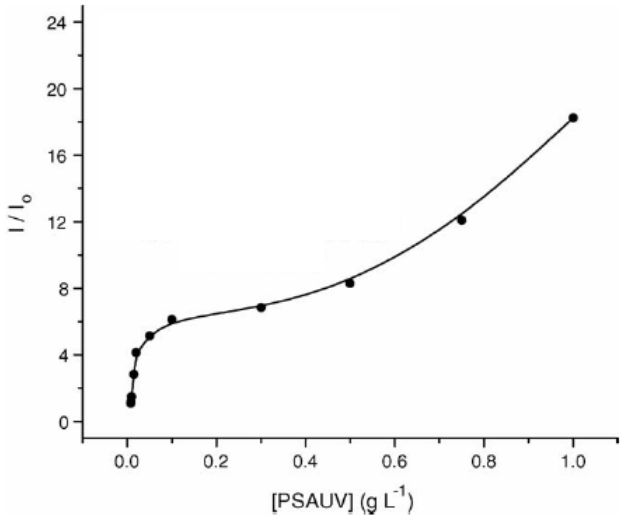

Figure 3-14: Ratio of pyrene's first emission band intensity vs. poly[sodium N-(11-acrylamidoundecanoyl)-L-valinate] concentration (reprinted from Roy *et al*) [39]

In other words, pyrene is being encapsulated at all concentrations, including those below the vesicle CAC. This contrasts with amphiphilic block copolymers where, at concentrations below the CAC, pyrene's fluorescence becomes independent of the concentration of polymer.[41] This indicates that the polymer forms intra-chain aggregates which, being independent of polymer concentration continue to encapsulate pyrene in a hydrophobic environment at concentrations below the CAC.

Interest in polysoaps comes from three distinct areas. Firstly, it has been suggested by some that the behaviour of polysoaps is closely analogous to that of proteins and other biological molecules. Therefore, they are seen as "toy box" biological molecules allowing a better understanding of the balance of physical processes which govern

their conformation. Secondly, they have a large capacity to be loaded with hydrophobic species meaning they are of potential interest in drug delivery and emulsion applications especially as many polysoaps are not surface active and therefore do not promote foaming. Thirdly, in more recent years these polymers have been used to solubilise lipid membrane proteins in bulk water, in relation to this application such polymers are usually named amphipols.[42]

3.4 Aims

The existent widespread use of maleic anhydride copolymers in the cosmetics industry along with an apparent market demand for time released and longer lasting formulations has stimulated interest in using such polymers as encapsulants.

To this end both hydrophilic and hydrophobic derivatives of E60 were synthesised and tested for: aggregation, capacity to encapsulate hydrophobic fluorophores and their response to changes in their structure and conditions of aggregation.

3.5 Results and discussion

3.5.1 Hydrophobically modified E60 derivatives

As has already been discussed, polyelectrolytes, which have a significant hydrophobic component, are able to self assemble into intramolecular and, in some cases, intermolecular aggregates.[39,40] Therefore, the effect of hydrolysed E60 (hE60) on pyrene's fluorescence was probed in order to determine whether any aggregation was occurring. This was achieved by preparing a variety of hE60 solution concentrations with a saturated aqueous pyrene solution ($6x10^{-7}$M) and then measuring the intensity

of pyrene's first emission band (I_1) (emission 373nm, excitation 339nm) and calculating the ratio of this value to the zero polymer concentration value (I_0) (figure 3-15).

The origin of this effect is that pyrene's emissions are quenched in polar environments, therefore, should self assembly occur the some of the pyrene will be encapsulated in the aggregates and excluded from the polar solvent. As a result, the intensity of the emission will increase. Therefore, the onset of self assembly will see pyrene's emission intensity become proportional to the polymer concentration.

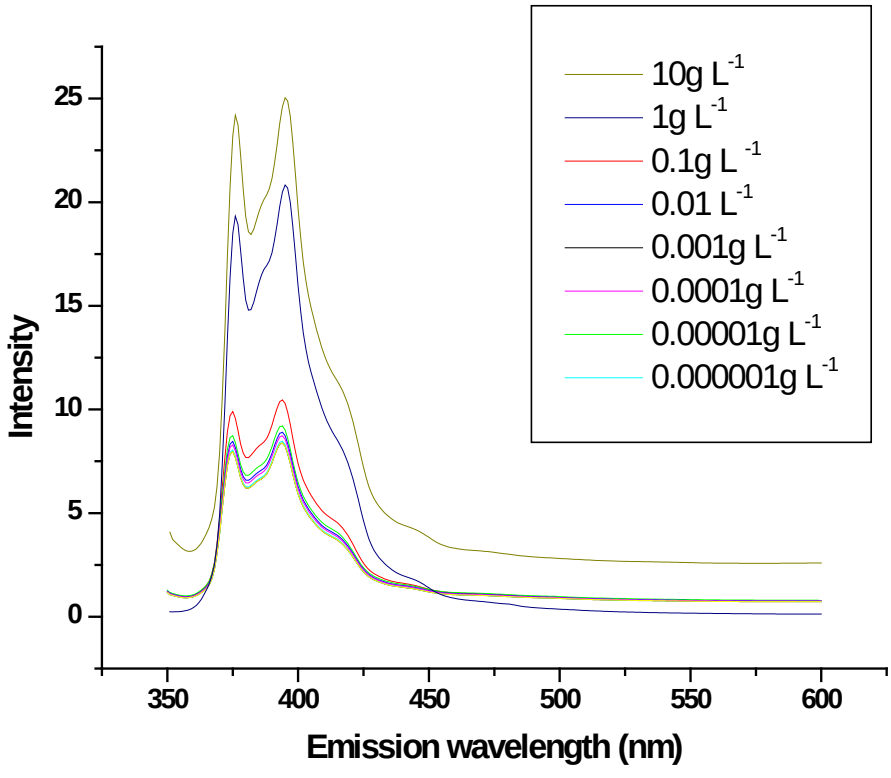

Figure 3-15: Emission spectra of pyrene in different concentrations of $hE60_{(aq)}$. Excitation wavelength 339nm

The origin of this effect is that pyrene's emissions are quenched in polar environments, therefore, should self assembly occur the some of the pyrene will be encapsulated in the aggregates and excluded from the polar solvent. As a result, the intensity of the emission will increase. Therefore, the onset of self assembly will see pyrene's emission intensity become proportional to the polymer concentration. This change in the relationship between emission intensity and polymer concentration is used to determine the critical aggregation concentration.

An alternative method to the one outlined here is to measure the ratio of pyrene first and third emission bands at different polymer concentrations. This is particularly sensitive as the third emission band is particularly quenched by polar environments. However, in this instance it is not particularly useful as the hydrophobic environments are comparatively polar and therefore the third emission band continues to be quenched even after the onset of both intra and inter chain aggregation.

By plotting the intensity of emission at 373nm in ratio with the intensity at zero polymer concentration it is possible to determine if self assembly is occurring.

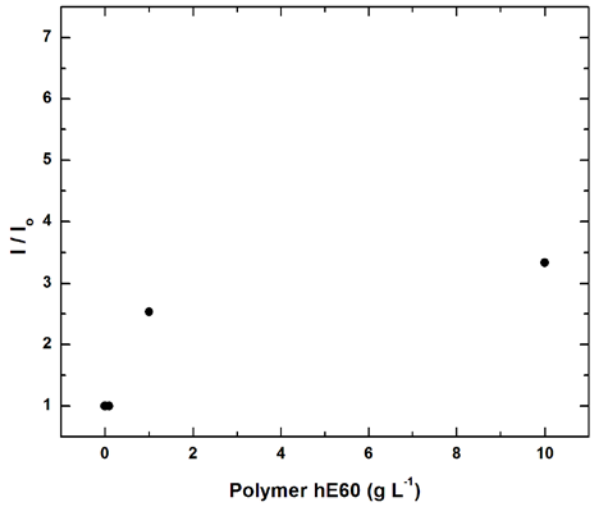

Figure 3-16: Plot of I/I_o vs. hE60 concentration (I is the intensity of pyrene's first emission band and I_o the intensity of pyrene's first emission band at zero polymer concentration).

The plot (figure 3-16) demonstrates a weak dependence of pyrene's fluorescence on hE60 concentration. However, were intramolecular aggregation occurring I_1/I_o would be concentration dependent at all concentrations and there is no evidence of intermolecular aggregation by light scattering. Therefore, it would seem this change in fluorescence is due to some other factor such as a significant change in solvent polarity at higher polymer concentration. Consequently, it was concluded that hE60 is unable to either aggregate or encapsulate pyrene across this concentration range. It should also be noted that these plots are often seen in the literature as log concentration vs. Intensity. However, this is typically done merely to create an appropriate scale. Typically, polymer aggregation occurs at low concentrations, circa

10^{-12} to 10^{-4} g L^{-1}, as a result the CAC is often found by serial factor 10 dilutions which, if plotted as a linear scale would be difficult to interpret. With polysoaps there is no region in which the polymer concentration is independent of pyrene's fluoresence intensity. Therefore, interchain aggregation is more easily resolved from intra- chain aggregation by probing over a smaller concentration range, in this case 0.1 to 10 g L^{-1}. As a result a linear plot can be used.

Previously, Hu *et al*[30] modified poly(maleic anhydride-alt-n-ethyl vinyl ether) with naphthylamine, dodecylamine and octylamine and in doing so reported the formation of intramolecular aggregates in all cases. Therefore, in order to try to induce either intra or inter molecular aggregation E60 was reacted with a series of hydrophobic amines (figure 3-17, table 3-1).

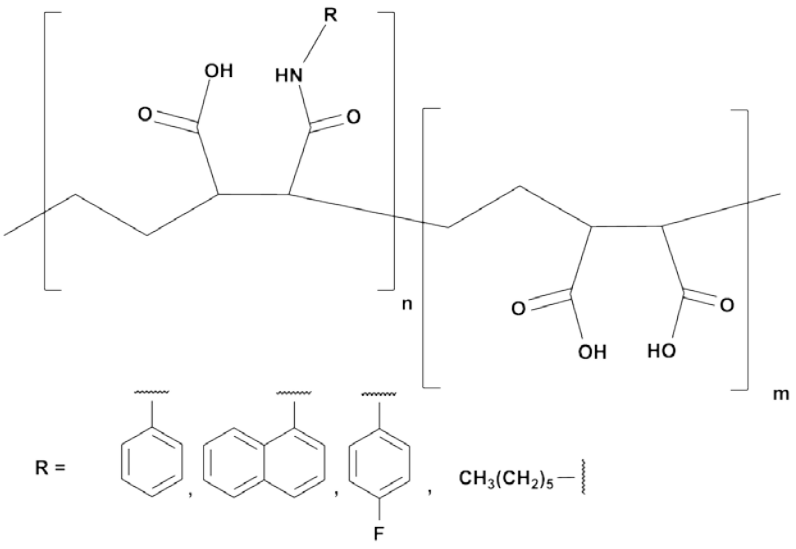

Figure 3-17: Hydrophobically modified E60 derivatives

Table 3-1: Hydrophobically modified polymers for aggregation

Code*	Amine	n†	m‡	M_n (Da)**
E60B20	Benzylamine	70	247	56,500
E60B50	Benzylamine	165	152	60,400
E60B80	Benzylamine	241	76	67,200
E60B100	Benzylamine	317	0	74,000
E60FB50	4-fluorobenzylamine	174	143	64,400
E60H50	Hexylamine	165	152	59,400
E60N50	Napthylmethylamine	152	165	66,900

*Code is based on the target anhydride to amide conversion with a particular amine, for example E60B50 E60B(enzylamide derivative at)50(% conversion to amide). B: benzylaminde; FB: 4-fluorobenzylamide; H: hexylamide; N: napthylmethylamide.

†: number of repeat units of amide (figure 3-17)

‡: number of repeat units of diacid (figure 3-17)

**: M_n calculated from ^{1}H NMR

Preparation of aqueous polymeric aggregates was brought about by three methods: firstly, the drop-wise addition of water to a stirred polymer DMF solution to a final DMF to water ratio of 1:9; secondly, the same procedure but followed by dialysis (≈ 12kDa mol. wt. cut off) against distilled water for 48 hours; thirdly, the addition of the DMF solution to the water to a final DMF to water volume ratio of 1:9 followed by dialysis against water for 48 hrs. The second technique, namely the addition of water followed by dialysis, is the standard procedure unless otherwise stated.

During the preparation of 1g L^{-1} polymer solutions it was found, somewhat surprisingly, that on the addition of water the solution became turbid indicating the formation of large, intermolecular aggregates. This was confirmed both by 90^{o} dynamic light scattering, and TEM (figure 3-18).

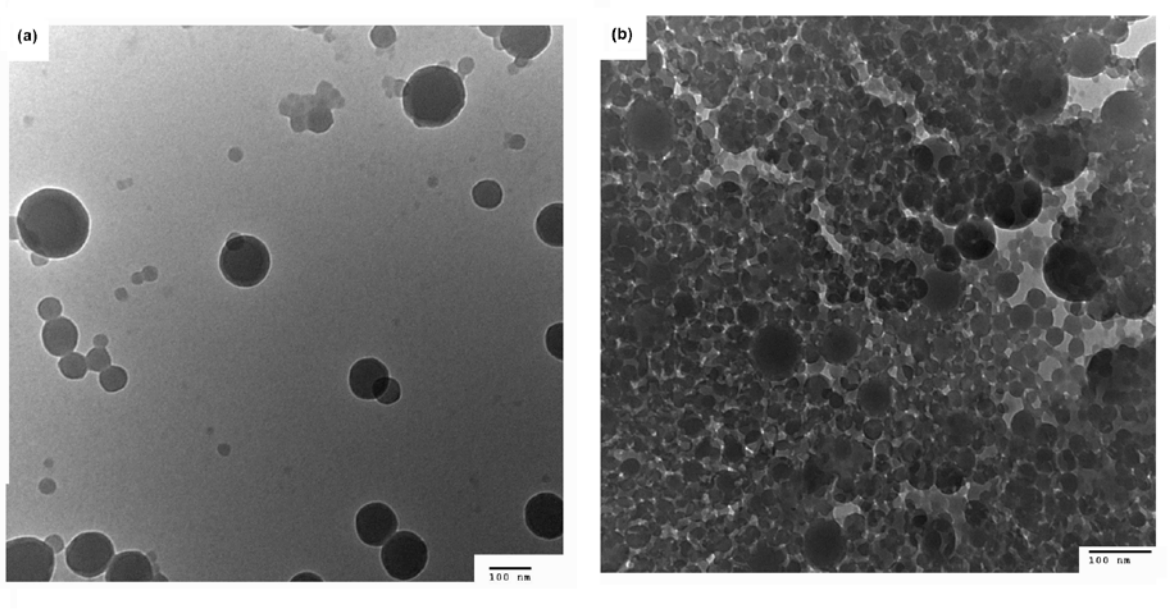

Figure 3-18: TEM images of E60B50 (a) 0.1mg mL^{-1} (b) 1mg mL^{-1}

In order to probe the effect of the degree and molecular nature of the hydrophobic modification, a series of 1mg mL^{-1} solutions were prepared by the careful drop-wise addition of water. The resulting aggregate sizes are given in table 3-2.

Table 3-2: Aggregate sizes as determined by both DLS and TEM.

Code	DLS (nm)*	DLS (nm)†	dpI	TEM (nm)ǂ
E60B20	40-48	123-146	0.22	36-172
E60B50	53-131	-	0.123	30-121
E60B80	124-128	-	0.095	101-142
E60B100	126-182	-	0.128	52-212
E60FB50	63-66	-	0.099	48-88
E60H50	30-66	-	0.134	28-92
E60N50	50-101		0.159	25-192

*DLS modal size of first distribution, † modal size of second distribution, ǂ quoted as a range.

The TEM and DLS values broadly concur although the range appears to be wider in the case of TEM.

A more detailed analysis of E60B20, E60B50, E60B80 and E60B100 aggregates demonstrates that the modal size and overall distribution increases with increasing hydrophobe incorporation (figures 3-19 and 3-20).

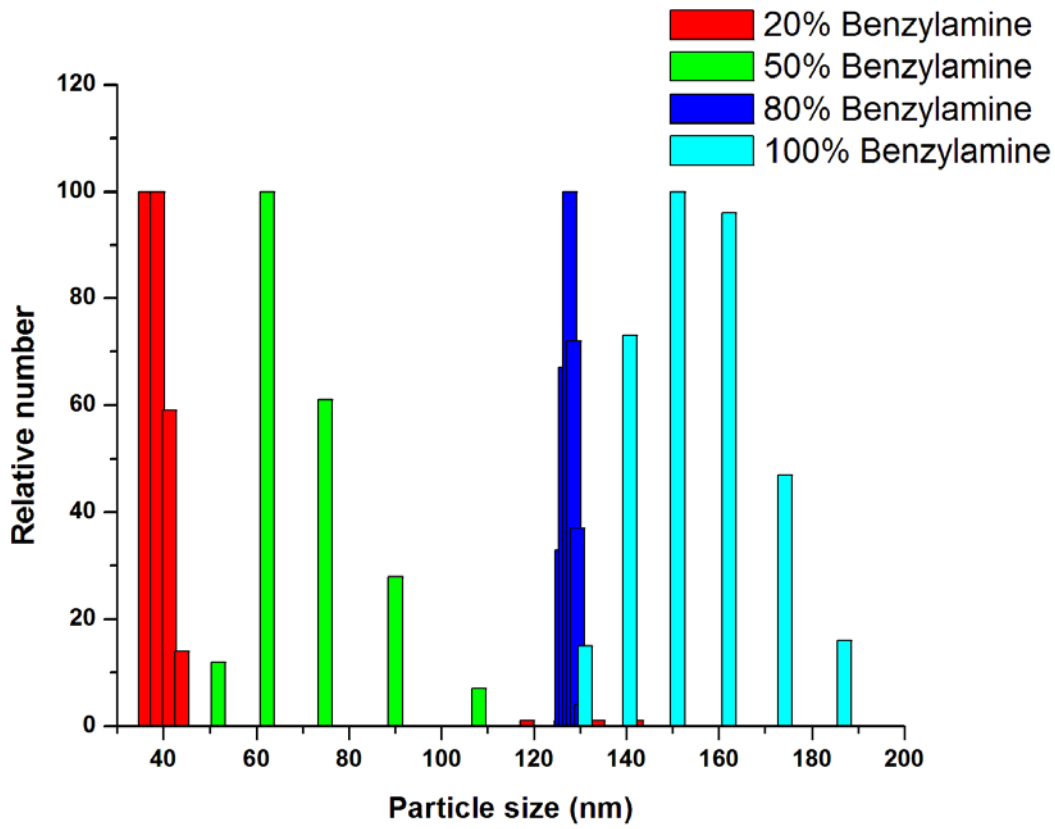

Figure 3-19: DLS distributions of aggregates containing increasing hydrophobe incorporation

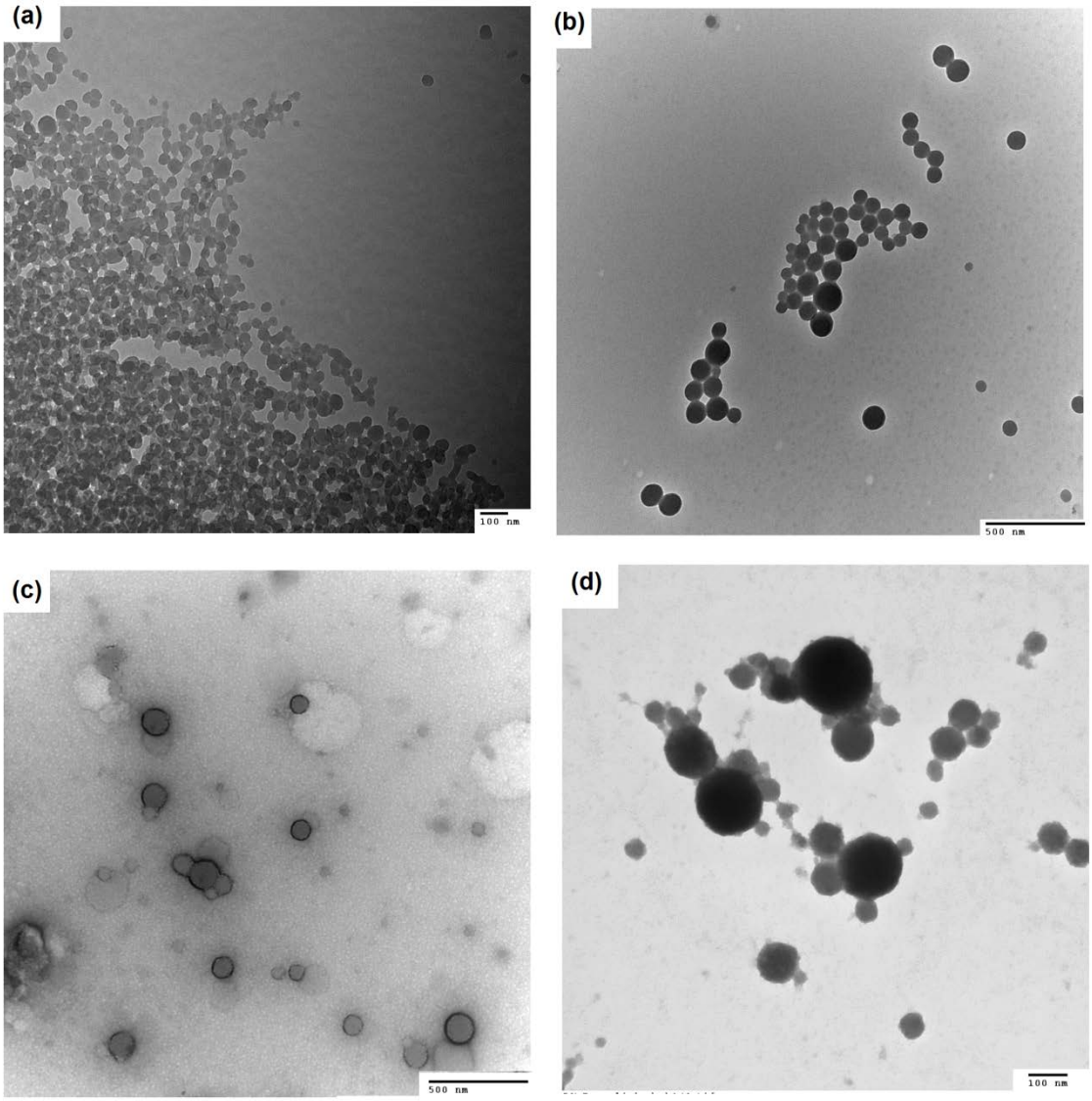

Figure 3-20: TEM images of aggregates from 1g L^{-1} (a) E60B100, (b) E60B80 (c) E60B50, and (d) E60B20. Aggregates were deposited from a 0.1g L^{-1}solution.

Figure 3-21 shows the structure of aggregates of E60B50, E60H50, E60N50, and E60FB50.

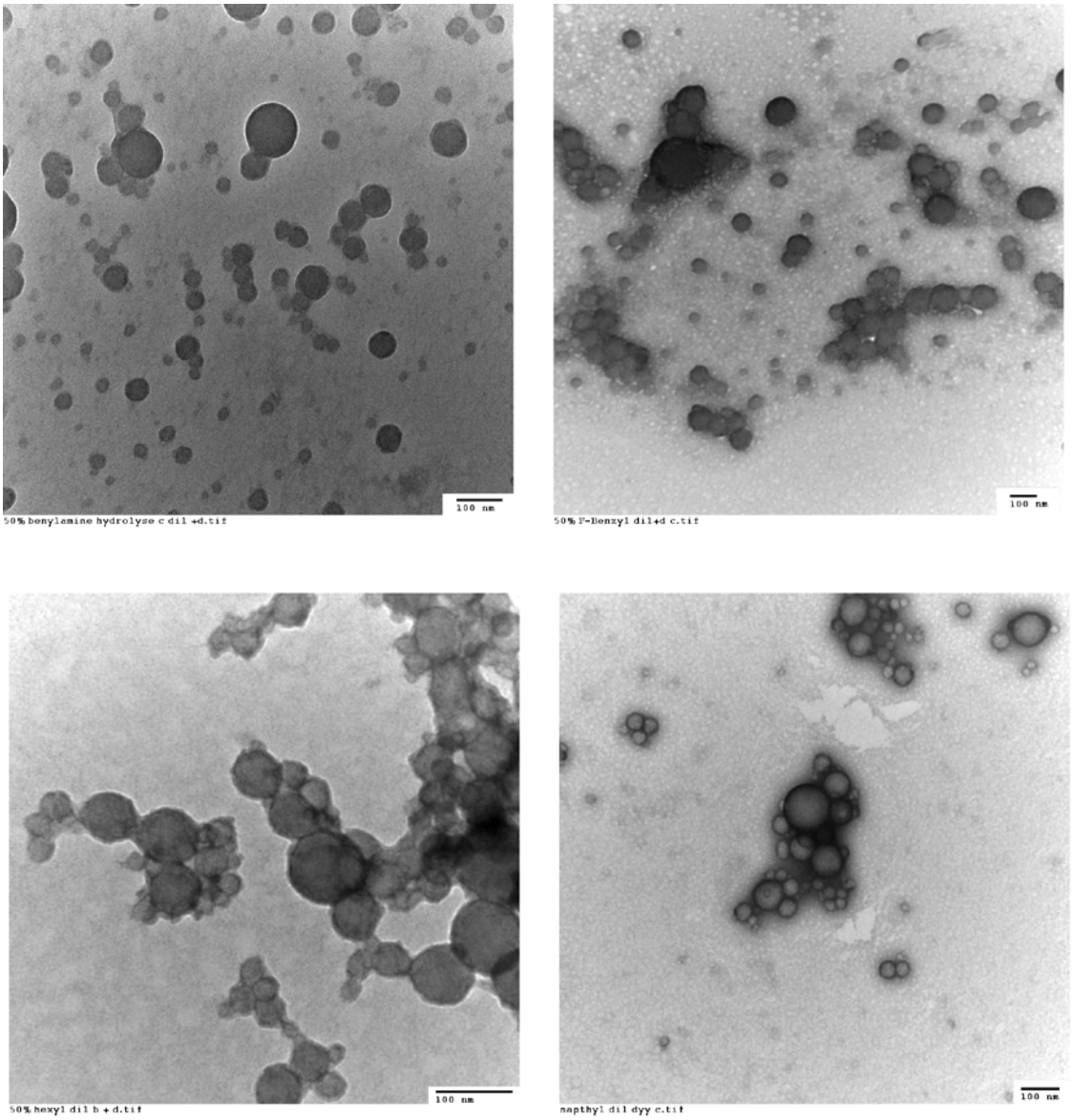

Figure 3-21: TEM images of: (a) E60B50, (b) E60FB50, (c) E60N50, and (d) E60H50 stained with uranyl acetate dye

While the modal size of the aggregates does not differ markedly between samples the distribution of sizes does appear to. Before this can be rationalised it was necessary to determine the mechanism of aggregation. This was achieved by two methods: NMR spectroscopy and hydrophobic fluorescence probes.

Firstly, NMR spectroscopy was employed to probe the composition of the corona and core of these aggregates. ^{1}H NMR relaxation times are influenced by changes in the

dynamic motion of protons. In particular, T_2 relaxation times decrease as molecular motion decreases and, in the glassy, immobile core of a polymeric aggregate, the proton signals can be significantly broadened, reduced or even broadened beyond detection of the NMR spectrometer. The corona protons, which are more mobile, are usually less affected.

In order to achieve this, E60B100 was dissolved in d_6-DMSO (a co-solvent for both the acid and benzylamide moieties) and D_2O (selective for only the diacid moieties) was added to form a final aggregate concentration of 10mg mL^{-1}. The solvent mixtures analysed are shown in table 3-3.The aromatic regions integral was compared with the ethylene regions integral. In a common solvent for both the hydrophilic and hydrophobic components, e.g. DMSO, the ratio of integrals should always be 5 to 4 (aromatic to ethylene). Any deviation from this indicates that the one of the groups in is in excess within the core of the aggregate.

Table 3-3: The ratio of aromatic peaks measured to theoretical value and ethylene, for a variety of solvent non-solvent mixtures

d_6-DMSO (mL)	**D_2O (mL)**	**I_A/I_{TA}***	**I_A/I_E†**
0.75	0.25	1	5/4
0.5	0.5	0.84	4.4/4
0.25	0.75	0.45	2.3/4
0.1	0.9	0.27	1.4/4

*I_A/I_{TA} ratio of measured aromatic integral to theoretical with respect to ethylene protons, †I_A/I_E ratio of measured aromatic integral to measured ethylene integral

As can be observed, the aromatic signal progressively decreases with increasing addition of D_2O; precipitation was observed to occur at 1:1 d_6-DMSO:D_2O. The signal broadening appears to occur in all the proton environments (figure 3-22). However, despite the fact that all signals appear to be suppressed, the ratio of ethylene to aromatic peaks (table 3-3) demonstrates that the aromatic peaks decrease relative to the ethylene protons indicating that the aromatic protons have a longer T_2 relaxation time and therefore are in a more restricted environment.

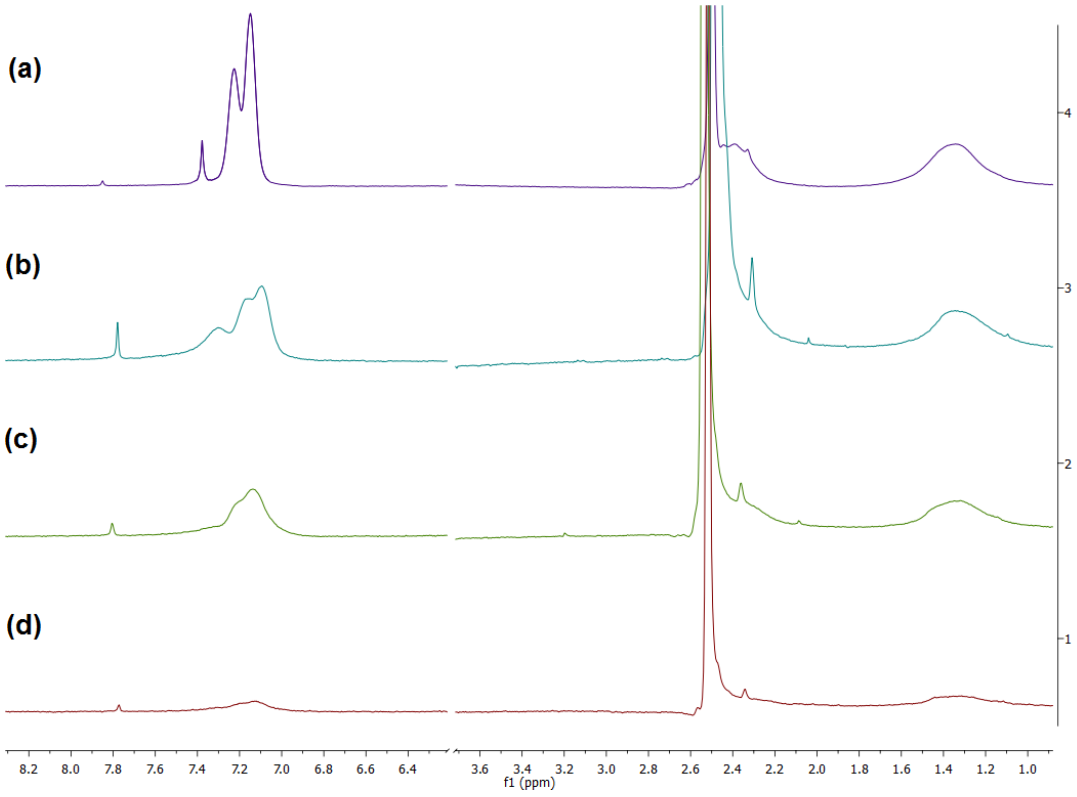

Figure 3-22: (400MHz, ^{1}H NMR): spectra of E60B100 10g L^{-1} in: (a) D_2O 0.25mL + d_6-DMSO 0.75mL, (b) D_2O 0.5mL + d_6-DMSO 0.5mL, (c) D_2O 0.75mL + d_6-DMSO 0.25mL, and (d) D_2O 0.9mL + d_6-DMSO 0.1mL

The maleic anhydride protons, which can be observed as a shoulder to the d_6-DMSO peak at 2.4ppm (figure 3-22 (a)), decrease markedly with increasing D_2O. This is, in

part, surprising as the maleic acid residues are likely to make up the hydrophilic component of the polymer so one might expect these protons to better retain their capacity for spin spin relaxation. However, in the case of E60B100 there are no diacid residues, only amidic – acid residues which means that the hydrophobic and hydrophilic components, the corona and the core, are separated by a single C-C backbone bond. This suggests that the conformational freedom of the hydrophilic moiety is severely restricted leading to the broadening of those signals.

The ^{1}H NMR spectra of E60B100 and E60B20 were compared in order to probe the importance of the number of diacid and hydrophobic moieties on the aggregates structure. Rather than precipitating from d_6-DMSO, d-methanol was used as the co-solvent which, subsequent to the addition D_2O, was removed under vacuum. This ensured that the presence of residual co-solvent did not distort the comparison (figure 3-23, table 3-4).

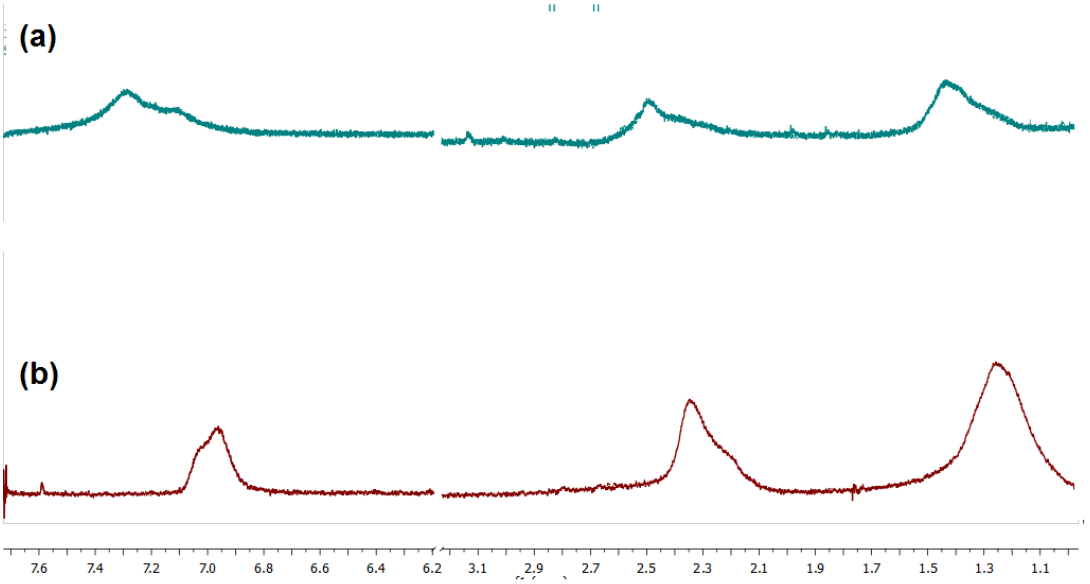

Figure 3-23: ^{1}H NMR spectra of (a) E60B100, and (b) E60B20 in D_2O

Table 3-4: Relative integrals of aromatic (I_A) and maleic anhydride (I_{MA}) protons, relative to ethylene (I_E = 4) for E60B100 and E60B20.*

Polymer	I_A (7.5-6.8ppm)	I_{MA} (2.9-2.2ppm)	I_E (1.7-1.0ppm)
E60B100	1.8 (5.0)	2.4 (1.9)	4
E60B20	0.9 (1.0)	1.8 (2.0)	4

* Values in brackets show the integral value relative to ethylene in d-methanol

Interestingly, while peak broadening is observed, especially in the aromatic region, in both cases the relative ratio of peaks in E60B20 is the same as the actual values as determined by d-methanol ^{1}H NMR. This indicates that in cases where the hydrophobe content is low, there is a fast exchange of hydrophobic residues between the core and corona. A tentative proposition for the structural forms is outlined in figure 3-24.

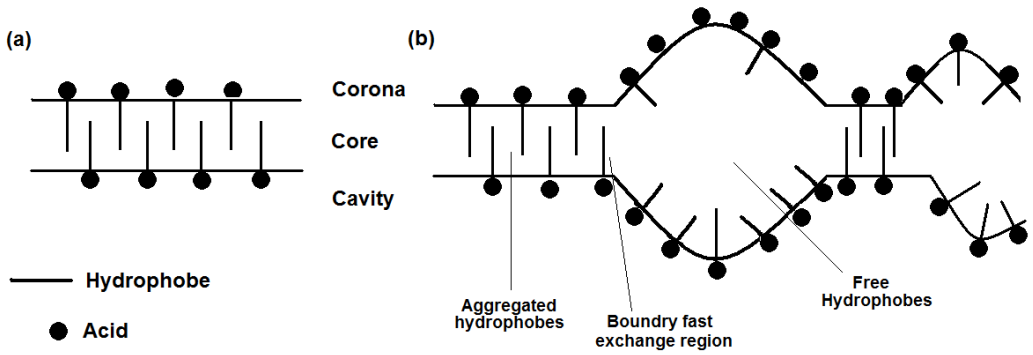

Figure 3-24: Proposed structure of inter-molecular aggregates in: (a) high hydrophobic content polymers, (b) low hydrophobic content polymers

In figure 3-24(a) the bilayer is proposed to be composed of two polymer chains whose length runs perpendicular to the surface normal. Conceptually this makes sense as there is no long distance asymmetry within the polymer therefore its amphiphilic nature, unlike that of di-block copolymers, is not a long distance phenomena. Rather, the amphipilicity occurs repetitively over a short distance, therefore it is necessary for the polymer to pack in this way (figure 3-25).

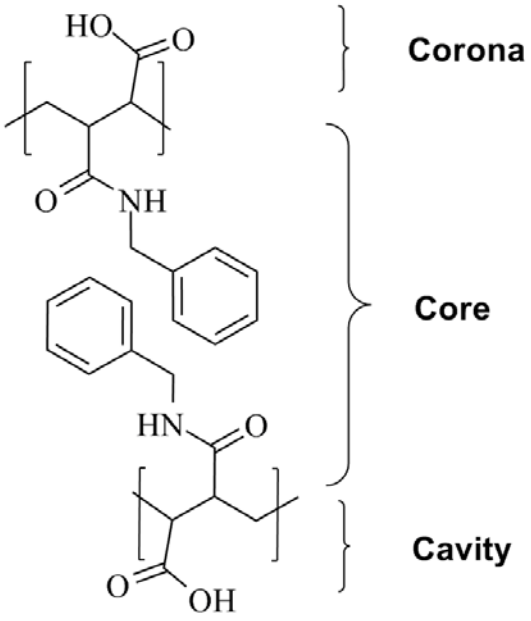

Figure 3-25: Proposed structure of the core and cavity of E60B polymers

A tentative structure for this is presented in figure 3-24(b). Such a structure would allow for fast exchange of the hydrophobic moieties, thereby explaining the strength of aromatic signals in the E60B20 ^{1}H NMR (table 3-3)

Further, qualitative evidence for the mobility of aggregated E60B20 chains is provided by dilution experiments. It was observed that upon dilution of E60B20 1gL^{-1} aggregate solutions to 0.1 g L^{-1} that over the course of four days the solution cleared

whereas E60B100 remained noticeably turbid. TEM of E60B20 solutions confirmed the dispersal of the aggregates (figure 3-26)

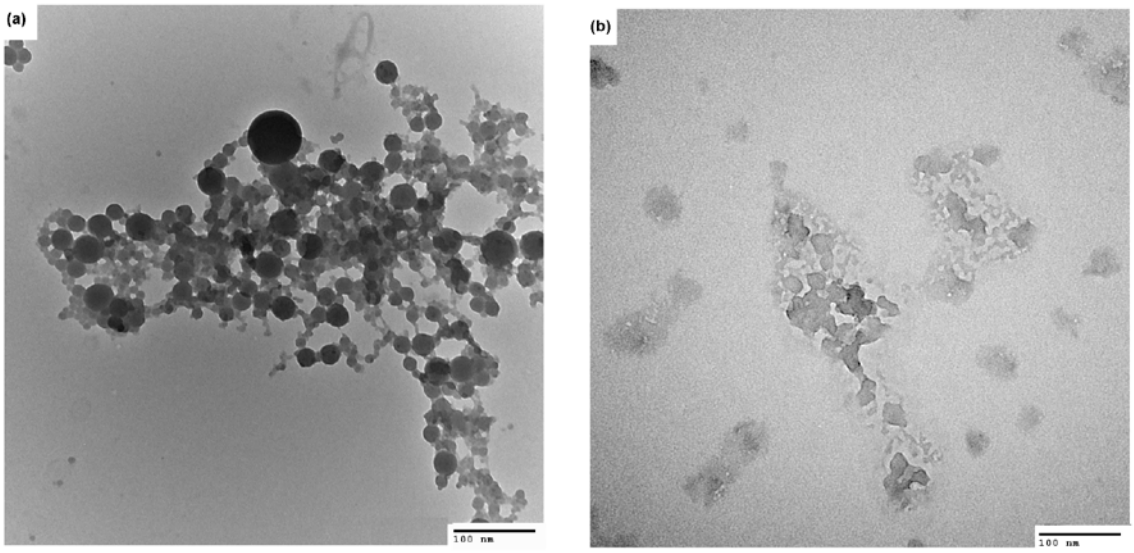

Figure 3-26: E60B20 0.05g L^{-1} after: (a) 6 hours, (b) 144 hours

Therefore, it appears that, as the concentration is reduced below the CAC, E60B20 aggregates are able to enter into solution as unimers. This is not the usual mechanism for polymeric aggregates where the entangled nature of the core kinetically freezes the structure.

Such a structure also provides an explanation for the trend observed that increasing hydrophobe content leads to an increase in aggregate size. The reason for this is twofold: firstly, an increase in the number of hydrophobes leads to an increase in the conformational rigidity of the chain in water, requiring it to pack into a structure with a reduced curvature; and secondly, an increase in the number of hydrophobic moieties results in a decrease in the number of diacid groups, thereby decreasing the amount of

inter chain repulsion. The importance of this second factor can be observed by precipitating the E60B50 and E60B10 into salt water ($NaCl_{(aq)}$,0.05M) (figure 3-27).

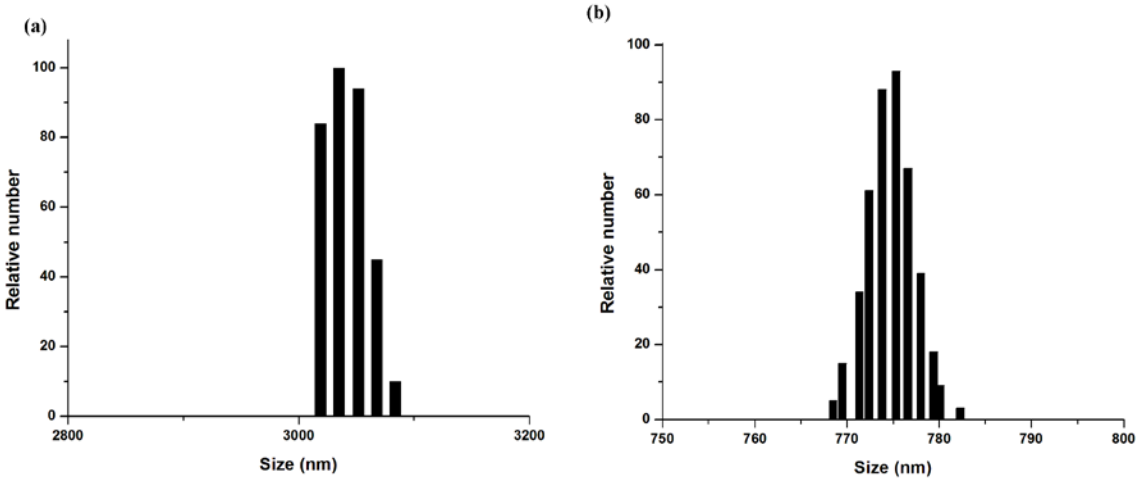

Figure 3-27: DLS of (a) E60B100; and (b) E60B10 in $NaCl_{(aq)}$ (0.05M)

As can be observed there is a dramatic increase in the aggregate size for E60B100 (figure 3-27 (a)) and E60B10 forms aggregates which are not observed in distilled water.

In order to further examine the effect of hydrophobic content on aggregation, pyrene was used as a fluorescent probe to determine the onset of intermolecular aggregation. This was achieved by precipitation of DMF solutions, across a range of concentrations, of E60B20, E60B50, E60B80, and E60B100 into saturated pyrene aqueous solutions. These were then dialysed over 36 hours against pyrene saturated water, and the fluorescence intensity of the pyrene I_1 emission band measured (excitation 339.0nm, emission 373.0nm). The results are shown in figure 3-28 and 3-29.

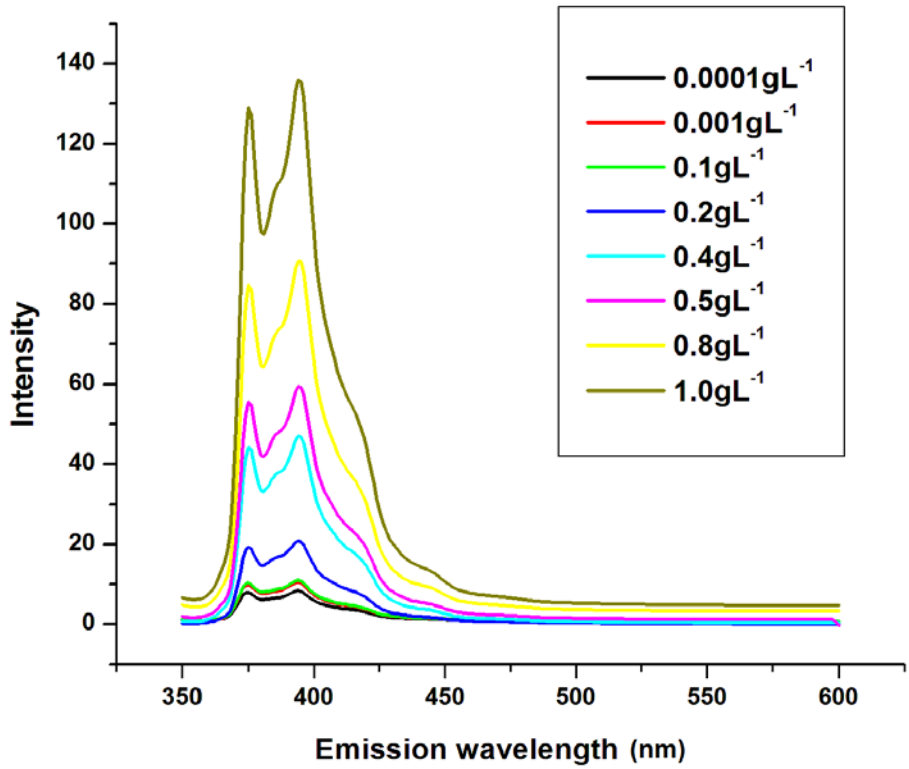

Figure 3-28: Pyrene emission spectrum with increasing polymer (E60B100) concentration (g L^{-1}). Note the rapid increase between samples 0.2gL and 1.0g L^{-1} which demonstrate the onset of inter-chain aggregation and the formation of large aggregates.

.

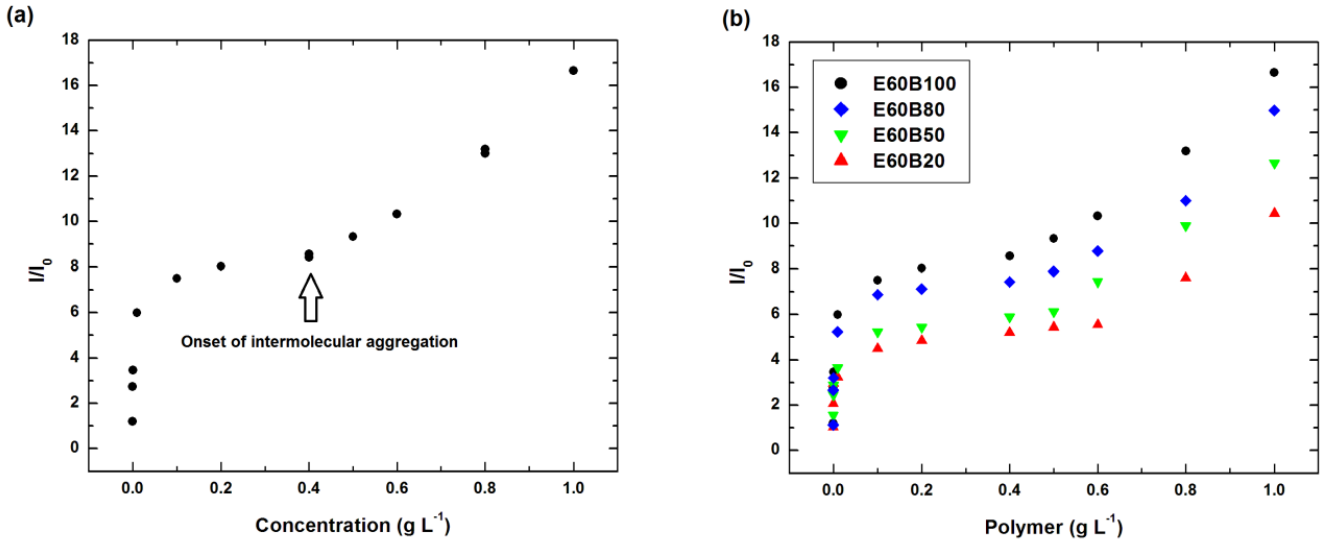

Figure 3-29: Plots of I_1/I_0 vs. polymer concentration with: (a) E60B100 intensity vs concentration plot and (b) a plot showing intensity vs concentration for E60B100, E60B80, E60B50 and E60B20. Note the onset of the third linear region is caused by the start of inter-chain aggregation.

Firstly, it is worth observing that in all cases there is no region, below 1g L^{-1}, where I_1/I_o is independent of polymer concentration, despite the fact there is no evidence, either by light scattering or TEM, of aggregates forming when C < 0.1g L^{-1}. This indicates that intramolecular aggregation is occurring and therefore, the pyrene is being immobilised within these intramolecular aggregates. In summary, at low concentration the polymers form intramolecular aggregates whereas at higher concentration intermolecular aggregates form (figure 3-30).

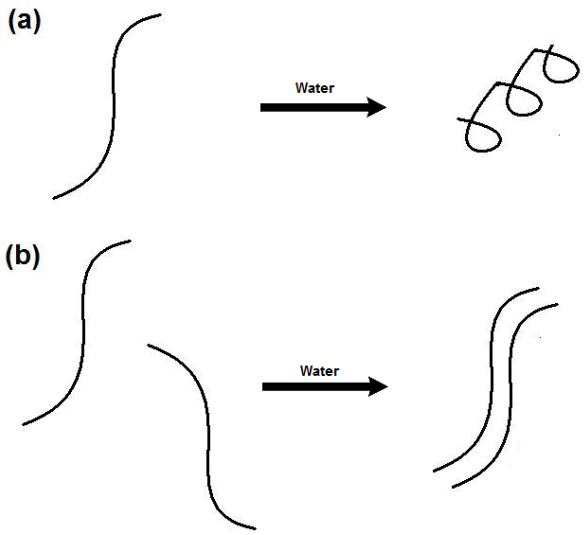

Figure 3-30: Schematic of aggregation: (a) low polymer concentration, and (b) high polymer concentration.

The CAC for these polymers are shown in table 3-5

Table 3-5: Calculated CAC from pyrene fluorescence

Polymer	CAC (g L^{-1})	CAC (mol dm^{-3})
E60B20	0.6	1.06×10^{-5}
E60B50	0.5	8.26×10^{-6}
E60B80	0.4	5.92×10^{-6}
E60B100	0.4	5.4×10^{-6}

While there is a definite correlation between hydrophobe content and CAC both in terms of g L^{-1} and mol dm^{-3}, it is not a particularly strong one, and all the values are

within a factor of ten of each other. This suggests that polymer concentration may be of greater influence in determining whether intra- or intermolecular aggregates are formed.

This can be understood in terms of the intramolecular regional micelle model (see section 3.3.2). Within this model two remote parts of the same chain encounter each other, and the subsequent superposition of their hydrophobic groups leads to the formation of a semi-stable intramolecular micelle. The probability of this event happening will be determined by the number of hydrophobic moieties along the backbone as well as numerous other factors such as perturbation length and molecular weight which combine determine how “easily” the two components find each other. However, for a given system there will be a characteristic probability of an intra chain superposition of hydrophobic groups.

If the concentration of polymer is increased the probability that two separate polymer chains’ hydrophobic groups will superpose increases. In other words as concentration is increased the degree of inter-chain aggregation rises relative to the degree of intra-chain aggregation. Therefore, at some critical concentration the probability of intra-chain aggregation becomes negligible and larger, interchain aggregates form.

This explains why the number of hydrophobic groups does not seem to affect significantly, the onset of interchain aggregation. Although the probability of two individual polymer chains superposing their hydrophobic groups decreases with decreasing hydrophobe content, so does the probability of remote regions of a polymer chain encountering each other.

In addition, this provides some insight as to why there are no clear trends associated with the hydrophobe's identity. While the size of the aggregate does appear to be dependent on the number of hydrophobes it does not significantly affect the CAC. Therefore, it could be that molecular mass is the more important factor.

The ability of these polymers to exist in either a water soluble conformation or aggregate perhaps explains the capacity of these polymers to efficiently form aggregates even at high concentrations (100mg mL^{-1}) without significant amounts of precipitation. Indeed, the polymers so readily form aggregates that the polymer solution can be added drop-wise, or even poured, into water without significant precipitation. Examples of polymer aggregates obtained by this mechanism are shown in figure 3-31.

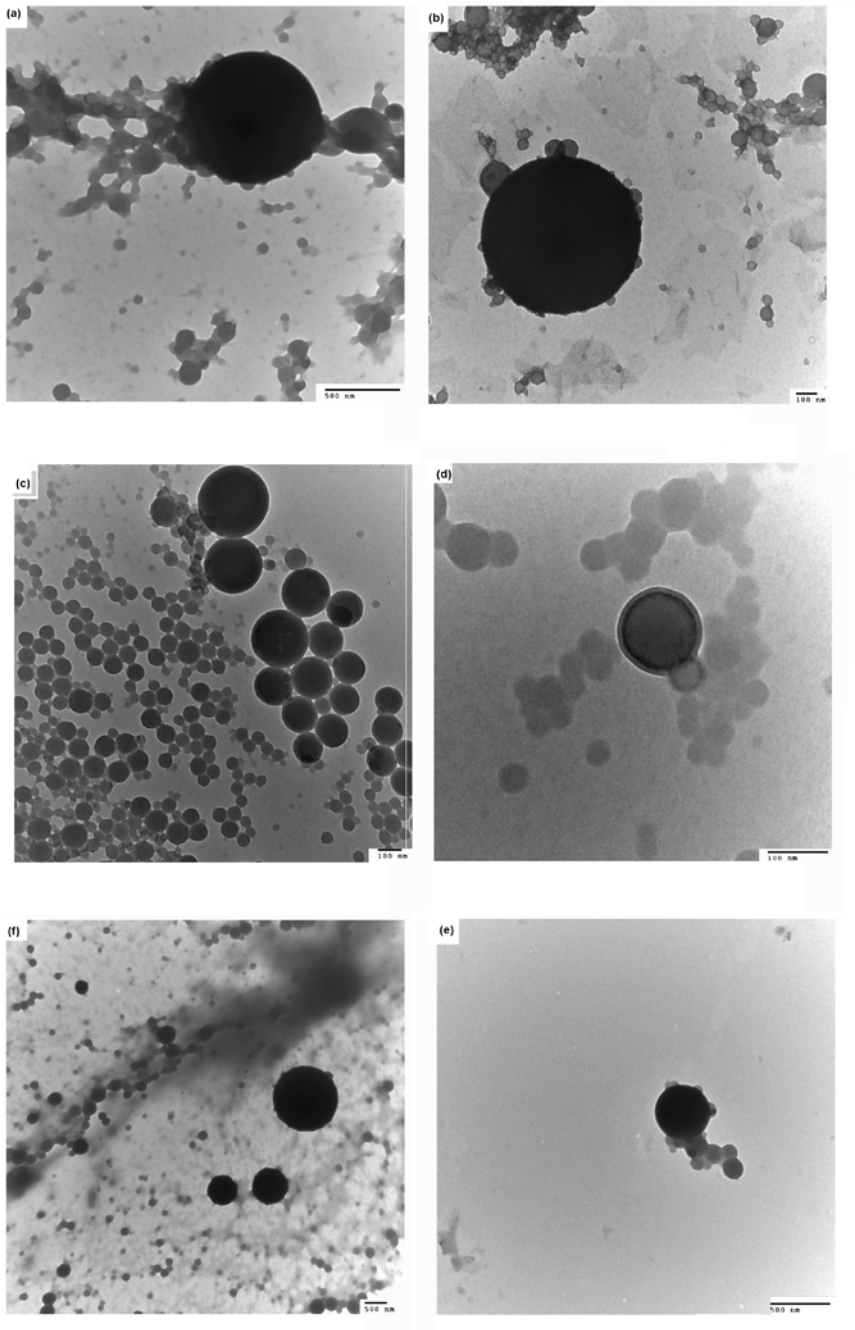

Figure 3-31: Examples of structures prepared from 100mg mL^{-1} from: (a)E60B50, (b) E60H50, (c) E60N50, (d) E60FB50, (e) E60B20, and (f) E60H50.

As can be observed in figure 3-31 the size distribution increases dramatically when the polymer solution is added to the water. This is presumably the result of rapid aggregation which results in the formation of non-equilibrium structures which are kinetically frozen.

Finally, in a recent paper Wooley *et al.*[8] demonstrated the stabilisation of micelles of poly(styrene)-b-(styrene-alt-maleic acid) by cross linking the maleic acid groups with a di-amine and carbodiimide, thereby creating inter-chain amide cross-links within the micelle's corona.

The ability to crosslink E60 aggregates presents the possibility to stabilise them both to changes in pH, an increase in which was observed to disperse the aggregates, and other effects such as dilution. In order to test the feasibility of doing so with E60 aggregates, a solution of E6050B was incubated overnight in the presence of 10 mol % cross linker (1,2-ethylenedioxy bis(ethylamine)) relative to the moles of carboxylic acid, 1-[3-(dimethylamino)propyl]-3-ethylcarbodiimide hydrochloride] and N-hydroxysuccinimide. This was followed by dialysis initially against $HCl_{(aq)}$ (6hrs) then against distilled water (72 hours).

No significant change was observed in the DLS distribution. Addition of DMF to a solution of E60B50 aggregates resulted in their dispersion whereas the cross-linked aggregates persisted. Comparison of the FT-IR spectra of E60B50 and cross-linked E60B50 demonstrated the incorporation of 1,2-ethylenedioxy bis(ethylamide) into the aggregates (figure 3-32).

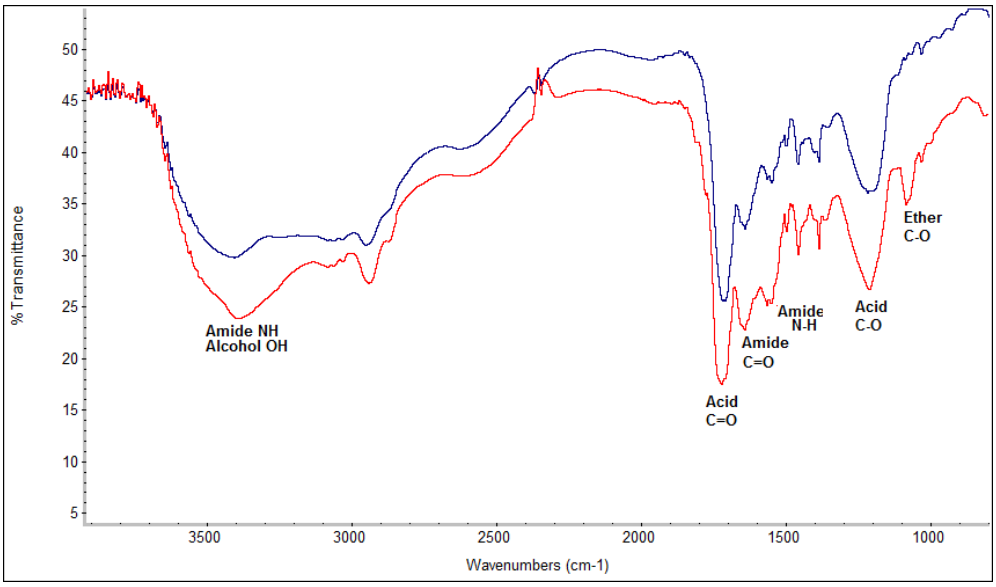

Figure 3-32: (KBr, FTIR) Spectra of: (blue) E60B50, and (red) cross-linked E60B50.

Table 6: Assignment of the principle peaks in fig 3-32

E60B50 (cm^{-1})	**Assignment**	**E60B50 cross-linked (cm^{-1})**	**Assignment**
3600-2750	Amide N-H Alcohol O-H	3600-2750	Amide N-H Alcohol O-H
2600 broad	C-H	2600 broad	C-H
1740 sharp	Acid C=O	1740 sharp	Acid C=O
1610 sharp	Amide C=O	1610 sharp	Amide C=O
1580 sharp	Amide N-H	1580 sharp	Amide N-H
1480	C-C	1476	C-C
1410	C-C	1410	C-C
1190	Acid C-O	1190	Acid C-O
		1096	Ether C-O

:

As can be observed, C-O stretches appear at circa 1100cm^{-1} and the amide C=O intensity, relative to acid C=O increases, indicating an increase in the number of amidic carbonyl groups.

3.5.2 Conclusion

A series of hydrophobically modified E60 derivatives were synthesised and demonstrated to aggregate both intra- and intermolecularly. The determining factor on inter- vs. intra molecular aggregation was demonstrated to be polymer concentration rather than the concentration of hydrophobe. In addition, it was shown that aggregates formed from polymers with low hydrophobic modification were not necessarily kinetically frozen and could undergo changes in response to concentration.

3.6 Hydrophilically modified E60 Derivatives

Much attention has been given in the literature to the addition of useful molecules to the surfaces of aggregates. As a result, it was decided to widen the scope and applicability of E60 based aggregates by attempting the synthesis of stable aggregates wherein some anhydrides persist which may then be usefully employed for further modification.

Poly(ethylene-alt-maleic anhydride) is not water soluble, consequently it was speculated that the appropriate hydrophilic modification of the polymer backbone would result in an aggregate wherein the anhydride moieties form the core. To this end E60 was reacted with ethanolamine in order to introduce hydrophilic hydroxyl bearing moieties (figure 3-33).

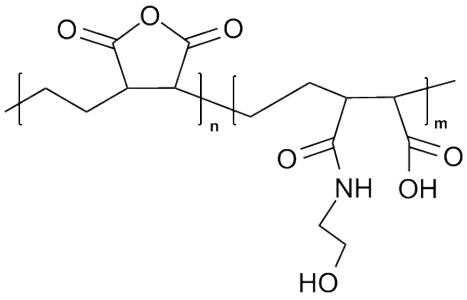

Figure 3-33: Structure of ethanolamine modified E60.

Trial and error, confirmed that modification with 2-8 mol% of ethanolamine (relative to anhydrides) was optimal in producing nano-scale aggregates. Subsequently, 2.5% modification was used and the resulting polymer named E60EA, the reaction being confirmed by ^{1}H NMR spectroscopy which demonstrates the presence of hydroxyl, acidic, maleic acid and ethylene-acid protons (figure. 3-34).

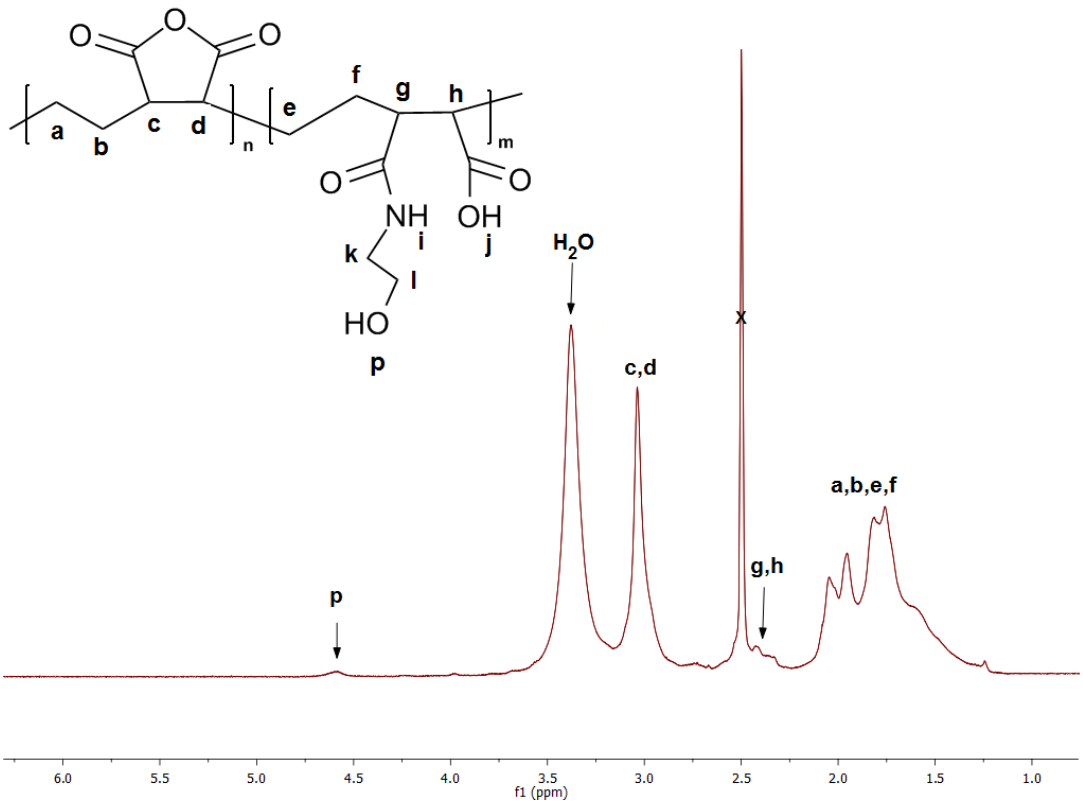

Figure 3-34: (400MHz, d6-DMSO) ^{1}H NMR spectrum of polymer E60EA

Following the addition of water to a 10 mg mL^{-1} solution of E60EA, aggregation was observed. This was replicated with d_6-DMSO and D_2O in order to acquire a ^{1}H NMR spectrum. The signals of ethylene and maleic anhydride protons were seen to decrease and broaden. The suppression of the maleic anhydride protons also allows the ethanolamine protons to be resolved confirming their occupancy of a mobile environment (figure 3-35).

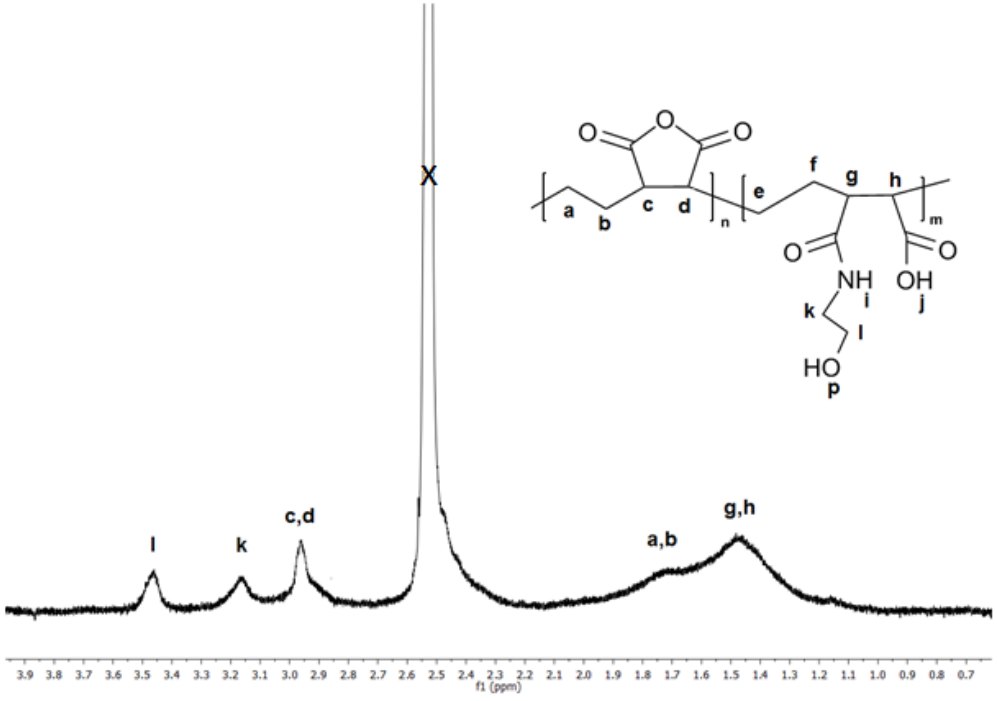

Figure 3-35: (400MHz, D_2O) ^1H NMR spectrum of E60EA aggregates

Unfortunately, the hydrolysis of the remaining anhydride moieties occurs within 24 hours of their aggregation in water. The result is the complete dispersal of the aggregates Therefore, to stabilise the structures to hydrolysis the polymer chains were crosslinked by the reaction of the anhydride moieties with (1,2-ethylenedioxy bis(ethylamine)) (figure 3-36).

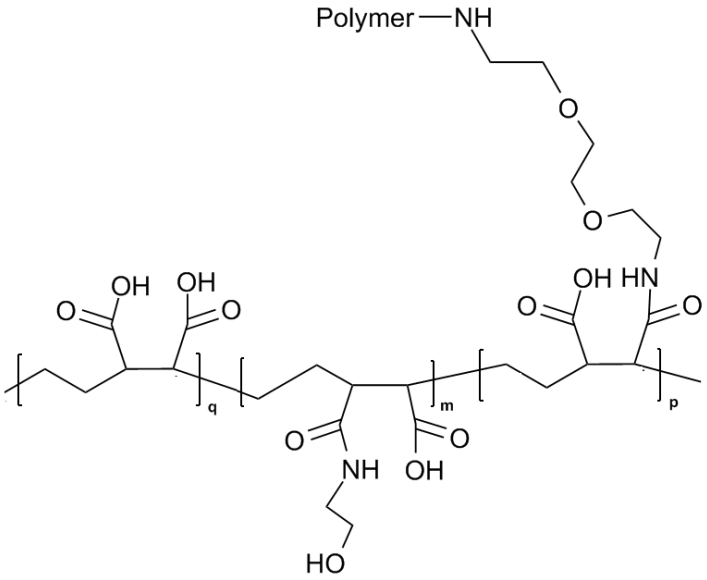

Figure 3-3633: Structure of crosslinked E60EA.

Cross-linking was confirmed by ^{1}H NMR spectroscopy (figure 3-37).

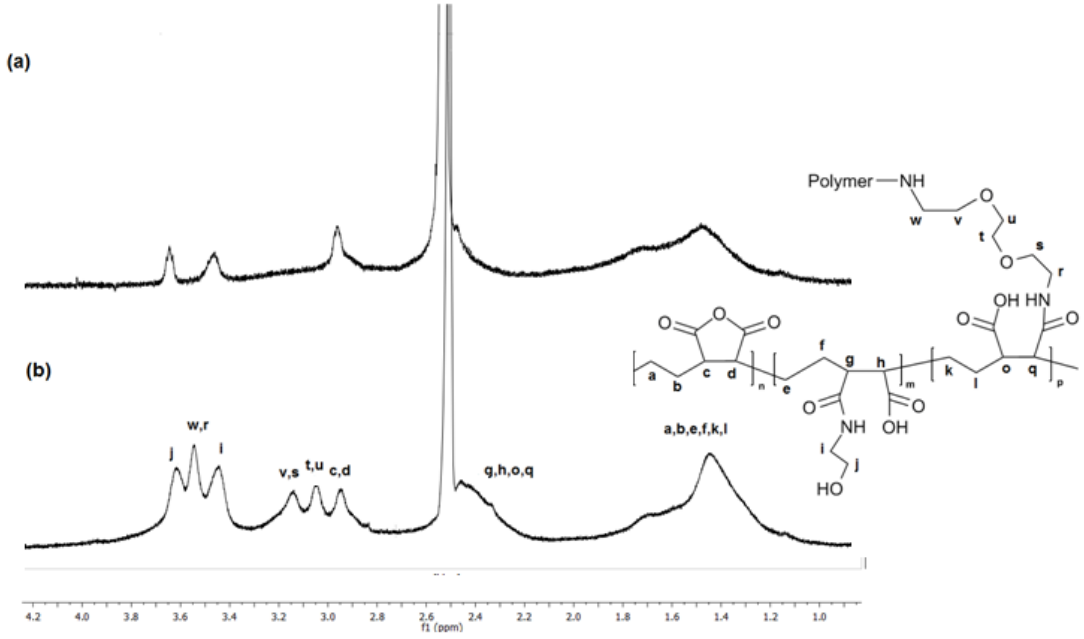

Figure 3-37: (400MHz, D_2O) ^{1}H NMR spectra of (a) E60EA aggregates and (b) crosslinked E60EA aggregates

Upon cross-linking the aggregates are unable to dissolve upon hydrolysis of the remaining anhydride moieties, thereby allowing their dialysis and subsequent collection of TEM images.

The swelling of the polymer aggregate, resulting from the hydrolysis of their remaining anhydride groups, leads to an decrease in the spin-spin relaxation times and consequently an increase in the intensity of the ^{1}H NMR signals.

A proposed mechanism of aggregation, crosslinking and hydrolysis is summarised in (figure 3-38).

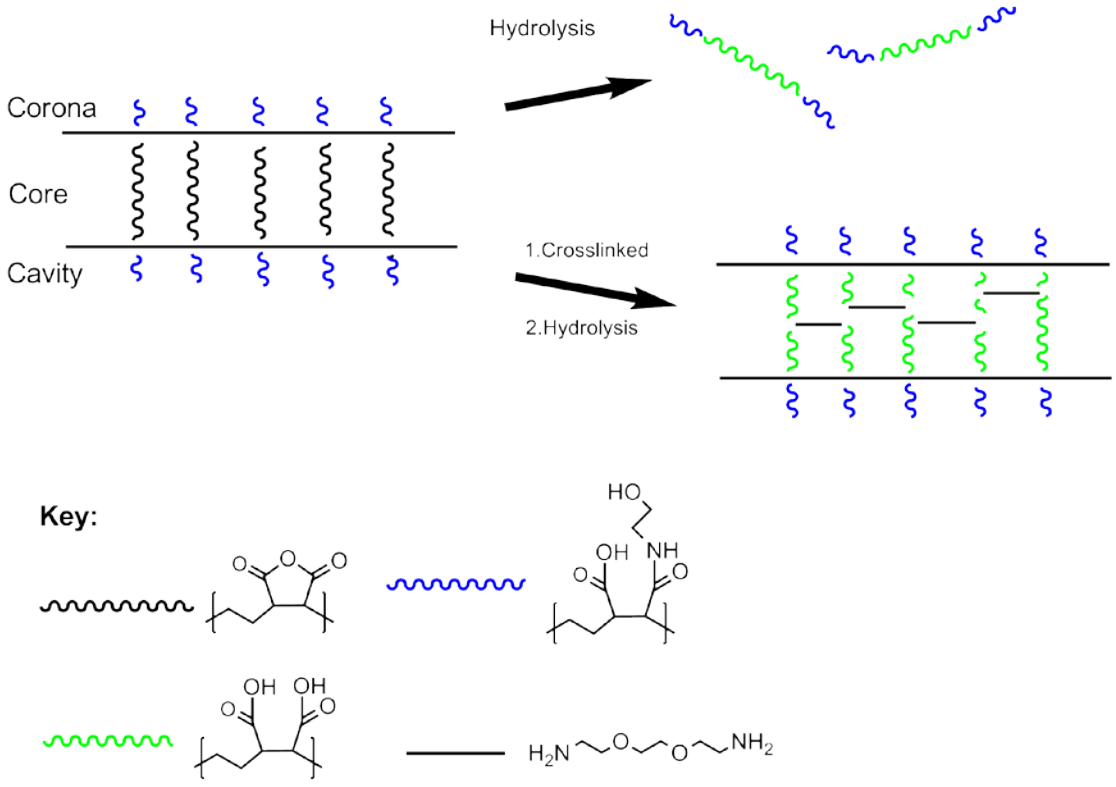

Figure 3-38: Idealised aggregate structure and cross linking process

It should be noted that figure 3-38 is an idealised system; in reality the addition of ethanolamine onto the polymer backbone occurs randomly and so the hydrophilic moieties will be randomly distributed across the polymer backbone. Consequently, the polymer chains are likely to be in a contorted conformation emerging and submerging into the core in order to maximise the number of ethanolamine moieties in the corona.

Over the short term (< 8hrs at room temperature) the anhydrides remain viable and are able to react with good nucelophiles, that is to say any nucelophile which is stronger than water. This was demonstrated by the reaction of cross-linked E60EA aggregates with benzylamine. Despite being dialysed over 7 days (8 hrs against 0.01M $HCl_{(aq)}$ - and 4 days against distilled water) the benzylamine moieties persisted as part of the aggregate structure, (figure 3-39).

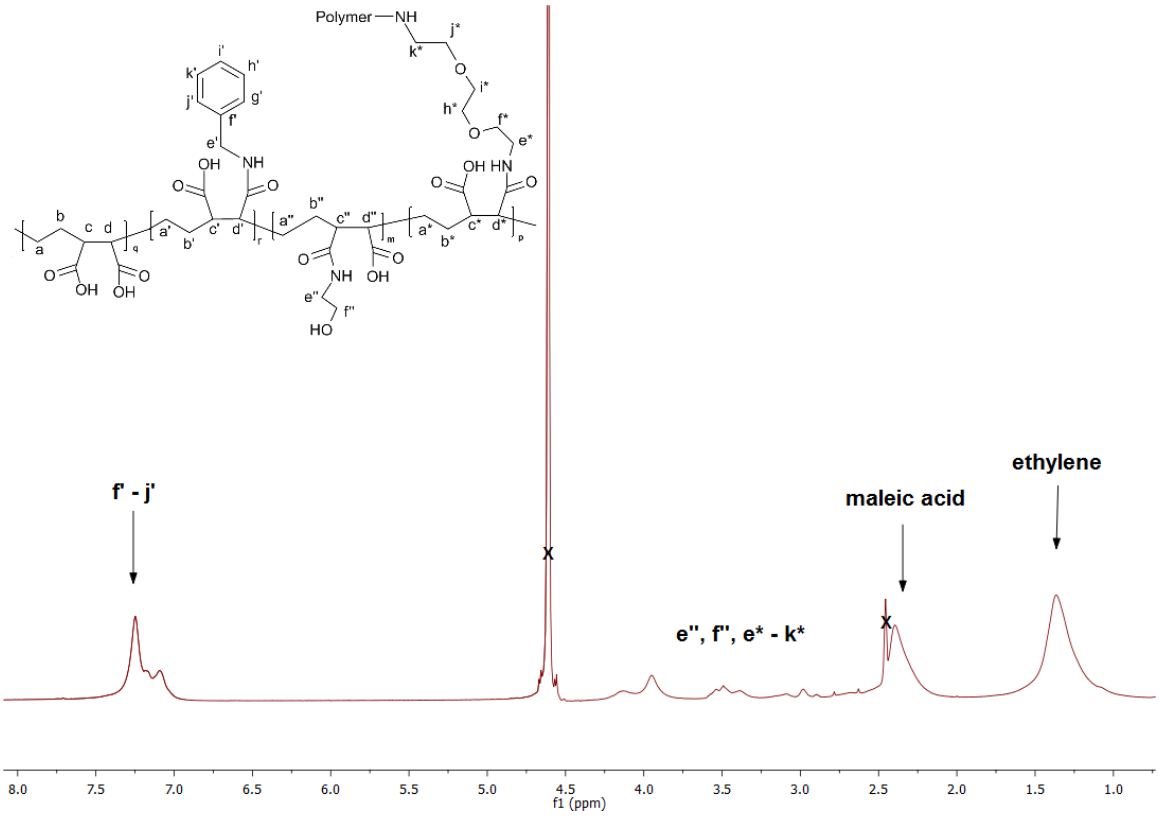

Figure 3-39: (400MHz, D_2O) ^1H NMR of benzylamine reacted cross-linked E60E

3.6.1 pH response of cross-linked E60EA

If the residual anhydride groups, within the aggregate, are not further reacted they will eventually hydrolyse. Therefore, the number of acidic groups increases markedly, consequently the crosslinked aggregates should be pH responsive. That is to say, at low pH the acidic groups are protonated whereas at elevated pH they are deprotonated. As a result, at elevated pH the inter/intra chain repulsion increases which, it was found, swelled the aggregate (figure 3-40).

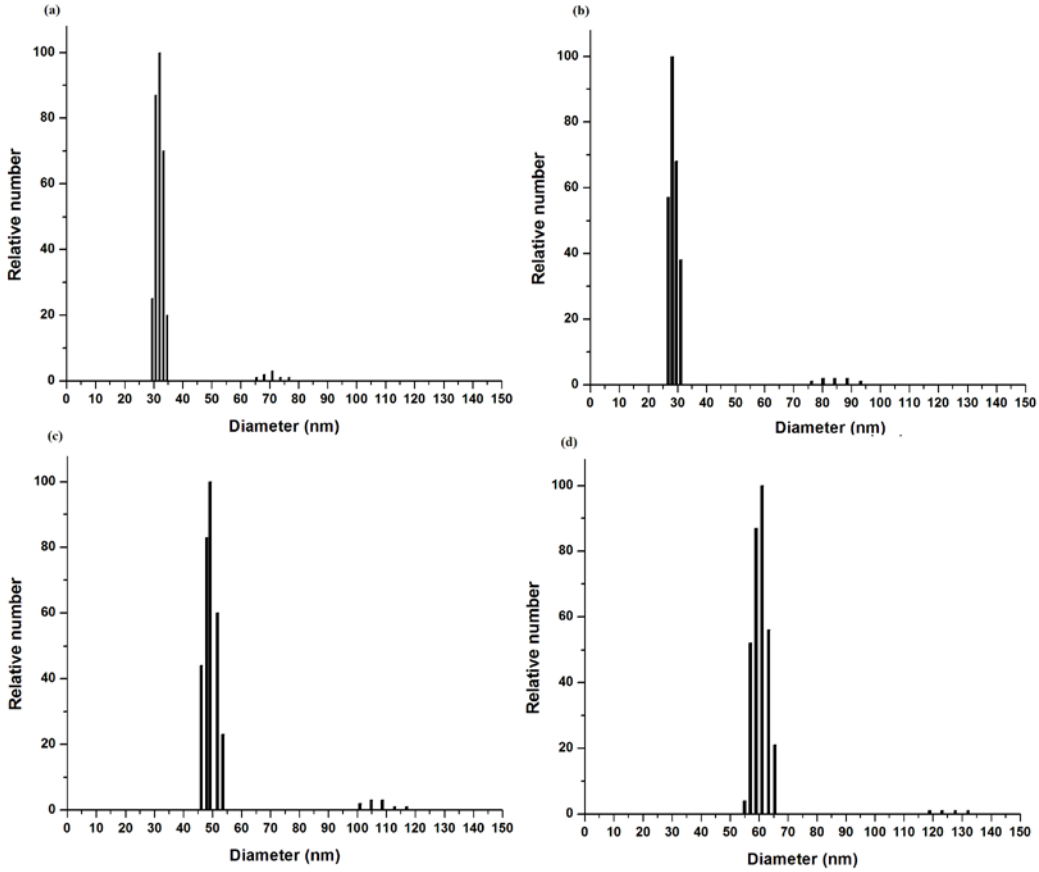

Figure 3-40: DLS plots of hydrolysed cross-linked E60EA aggregates at: (a) natural pH, (b) pH 2, (c) pH 7, and pH 9. pH adjustments were made by the dropwise addition of 1M $HCl_{(aq)}$ or 1M $NaOH_{(aq)}$ to 100mL of a 10mg mL^{-1} crosslinked E60EA solution

As figure 3-40 demonstrates, the particles swell noticeably when taken to elevated pH, corresponding to an increase in the charge density along the polymer backbone as the acid groups are deprotonated. The influence of pH is even more marked in the TEM images (figure 3-41). In addition to 10% crosslinked polymers already outlined (see section 3.6), TEM images of aggregates to which only 1 mol% of crosslinker (to anhydride) was added are shown. These lightly cross-linked aggregates were observed

to swell into less well defined structures. However, due to the low incorporation of cross-linker no further spectral analysis was conducted on these.

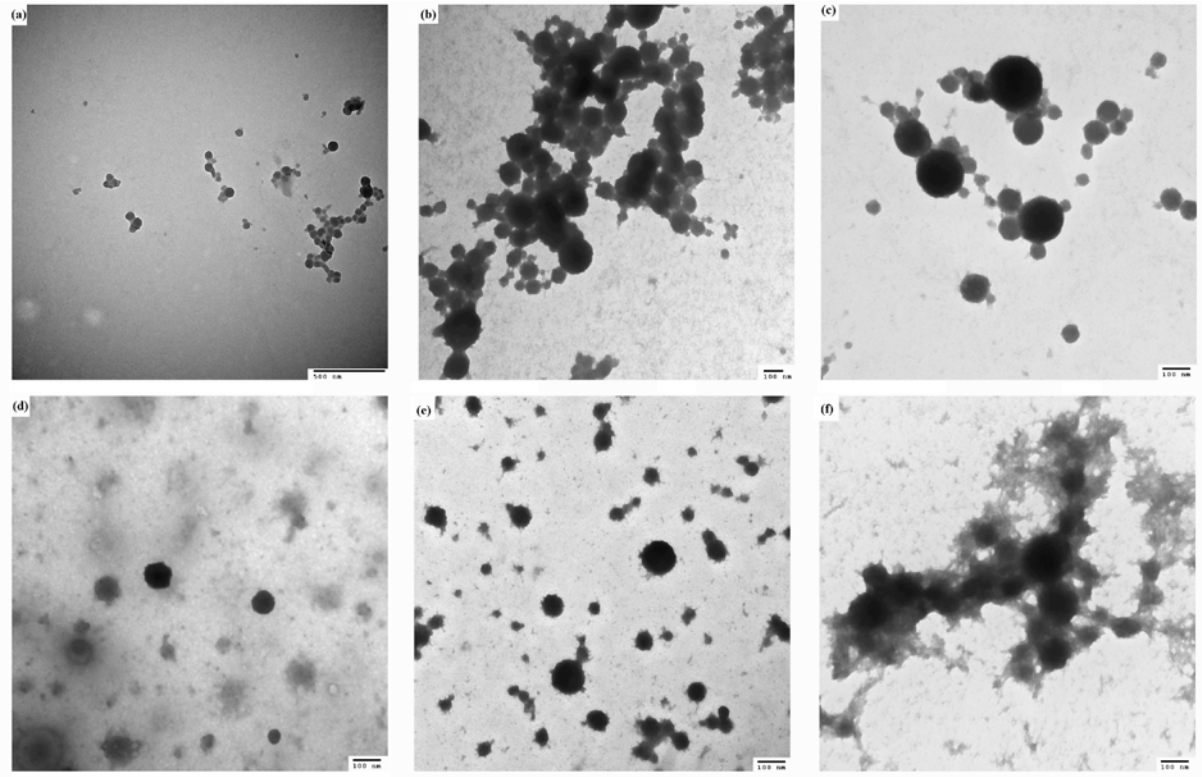

Figure 3-41 TEM images of (a) 10% cross-linked E60EA pH 3, (b) 10% cross-linked E60EA pH7. (c) 10% cross-linked E60EA pH 9, (d) 1% cross-linked E60EA pH 3, (e) 1% cross-linked E60EA pH7, and (f) 10 cross-linked E60EA pH 9

3.6.2 Conclusion

The hydrophilic modification of E60 proved successful in forming vesicle sized aggregates, and subsequent partial cross-linking of the anhydrides stabilised the aggregates to hydrolysis and further chemical modification. It has been demonstrated that immediately after cross-linking there are sufficient maleic anhydride units for further nucleophilic addition. Potentially, this would allow these aggregates to be

used as covalent carriers for compounds. The pH dependence of the aggregates size may allow for a better access to any covalently immobilised compound. Consequently, this represents a viable supramolecular carrier for useful compounds.

3.6.3 Future work

3.6.3.1 Hydrophobically modified poly(ethylene-alt-maleic anhydride)

The ability of E60B20 to behave as a small molecule surfactant, that is to say the aggregates disperse at concentrations below the CAC, presents the opportunity to have a concentration-dependent encapsulent. In other words, the aggregates above the CAC could be loaded with a suitable molecule and then, upon dilution, the kinetics of release would increase significantly, as the surface area to volume ratio of intramolecular micelles would be much closer to unity than for larger aggregates. Therefore, a detailed study of the release kinetics of fluorescent dyes would be instructive, as would the covalent immobilisation of fluorophores onto the polymer backbone which, if suitably chosen, would give an indication of interchain separation and the degree of intermolecular aggregation with concentration.

Secondly, there is the potential to modify the polymer with a mixture of different hydrophobes which may allow for the compartmentalised encapsulation of different molecules.

Thirdly, preliminary results for the polymer's addition to non-basic, high ionic strength systems resulted in a much increased aggregate size, for example 0.05M $NaCl_{(aq)}$ appears to cause E60B100 aggregates to form which are 4.5μm in size (by

DLS). Further experiments are necessary to probe the effect of ionic strength on aggregation.

Finally, Wooley *et al* has outlined a synthesis for poly(styrene)-b-(styrene-alt-maleic anhydride) copolymers. After hydrolysis of the anhydride, the system is able to self-assemble into micelles with the styrene block forming the core. Given the results of the work presented here it would be interesting to examine how hydrophobic modification of the maleic anhydride copolymer block would affect this system's ability to act as an encapsulent. It may be possible to create a system wherein a conventional hydrophobic core is formed yet the micelles corona is composed of multiple intramolecular micelles. This may affect the release rate of these nanoparticles as hydrophobic molecules leaching from the core enter into the intramolecular micelles. In addition, this may provide another route to compartmentalised encapsulation.

3.6.3.2 Hydrophilically modified E60

It would be interesting to use these polymers as covalent carriers of useful compounds, particularly hydrophobic ones. The pH responsiveness of these cross-linked aggregates presents the opportunity to create a system wherein the core contains a hydrophobic catalyst, the accessibility to which could be modulated by varying the pH. Similarly, changes in the solvent polarity or ionic strength could be used to similar effect.

3.7 Experimental Section

3.7.1 Materials and Instrumentation

All chemicals were purchased from standard chemical suppliers and used without further purification unless otherwise stated. Dry solvents were purchased from Fischer Scientific and dried by passage through two alumina columns using an Innovative Technology Inc. solvent purification system and stored under N_2. Dialysis was carried out against deionised water (containing, where appropriate, dissolved acid/base/salt as stated in the experimental section) using dialysis membranes (Medicell International Ltd, Size 5, Inf Dia 24/32" - 19.0mm) with a cut off of approximately 12000 Daltons. Dialysed samples were freeze dried using a Christ Alpha 2-4 LSC.

NMR spectra were recorded using a Varian Inova 500 spectrometer at 499.87 (1H) and 125.67 MHz (13C, 1H decoupled at 500 MHz), a Bruker Avance 400 spectrometer at 400.13 MHz (1H) or 100.26 MHz (13C, 1H decoupled at 400 MHz) or a Varian Inova-700 spectrometer at 700MHz (1H) and 176MHz (13C), at ambient temperature in CDCl3, DMSO, D2O, MeOD. NMR spectra were analysed using MestReNova v6.04 software and referenced internally to the residual protons in the NMR solvent. IR spectra were recorded on a Nicolet Nexus FT-IR spectrometer either as pressed KBr disks or as thin films cast on KBr discs from a suitable solvent. Spectra were analysed using Omnic version 5.1 software. Dynamic light scattering measurements were performed on a Brookhaven Instruments 90 ZetaPlus Paticle Sizer. The temperature was fixed at 23 °C and samples were allowed to equilibrate to this temperature before measurements were recorded. Three runs with an average of

10 scans each were performed. Data was analysed with Brookhaven ZetaPlus Particle Sizing Software version 3.72. Samples for TEM analysis were prepared by deposition of a drop of the particle solution on to a carbon-coated copper grid and the excess solution removed using filter paper, leaving a thin film of the aggregates. The samples were imaged using a Hitachi H7600 microscope. Fluorescence measurements were performed using a JASCO FP-6200 Spectrofluorometer.

3.7.2 Polymer preparation

Samples of purified E60 were heated to 120^{o}C overnight under vacuum. Subsequently, the samples were stored in a dessicator and used within 12 hours.

3.7.3 Benzylamine modification poly(ethylene-alt-maleic anhydride) to 100% amide

E60 (1.00g, 0.025mmol, 0.0079mol anhydride) was dissolved into anhydrous DMF at a concentration of 10% w/v. Benzylamine (0.85g, 0.0087mol) was dissolved into 1mL of DMF and added drop wise to the polymer solution with vigorous stirring for 10 min. To this 2mL of distilled water was added and the solution heated to 60^{o}C for 2h. The solution was then transferred to a dialysis bag (12kDa molecular weight cut off, Sigma) and then dialysed against $HCl_{(aq)}$ (1000mL, 0.05M) for 8h the distilled water for a further 48h with frequent water changes. The polymer was then recovered by freeze drying.

This procedure was repeated for the synthesis of E60B10, E60B20, E60B50, and E60B80 with an appropriate amount of benzylamine. E60B10 benzylamine (0.085g, 0.00087mol); E60B20 benzylamine (0.170g, 0.0016mol), E60B50 (0.425g, 0.0040mol); E60B80 (0.680g, 0.00634mol)

3.7.3.1 Characterisation of E60B100

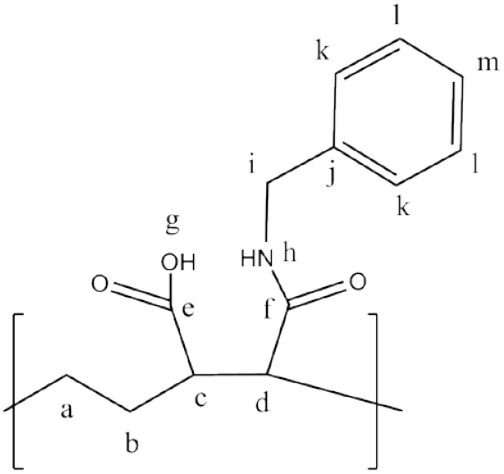

^{1}H NMR: δ_H (400MHz, d_6-DMSO): 9.8-8.35 (br, h); 7.42-6.9 (br, k, l, m); 4.55-4.05 (br, i); 2.8-2.2 (br ov, c, d); 2.1-1.05 (br, a, b.)

FTIR ν_{max} (KBr)/cm^{-1}: 3340 (strong) acid OH, N-H; 3014, (weak) C-H sp^3, 2967 (strong) C-H sp^3; 1723 (strong) acid C=O; 1642 (strong) amide C=O; 1561 amide II band N-H; 1498 aromatic C=C.

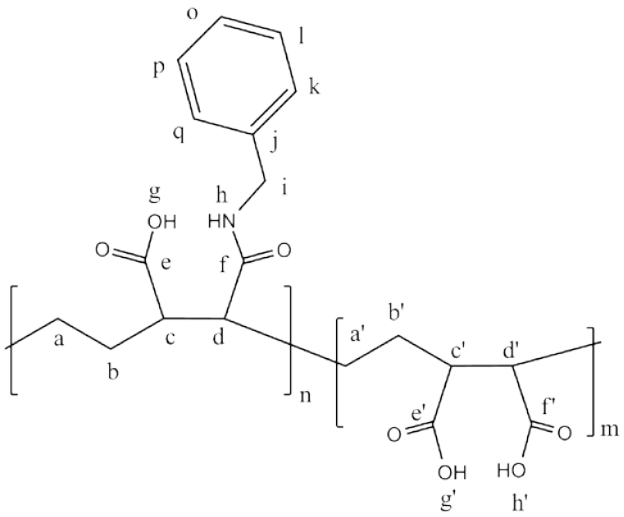

^{1}H NMR: δ_H (400MHz, d_6-DMSO): 9.8-8.35 (br, h); 7.42-6.9 (br, k, l, o, p, q); 4.55-4.05 (br, i); 2.8-2.2 (br ov, c, d, c',d'); 2.1-1.05 (br ov, a, b, a', b')

3.7.4 Fluorobenzylamide poly(ethylene-alt-maleic anhydride) derivatives

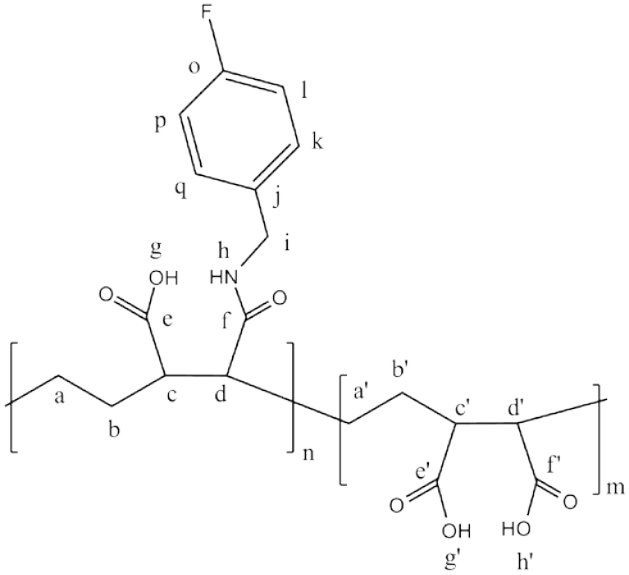

^{1}H NMR: δ_H (400MHz, d_6-DMSO): 8.2-9.8 (br m, h); 7.3-6.9 (br, k, l, p, q); 5.6-4 (br, i); 2.6-2.1 (br, ov, c', d', c, d); 2-1.05 (br m, a, b, a', b').

FTIR ν_{max} (KBr)/cm^{-1}: 3347 (strong) acid OH, N-H; 2962 (strong) C-H sp^3; 1717 (strong) acid C=O; 1639 (strong) amide C=O; 1561cm^{-1} amide II band N-H; 1498 aromatic C=C; 1411 aromatic C=C; 1187 acid C-O.

3.7.5 Hexylamide poly(ethylene-alt-maleic anhydride) derivatives

E60 (1.00g, 0.025mmol, 0.0079mol anhydride) was dissolved into anhydrous DMF at a concentration of 10% w/v. Hexylamine (0.401g, 0.0040mol) was dissolved into 1mL of DMF and added drop wise to the polymer solution with vigorous stirring for 10 min. To this 2mL of distilled water was added and the solution heated to 60^{o}C for 6h.

The nascent gel and solution was then transferred to a dialysis bag (12kDa molecular weight cut off, Sigma) and dialysed against $HCl_{(aq)}$ (1000mL, 0.05M) for 12h the distilled water for a further 48h with frequent water changes. The polymer was then recovered by freeze drying.

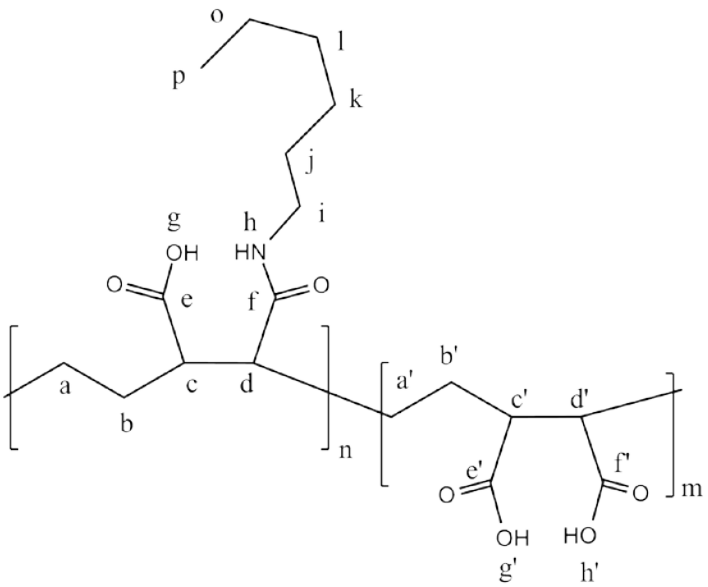

^{1}H NMR: δ_H (400MHz, d_6-DMSO): 8.3-7.8 (br s, h); 3.1-2.85 (br, i); 2.6-2.1 (br m, ov, c, d, c', d'); 2.1-0.9 (br ov, a, b, j, k, l, o, a', b'); 0.88 (br, p).

FTIR ν_{max} (KBr)/cm^{-1}: 3335 (strong) acid OH, N-H;, 2967 (strong) C-H sp^3; 1722 (strong) acid C=O; 1641 (strong) amide C=O; 1562 amide II band N-H.

3.7.6 Napthylmethylamide poly(ethylene-alt-maleic anhydride) derivatives

The same procedure was followed as benzylamine (section 3.83) but benzylamine was substituted for napthymethylamine (0.0040mol, 0.623g).

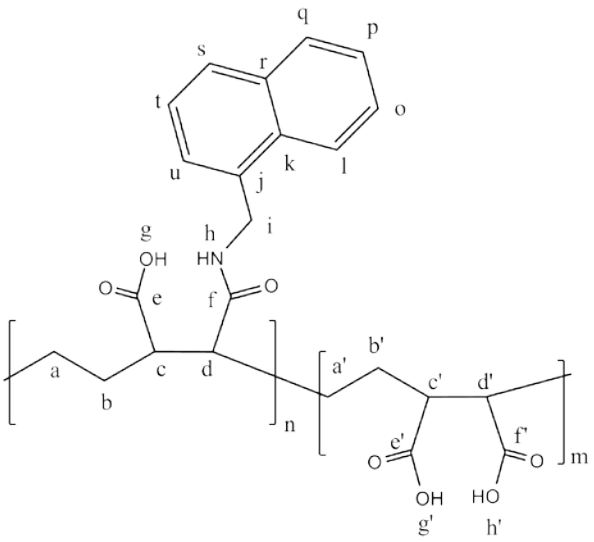

^{1}H NMR: δ_H (400MHz, d_6-DMSO): 9.9-8.1 (br, h); 8.1-7.2 (br m ov, l, o, p, q, s, t, u); 4.96-4.35 (br, i); 2.9-2.2 (br m ov, c, d, c', d'); 2-1.05 (br, a, b, a', b').

FTIR ν_{max} (KBr)/cm^{-1}: 3349 (stonrg) acid OH, N-H; 2958cm^{-1} (strong) C-H sp^3; 1719 (strong) acid C=O; 1641cm^{-1} (strong) amide C=O; 1560cm^{-1} amide II band N-H; 1498 aromatic C=C; 1406 aromatic C=C; 1195 acid C-O, 753, 701.

3.7.7 Micelle preparation

3.7.7.1 Addition to water with dialysis

The polymer was dissolved to a concentration between 0.05mg mL^{-1} and 100mg mL^{-1} in DMF (1mL). The solution was then stirred and distilled water (9mL) was added dropwise to the solution. After the complete addition of water, the mixture was transferred to a dialysis bag (12kDa molecular weight cut off) and dialysed against distilled water (1000mL) for 36h with frequent water changes. The mixture was then recovered, and either used without further purification or the polymer was isolated by freeze drying.

3.7.7.2 Addition of water without dialysis

The polymer was dissolved to a concentration between 0.05mg mL^{-1} and 100mg mL^{-1} in DMF (1mL). The solution was then stirred and distilled water (9mL) was added dropwise to the solution. The mixture was then used without further purification.

3.7.7.3 Addition of polymer DMF solution to water

The polymer was dissolved to a concentration between 0.05mg mL^{-1} and 100mg mL^{-1} in DMF (1mL). This was then added, either drop wise or poured, into distilled water. The mixture was then dialysed against distilled water and then used without further purification.

3.7.7.4 Addition of $NaCl_{(aq)}$

The same procedure was followed as with the addition of water to polymer DMF solution (see section 3.7.7.3) but $NaCl_{(aq)}$ (0.05M) was substituted for distilled water.

3.7.8 NMR micelles

3.7.8.1 E60B100 from DMSO

E60B100 was dissolved into d_6-DMSO and D_2O was added in varying relative volumes to give a final polymer concentration of 10mg mL^{-1}. The samples were allowed to equilibrate for 36h is a sealed NMR tube. ^1H NMR spectra were then collected (400MHz, 1024 scans).

3.7.8.2 E60B20 and E60B100 from methanol

E60B20 was dissolved into d-methanol to a concentration of 10mg mL^{-1}. To this D_2O was added drop wise with efficient stirring. The d-methanol was then removed under

vacuum, and the aqueous dispersion allowed to equilibrate 32h in a sealed NMR tube. ^{1}H NMR spectra were then collected (400MHz, 1024 scans).

3.7.9 Crosslinked aggregates

E60B50 aqueous aggregated solution (100mL) was prepared as section 3.8.7.1 to a concentration of 1mg mL^{-1}. To this solution 2,2(ethylene dioxy)-bis-ethylamine was added in 10 mol% to the moles of polymer carboxylic acid (0.012g, 0.0643mol). To this EDC.HCl (0.055g, 0.29mmol) was added with N-hydroxysuccinimide (0.041g,0.34mmol). The solution was then allowed to stir overnight before being transferred into a dialysis bag (12kDa cut off) and dialysed against distilled water for 6 days with frequent changes of water. The material was then recovered by freeze drying.

FTIR ν_{max} (KBr)/cm^{-1}: 3399 (strong, ov) acid O-H and N-H; 3089 (weak) C-H sp^2; 2943 C-H sp^3; 1721 (strong) acid C=O; 1640 (strong) amide C=O; 1567 amide II band N-H; 1459 aromatic C=C; 1394 aromatic C=C; 1209 C-O acid, 1190 C-O ester.

3.7.10 Determination of critical aggregation concentration

Critical aggregation concentration was determined by the following standard procedure. An acetone solution of pyrene was prepared ($6x10^{-3}$M) was added to distilled water so that, after the removal of acetone by rotary evaporation, the final pyrene concentration of $6x10^{-7}$M. This was then added to stirred polymer DMF solutions with concentrations between 0.000001mg mL-1 and 10mg mL-1. The resulting dispersion was then dialysed against aqueous pyrene (1000mL, $6x10^{-7}$M) for 72h with frequent changes of the aqueous pyrene. The solutions were then recovered

and the fluorescence spectrum recorded (λ_{exc} 339 nm) at room temperature and the CAC values were obtained from plots of the ratio I_1 emission band to the zero polymer concentration I_1 emission band (I_1 intensity at 373nm) versus polymer concentration.

3.7.11 Ethanolamine modified poly(ethylene-alt-maleic anhydride)

E60 (5.00g, 0.125mmol, 0.040mol anhydride) was dissolved into anhydrous DMSO (22.5mL). Ethanolamine (0.061g, 0.99mmol) was dissolved in DMF (2.5mL) and added drop wise to the stirred polymer solution. The solution was allowed to stir for a further 10 minutes. The polymer was either used as prepared or isolated by precipitation into a 10 volume excess of DCM.

3.7.11.1 Characterisation

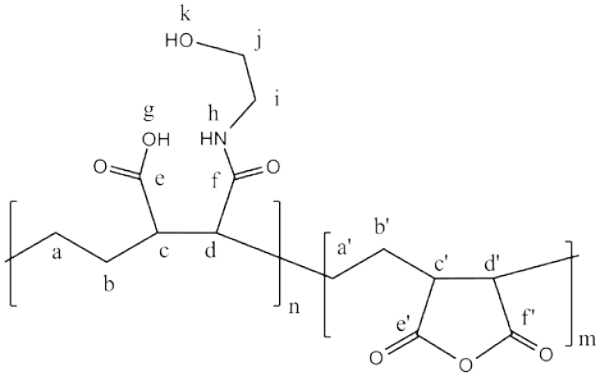

^{1}H NMR: δ_H (400MHz, D_2O): 4.63 (br, k); 3.1-2.78 (br, c', d'); 2.6-2.25 (bro v, c, d); 2.1-1.4 (bro v, a, b, a', b')

3.7.12 Preparation of poly(ethylene-alt-maleic anhydride) aggregates

A sample of E60E was used as prepared (section 3.7.11), and diluted to a concentration of 100mg mL^{-1}, 10mL of this solution was added dropwise to 100mL of vigorously stirred water.

This was procedure was repeated with deuterated solvent with E60E (0.50g) dissolved in 5mL d_6-DMSO. A 0.5mL sample of this was then added drop wise to vigorously stirred D_2O (5mL). A ^1H NMR was then taken (400MHz, 1028 scans).

3.7.13 Hydrolysis of ethanolamide modified poly(ethylene-alt-maleic anhydride) derivative

The hydrolysis of E60E aggregates was followed by ^1H NMR by allowing the NMR solution prepared (section 3.7.11) to hydrolyse in D_2O at room temperature.

3.7.13.1 Characterisation

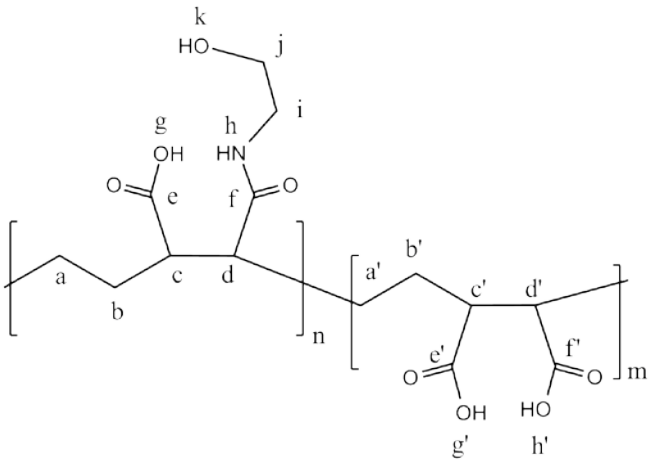

^1H NMR: δ_H (400MHz, D_2O): 4.63 (br, k); 2.7-2.25 (bro v, c, d, c', d'); 2.1-1.4 (bro v, a, b, a', b').

3.7.14 Crosslinked modified poly(ethylene-alt-maleic anhydride) aggregates

E60E aggregate solution was used as prepared (section 3.8.11), to this 2,2'-(ethylenedioxy)-bis-(ethylamine) (6mg, 0.040mmol) was added from an aqueous stock solution of 2,2'-(ethylenedioxy)-bis-(ethylamine) (62mg mL^{-1}). The solution was allowed to stir for 1h before being transferred into a dialysis bag (12kDa molecular mass cut off) and then dialysed against distilled water (1000mL) for 48h, with frequent water changes.

This procedure was repeated with E60E in a deuterated solvent as prepared in section 3.8.12 to a final polymer aggregate dispersion concentration of 10mg mL^{-1}. The solution was stirred and to this 2,2'-(ethylenedioxy)-bis-(ethylamine) was added as 10µl from D_2O stock solution (58mg mL^{-1}). A ^1H NMR spectrum was then recorded (400MHz, 1028 scans).

3.7.14.1 Characterisation

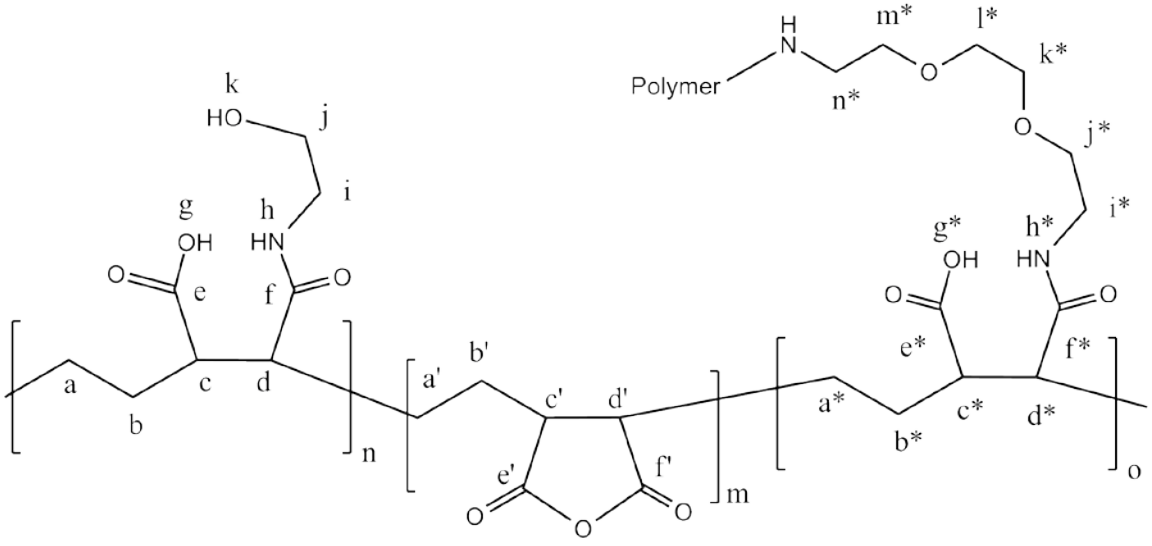

^{1}H NMR: δ_H (400MHz, D_2O): 3.7-2.73 (br, m, ov, j, i, i*, j*, k*, l*, m*, n*, c', d'; 2.5-2.1 (br, ov, c, d, c*, d*); (1.19-1.1, br, a, b, a', b', a*, b*)

3.7.15 Hydrolysis of crosslinked ethanolamine modified poly(ethylene-alt-maleic anhydride) aggregates

Crosslinked E60E solution was sampled as prepared (see section 3.8.14) and incubated for 36h at room temperature. This was repeated for the ^{1}H NMR aggregate solution prepared in section 3.7.14.

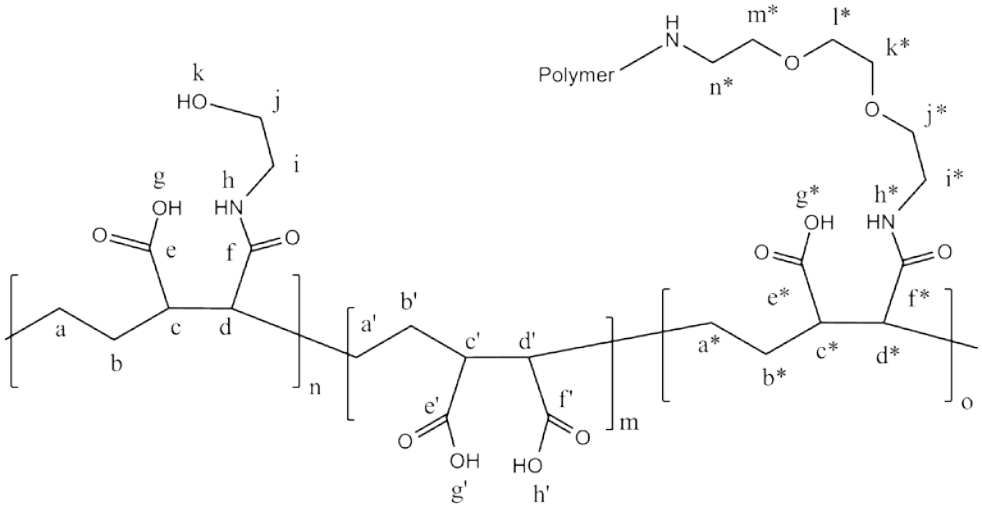

^{1}H NMR: δ_H (400MHz, D_2O): 3.7-2.7 (br, m, ov, i*, k*, l*, m*, n*, i, j; 2.6-2.2 (br, ov, c', d', c*, d*, c, d); 1.7-1.1 (br, ov, a, b, a', b', a*, b*)

3.7.16 Benzylamine functionalised cross linked ethanolamide E60 aggregates

A cross linked E60E aggregate solution was prepared as outlined in sections (3.7.12) and (3.7.14). To a 10mL aggregate solution (10mg mL^{-1}) benzylamine (0.043g, $3.96x10^{-4}$) was added. A 1mL sample was then taken and the solution dialysed (12kDa molecular weight cut off) against $HCl_{(aq)}$ (0.05M, 10mL) 6h, then against distilled water overnight. Then 0.5mL of the solution was then transferred into a new dialysis

bag (12kDa molecular weight cut off) and dialysed against D_2O (5mL) is a sealed vessel. Dialysis was allowed to occur over 3 days with 6 changes of the D_2O. The resulting solution was then analysed by ^1H NMR.

3.7.16.1 Characterisation

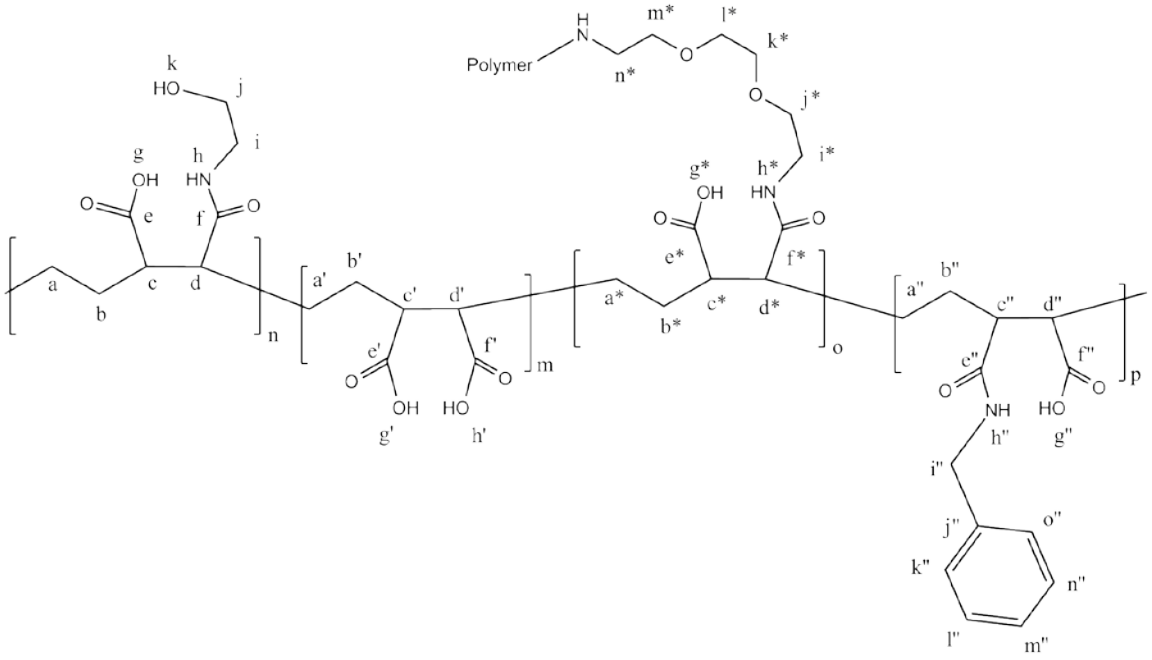

^1H NMR: δ_H (400MHz, D_2O): 7.4-7.05 (br, m, k''. l'', m'', n'', o''); 4.25-2.75 (br, m, ov, i*, j*, k*, l*, m*, n*, i, j); 2.5-2.3 (br, ov, c, d, c', d', c*, d*, c'', d''); 1.5-1.1 (br, ov, a, b, a', b', a*, b*, a'', b'').

3.8 References

(1) Fenyman, R. P. *The Pleasure of Finding Things Out: The Best Short Works of Richard P. Fenyman*, 1 ed.; Basic Books: Cambridge, 2000.

(2) Stryer, L. *Biochemistry*, 3 ed.; W. H. Freeman & Company: New York, 1988.

(3) Konrad, O.; Lankau, T. *Journal of Chemical Education* **2007**, *84*, 864.

(4) Rezus, Y. L. A.; Bakker, H. *Journal of Physical Review Letters* **2007**, *125*, 9853.

(5) Atkins, P. *The Elements of Physical Chemistry*, 3 ed.; Oxford University Press: Oxford, 2001.

(6) Tonford, C. *Science* **1978**, *200*, 1012.

(7) Hendrick, J. L.; Trollsas, M.; Hawker, C. J.; Claesson, H.; Heise, A.; Miller, R. D.; Mecerreyes, D.; Jerom, R. *Macromolecules* **1998**, *31*, 8691.

(8) Harrisson, S.; Wooley, K. L. *Chemical Communications* **2005**, 3259.

(9) Zhang, X.; Matyjaszewski, K. *Macromolecules* **1999**, *32*, 1763.

(10) Israleachvili, J. N. *Intermolecular Surface Forces*, 2 ed.; Academic Press: London, 1992.

(11) Zhang, L.; Eisenberg, A. *Polymers for Advanced Technologies* **1998**, *9*, 667.

(12) Evans, D. F.; Wennerstrom, H. *The Colloidal Domain: Where Physics, Chemistry, Biology and Technology Meet*; VCH: New York, 1994.

(13) Cameron, N. S.; Corbierre, M. K.; Eisenberg, A. *Canadian Journal of Chemistry* **1999**, *77*, 1311.

(14) Antonietti, M.; Forster, S. *Advanced Materials* **2003**, *15*, 1323.

(15) Roger, C.; Liu, W.; Pallier, A.; Brestaz, M.; Pantoustier, N.; Tribet, C. *Macromolecules* **2007**, *40*, 4276.

(16) Kotz, J.; Kosmella, S.; Beitz, T. *Progress in Polymer Science* **2001**, *26*, 1199.

(17) M. Joan Comstock. *Polymers in Aqueous Media: Performance through association*; American Chemical Society: Washington D.C., 1989; Vol. 223.

(18) Strauss, U. P.; Gershfield, N. L. *Journal of Physical Chemistry* **1954**, *58*, 747.

(19) Strauss, U. P.; Jackson, E. *Journal of Polymer Science* **1951**, *6*, 649.

(20) Dublin, P. L.; Strauss, U. P. *Journal of Physical Chemistry* **1967**, *71*, 275.

(21) Dublin, P. L.; Strauss, U. P. *Journal of Physical Chemistry* **1970**, *74*, 2842.

(22) Shih, L. B.; Luccas, M. H.; Warner, R. J. *Polymer Preprints* **1986**, *27*, 288.

(23) Qiu, Q.; Lou, A.; Somasundaran, P.; Pethica, B. A. *Langmuir* **2002**, *18*, 5921.

(24) Miyashita, T.; Arito, Y.; Matsuda, M. *Macromolecules* **1991**, *24*, 872.

(25) Shih, L. B.; Sheu, E. Y.; Cheng, H. *Macromolecules* **1988**, *21*, 1387.

(26) Shih, L. B.; Mauer, D. H.; Verbrugge, C. J.; Wu, C. F.; Chang, S. L.; Chen, S. H. *Macromolecules* **1988**, *20*, 1331.

(27) Hsu, J. L.; Strauss, U. P. *Journal of Physical Chemistry* **1987**, *91*, 6238-6241.

(30) Hu, Y.; Kramer, M. C.; Boudreaux, C. J.; McCormick, C. L. *Macromolecules* **1995**, *28*, 7100-7106.

(31) Anton, P.; Koberle, P. *Die Makromolekulare Chemie* **1993**, *194*, 1.

(32) Strauss, U. P.; Barbieri, B. W. *Macromolecules* **1982**, *15*, 1347.

(33) Chu, D. Y.; Thomas, J. K. *Macromolecules* **1990**, *23*, 4185.

(34) Nagai, K.; Elias, H. G. *Kolloid Z. Z. Polymer* **1972**, *250*, 334.

(35) Newkone, G. R.; Moorefield, C. N.; Baker, G. R.; Saunders, M. J.; Grossman, S. H. *Angewandte Chemie* **1991**, *103*, 1207.

(36) Turro, N. J.; Barton, J. K.; Tomalia, D. A. *Accounts of Chemical Research* **1991**, *24*, 332.

(37) Borisov, O. V.; Halperin, A. *Langmuir* **1995**, *11*, 2911.

(38) Hugouvieux, V.; Axelos, M. A. V. *Macromolecules* **2009**, *42*, 392.

(39) Nayak, R. R.; Roy, S.; Dey, J. *Colloid Polymer Science* **2006**, *285*, 219.

(40) Nayak, R. R.; Roy, S.; Dey, J. *Polymer* **2005**, *46*, 12401.

(41) Gao, B.; Tang, Z.; He, S. *Colloid Polymer Science* **2006**, *284*, 710.

(42) Tribet, C.; Audebert, R.; Potpot, J. L. *Proceedings of the National Academy of Science* **1996**, *93*, 15047.

(43) Zdanowicz, V. S.; Strauss, U. P. *Journal of Physical Chemistry B* **1998**, *102*, 40.

(44) Yokoyama, M.; Miyauchi, M.; Yamada, N.; Okano, T.; Sakurai, Y.; Kataoka, K.; Inoue, S. *Cancer Research* **1990**, *50*, 1693.

(45) Watson, J. D.; Crick, F. H. C. *Nature* **1953**, *171*, 4356.

(46) Turner, M. S.; Joanny, J. F. *Journal of Physical Chemistry* **1993**, *97*, 4825.

(47) Tonge, S. R.; Tighe, B. J. *Advanced Drug Delivery Reviews* **2001**, *53*, 109-122.

(48) Nayak, R. R.; Roy, S.; Dey, J. *Colloid Polymer Science* **2006**, *285*, 219.

(49) Lutz, J. F.; Laschewsky, A. *Macromolecular Chemistry and Physics* **2005**, *206*, 813.

(50) Kramer, M. C.; Steger, J. R.; Hu, Y.; McCormick, C. L. *Macromolecules* **1996**, *29*, 1992.

(51) Kaewsaiha, P.; Matsumoto, K.; Matsuoka, H. *Langmuir* **2007**, *23*, 9162.

(52) Han, J.; Silcock, P.; McQuilan, A. J.; Bremer, P. *Colloid Polymer Science* **2008**, *286*, 1605.

(53) Eckert, A. R.; Webber, S. E. *Macromolecules* **1996**, *29*, 560.

(54) Discher, B. M.; Won, Y. Y.; Ege, D. S.; Lee, J. C.-M.; Bates, F. S.; Discher, D. E.; Hammer, D. A. *Science* **1999**, *284*, 1143.

(55) Discher, B. M.; Bermudez, H.; Hammer, D. A.; Discher, D. W.; Won, Y. Y.; Bates, F. S. *Journal of Physical Chemistry B* **2002**, *106*, 2848.

(56) Cochin, D.; Candau, F.; Zana, R.; Talmon, Y. *Macromolecules* **1992**, *25*, 4220.

Chapter Four: **Poly(ethylene-alt-maleic anhydride) for Surface Applications**

4.1 Introduction

Since maleic anhydride copolymers first appeared in the patent literature they have found multiple applications in thin film and glass size applications, principally as adhesion layers between different materials.[1] Therefore, it is perhaps surprising, given that maleic anhydride copolymers appear in the literature as early as the 1950s, that their first use in the academic literature for monolayer surface applications does not appear until Bergbreiter *et al*'s 1997 publication[2].

Bergbreiter *et al*'s described the immobilisation of poly(methyl vinyl ether-alt-maleic anhydride) onto an amino-silated glass slide, and the subsequent reaction of the remaining anhydrides with a amine terminated dendrimer. The result was to immobilise the dendrimer in such a way so that one hemisphere became tethered to the surface via amide bonds while the other retained its free amines. They were then able to add sequential layers of maleic anhydride copolymer, dendrimer and so on building up an ever thickening film

Badyal *et al.*[3,4] have since confirmed the reactivity of amino silane immobilised maleic anhydride copolymers by observing changes in the surface's XPS spectrum before and after its exposure to a variety of alcohols and amines.[3,4]

Since this early work interest in these polymers has been steadily growing with maleic anhydride copolymer thin films or monolayers finding application in areas such as: the

immobilisation of cellulose, the immobilisation of nucleic acid probes, and the preparation of biocompatible glycopolymer bearing surfaces.[2,5-7]

It is perhaps unsurprising that this growing interest should have developed. In a recent review article Gauthier *et al.*[8] provided a thorough discussion of polymer's which are capable of reacting post polymerisation. In summary, the principle difficulties with such polymers are either: in difficultly of synthesis, the loss of reactivity to unwanted side reaction, or functional groups with too low a reactivity for reasonable conversion.

In contrast the maleic anhydride functional group will readily react with reasonably strong nucleophiles, but is reasonably stable to moisture and alcohols at room temperature. In addition, should hydrolysis occur this can easily be reversed (chapter one). In this context, it is their moderate reactivity which makes maleic anhydride copolymers attractive.

As a result, maleic anhydride copolymers are potentially interesting in surface applications where it is desirable that reactions should go to both in high yield which, in addition to requiring reasonably reactive groups, also requires the reactive sites along the polymer chain to survive the surface's preparation.

4.1.1 Hydrophobic surfaces

4.1.1.1 Wetting

Wetting describes the process in which a liquid contacts with a surface, the characteristics of this contact are the result of the balance of intermolecular forces which is determined by the identity of the solid surface, the liquid and the wider fluid.

It should be noted that this description implies no identity for either the liquid or fluid. For example, the liquid could be a drop of dichloromethane and the fluid water. However, for the sake of both clarity and brevity the remainder of this chapter will consider systems wherein the liquid is water and the fluid air.

The most important measurable value, which is dependent on the balance of these forces, is the liquid's contact angle (θ) which is defined as the angle between the tangent to water – air interface and the tangent to the solid air interface at the point at which all three phases meet (figure 4-1)

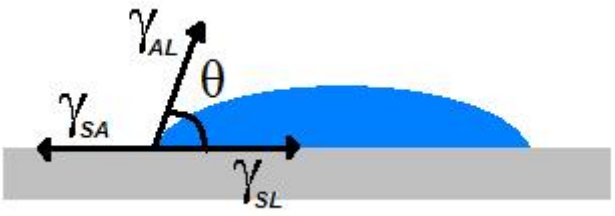

Figure 4-1: Droplet on a solid surface

Where Υ_{SA}, Υ_{SL} and Υ_{AL} are the free energies of the surface air, surface liquid, and air liquid interfaces respectively. The effect of these three energies on the contact angle is described by the Young equation (eqn. 4-1).[9]

$$\cos\theta = \frac{\gamma_{SA} - \gamma_{SL}}{\gamma_{AL}} \qquad \text{(eqn 4-1)}$$

The contact angle is in inverse relation to the fluids capacity to wet the surface, the higher the contact angle the lower the surface wetting (table 4-1).

Table 4-1: Relation of wetting to contact angle

θ	Degree of wetting
0^o	Complete
$0^o < \theta < 90^o$	High
$90^o < \theta < 150^o$	Low
$\theta < 150^o$	Complete non-wetting

However, it is important to note that the Young's relation describes an idealised system in that it assumes a perfectly smooth and chemically homogenous surface. Therefore, any deviation from such a system requires the use of alternative models of which there are two principle examples namely the Wenzel and Cassie-Baxter model.[10,11]

In the case of surfaces which are not perfectly smooth, that is to say surfaces with a surface roughness, the total surface area of the solid is greater than the apparent, projected, surface area. As a result, the contact area between the water and surface is greater than is apparent from the drop's dimensions.

Wenzel was the first to present a solution to this problem by adaptation of the Young equation (equation 4-2).[11]

$$\cos\theta_w = r\ \cos\theta \qquad \text{(eqn 4-2)}$$

Where θ_w is the Wenzel contact angle, and r is the roughness ratio (ratio between the actual and projected surface area). However, this model in turn assumes that water droplet entirely penetrates the surface textures (figure 4-2 (a)).

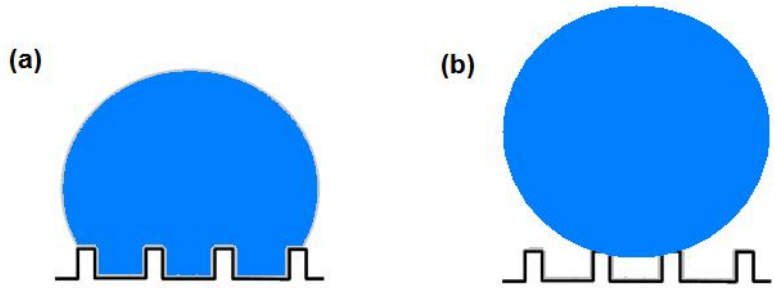

Figure 4-2: (a) Wenzel wetting: the water fully penetrates the surface texture, (b) in-homogenous wetting the water droplet fails to enter the texture

However as figure 4-2(b) shows it is possible that the water droplet sits in a position where it contacts only the top of the asperities, in which case the air forms a partial layer between the surface and droplet. This is so called in-homogenous wetting and in such instances it is necessary to apply the Cassie-Baxter model which was developed to describe the wetting behaviour of chemically heterogeneous surfaces (figure 4-3).

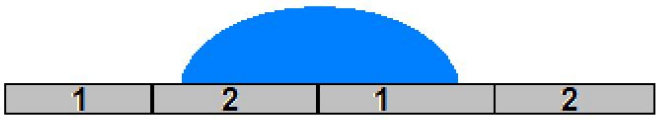

Figure 4-3: Representation of a chemically heterogeneous surface where 1 and 2 represent different surface chemistries.

In such an instance it is possible to calculate the surface's apparent contact angle based on the surface area fraction of each chemistry beneath the droplet's footprint (equation 4-3).

$$\cos\theta_{CB} = \chi_1 \cos\theta_1 + \chi_2 \cos\theta_2 \qquad \text{(eqn. 4-3)}$$

Where θ_{CB} is the Cassie Baxter contact angle, χ_1 and χ_2 are the surface area fraction of surface components 1 and 2 respectively, and θ_1, θ_2 the individual contact angle of components 1 and 2.

As previously stated inhomogeneous wetting leads to air (fluid) becoming trapped between the liquid droplet and the surface. The result is that the air makes up part of the water droplets surface contact area and so contributes to the apparent contact angle.

In the second instance (figure 4-2(b)) the water does not successfully penetrate into the roughened structure and air becomes trapped between the water droplet and the solid interface. As a result the air forms a component of the surface liquid interface

and contributes to the apparent contact angle. Under these circumstances the situation is best described by the Cassie Baxter model wherein air forms the in which component (equation 4-4).

$$\cos\theta_{CB} = f\, r_f \;\; \cos\theta - \; (1 - f) \qquad \text{(eqn. 4-4)}$$

Where f is the projected area fraction of the solid wetted by the droplet and r_f is the roughness ratio.

4.1.1.2 Water repellent surfaces

Water repellent surfaces are remarkably abundant in nature with myriad species of fungi, insects and plants displaying at least some, but in many cases dramatic, water repellency. The topography of several representative examples of these surfaces has been thoroughly examined by Bathlott and Neinhuis[12] and while myriad different surface morphologies are evident, the most effective ones are extremely rough and often have two different scales of roughness in order to maximise the roughness ratio.

Synthetic mimics of such materials are nearly as diverse as those nature with routes to such surfaces including: fibres, particle aggregation, lithography, crystal growth, phase separation, porous inorganic structures, etching, and diffusion limited growth.[2,13,14] Such surfaces have already been reviewed thoroughly elsewhere[15], however, it is worth briefly examining some individual techniques.

Fibres and woven fabrics are relatively easy to make hydrophobic surfaces and even super-hydrophobic due to the textured nature of their surface which occurs of a relatively long length scale.[16] Recent developments in the field include the sputtering of hydrophobic groups by laser and plasma deposition onto the fibres surface.[17] It is important to note that the deposition of many of these hydrophobic groups onto a flat surface does not give rise to water repellency. Therefore, the rough surface textures of the fibres are essential to its hydrophobic behaviour.

A common route to such surfaces is via phase separation, usually the precipitation of a polymer out of a solvent onto the surface.[18] This process is usually quite slow one, sometimes over several hours to days, this is because in order to maximise the surface roughness the precipitating material must be given sufficient time and mobility to form large scale structures. An elegant example of this technique is provided by Chang *et al.*[19] who precipitated poly(vinyl phenol)-b-(styrene) onto a surface. The resulting spherical surfaces structures had a micro-porous resulting from the phase separation of the styrene and phenol blocks.

However, despite being easy to create the commercialisation and exploitation of such technologies has, relative to the academic literature, been lacklustre. This is because the surfaces are generally quite fragile, they often involve multiple steps to achieve the desired result, and the films are easily contaminated by absorbing oils. Consequently, while the basic research in much of this area has already been done, there remain significant technical challenges to surmount.

.

4.2 Aims

4.2.1 Water repellent surfaces

There is a clear interest in developing water repellent surface, however, currently the technical limitations, such as their fragility and the fact they are often opaque limits their application. In addition, many of the processes outlined involve multiple steps which represent a barrier to both their commercialisation.

As a result, an attempt was made to make a water repellent surface from E400 (high molecular mass poly(ethylene-alt-maleic anhydride) within as few steps as possible.

4.3 Results and discussion: Hydrophobic surfaces

E400 represents an interesting route to hydrophobic surface because the polymer can be introduced to the surface from a volatile solvent, such as acetone, and the subsequently reacted with a fluorine bearing amine. This potentially represents an easy way to create fluorinated surfaces without the need to use techniques such as plasma deposition.

In addition, a suitably functionalised surface, such as an amino-silated glass substrate, allows the polymer to be covalently tethered to the solid improving its adhesion and durability, also there is the potential to cross link the structure with di- amino or di-hydroxy molecules with potential further benefits to the structures stability.

To this end a series of surfaces were prepared by reaction of E400 with amino-silated silicon wafers (figure 4-4).

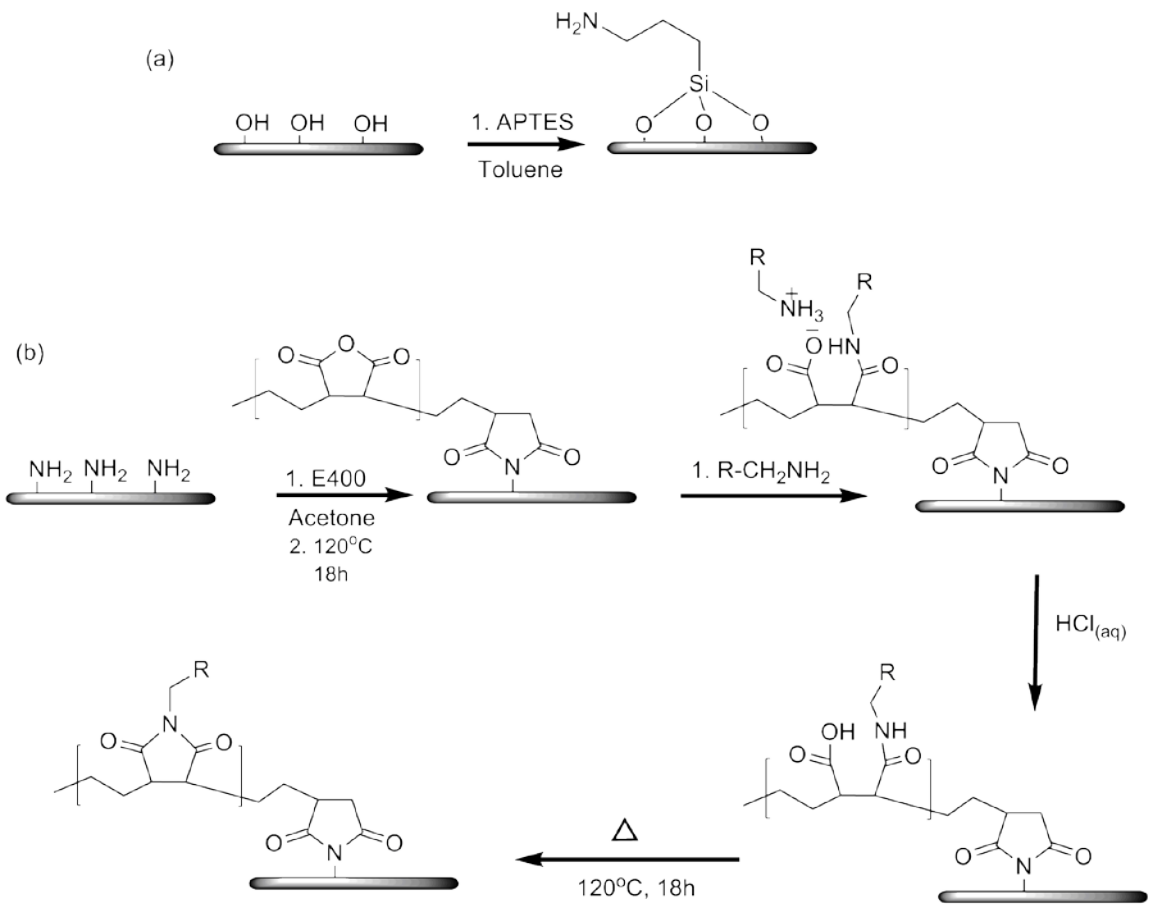

Figure 4-4: Immobilisation of E400 onto aminosilated glass slides (a) silation of glass slide with 3-aminopropyl(triethoxysilane); (b) immobilisation of E400 and its subsequent reaction with an amine

In order to confirm the viability of the immobilised polymer chains several silicon wafers were prepared for XPS. Samples submitted included: a blank silicon wafer, a 3-aminopropyltriethoxy silane coated wafer, a polymer coated silated wafer, and polymer coated wafer which had been prior exposed to 4-fluorobenzylamine (table 4-2).

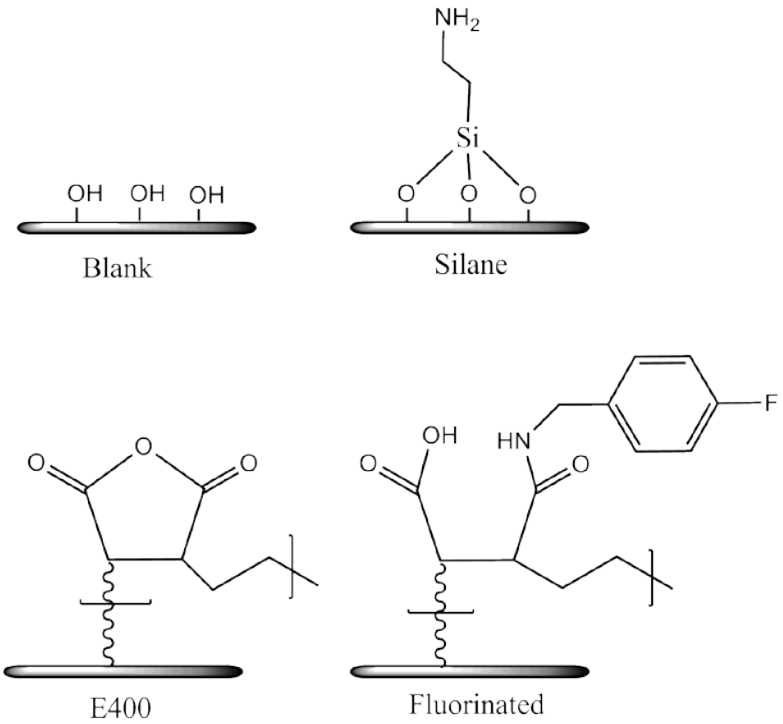

Figure 4-5: Surfaces prepared for XPS (table 4-2)

Table 4-2: Elemental composition of silicon wafer surfaces by XPS

Surface	Elemental composition (%)
Blank	Na (5.5), O (52.8), C (13.2), Si (21.4), Cl (0.2), N (0.3)
Silated	Na (0.0), O (30.2), C (40.7). Si (23.8), Cl (0.2), N (5.8)
E400	Na (0.3), O (25.0), C (55.7), Si (15.1), Cl (0.4), N (3.9)
Fluorinated	Na (1.0), O (26.5), C (48.1), Si (16.5), Cl (0.5), N (4.0), F (4.0)

As table 4-2 shows, the elemental composition of the surfaces changes markedly in the nitrogen and fluorine region. The initial increase in relative nitrogen content (blank to silane) is the result of the amino-silane's reaction with the surface. This

subsequently decreases when E400 is introduced (silane to E400), however, upon the surfaces exposure to an amine the nitrogen content increases indicating the immobilisation of the amine onto the surface (E400 to fluorinated). In addition to this fluorine appears in the elemental surface composition. This process was also followed semi-empirically by contact angle measurement.

High resolution XPS is especially useful in examining carbon environments, in particular between aliphatic, C-O and C=O (or O-C-O) environments. Table (4-3) summarises the relative amount of carbon in each of these environments for each sample.

Table 4-3: Relative amount of aliphatic, C-O and C=O on the wafers surface

Carbon	Si reference	Silane	E60	Fluroinated
C 1s aliphatic	80.2	71.6	67.9	63.5
C 1s C-O	14.3	22.8	16.6	15.1
C 1s C=O (or O-C-O)	5.5	5.6	15.5	12.3

The composition of carbon on the blank reference substrate is as would be expected of so called adventitious carbon, in other words contaminants deposited from the air or vacuum.

The increase in the number of C=O environments between the silane sample and the E60 sample indicates the successful deposition of poly(ethylene-alt-maleic anhydride).

As a result, it can be concluded that immobilisation of E400 on an amino-silane surface results in a surface bearing anhydride which are viable for further reaction.

In order to try and assess the possibility of achieving super hydrophobic several amines were reacted with E400 immobilised surfaces in order to determine the resulting contact angle.

Table 4-4: Contact angles of surfaces reacted with various amines

Amine	Θ (^{o})*	Error (^{o})	Θ (^{o})†	Error(^{o})
Control E400	48	4.6	52	3.0
Propylimide	63	3.4	72	5.7
Hexylimide	65	2.1	81	4.2
Dodecylimide	72	2.3	78	3.3
Benzylimide	68	4.1	74	4.1
Pentafluoropropylimide	74	2.3	76	2.2
4-Fluorobenzylimide	76	3.1	82	4.2

*After reaction with amine but prior to imidization

†After heating (120^{o}C, vacuum oven) to form the imide

As can be observed (table 4-4) none of the above reactions resulted in a significantly hydrophobic surface with values below 90^o. Consequently, it was necessary to introduce a significant amount of roughness into the surface to try and trap air between the water droplet and surface and so bring about Cassie-Baxter

(inhomogeneous) wetting. However, for the system to be of commercial value it is also necessary that as few steps as possible be involved in its synthesis.

The phase separation of two polymers cast onto a surface from a co-solvent is a well understood thermodynamic phenomena. The two polymers separate into distinct solid phases because the enthalpy of mixing is usually unfavourable. As a result the film comes to be composed of separate, chemically homogeneous, micro-domains.

This phenomenon was employed in order to try and create large scale texturing on a surface. This was achieved by spin casting films of poly(methyl methacrylate) and E400 from acetone, followed by the films immersion in a solvent (THF) selective for the methacrylate polymer. The result is to create troughs in the surface where the methacrylate had dissolved and peaks composed of E400 (figure 4-6).

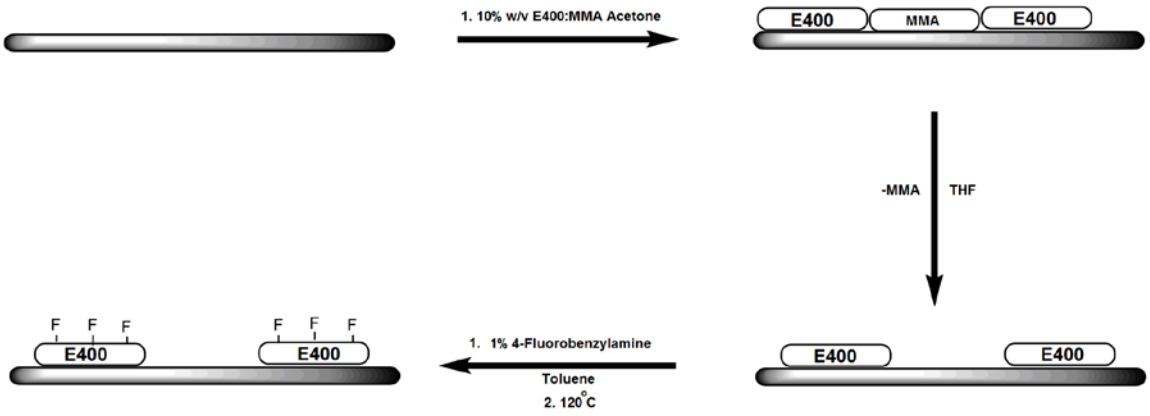

Figure 4-6: Preparation of E400 roughened surfaces

Figure 4-7 shows the phase separation of E400 and PMMA on the silicon wafer. The maximum peak height on the surface was observed to be 96.2nm above the minimum.

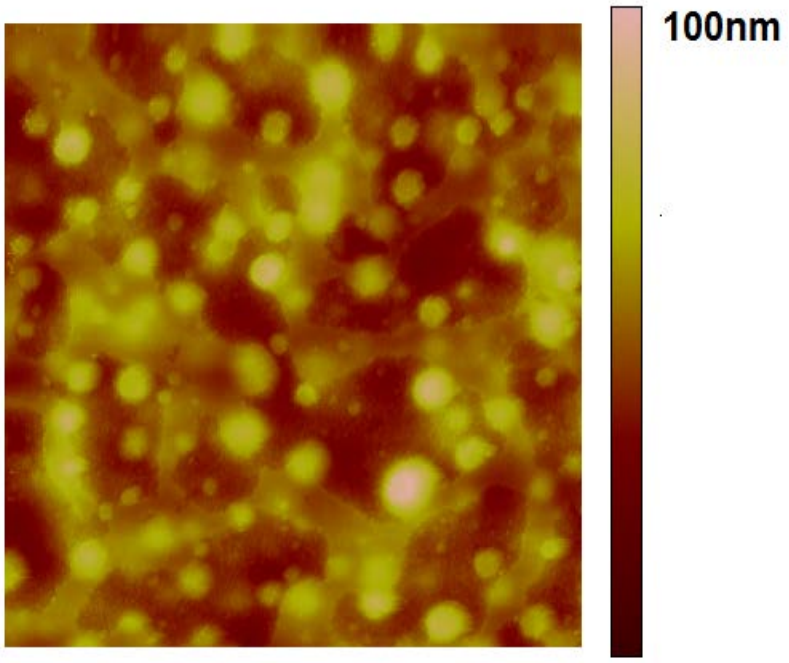

Figure 4-7: AFM image (2.5µm x 2.5µm) of E400:MMA spin coated surface

Upon immersion in THF (figure 4-8) the polymer film was observed to significantly roughen with the highest peak growing from 96.5nm to 659nm.

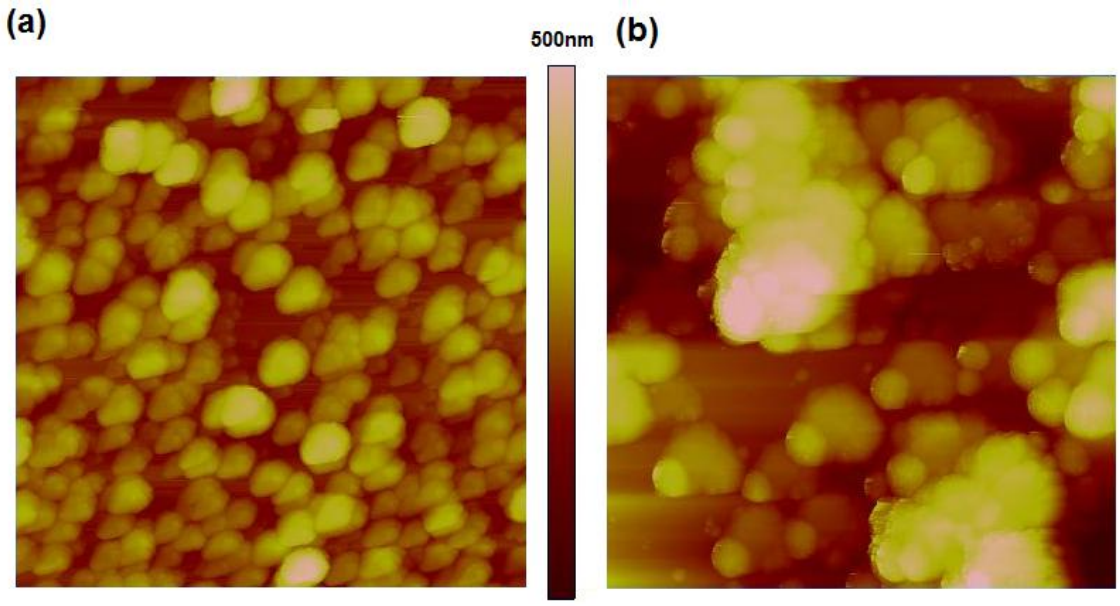

Figure 4-8: AFM image (2.5µm x 2.5µm) of E400:MMA spin coated surface after (a) 5h in THF, and (b) 18h in THF

Subsequent to the reaction of the surfaces with 4-fluorobenzylamine the contact angle was observed to be 92^{o} +/- 7, a significant increase on a comparable flat surface of 76^{o} still short, however, of a water repellent surface. However, a significant increase was brought about. It would be useful to determine both the advancing and receding contact angles for these materials. The measurements are typically taken by expanding or contracting the droplet contact with a surface. The most well known method of doing this is to tilt the sample to a critical angle beyond which the water droplet would roll. The angle of the droplet in the 'down hill' direction is termed the advancing angle, as the droplet is advancing onto new surface, whereas the opposite is termed the receding angle, as the droplet retreats. This hysteresis provides an insight into the surface architecture, as partially wetted surface structures will tend to make the droplet stick in place, i.e. large hysteresis whereas completely de-wetted surfaces will

tend to allow the droplet to roll i.e. low hysteresis. Due to lack of facilities we were unable to measure these parameters but clearly and future work would benefit from taking such measurements.

4.3.1 Conclusion

The principle of surface roughening for hydrophobic application by utilising phase separation was demonstrated. The results although short of the desired values are significantly above those of flat surfaces of similar composition. Therefore, with optimisation it may be possible to achieve the desired result, perhaps by simply varying the poly(methyl methacrylate) to E400 ratio

4.4 Experimental

4.4.1 Materials and Instrumentation

All silicon wafers (single side polished, 500μm thick) were purchased from Si-mat Silicon Materials. AFM measurements were collected on a Digital Instruments Nanoscope IV scanning probe microscope. Measurements were taken in tapping mode using a Budget Sensors Tap 300 AFM tip (100MHz, 40Nm^{-1}). XPS spectra were collected on a Kratos Axis Ultra DLD X-ray Photoelectron Spectroscopy Instrument. XPS measurements were collected in Fixed Analyser Transmission mode 20eV pass energy, with a aperture of 300x700μm at a take off angle of 90^{o} and acceptance angle of 30^{o}. The chamber pressure was maintained at pressures below 8x10^{-9} Torr and analysis was conducted on CASAXPS software. Contact angle measurements were made on a Goniometer via the sessile drop method with 10μL of distilled water, in triplicate.

4.4.2 Silicon wafer cleaning procedure

Silicon wafers were cut to an appropriate size then immersed in hexane (1h), methanol (1h), then a hydrochloric acid methanol bath (1:1 v/v, 6h). The polymers were then rinsed with deionised water and the immersed in piranha solution (5mL 30% H_2O_2, 15mL concentrate H_2SO_4). The wafer was then washed with copious water before being dried under vacuum (120^oC, 18h). Wafers were then used within 24h of their preparation.

4.4.3 Amino silation of silicon wafers

A solution of 3-aminopropyl-(triethoxy)silane was prepared in toluene (10mM) and a freshly cleaned silicon wafer immersed in it (4h). The silicon wafer is then removed, washed with copious amounts of toluene, sonicated in toluene then dried in a vacuum oven (90^oC, 18h). The silated wafers were used within 24h of their preparation.

4.4.4 Immobilisation of poly(ethylene-alt-maleic anhydride) onto aminosilated silicon wafers

An acetone solution of E400 (0.1% w/v) was prepared and a freshly prepared amino silated wafer immersed within it for 10min. The wafer was then removed washed with copious amounts of acetone and dried in a vacuum oven (120^oC, 8h). The wafers were then used within 24h.

4.4.5 Reaction of poly(ethylene-alt-maleic anhydride) functionalised slides

E400 functionalised slides were first heated to 120^oC under vacuum (2h) to ensure the anhydrides are ring closed. The polymer was then exposed to a 1% v/v of an appropriate amine in toluene. The mixture was allowed to stand for 10min, then the

silicon wafer was removed, washed with copious amounts of toluene, rinsed with methanol, washed in $HCl_{(aq)}$ and then rinsed with copious amounts of distilled water.

The wafers were then dried and used, or else heated to 120^{o}C overnight to ring close the amidic acid to the imide.

4.4.6 Preparation of poly(ethylene-alt-maleic anhydride) – poly(methyl methacrylate) films

E400 was heated in a vacuum oven (120^{o}C, 18h) and poly(methyl methacrylate) (120kDa, Sigma) was dissolved into acetone to a concentration of 10% w/v. An E400 solution was then prepared to 10% w/v and the solutions mixed at 1:1 v/v. The solutions were then stirred for 30 minutes. 10μL of this solution was then spun onto a silicon wafer (2,000rpm, 40s spin). The nascent film was then dried in under vacuum at room temperature (18h). An AFM image was then collected.

The silicon wafer was then immersed into THF for a length of time varying between 1 and 18h. The samples were then dried, heated to 120^{o}C under vacuum, and then the contact angle measured. The silicon wafer was then immersed into a toluene solution of 4-flurobenzylamine for 10min, then dried, rinsed with acid, the copious amounts of water, and then heated to 120^{o}C (18h) before another contact angle was made and an AFM image collected.

4.5 References

(1) Barr, D. A.; Buteux, R. H. B.: Great Britain, 1964.

(2) Liu, Y.; Bruening, M. L.; Bergbrietier, D. E.; Crow, R. M. *Angewandte Chemie International Edition* **1997**, *36*, 2114.

(3) Evenson, S. A.; Fail, C. A.; Badyal, J. P. S. *Journal of Physical Chemistry Part B* **1998**, *102*, 3500.

(4) Evenson, S. A.; Fail, C. A.; Badyal, J. P. S. *Journal of Physical Chemistry Part B* **2000**, *104*, 10608.

(5) Pompe, T.; Zschouche, S.; Herold, N.; Salchert, K.; Gouzy, M. F.; Sperling, C.; Werner, C. *Biomacromolecules* **2003**, *4*, 1072.

(6) Uzawa, H.; Ito, H.; Izumi, M.; Tokuhisa, H.; Taguchi, K.; Minoura, N. *Tetrahedron* **2005**, *61*, 5895.

(7) Freudenberg, U.; Zschoche, S.; Simon, F.; Janke, A.; Schmidt, K.; Behrens, S. H.; Auweter, H.; Werner, C. *Biomacromolecules* **2005**, *6*, 1628.

(8) Gauthier, M. A.; Gibson, M. I.; Klok, H. A. *Angewandte Chemie International Edition* **2009**, *48*, 48.

(9) Callies, M.; Quere, D. *Soft Matter* **2005**, *1*, 55.

(10) Cassie, A. B. D.; Baxter, S. *Transactions of the Faraday Society* **1944**, *40*, 546.

(11) Wenzel, R. N. *Industrial Engineering and Chemistry* **1936**, *28*, 988.

(12) Neinhuis, C.; Barthlott, W. *Annals of Botany* **1997**, *79*.

(13) Quian, B.; Shen, Z. *Langmuir* **2005**, *21*, 9007.

(14) Ma, M. L.; Krikorian, V.; Yu, J. H.; Thomas, E. L.; Rutledge, G. C. *Nano Letters* **2006**, *6*, 2969.

(15) Roach, P.; Shirtcliffe, N.; Newton, M. I. *Soft Matter* **2007**, *4*, 224.

(16) Gao, L. C.; McCarthy, T. J. *Langmuir*, *22*, 5969.

(17) Zhang, J.; France, P.; Radomyselskiy, A.; Datta, S.; Zhao, J.; Ooij, W. v. *Journal of Applied Polymer Science* **2006**, *88*, 1473.

(18) Erbil, H. Y.; Demirel, A. L.; Avci, Y.; Mert, O. *Science* **2003**, *299*, 1377.

(19) Tung, P. H.; Kuo, S. W.; Jeong, K. U.; Cheng, S. Z. D.; Huang, C. F.; Chang, F. C. *Macromolecular Rapid Communications* **2007**, *28*, 271.

(20) Chambers, L. D.; Stokes, K. R.; Walsh, F. C.; Wood, R. J. K. *Surfactant Coating Technology* **2006**, *201*, 3642.

(21) Werner, C.; Maitz, M. F.; Sperling, C. *Journal of Materials Chemistry* **2007**, *22*, 339.

(22) Wisniewski, N.; Reichert, M. *Colloids and Surfactants Part B* **2000**, *18*, 197.

(23) Ekin, A.; Webster, D. C.; Daniels, J. W.; Stafslien, S. J.; Casse, F.; Callow, J. A. *Journal of Coating Technology* **2007**, *4*, 435.

(24) Jeon, S. I.; Andrade, J. D. *Journal of Colloid and Interface Science* **1991**, *142*, 159.

(25) Szleifer, I. *Biophysical Journal* **1997**, *72*, 595.

(26) Feldman, K.; Hahner, G.; Spencer, N. D.; Harder, P.; Grunze, M. *Journal of the American Chemical Society* **1999**, *121*, 10134.

(27) Kane, R. S.; Deschatelets, P.; Whitesides, G. M. *Langmuir* **2003**, *19*, 2388.

(28) Arakawa, T.; Timasheff, S. N. *Biochemistry* **1985**, *24*, 6756.

(29) Ishihara, K.; Aragaki, R.; Tomoko, U.; Watenabe, A.; Nakabayashi, N. *Journal of Biomedical Materials Research* **1984**, *24*, 1069.

(30) Hayward, J. A.; Chapman, D. *Biomaterials* **1984**, *5*, 135.

(31) Krishnan, S.; Weinman, C. J.; Ober, C. K. *Journal of Materials Chemistry* **2008**, *18*, 3405.

(32) Kitano, H.; Kawasaki, A.; Kawasaki, H.; Morokoshi, S. *Langmuir* **2005**, *21*, 11932.

(33) Chang, Y.; Chen, S.; Zhang, Z.; Jiang, S. *Langmuir* **2006**, *29*, 2222.